

# Fundamentals of Hydrogen Safety Engineering II

Vladimir Molkov

A photograph of a car at night, with its headlights on and large flames erupting from the front. The car appears to be a dark-colored sedan. The flames are bright orange and yellow, reaching up to the hood of the car. The background is dark, suggesting a nighttime setting.

Part II

Download free books at

**bookboon**.com

Vladimir Molkov

# Fundamentals of Hydrogen Safety Engineering II

---

Fundamentals of Hydrogen Safety Engineering II

© 2012 Vladimir Molkov & [bookboon.com](http://bookboon.com)

ISBN 978-87-403-0279-0

# Contents

<b>1</b>	<b>Introduction</b>	<b>Part I</b>
1.1.	Why hydrogen?	Part I
1.2.	Public perception of hydrogen technologies	Part I
1.3.	The importance of hydrogen safety	Part I
1.4.	Hazards, risk, safety	Part I
1.5.	Hydrogen safety communication	Part I
1.6.	The subject and scope of hydrogen safety engineering	Part I
1.7.	The emerging profession of hydrogen safety engineering	Part I
1.8.	Knowledge gaps and future progress	Part I
<b>2</b>	<b>Hydrogen properties and hazards</b>	<b>Part I</b>
2.1.	Physical and chemical properties	Part I
2.2.	Combustion properties	Part I
2.3.	Comparison with other fuels	Part I
2.4.	Health hazards	Part I
2.5.	Concluding remark	Part I
<b>3</b>	<b>Regulations, codes and standards and hydrogen safety engineering</b>	<b>Part I</b>

**YOU THINK.  
YOU CAN WORK  
AT RMB**

**RAND MERCHANT BANK**  
A division of FirstRand Bank Limited  
Traditional values. Innovative ideas.

Rand Merchant Bank uses good business to create a better world, which is one of the reasons that the country's top talent chooses to work at RMB. For more information visit us at [www.rmb.co.za](http://www.rmb.co.za)

Thinking that can change your world

Rand Merchant Bank is an Authorised Financial Services Provider



Click on the ad to read more



<b>4</b>	<b>Hydrogen safety engineering: framework and technical subsystems</b>	<b>Part I</b>
4.1.	Framework	Part I
4.2.	Technical sub-systems	Part I
<b>5</b>	<b>Unignited releases</b>	<b>Part I</b>
5.1.	Expanded and under-expanded jets	Part I
5.2.	Under-expanded jet theories	Part I
5.3.	The similarity law for concentration decay in momentum-dominated jets	Part I
5.4.	Concentration decay in transitional and buoyancy-controlled jets	Part I
<b>6</b>	<b>Dispersion of hydrogen in confined space</b>	<b>Part I</b>
6.1.	Dispersion of permeated hydrogen in a garage	Part I
6.2.	The pressure peaking phenomenon	Part I
<b>7</b>	<b>Ignition of hydrogen mixtures</b>	<b>Part I</b>
7.1.	Overview of hydrogen ignition mechanisms	Part I
7.2.	Spontaneous ignition of sudden releases	Part I
<b>8</b>	<b>Microflames</b>	<b>Part I</b>
8.1.	Quenching and blow-off limits	Part I



Discover the truth at [www.deloitte.ca/careers](http://www.deloitte.ca/careers)

**Deloitte.**

© Deloitte & Touche LLP and affiliated entities.



Click on the ad to read more

Click on the ad to read more

<b>9</b>	<b>Jet fires</b>	<b>Part I</b>
9.1.	Introduction to hydrogen jet fires and safety issues	Part I
9.2.	Chronological overview of hydrogen jet flame studies	Part I
9.3.	The drawback of Froude-based correlations	Part I
9.4.	The similitude analysis and a dimensional correlation	Part I
9.5.	The jet flame blow-off phenomenon	Part I
9.6.	The novel dimensionless flame length correlation	Part I
9.7.	Flame tip location and equivalent unignited jet concentration	Part I
9.8.	Separation distances from a hydrogen leak	Part I
9.9.	Effect of nozzle shape on flame length	Part I
9.10.	Effect of jet attachment of flame length	Part I
9.11.	Pressure effects of hydrogen jet fires	Part I
9.12.	Summary	Part I
<b>10</b>	<b>Deflagrations</b>	<b>10</b>
10.1.	General features of deflagrations and detonations	10
10.2.	Some observations of DDT in hydrogen-air mixtures	13
10.3.	Vented deflagrations	15
10.4.	Large eddy simulation (LES) of large-scale deflagrations	54

**I WANT TO CHANGE DIRECTION,  
AND THE WORLD.**

**GOT-THE-ENERGY-TO-LEAD.COM**

We believe that energy suppliers should be renewable, too. We are therefore looking for enthusiastic new colleagues with plenty of ideas who want to join RWE in changing the world. Visit us online to find out what we are offering and how we are working together to ensure the energy of the future.

**RWE**  
The energy to lead

<b>11</b>	<b>Detonations</b>	<b>141</b>
11.1.	Direct initiation of detonation	141
11.2.	LES of hydrogen-air detonations	141
<b>12</b>	<b>Safety strategies and mitigation techniques</b>	<b>178</b>
12.1.	Inherently safer design of fuel cell systems	179
12.2.	Mitigation of release consequences	180
12.3.	Reduction of separation distances for high debit pipes	180
12.4.	Mitigation by barriers	181
12.5.	Mitigation of deflagration-to-detonation transition (DDT)	181
12.6.	Prevention of DDT within a fuel cell	182
12.7.	Detection and hydrogen sensors	182
	<b>Concluding remarks</b>	<b>184</b>
	<b>Acknowledgements</b>	<b>189</b>
	<b>Appendix 1. Glossary</b>	<b>190</b>
	<b>References</b>	<b>193</b>

[bookboon.com](http://bookboon.com)

# Corporate eLibrary

See our Business Solutions for employee learning

[Click here](#)



**Disclaimer.** Author does not make any warranty or assumes any legal liability or responsibility for the accuracy, completeness, or any third party's use of any information, product, procedure, or process disclosed, or represents that its use would not infringe privately owned rights. Any electronic website link in this book is provided for user convenience and its publication does not constitute or imply its endorsement, recommendation, or favouring by the author.

The first part of this book is available in  
**"Fundamentals of Hydrogen Safety Engineering I"**

# 10 Deflagrations

## 10.1. General features of deflagrations and detonations

There are two types of “combustion explosions”, i.e. deflagrations and detonations. There are other types of “explosions”, e.g. “physical explosions” of vessels by overpressure above the established limit due to overfill, as a result of runaway reaction, etc. The word “explosion” is rather a jargon and we will avoid applying it in this book where possible. Sometimes the use of term “explosion” could generate misunderstanding. For example, some standards do introduce wrongly from author’s point of view so-called “explosion limit”. This is done in spite of the fact that there can be a significant difference between the “flammability limit”, which is relevant for deflagrations, and “detonability limit” (see further in this section).

Let us overview the most general features of gaseous deflagrations and detonations. Deflagration propagates with velocity below the speed of sound in the unburned mixture while detonation with velocity above the speed of sound. Deflagration front propagates by diffusion of active radicals and heat from combustion products to unburned flammable mixture. A detonation front is in principle different from a deflagration front. It is a complex of coupled leading shock and following the shock reaction zone as was for the first time suggested by Chapman (1899) and Jouguet (1905–1906).

The stoichiometric hydrogen-air mixture flame propagation velocity in the open quiescent atmosphere in a 20 m diameter hemispherical cloud is growing up to 84 m/s, and an explosion overpressure is of the order of 10 kPa in the near field. Then, pressure in a blast wave decays inversely proportional to radius, while for high explosives the pressure decays inversely proportional to radius squared. The maximum deflagration pressure to initial pressure ratio in a closed vessel is essentially higher and equals to 8.15 (BRHS, 2009). Detonation propagates faster than the speed of sound with the Chapman-Jouguet (CJ) velocity and the CJ pressure, which for stoichiometric hydrogen-air mixture are 1968 m/s and 1.56 MPa respectively (BRHS, 2009).



Detonation is the worst case scenario for hydrogen accident. The detonability range of hydrogen in air 11–59% by volume (Alcock et al., 2001) is narrower and within the flammability range of 4–75% by volume. It is worth noting that the detonability limits are not fundamental characteristics of the mixture as they strongly depend on the size of the experimental set up where they are measured. Indeed, a diameter of the tube, where detonation can propagate, should be of the order of a detonation cell size. However, the detonation cell size increases with approaching the detonability limits. Thus, the larger is the scale of an experimental apparatus the smaller is the lower detonability limit (the larger is the upper detonability limit). The important conclusion for practical applications is that the detonability limits of hydrogen-air mixture of the same concentration expand with the scale of a flammable cloud. This explains the difference between the lower detonability limit of hydrogen 11% by volume reported by Alcock et al. (2001) and the “underestimated” value of 18% published in standard ISO/TR 15916:2004. Experimental values of the detonation cell size for a stoichiometric hydrogen-air mixture are in the range 1.1–2.1 cm (Gavrikov et al., 2000).

Once initiated, detonation will propagate as long as the mixture is within the detonability limits subject of sufficient size of the cloud. The detonation wave is led by a von Neumann (1942) pressure spike, which has a short spatial scale of the order of one intermolecular distance, and is about double the CJ pressure. The detonation front has complicated 3D structure. The example of the hydrodynamic structure of detonation with characteristic cells is shown in Fig. 10–1 (Radulescu et al., 2005).

An advertisement for SKF. It features a woman with long dark hair smiling in the foreground. In the background, a white wind turbine is visible against a blue sky. The text 'Brain power' is written in large white letters on the left. On the right, there is a block of text about wind energy and SKF's role. At the bottom left, there is a call to action to visit the SKF website. The SKF logo is in the bottom right corner.

Brain power

By 2020, wind could provide one-tenth of our planet's electricity needs. Already today, SKF's innovative know-how is crucial to running a large proportion of the world's wind turbines.

Up to 25 % of the generating costs relate to maintenance. These can be reduced dramatically thanks to our systems for on-line condition monitoring and automatic lubrication. We help make it more economical to create cleaner, cheaper energy out of thin air.

By sharing our experience, expertise, and creativity, industries can boost performance beyond expectations.

Therefore we need the best employees who can meet this challenge!

The Power of Knowledge Engineering

Plug into The Power of Knowledge Engineering.  
Visit us at [www.skf.com/knowledge](http://www.skf.com/knowledge)

**SKF**

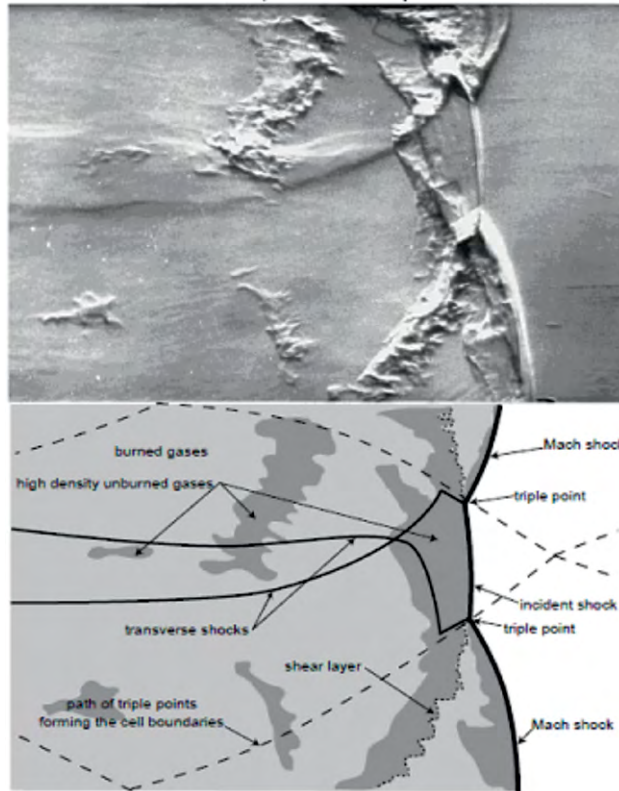


**Figure 10–1.** Schlieren photograph of the hydrodynamic structure of detonation (Radulescu et al., 2005).

The detonation cell size is a function of a mixture composition. Figure 10–2 shows results of the classical work by Lee on dependence of detonation cell size on concentration of hydrogen in air (Lee, 1982).

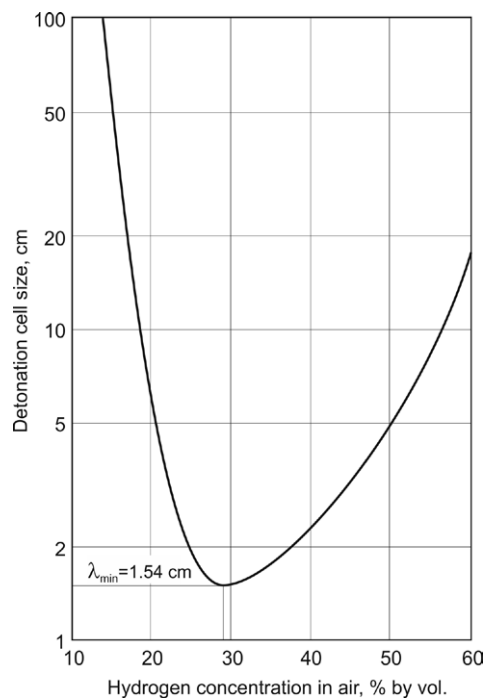


**Figure 10–2.** Detonation cell size as a function of hydrogen concentration in air (Lee, 1982).

## 10.2. Some observations of DDT in hydrogen-air mixtures

Hydrogen is prone to the deflagration-to-detonation transition (DDT). DDT can happen in different environment, including tubes, enclosures, etc.

The experimentally observed run-up distance for transition from deflagration-to-detonation (DDT) in stoichiometric hydrogen-air mixture in a tube has typical length to diameter ratio of approximately 100. The DDT phenomenon is still one of the challenging subjects for combustion research. Different mechanism are responsible for a flame front acceleration to a velocity close to the speed of sound in an unburned mixture, including but not limited to turbulence in an unburned mixture, turbulence generated by flame front itself, and various instabilities such as hydrodynamic, Rayleigh-Taylor, Richtmyer-Meshkov, Kelvin-Helmholtz, etc. Then, there is a jump from the sonic flame propagation velocity to the detonation velocity, which is about twice of the speed of sound at least for near stoichiometric hydrogen-air mixture. The detonation wave is a complex of precursor shock and combustion wave propagates with a speed of von Neumann spike and its description can be found elsewhere (Zbikowski et al., 2008). Detonation front thickness is a distance from the precursor shock to the end of reaction zone where the Chapman-Jouguet condition (sonic plane) condition is reached.

The presence of obstacles in a tube can essentially reduce run-up distance for DDT. This is thought due to significant contribution of the Richtmyer-Meshkov instability just before the DDT. Indeed, the Richtmyer-Meshkov instability increases a flame front area in both directions of a shock passage through the flame front as opposite to the Rayleigh-Taylor instability, when only one direction is unstable to the pressure gradient (acceleration of flow in direction from lighter combustion products to heavier unburned mixture). The initiation of detonation during DDT is thought to happen in a so-called hot spot(s), which potentially could be located within the turbulent flame brush or ahead of it, e.g. in a focus of a strong shock reflection. The peculiarities of DDT mechanisms are not affecting parameters of a steady-state detonation wave following it.

DDT was observed during mitigation of deflagration in enclosure by the venting technique. Venting of a 30% hydrogen-air deflagration in a room-like enclosure with an internal jet camera and initially closed venting panels resulted in DDT with overpressures up to 3.5 MPa in experiments performed in the Kurchatov Institute by Dorofeev et al. (1995a). DDT was initiated a few milliseconds after the destruction of the venting panels. The photographs show the formation of an outflow followed by a localized explosion inside the enclosure near the panel. No effect of the igniting jet size, emerging from the jet camera, on the onset of detonation was observed. The volume size of the jet camera also had no effect, indicating the local character of the detonation onset. Authors suggested that the onset of detonation was not directly connected with jet ignition, but was specifically linked to the sudden venting. Indeed, a needle-like structured flame front with developed combustion surface can be induced by the venting as observed in experiments of Tsuruda and Hirano (1987). Flame front instabilities, in particular Rayleigh-Taylor instability, and rarefaction waves propagating into the enclosure after the destruction of the venting panel increase the mixing of the unburnt mixture and combustion products that can facilitate formation of “hot spots”. In partially reacted mixtures this may create an induction time gradient thereby establishing the conditions for DDT, e.g. by pressure wave amplification by the SWACER (Shock Wave Amplification by Coherent Energy Release, a term introduced by Lee et al., 1978) mechanism theoretically predicted by Zeldovich et al. (1970). The possibility of DDT initiation during a reflection of a pressure wave generated by the camera jet combustion cannot be excluded as well (this could “naturally” coincide with the start of the venting panel opening).

DDT was observed in a large-scale test carried out by Pfortner and Schneider (1984) in Fraunhofer ICT (Germany). The experimental set up included a “lane” (2 parallel walls 3 m apart with height 3 m and length 12 m) and an enclosure (driver section) of sizes  $L \times W \times H = 3.0 \times 1.5 \times 1.5$  m (6.75 m<sup>3</sup> volume) with an initially open to the “lane” vent of 0.82x0.82 m. The “lane” and the enclosure were filled with the same 22.5% hydrogen-air mixture kept under a plastic film. Venting of 22.5% hydrogen-air deflagration initiated at the rear wall of the enclosure by five ignitors into the partially confined space simulating a “lane” resulted in DDT. At a time of 54.61 ms after ignition the DDT occurred in the “lane” at the ground level, when the accelerated flame emerged from the driver section touched the ground.

The onset of detonation in a 17% hydrogen-air deflagration was experimentally observed in a laboratory-scale study by Ferrara et al. (2005). The experimental rig was a cylindrical vessel with a volume of  $0.2 \text{ m}^3$  ( $L \times D = 1.0 \times 0.5 \text{ m}$ ) connected to a dump vessel of a volume of approximately  $50 \text{ m}^3$  through a gate valve of diameter 16.2 cm and vent pipe ( $L = 1 \text{ m}$ ,  $D = 16.2 \text{ cm}$ ). The mixture was prepared by partial pressures in the primary vessel only. Ignition was initiated immediately after opening of the gate valve at the rear wall by a 16 J combustion engine spark plug. A sudden detonation spike of 1.5 MPa appeared in the pressure transients in the vessel only, well after the leading edge of the flame had left the vessel-duct assembly. Supposedly, the short backflow of products from the duct to the vessel led to turbulisation of combustion inside the vessel as was demonstrated in author's previous research back to 1980th (Molkov et al., 1984). The entrainment of unburned mixture pockets by the high velocity hot gases can lead to violent ignition and, under certain circumstances, detonation as demonstrated by Lee and Guirao (1982). For a 17% hydrogen-air mixture at 0.1 MPa and 300 K the detonation cell size is about 15-16 cm and reduces to 4 cm at 400 K following data in the report by Breitung et al. (2000). This could be a possible explanation of no detonation onset in a 16.2 cm diameter pipe and detonation onset in 50 cm diameter vessel, where unburned mixture was preheated by explosion pressure compression to at least 400 K (Ferrara et al., 2005). The occurrence of a detonation wave in the main vessel in similar venting configurations was reported by Medvedev et al. (1994) on even a smaller scale for highly reactive mixtures with initial pressures higher than ambient.

### 10.3. Vented deflagrations

#### 10.3.1. Pressure peaks structure

The phenomenon of double peak pressure structure for vented gaseous deflagrations has been well established since the beginning of research at 1950<sup>th</sup>, but it has not been explained on a satisfactory theoretical basis for a long time (Butlin, 1975). The existence of a two-peak pressure structure during venting of deflagration was demonstrated theoretically by models of Yao (1974), Pasman et al. (1974), Bradley and Mitcheson (1978), Molkov and Nekrasov (1981). The example of typical two peaks structure experimental pressure transient is presented in Fig. 10-3 (Dragosavic, 1973). The first peak is due to vent opening and the second peak is due to high combustion rate (large surface area) at the end of the deflagration.

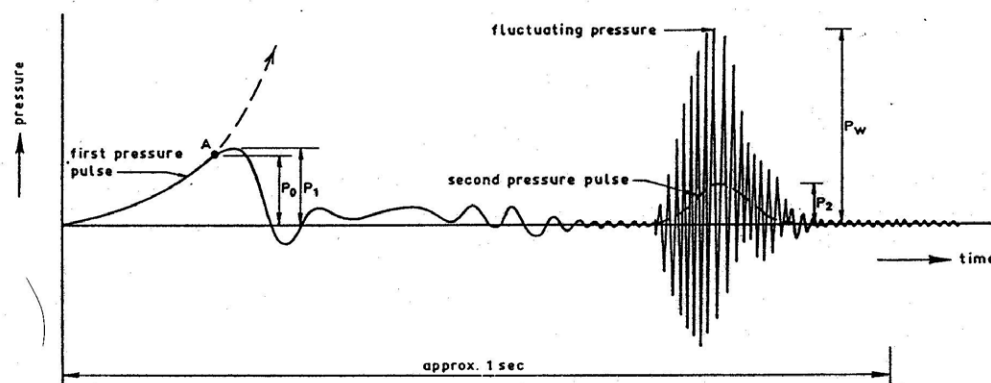


**Figure 10-3.** Typical experimental pressure-time curve with two characteristic peaks  $P_1$  and  $P_2$  (Dragosavic, 1973). Here  $P_0$  is the vent opening pressure.

Later in Cooper et al. (1986) revealed a more complex four-peak pressure structure for rectangular enclosures and very low vent release pressures (see Fig. 10-4, top graph). Analysis of film records showed that pressure peak  $P_1$  is associated with vent opening and venting of unburned gas from enclosure (Fig. 10-4, top, middle, bottom). Due to higher velocity of hot gas compared to cold gas at the same pressure drop, burned gas venting begins almost immediately after the pressure peak  $P_1$ , when vent opening pressure is above 7.5 kPa (Fig. 10-4, middle, bottom), and thus contributes significantly to the fall in pressure at this stage of vented deflagration. The second peak  $P_2$  is due to “external explosion” or highly turbulent combustion of unburned mixture pushed out of the vessel. External combustion is not important at higher vent opening pressures since only small amount of unburned gas is ejected from the enclosure prior to its ignition, and the second peak can no longer be seen on pressure transients. Decrease of flame front area after flame touches the enclosure walls is responsible for the third peak  $P_3$ . Cooper et al. (1986) stated that the fourth peak  $P_4$  is generated when pressure waves resulting from the combustion process couple with the acoustic modes of the vessel and set up sustained pressure oscillations thus satisfying the Rayleigh criterion (Rayleigh, 1945). The third  $P_3$  and fourth  $P_4$  peaks still occur at failure pressure 7.5 kPa (see Fig. 10-4, middle). At the highest vent opening pressure of 21.7 kPa (Fig. 10-4, bottom) only two peaks are observed. The second major peak is clearly due to acoustically enhanced combustion (Cooper et al., 1986). The peak  $P_3$  is no longer observed since the onset of the rapid combustion process responsible for  $P_4$  occurs prior to any significant reduction in flame area due to interaction of the flame front with the enclosure walls.



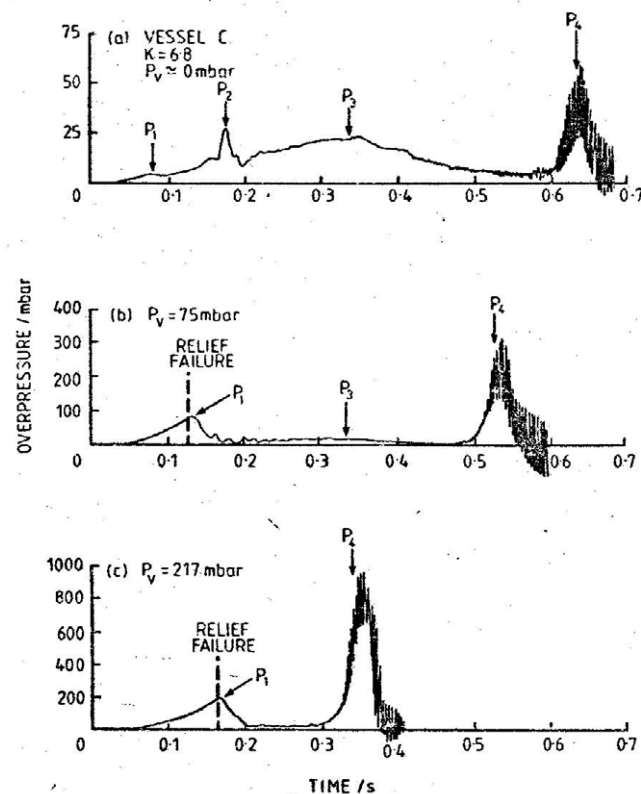


**Figure 10-4.** Pressure transients (Cooper et al., 1986): with four peaks at low vent opening pressure (top), three peaks at medium vent opening pressure (middle), two peaks at high vent opening pressure (bottom).

With us you can  
shape the future.  
Every single day.

For more information go to:  
[www.eon-career.com](http://www.eon-career.com)

Your energy shapes the future.

**e-on**

It is worth noting that by increasing the failure pressure of relief panel above 7.5 kPa two pressure peaks becoming the dominant features of the observed pressure-time profiles (Fig. 10–4, middle and bottom graphs). This value has to be confirmed for hydrogen-air deflagrations as experiments by Cooper et al. (1986) were carried out with other flammable gas. Requirements in many industrial situations preclude the use of low failure pressure reliefs. In circumstances where a high failure pressure relief is employed the four pressure peaks identified by Cooper et al. (1986) will not all be discernible on any pressure trace as can be seen in Fig. 10–4. Moreover, the relative ease, with which the fourth acoustically driven peak can be significantly reduced in magnitude or eliminated altogether, suggests that in most practical situations acoustically enhanced pressures will be of little or no importance (Cooper et al., 1986; van Wingerden and Zeeuwen, 1983).

### 10.3.2. Lumped parameter models of vented deflagrations

Why bother trying to improve lumped parameters models of vented deflagrations, when there exist much more powerful tools of computational fluid dynamics (CFD)? An answer given by Rasus and Krause (2001) is hard to disagree with: “For practical purposes, the detailed modelling of vented explosions, e.g. based on CFD codes, can be excessively sophisticated and time consuming and even not feasible for large and complex geometries”.

First lumped parameter theories of vented explosion dynamics were presented by Yao (1974) and Pasman et al. (1974). Detailed theory of spherical vented gaseous deflagration was published by Bradley and Mitcheson (1978). Further developments were made by an original theory of Molkov and Nekrasov (1981) when for the first time two lumped parameters were introduced into the model (turbulence factor and discharge coefficient). Over the years, the theory has been shown to predict reasonably well dynamics of gaseous deflagrations for both closed and vented enclosures for a wide range of explosion conditions. The history of development of this model is outlined briefly in (Molkov, 1995). Razus and Krause (2001) published a comparative study of a number of vent sizing approaches. From their work, Fig.1 p. 14, one can see that the model (Molkov and Nekrasov, 1981) compares favourably to its analogues in predicting vented deflagration overpressures. The accuracy of the model predictions for different fuel-air mixtures has been found to be higher in 90% cases of available experimental data (Molkov, 1999a) than those made using the approach offered in the standard NFPA 68 (2002).

The model by Molkov and Nekrasov (1981) has been successfully used since then for enclosures with inertia-free covers. The increase of the mass burning rate due to the growth of flame front area, flame front instabilities, and turbulence generated by venting process is taken into account by the turbulence factor,  $\chi$ , which is the first lumped parameter of the model. The second lumped parameter is the generalised discharge coefficient,  $\mu$ , whose value takes into account possible gas movement inside the enclosure that gives larger values as compared to small orifices in large vessels, when gas velocity within the vessel can be taken as zero with high accuracy.

The model (Molkov and Nekrasov, 1981) has been validated broadly against experiments with non-inertial vent covers for different fuel-air mixtures, see e.g. (Molkov et al., 2000). The code CINDY, developed at the University of Ulster, includes the mentioned deflagration model, augmented by features enabling the user to predict pressure dynamics for various inertial vent cover designs, providing safety engineers with a sorely needed tool for vent sizing of inertial covers. Features of the CINDY code include several vent cover opening mechanisms, an option of multiple vents, original modelling of gas flows nearby the vent cover, and user-controlled variation of the turbulence factor and discharge coefficient over time.

### 10.3.3. Vented deflagrations with inertial vent covers

The first studies on the influence of vent cover inertia on explosion pressure were performed in the UK in the 1950's by Wilson (1954), Cubbage and Simmonds (1955). Korotkikh and Baratov (1978) suggested that the cause of building destruction by internal deflagration was in most cases not insufficient vent area but excessive inertia of vent cover(s) and high release pressure. An important issue in inertial cover design is the upper limit of inertia that a given application might accept. Above the upper limit, the design might fail to open sufficiently, negating its purpose. To neglect the influence of vent cover inertia different values have been suggested: from 10 kg/m<sup>2</sup> (Bartknecht, 1978) to 120 kg/m<sup>2</sup> in relevant Russian standard. Details of the published results of various investigators into inertial effects are summarised in Molkov et al. (2004a).

In this section we present the next step in development that enables the lumped parameter model by Molkov and Nekrasov (1981) to take into account inertial venting devices of various types (Grigorash et al., 2004). We start with presenting a modification of the governing equations to include multiple vents of arbitrary nature acting concurrently. We continue with a description of our modelling of two types of inertial venting devices: translation panels, that include spring-loaded valves, and hinged doors. We conclude with reproducing our validation results for both types of these covers against the experiments by Höchst and Leuckel's (1998) on vented gaseous deflagrations with inertial covers (surface density up to 124 kg/m<sup>2</sup>) in a large-scale 50-m<sup>3</sup> silo, and experiments of Wilson (1954) with spring-loaded venting valves.

#### 10.3.3.1. Model assumptions and derivation of governing equations

It is assumed that a deflagration in uniform gaseous flammable mixture is initiated by an ignition source with low energy release like a spark. The “low” means negligible in comparison with the internal energy of the mixture. The ignition source may reside anywhere inside an enclosure of arbitrary shape, volume  $V$ , with the ratio of the longest overall dimension to the shortest one not more than 5:1 (when pressure non-uniformity and wave effects could become important). The initial pressure and temperature are equal  $p_i$  and  $T_{ui}$  respectively. In general case, obstacles can be distributed throughout the enclosure.

A premixed flame propagates from the point of ignition throughout the mixture at conditions of changing in time temperature of unburnt mixture  $T_u(t)$  and pressure  $p(t)$  with burning velocity  $S_u(T_u, p)$ . The Mach number,  $S/c_u$ , relating the flame velocity  $S$  and the speed of sound  $c_u$  in the unburnt mixture, doesn't exceed the value of about 0.1. This allows one to consider pressure uniform throughout the space of enclosure, and changing only in time. The flamelet model of turbulent combustion is assumed for the conversion of fresh gases into combustion products. The conversion happens in the flame front that is negligibly thin. Heat losses are neglected because the deflagration time is short in comparison with the characteristic heat transfer time from hot gases to walls and obstacles. The difference between the calculated adiabatic isochoric complete combustion pressure and the experimental one is roughly 10% (Kumar et al., 1989). Compression and expansion of gases comply with the adiabatic equation. Maché effect is neglected. Indeed, it was shown previously that the influence of the phenomenon of non-uniform distribution of temperature throughout the space of the vessel is negligible, even for burning velocity determination by constant volume bomb technique (Metghalchi and Keck, 1982). This is even more correct for vented deflagration where the pressures are less due to venting. The specific heats ratios of unburnt  $\gamma_u$  and burnt  $\gamma_b$  gases are constant during deflagration. The molecular masses of unburnt and burnt gases are constant too. The gases themselves are assumed ideal.

Vents may appear as single or multiple units, either inertia-free or inertial of mass  $m$ . A latching pressure  $p_v$  may be used to prevent vent opening until the target pressure is reached. An inertia-free vent opens instantaneously. The venting area  $F_j$  of each vent  $j$  with inertial cover varies with time, since inertial covers open gradually. The area  $F_j$  is calculated as the gap area between the edges of the cover and the vent opening, depending on the type of the cover (translating panel or hinged door), its size, and, in case of hinged doors, shape.

be > your degree

Bring your talent and passion to a global organization at the forefront of business, technology and innovation. Discover how great you can be.

Visit [accenture.com/bookboon](https://accenture.com/bookboon)

**Be greater than.**  
consulting | technology | outsourcing

**accenture**  
High performance. Delivered.

© 2013 Accenture  
All rights reserved.

Derivation of the vented deflagration model for the case of a single inertia-free venting device can be found elsewhere (Molkov and Nekrasov, 1981; Molkov, 1995). Here we will demonstrate how the model, and this derivation, changes in the case of multiple inertial venting devices. At the same time, let us introduce the entire necessary notation.

Let us refer the real flame front area  $F_f(t)$  at any moment  $t$  of time to the surface area  $F_s(t) = 4\pi r_b^2$  of a sphere of radius  $r_b$  to which burnt gas inside the enclosure could be gathered at the same moment, and call this ratio, according to historically settled terminology, a turbulence factor  $\chi(t) = F_f(t)/F_s(t)$ . Here  $\pi_0$  denotes “pi” number. The dependence of the burning velocity on temperature and pressure can be expressed as, see e.g. (Nagy et al., 1969; Bradley and Mitcheson, 1978),  $S_u = S_{ui} (T_u/T_{ui})^m (p/p_i)^n$ , where subscript “i” stands for initial conditions. From the adiabatic equation  $pV^\gamma = \text{const}$  together with the ideal gas state equation one can easily derive the relationship, in which the dimensionless pressure is the ratio of current pressure to initial pressure in the vessel  $\pi = p/p_i$

$$T/T_i = (p/p_i)^{(\gamma-1)/\gamma} = \pi^{1-1/\gamma}. \quad (10-1)$$

This proportion allows one to express the burning velocity in the form

$$S_u = S_{ui} \pi^\varepsilon, \quad (10-2)$$

where the values of thermokinetic factor  $\varepsilon = m + n - m/\gamma_u$  along with the initial burning velocity  $S_{ui}$  can be determined by the inverse problem method, i.e. by processing a pressure transient recorded in a closed spherical bomb, and are tabulated for some mixtures, see e.g. references in (Molkov, 1995). Denote  $\sigma_u = \rho_u/\rho_i$  the relative density of the unburnt gas, where  $\rho_i$  and  $\rho_u$  are the initial and the current unburnt gas densities respectively. From the adiabatic equation written in the form  $p(m/\rho)^\gamma = \text{const}$ , where  $m$  is the mass, for both the initial and the current densities, one can see that

$$\sigma_u = \pi^{1/\gamma_u} \quad (10-3)$$

Denote  $n_u = m_u/m_i$  and  $n_b = m_b/m_i$  the relative masses;  $\omega_u = V_u/V$  and  $\omega_b = V_b/V$  the relative volumes of unburnt and burnt gases. Volume conservation within the gas gives  $\omega_u + \omega_b = 1$ . Then for the average relative density of burnt gases throughout the enclosure we have

$$\langle \sigma_b \rangle = \frac{\langle \rho_b \rangle}{\rho_i} = \frac{n_b}{\omega_b} = \frac{n_b \sigma_u}{\sigma_u - n_u}. \quad (10-4)$$

For further simplicity of derivation it is useful to imagine, in the mathematical sense only, that we deal with spherical flame propagation in a spherical vessel of radius  $a$

$$a = \left( \frac{3V}{4\pi_0} \right)^{1/3} \quad (10-5)$$

Then the dimensionless radius of our imaginable spherical flame can be calculated as

$$r(t) = \frac{r_b(t)}{a} = \left( \frac{V_b}{V} \right)^{1/3} = \left( 1 - \frac{V_u}{V} \right)^{1/3} = \left[ 1 - \frac{n_u(t)}{\sigma_u} \right]^{1/3} = \left[ 1 - \frac{n_u(t)}{\pi^{1/\gamma_u}} \right]^{1/3}. \quad (10-6)$$

According to the flamelet model of turbulent combustion, the burning rate of fresh gases is  $dm_u / dt = -F_f \rho_u S_u$ . Using notation for  $\chi$  and formulae (10-2) and (10-3) gives

$$\frac{dm_u}{dt} = -4\pi_0 r_b^2 \rho_i \sigma_u \chi S_{ui} \pi^\varepsilon. \quad (10-7)$$

The above formula expresses the instantaneous change in the unburnt gases mass within the vessel due to combustion. In the following, we account for the other change to this mass is due to venting.

To distinguish between the unburnt and burnt gas outflows, the fraction of the area  $F_j(t)$  of a vent “j” occupied by burnt gas during outflow at any moment is denoted  $A_j(t)$ . Then unburnt gases occupy  $(1 - A_j(t))$  fraction of  $F_j(t)$ . In the most general case of vented deflagration, only unburnt gases outflow from a vent at the beginning of venting,  $A=0$ . After that, joint outflow of unburnt and burnt gases takes place. At the end of the process, the outflow has to be accomplished by burnt gases only,  $A=1$ . An exception is the case of ignition in the close proximity of a relatively small vent, when burnt gases occupy the whole of the vent cross-section from the very start of venting,  $A=1$ .

In 1997 author has analyzed motion pictures of vented deflagrations by various authors and showed that, in general,  $A=r^2$  is a reasonable estimate of the joint outflow. Particularly, this estimate is closer to the experimental results than the Yao's (1974) estimate  $A=n_b/(n_b+n_u)$ . It should be noticed, however, that the estimate  $A=r^2$  gives unsatisfactory results under the special condition that the maximum deflagration pressure is comparable to the vent release pressure (denoted  $p_v$  below). In the CINDY code, created at the University of Ulster, the user can control the estimate of A, by choosing the location of the ignition source position relative to the vent, as follow

$$A = \begin{cases} 1, & \text{if the ignition source is very close to the vent;} \\ 0, & \text{if the ignition source is very far from the vent;} \\ r^2, & \text{if the ignition source is in the middle of the enclosure.} \end{cases}$$

For each vent, the orifice equations for calculation of mass flow rate for subsonic and sonic regimes published elsewhere (Bradley and Mitcheson, 1978) give the mass rate of discharge  $G_{ju}$  of unburnt and  $G_{jb}$  of burnt gases. With our notation for relative pressure and density, the mass rate of discharge of any gas is

$$G = \mu F p_i^{1/2} \rho_i^{1/2} R^\# \quad (10-8)$$

where  $R^\#$  is the outflow parameter given by

$$R^\# = \left\{ \frac{2\gamma}{\gamma-1} \pi \sigma \left[ \left( \frac{p_a}{p_i \pi} \right)^{2/\gamma} - \left( \frac{p_a}{p_i \pi} \right)^{(\gamma+1)/\gamma} \right] \right\}^{1/2} \quad \text{and} \quad R^\# = \left[ \gamma \left( \frac{2}{\gamma+1} \right)^{\frac{\gamma+1}{\gamma-1}} \pi \sigma \right]^{1/2} \quad (10-9)$$



for subsonic regime and sonic regime, respectively. The transition from the subsonic to the sonic regime of discharge happens when the pressure exceeds the critical value

$$\pi \geq \left( \frac{p_a}{p_i} \right) \cdot \left( \frac{1+\gamma}{2} \right)^{\gamma/(\gamma-1)} . \quad (10-10)$$

The unburnt and burnt versions of  $R^\#$  and the critical pressure are obtained by (10-9) and (10-10) with substituting the unburnt and burnt versions of  $\gamma$  and  $\sigma$  in these formulae.

Taking into account formula (10-7) for mass burning rate, and simultaneous discharge of unburnt and burnt gases from  $N$  vents, the rate of change of the unburnt gases mass becomes

$$\frac{dm_u}{dt} = -4\pi_0 r_b^2 \rho_i \sigma_u \chi S_{ui} \pi^\varepsilon - \sum_{j=1}^N (1-A_j) G_{uj} . \quad (10-11)$$

From now on, the limits of summation will be the same everywhere and we omit them from the summation sign. Using formulae (10-3), (10-5) and (10-6), and going over to relative mass and dimensionless time in (10-11), gives

$$\frac{dn_u}{d\tau} = -3 \cdot \left[ \left( 1 - n_u \pi^{-1/\gamma_u} \right)^{2/3} \chi \pi^{\varepsilon+1/\gamma_u} + \sum \frac{a(1-A_j)G_{uj}}{3m_i S_{ui}} \right] . \quad (10-12)$$



"I studied English for 16 years but...  
...I finally learned to speak it in just six lessons"

Jane, Chinese architect

ENGLISH OUT THERE

Click to hear me talking before and after my unique course download

Recall the Newton-Laplace formula for the speed of sound at the initial conditions  $c_{ui} = \sqrt{\gamma_u p_i / \rho_i} = \sqrt{\gamma_u R T_{ui} / M_{ui}}$ . With (10–8) and this formula it is easy to rewrite the discharge term in (10–12) in the form

$$\sum \frac{a(1-A_j)G_{uj}}{3m_i S_{ui}} = WR_u^\# \frac{\sum (1-A_j)\mu_j F_j}{\sum \mu_j F_j}, \quad (10-13)$$

where  $W$  is the transient venting parameter, dependent on the varying current venting areas

$$W = \frac{a\sqrt{p_i \rho_i}}{3m_i S_{ui}} \sum_{j=1}^N \mu_j F_j = \frac{c_{ui} \sum \mu_j F_j}{(36\pi_0)^{1/3} V^{2/3} S_{ui} \sqrt{\gamma_u}}. \quad (10-14)$$

With (10–13) and (10–14), equation (10–12) becomes

$$\frac{dn_u}{d\tau} = -3 \left[ \chi \pi^{\varepsilon+1/\gamma_u} (1 - n_u \pi^{-1/\gamma_u})^{2/3} + WR_u^\# \frac{\sum (1-A_j)\mu_j F_j}{\sum \mu_j F_j} \right]. \quad (10-15)$$

Reasoning analogously brings about the equation for the rate of change of mass of burnt gases

$$\frac{dn_b}{d\tau} = 3 \left[ \chi \pi^{\varepsilon+1/\gamma_u} (1 - n_u \pi^{-1/\gamma_u})^{2/3} - WR_b^\# \frac{\sum A_j \mu_j F_j}{\sum \mu_j F_j} \right] \quad (10-16)$$

Equations (10–15) and (10–16) are two of the three governing differential equations of this model. The third equation that describes the change in the relative pressure is obtained from the laws of conservation, as follows. Conservation of mass gives

$$n_b + n_u + \int_0^t \sum \frac{A_j G_{bj} + (1-A_j)G_{uj}}{m_i} dt = 1. \quad (10-17)$$

The mass flux of the unburnt gases through every vent reduces the energy of the system by the sum of the amount of the internal energy of the escaped gas and the work required to move this mass through the vent cross-section. Therefore, conservation of energy per mass unit gives

$$u_i = \int_{n_b} u_b dn_b + \int_{n_u} u_u dn_u + \int_0^t \left[ \left( u_b + \frac{p}{\rho_b} \right) \sum \frac{A_j G_{bj}}{m_i} + \left( u_u + \frac{p}{\rho_u} \right) \sum \frac{(1-A_j)G_{uj}}{m_i} \right] dt. \quad (10-18)$$

The internal energy of a mass unit of the unburnt and burnt gases changes in consequence of adiabatic compression or expansion respectively as (Babkin and Kononenko, 1967)

$$u_u = u_i + \frac{(T_u - T_{ui})c_{vu}}{M_{ui}} \quad \text{and} \quad u_b = u_{bi} + \frac{(T_b - T_{bi})c_{vb}}{M_{bi}}, \quad (10-19)$$

where  $c_v$  denotes the specific heat per mole at isochoric conditions. Since the combustion takes place at a constant initial pressure, the enthalpy is conserved  $u_i + RT_{ui} M_{ui}^{-1} = u_{bi} + RT_{bi} M_{bi}^{-1}$ , and this leads to

$$u_b = u_i + \frac{RT_{ui}}{M_{ui}} - \frac{RT_{bi}}{M_{bi}} + \frac{(T_b - T_{bi})c_{vb}}{M_{bi}}. \quad (10-20)$$

Substitution of (10-19) and (10-20) to the energy equation (10-18) followed by simplifications using the mass conservation equation (10-17), the gas state equation in the form  $p/\rho = RT/M$  and the specific heats equation  $c_p - c_v = R$  gives

$$R \frac{T_{ui}}{M_{ui}} = c_{pb} \frac{T_{bi}}{M_{bi}} n_b + c_{pu} \frac{T_{ui}}{M_{ui}} n_u - c_{vb} \int_{n_b} \frac{T_b}{M_{bi}} dn_b - c_{vu} \int_{n_u} \frac{T_u}{M_{ui}} dn_u + \int_0^t \frac{c_{pb}(T_{bi} - T_b)}{m_i M_{bi}} \sum A_j G_{bj} dt + \int_0^t \frac{c_{pu}(T_{ui} - T_u)}{m_i M_{ui}} \sum (1 - A_j) G_{uj} dt \quad (10-21)$$

By the assumption of uniform distribution of temperature in the combustion products, the ideal gas state equation, and formulae (10-3) and (10-4), one has

$$\int_{n_b} \frac{T_b}{M_{bi}} dn_b = \frac{T_{ui}}{M_{ui}} \sigma_u^{\gamma_u-1} (\sigma_u - n_u) \quad (10-22)$$

Multiply both parts of (10-21) by  $M_{ui}$ , divide them by  $c_{vb} T_{ui}$  and simplify the result using equations (10-22), (10-1), (10-3),  $\gamma = c_p / c_v$  and  $\gamma - 1 = R / c_v$  to obtain

$$\pi + \gamma_b - 1 = n_u \frac{\gamma_u - \gamma_b}{\gamma_u - 1} \pi^{1-1/\gamma_u} + \frac{\gamma_u (\gamma_u - 1)}{\gamma_u - 1} \left\{ n_u + \int_0^t (1 - \pi^{1-1/\gamma_u}) \frac{\sum (1 - A_j) G_{uj}}{m_i} dt \right\} + \gamma_b \left\{ E_i n_b + \int_0^t \left[ E_i - \pi^{1-1/\gamma_u} \left( \frac{\pi^{1/\gamma_u} - n_u}{n_b} \right) \right] \frac{\sum A_j G_{bj}}{m_i} dt \right\}. \quad (10-23)$$

Differentiation of this equation with respect to the relative time  $\tau$ , and simplification using formulae (10-13), (10-15) and (10-16) yields equation for dimensionless pressure

$$\frac{d\pi}{d\tau} = 3\pi \frac{\chi(\tau) Z \pi^{\varepsilon+1/\gamma_u} (1 - n_u \pi^{-1/\gamma_u})^{2/3} - \gamma_b W R_\Sigma}{\pi^{1/\gamma_u} - \frac{\gamma_u - \gamma_b}{\gamma_u} n_u}, \quad (10-24)$$

where  $W$  is defined by (10-14),  $R_\Sigma$  is the outflow contribution

$$R_\Sigma = R_u^\# \frac{\sum [1 - A_j(\tau)] \mu_j F_j(\tau)}{\sum \mu_j F_j(\tau)} + R_b^\# \left( \frac{\pi^{1/\gamma_u} - n_u}{n_b} \right) \frac{\sum A_j(\tau) \mu_j F_j(\tau)}{\sum \mu_j F_j(\tau)} \quad (10-25)$$

and  $Z$  is the auxiliary quantity

$$Z = \gamma_b \left[ E_i - \frac{\gamma_u}{\gamma_b} \frac{\gamma_b - 1}{\gamma_u - 1} \right] \pi^{\frac{1-\gamma_u}{\gamma_u}} + \frac{\gamma_b - \gamma_u}{\gamma_u - 1}.$$

Thus, equations (10–15), (10–16) and (10–24) constitute the system of governing equations. At the beginning of the integration ( $\tau = 0$ ) of the governing equations, the following conditions are assumed:  $\pi = 1$  since the pressure equals  $p_i$ ;  $n_u = 1$  and  $n_b = 0$  since nothing has burnt yet. The integration of the governing equations can be done by any known method of solution of a system of ordinary differential equations. At any given moment of time, a number of dimensional deflagration parameters can be obtained, using the following simple formulae:  $t = \tau \times a / S_{ui}$  – the time of deflagration, sec;  $p = \pi \times p_i$  – the current pressure, Pa;  $S_u = S_{ui} \times \pi^\varepsilon$  – the current burning velocity, m/sec;  $r_b = r \times a$  – the current radius of the imaginable spherical flame, m;  $T_u = T_{ui} \times \pi^{(\gamma_u - 1) / \gamma_u}$  – the current temperature, K.

### 10.3.3.2. Modelling of vent covers

Equations (10–15), (10–16) and (10–24) above depend on the current venting area that changes with time, but the character of this change is not specified. This allows vent covers of any type to be “plugged in” the calculations, as long as the value of the current venting area  $F(t)$  can be calculated at each integration step. For any vent cover, in conditions of pressure growing with time, at some moment  $t_{vj}$ , when the internal explosion pressure is equal to the pre-set “latch release” pressure  $p_{vj}$ , the release of vent cover “j” occurs and outflow of gases from enclosure through vent “j” begins into the space. Depending on the vent cover type, the venting area either immediately becomes equal to the nominal vent area  $F_N$  (non-inertial or light vent covers, or rupture membranes) or increases gradually while vent cover moves away by the pressure force. Two common types of inertial venting devices are translation panels and hinged doors. The spring-loaded vent covers make a sub-class of the translation panels.

**DUKE**  
THE FUQUA  
SCHOOL  
OF BUSINESS

**BUSINESS HAPPENS**

**HERE.**

[www.fuqua.duke.edu/globalmba](http://www.fuqua.duke.edu/globalmba)

**Learn More >**

### Translation panels

A translation panel is an inertial cover modeled as a flat solid body. Vertically translating panels may move either upwards from or downwards towards their starting position, while horizontally translating panels can only move horizontally away from their starting position. The translation of the panel is either unrestricted or constrained by an inelastic arrester or a linear spring.

The force of reduced pressure that invokes movement of a translation panel deserves separate attention. With the simplest approach to model vent cover displacement, the force  $f(t)$  of reduced pressure is

$$f(t) = [p(t) - p_a] \cdot F_N. \quad (10-26)$$

Equation (10-26) assumes the same magnitude of pressure applied across the entire internal ( $p(t)$ ) and external ( $p_a$ ) surfaces of the vent cover. Application of the CINDY code, utilizing (10-26) to simulate both pressure and displacement in experiments by Höchst and Leuckel (1998) showed that while overpressures are successfully matched, backfitted displacements were too rapid compared to the experimental data (Molkov et al., 2003).

To account for the excessive displacement that the simple approach with (10-26) produces, consider the vent cover that has already travelled some distance away from the vent cross-section. The cover obstructs gases escaping from the vessel, and makes the gas flow change its direction by  $90^\circ$ . Thus some time after vent release, a jet forms under the moving vent cover. Molkov et al. (2003) have derived for a circular cover of radius  $R_0$  that taking this jet effect into account halves the value of the initial pressure force (10-26) as will be demonstrated in the next section

$$f(t) = \frac{[p(t) - p_a] \cdot \pi_0 R_0^2}{2} = \frac{[p(t) - p_a] \cdot F_N}{2}. \quad (10-27)$$

Simulations with CINDY code written according to the developed model showed that taking the jet effect into account by formula (10-27) produces a good match of the simulated panel displacement and pressure transients with the experimental data by Höchst and Leuckel (1998).

All in all, the procedure to calculate the pressure force is as follows. If a massive panel is completely covering a vent then the static pressure force that must overcome the gravity or spring load to lift the panel is given by formula (10-26). Formula (10-27) represents the pressure force when the jet effect is accounted for. We assume that transition from the “pressure” regime of formula (10-26) for the closed vent to the “jet” regime of formula (10-27) for the partially open vent is *continuous*. In the absence of evidence to the contrary, it is in direct proportion to the current venting area. The “jet fraction” parameter  $A_{jet}$  decides the fraction of the nominal venting area  $F_N$  at reaching which the vent finds itself in the “jet” regime.

At present, on each step of integration the panel motion is treated as uniformly accelerated. The CINDY code calculates the panel acceleration from the balance of forces

$$m \cdot a(t) = f(t) - k \cdot l - m \cdot g, \quad (10-28)$$

where  $a(t)$  is the vent cover acceleration,  $f(t)$  is the pressure force described above,  $m$  is the panel mass. The gravity acceleration  $g$  is directional. If the vent is located in the floor of the enclosure, formula (10-28) can be used with negative  $g$ . If the translation panel is mounted on the wall of the enclosure, then the gravity effects are neglected by setting  $g=0$ . If spring load is present, its contribution is expressed via the linear spring (Hooke's) constant  $k$ , N/m, and the current panel displacement  $l$ , m. The venting area is calculated as the gap area between the edges of the panel and the vent opening, as  $F=lp$ , where  $p$  is the vent panel perimeter. This area is zero for a closed vent and is allowed to increase until it reaches the maximum value equal to the nominal vent area  $F_N$ .

### Hinged doors

A hinged door is an inertial cover modelled as a solid rectangle able to swing about one of its edges, the hinge, fixed on the enclosure (see Fig. 10-5). Denote  $b$  the length of the hinged side, i.e. the length of the door;  $L$  the length of the pivoting side, i.e. the width of the door. Then the nominal area of the vent opening and the area of the hinged door is  $F_N = bL$ .

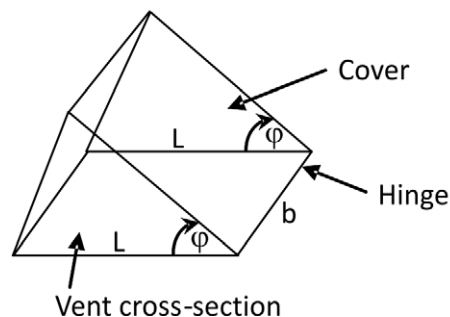


Figure 10-5. Hinged door.

Let  $\varphi$  be the angle between the vent opening and the hinged door. We assume the current venting area  $F(\varphi)$  to be the gap area between the edges of the cover and the vent opening. The gap, see Fig. 10-5, is formed from one rectangular region, based on the door edge opposite to the hinge, and two triangular regions, based on the pivoting edges of the door. The current venting area is then

$$F(\varphi) = 2L \cdot \sin\left(\frac{\varphi}{2}\right) \cdot \left(b + L \cdot \cos\left(\frac{\varphi}{2}\right)\right). \quad (10-29)$$

This area is zero for a closed vent ( $\varphi=0$ ) and is allowed to increase until it reaches the maximum value equal to the nominal vent area  $F_N$ . For angles  $\varphi > \varphi_N$  the venting area stays equal to  $F_N$ . We assume that the door is inelastically arrested at  $\varphi = 90^\circ$ .



To calculate the gas pressure force acting on the hinged door, we take into account the following. When the vent is closed, the pressure force is uniform throughout the door surface, and is determined as  $f = p(t)F_N = p(t)bL$ . When the vent commences to open, the picture changes. Firstly, the pressure of the moving gases on the door is smaller than the pressure inside the enclosure. Secondly, the pressure is not uniform along the door surface any more.

We address the first issue by using the continuity law for the gas flowing between the enclosure insides, the vent cross-section and the current venting area(10–29). We deal with the second issue assuming that the pressure along the door surface changes as a linear function of the position on the width of the door. That results in the following formula for the torque applied by the gas static pressure force to turn the door on its hinge (Molkov et al., 2004b)

$$T_{pressure} = \frac{bL^2}{6}(p(t) - p_a) \cdot \left[ 1 - \frac{F^2(\varphi)}{(bL)^2} \right]. \quad (10-30)$$

Our assumed linear change of pressure results in very easy derivations, picking up at least a part of the actual pressure change on the turning door. However, one realizes that the true pressure distribution may be anything but linear; the whole vent cover pushing phenomenon being three-dimensional, non-stationary and dependent on the geometry of the cover and vent opening. To date, we have not been able to find a suitable theoretical explanation of the gas pressure distribution on the opening door. Therefore, it was decided to settle on the linear distribution augmented by an empirical coefficient  $C_{jet}$  as follows

$$T_{pressure} = \frac{bL^2}{6C_{jet}}(p(t) - p_a) \cdot \left[ 1 - \frac{F^2(\varphi)}{(bL)^2} \right]. \quad (10-31)$$

The  $C_{jet}$  will compensate for the true non-linear, non-stationary and geometry dependent character of the hinged door movement. Notice that when the door is closed,  $\varphi = 0$ , formula (10–30) gives 3 times smaller value than the torque should be

$$T_{pressure, closed} = \frac{bL^2}{2}(p(t) - p_a). \quad (10-32)$$

Therefore, we have to use different formulae for a closed or almost closed door and a sufficiently wide open door. When the door is shut or is opened within some small range of angles, we apply formula (10–32). Above a certain angle, we have to apply formula (10–31). Similarly to translation panels, transition from the “internal pressure” regime of formula (10–32) to the “jet” regime of formula (10–31) is assumed to be linear with respect to  $F(\varphi)$ (10–29), with the empirical parameter  $A_{jet}$  looking after distinguishing between the two regimes. For consistency, we have to assume  $C_{jet} > 1/3$ , such that formula (10–31) would not result in a value greater than formula (10–32) would, for the same pressures and the cover dimensions.

The applicability of formula (10-31) is limited in the angle  $\varphi$  of the door opening. The formula will work only for the angles at which the current venting area  $F(\varphi)$  is less than the nominal area  $F_N$ . At a certain angle  $\varphi_N$  such that  $F(\varphi_N)=F_N$  the area of the flow through the gap between the enclosure and the vent cover is equal to the area of the flow from an unrestricted vent of the same area. At  $\varphi > \varphi_N$ , the vent is considered fully open. The continuing opening of the door does not affect the pressure dynamics inside the vessel. In our calculations, therefore, we assume that at angles of opening larger than  $\varphi_N$ , only gravity affects the door motion.

Having obtained the above formulae for the pressure force torque, one can determine the angular acceleration of the door from the following torque balance equations

$$\frac{\alpha m L^2}{3} = T_{pressure} - \frac{mg L \sin(\varphi)}{2} \quad (10-33)$$

for wall-mounted vents and

$$\frac{\alpha m L^2}{3} = T_{pressure} - \frac{mg L \cos(\varphi)}{2} \quad (10-34)$$

## Join American online LIGS University!

Interactive Online programs  
BBA, MBA, MSc, DBA and PhD

### Special Christmas offer:

- ▶ enroll **by December 18th, 2014**
- ▶ **start studying and paying only in 2015**
- ▶ **save up to \$ 1,200** on the tuition!
- ▶ Interactive Online education
- ▶ visit [ligsuniversity.com](http://ligsuniversity.com) to find out more!

Note: LIGS University is not accredited by any nationally recognized accrediting agency listed by the US Secretary of Education. More info [here](#).

for ceiling-mounted vents. The gravity acceleration  $g$  in these equations acts against the opening of the door. Equation (10-34) thus represents a ceiling-mounted vent, and equation (10-33) represents a wall-mounted vent with the door hinged at its top horizontal edge. Letting  $g = 0$  gives a wall-mounted vent with the door hinged at its vertical (side) edge. Letting  $g < 0$  gives the situation when gravity helps the door opening. Then equation (10-34) represents a floor-mounted vent that opens downwards. Equation (10-33) represents a wall-mounted vent with the door hinged at its bottom horizontal edge, a device that can be found, e.g. in (Zalosh, 1978).

### Comparison with experiments

Our models of vented deflagration with inertial vent covers described in the previous section depend on empirical parameter  $A_{jet}$  and also  $C_{jet}$  for hinged doors. To find the values of these parameters and to check the overall plausibility of the models, we have validated them against large scale experiments on vented methane-air deflagrations (Höchst and Leuckel, 1998). The paper by Höchst and Leuckel (1998) is rare in that it contains both pressure and displacement histories, for both translation panels and hinged doors. In what follows, “experiment 3-A” or “3-A” denotes experimental results plotted in Fig. 3a on page 92 of (Höchst and Leuckel, 1998), similarly “3-B”, “3-C” and “3-D” correspond to Figs. 3b, 3c and 3d on page 92 of (Höchst and Leuckel, 1998). All experiments were performed in a 50-m<sup>3</sup> silo with a venting device(s) on its top. In explosions 3-A and 3-C the cover of a single vent was a circular translation panel of inertia 89 kg/m<sup>2</sup> and 42 kg/m<sup>2</sup> with an arrester. Explosions 3-B and 3-D were vented each with a couple of rectangular hinged doors of inertia 124 kg/m<sup>2</sup> and 73 kg/m<sup>2</sup>. Explosions 3-A and 3-B were performed in initially quiescent mixtures, 3-C and 3-D in fan-assisted turbulent mixtures.

For venting with translation panels, cases 3-A and 3-C, a detailed description of the cover dimensions, initial values, and matching the model to the data is done in (Molkov et al., 2003). Here, Fig. 10-6 compares our best-match computed transients with the experimental results.

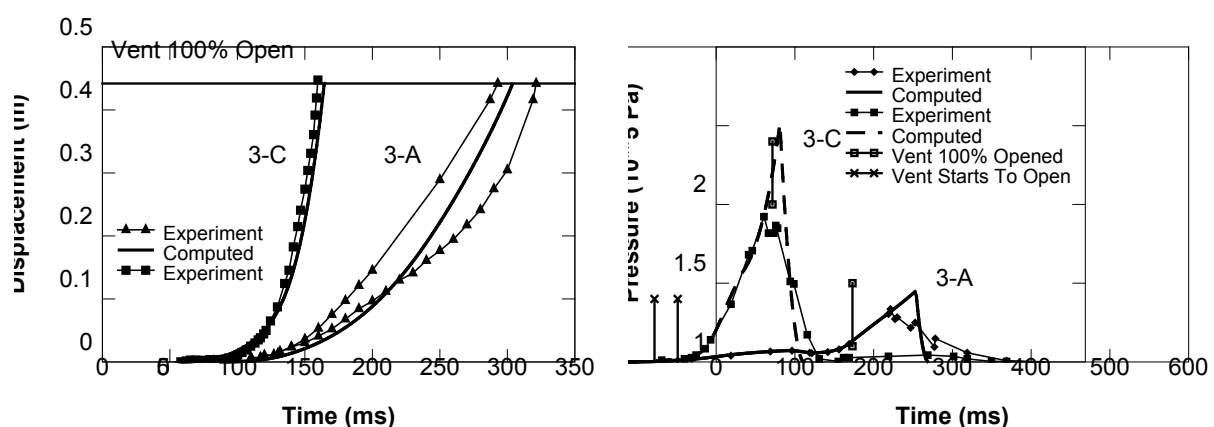


**Figure 10-6.** Comparison with the experiment by Höchst and Leuckel (1998) for translation panels: displacements (left); pressures (right).

Höchst and Leuckel (1998) noticed that their translation panel in experiment 3-A was 3 degrees tilted in motion. The displacement curves for 3-A reflect the movement of the faster and the slower edge of the panel, respectively. In experiment 3-C there was no panel tilt. All the four computed curves in Fig. 10–6 were achieved with the same value of the empirical vent cover parameter:  $A_{jet} = 0.1$ .

Validation of the case with spring-loaded covers is presented for a number of experiments in paper by Molkov et al. (2005). Example of our calculations of experiment 17A (Wilson, 1954) are shown in Fig. 10–7 for both displacement and pressure dynamics. Results indicate that the model matches the experiment with spring-loaded inertial covers well, in a way similar to the translation panels described above. The main details of experiment 17A (Wilson, 1954) in the apparatus with free volume of 1.72 m<sup>3</sup> and a single spring-loaded valve, opening outwards horizontally, of the 0.46 m diameter are: 2% by volume pentane-air mixture, 40.1 kg vent cover (244.5 kg/m<sup>2</sup> surface density).

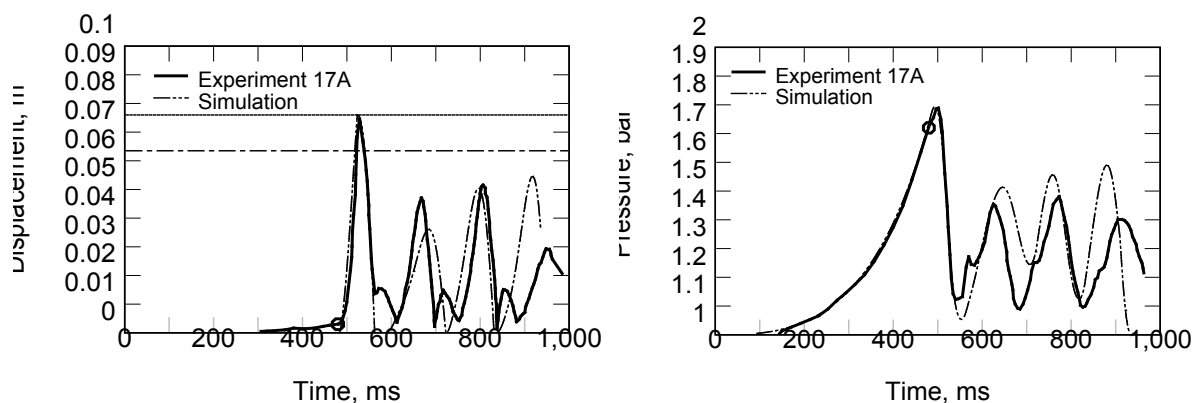



**Figure 10–7.** Comparison with Wilson (1954) experiment 17A (Molkov et al., 2005): o – start of the valve opening.

For venting with hinged doors, cases 3-B and 3-D (Höchst and Leuckel, 1998), the initial data were as follows. Each test was performed with two identical doors that acted simultaneously, exhibiting the same behaviour. From the experimental data by Höchst and Leuckel (1998) we derived that in the case 3-B each door mass was 118.7 kg and the opening pressure was  $1.03 \times 10^5$  Pa, in the case 3-D the respective values were 69.88 kg and  $1.02 \times 10^5$  Pa. The other parameters were the same in both cases:  $\gamma_u = 1.39$ ,  $\gamma_b = 1.25$ ,  $\varepsilon = 0.3$ ,  $S_{ui} = 0.38$  m/s,  $M_{ui} = 27.24$  kg/kmol,  $T_{ui} = 298$  K,  $E_i = 7.4$ ,  $V = 50$  m<sup>3</sup>,  $p_a = p_i = 1.0 \times 10^5$  Pa,  $b = 1.383$  m and  $L = 0.692$  m. Figure 10–8 presents our best-match computed curves in comparison with the experimental transients. Simulations completed when there was no unburnt gases left. In the case 3-B, this happened before the doors have reached 70° of opening.

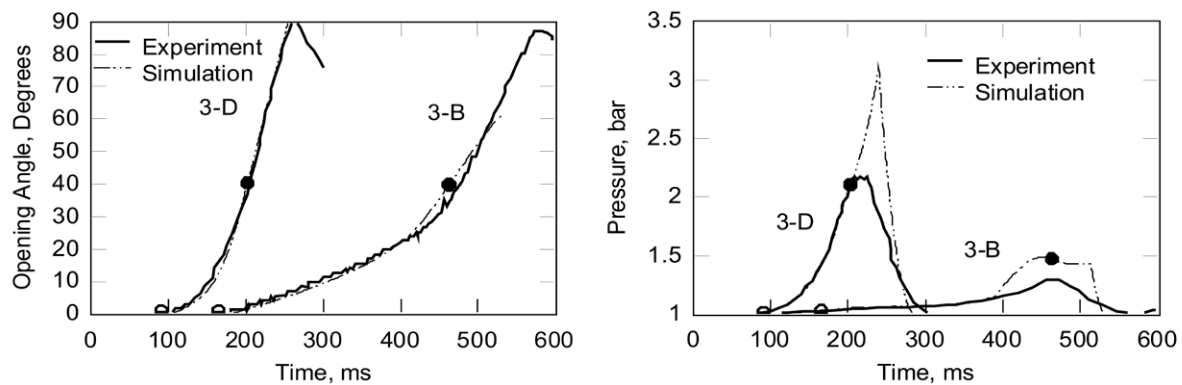



**Figure 10-8.** Comparison with hinged doors experiments 3-B, 3-D ( $\mu = 1.2$ , o – vent starts to open, ° – vent 100% open): left – opening angles; right – pressures.

For hinged vent covers,  $A_{jet}$  and  $C_{jet}$  were determined through matching of CINDY code predictions of experiments 3-B and 3-D.  $A_{jet}$  for the hinged covers was selected for the same reason as for the translating covers: it represents a threshold below which jetting flows are not yet fully established. Then sequences of values of  $\chi$  and  $\mu$  were found giving the best fit of the calculated pressure to the experiments. The calculated versus experimental cover angular displacements were then compared and a new  $A_{jet}$  selected as necessary. When both the calculated and experimental pressures and displacements were well matched,  $A_{jet}$  had a value of 0.05. The best overall curve match was achieved at  $C_{jet} = 1.4$ . The optimization of the found empirical values of  $A_{jet}$ ,  $C_{jet}$  is discussed in detail in (Molkov et al., 2004b). The turbulence factor  $\chi$  varied as a piecewise-linear function as the calculations progressed, the best-fit values of  $\chi$  for the two experiments were as shown in Fig. 10-9.



**MASTER IN MANAGEMENT**

**#1** EUROPEAN  
BUSINESS  
SCHOOL  
FINANCIAL TIMES  
2013








**#gobeyond**

**Because achieving your dreams is your greatest challenge.** IE Business School's Master in Management taught in English, Spanish or bilingually, trains young high performance professionals at the beginning of their career through an innovative and stimulating program that will help them reach their full potential.

- Choose your area of specialization.
- Customize your master through the different options offered.
- Global Immersion Weeks in locations such as Rio de Janeiro, Shanghai or San Francisco.

*Because you change, we change with you.*

www.ie.edu/master-management
mim.admissions@ie.edu



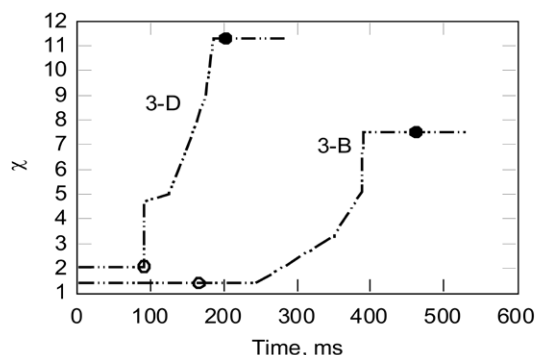


Figure 10-9. Experiments 3-B, 3-D:  $\gamma(\mu = 1.2)$ , o – vent starts to open, • – vent 100% open).

### 10.3.3.3. Inertial vent cover jet effect

Here we will demonstrate that the formation of a jet of escaping gases under a vent cover drastically influences transient explosion pressure and cover movement. Mathematical modelling of the pressure distribution, including the effect of jetting flow of deflagration products, results in a pressure force on vent cover half that predicted by traditional “straight forward” theory (applied in the previous section). It is determined by comparison with experimental data that the change from full pressure to reduced due to jet effect pressure on the inertial vent panel comes when the virtual venting area reaches 5–10% of the full venting area.

Disadvantages of thin bursting discs and similar devices include their sensitivity to fatigue caused by pressure fluctuations, poor heat insulation from the external environment, which often causes problems, e.g. with water condensation, unplanned “increase” of their mass, e.g. due to snow deposition, etc. To avoid these problems with above mentioned venting devices an inertial explosion door or pop-out panel can be applied. There are many types of explosion doors and similar pressure venting elements as considered in previous section: translation, spring-loaded, hinged. During vent cover movement, the size of the opening between the venting element and the vessel is taken as the actual venting area.

Translating pressure relief devices can be dangerous in operation because they could become missiles if unrestrained. Debris missiles and their trajectories have already received attention in the safety engineering community, see for example studies by Efimenko et al. (1998), Kao and Duh (2002), Baker et al. (1983), etc. It is important to accurately model forces acting on vent cover to predict distances at which unrestrained inertial venting elements could have damaging action and thus affect separation distance.

Let us consider a typical deflagration protection system, when a heavy vent cover is located over the vent at the top of enclosure, e.g. the restrained vertically translating cover used by Höchst and Leuckel (1998). The simplest “obvious” approach to model vent cover displacement is as follows. The total pressure force applied to the vent cover consists of the pressure force, due to the difference of the pressure on its internal (transient explosion pressure inside enclosure) and external (atmospheric pressure) surfaces.

In simplified “uncorrected” approach the pressure force is equal to  $f(t) = [p(t) - p_a]A$ , where  $A$  is the nominal vent area,  $\text{m}^2$ ;  $p(t)$  is the transient explosion pressure inside the vessel, Pa;  $p_a$  is atmospheric pressure, Pa; and  $f(t)$  is the total force applied to the vent cover, N. This equation assumes the same magnitude of pressure applied across the entire internal,  $p(t)$ , and external,  $p_a$ , surfaces of the vent cover. That is definitely true at the moment of cover release. However, the use of this equation gives too fast calculated displacement of the inertial vent cover as compared to experimental displacement recorded by Höchst and Leuckel (1998).

Several phenomena affecting inertial vent cover displacement were examined, including drag effects of the moving cover, air cushioning effects of the vent cover on its constraints, and vent cover jet flows affecting the pressure distribution on the internal vent cover surface (Molkov et al., 2003). The results of the drag effect and air cushioning effect analyses suggested that these phenomena were insufficient to account for the experimentally observed displacement of the circular inertial vent cover. Only the vent cover jet flows effect provided the successful modelling of the relationship between pressure forces generated by a deflagration and the motive behaviour of a translating inertial vent cover.

### ***Drag effect***

A drag force can be modelled by formula

$$-C_D \frac{\rho u^2}{2} A, \quad (10-35)$$

where  $C_D$  is the drag coefficient;  $\rho$  is the gas density,  $\text{kg}/\text{m}^3$ ;  $u$  is the gas velocity,  $\text{m}/\text{s}$ ; and  $A$  is the vent cover area. For experiments by Höchst and Leuckel (1998), when vent panels moved vertically upward, the following general form of the second Newton’s law is applied  $f(t) = [p(t) - p_a]A - m \cdot g$ . The drag force was added to the right-hand side of equation (10-35). It was found that a drag coefficient  $C_D$  well over 1000 would be required to properly match the model displacement predictions to the experimental data. However, the literature clearly indicated that a circular plate perpendicular to the flow should have a drag coefficient,  $C_D$ , of 1.1–1.2, see e.g. (Haberman and John, 1988). A review of the available literature further corroborated these values.

### ***Air cushioning effect***

The air cushioning effect between vent cover and damping material (Höchst and Leuckel, 1998) was estimated next. The potential for air cushioning, affecting the motion of a translating cover, occurs when the cover translation is restricted. If the cover is constrained by a frame including an arrester consisting of a solid piece of material, then air between the cover and the frame may act as a cushion, slowing the cover velocity as in experiments by Höchst and Leuckel (1998).



The Euler equation, assuming quasi-steady flow, states

$$\frac{dp}{\rho} + gdh + udu = 0, \quad (10-36)$$

where  $p$  is the local pressure, Pa;  $\rho$  is the gas density, kg/m<sup>3</sup>;  $h$  is the vertical height, m; and  $u$  is the gas velocity, m/s. In approximation of an incompressible fluid that is valid for a gas when its characteristic velocities are much less than the speed of sound, the above equation results by integration in the Bernoulli equation for incompressible flow

$$\frac{p}{\rho} + gh + \frac{u^2}{2} = \text{const} \quad (10-37)$$

Since the vertical distances are small, the altitude-related term, i.e.,  $gh$ , can be neglected.

Figure 10-10 shows a typical translating vent cover and damper/arrester, where  $R_0$  is the radius of the circular cover, m;  $L(t)$  is the distance between the cover and the arrester, m;  $t$  is time, sec; and  $u_{R_0}^e(t)$  is the gas velocity at the outermost diameter of the exterior side of the cover, m/s.

# SMS from your computer

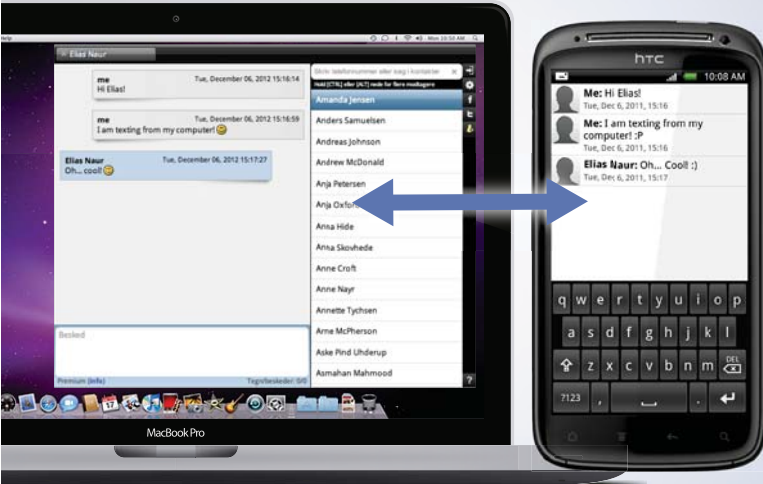
...Sync'd with your Android phone & number


**FREE**  
30 days trial!

Go to

[BrowserTexting.com](http://BrowserTexting.com)

and start texting from  
your computer!




**BrowserTexting**

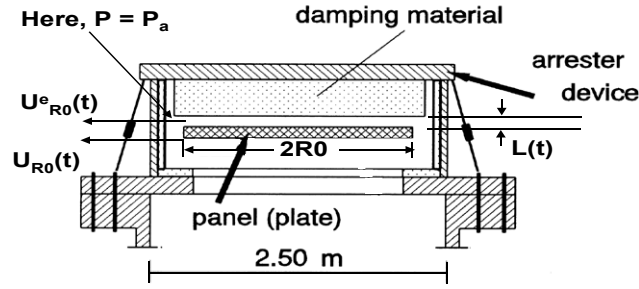


**Figure 10–10.** Arrested translating vent panel of Höchst and Leuckel (1998).

The decrease in volume of the space between the cover and the constraining frame is

$$\Delta V(t) = \pi R_0^2 \cdot \Delta L(t). \quad (10-38)$$

The gas volume flowing out of the space between the cover and the damper through the side of a cylinder, defined by the outermost radius of the cover, can be written as

$$\Delta V(t) = 2\pi R_0 \cdot L(t) \cdot u_{R_0}^e(t) \cdot \Delta t. \quad (10-39)$$

Based on the assumption of gas incompressibility the volumes given by last two equations can be set equal, allowing for the following expression for  $u_{R_0}^e(t)$

$$u_{R_0}^e(t) = \frac{R_0}{2L(t)} \cdot \frac{\Delta L(t)}{\Delta t} = \frac{R_0}{2L(t)} \cdot u_L(t), \quad (10-40)$$

where  $u_L(t)$  is the velocity of the vent cover at moment  $t$ . The relationship in equation (10–40) will remain true for any radius  $r < R_0$  and the respective gas velocity  $u_r^e(t)$

$$u_r^e(t) = \frac{r}{2L(t)} \cdot u_L(t). \quad (10-41)$$

Dividing equation (10–41) by equation (10–40) and re-arranging results in

$$u_r^e(t) = u_{R_0}^e(t) \frac{r}{R_0}, \quad (10-42)$$

which relates radius and gas velocity for  $0 < r \leq R_0$ .

In determining the pressure distribution above the cover in the cushion the pressure at the edge of the vent cover  $R_0$  is atmospheric pressure,  $p_a$ . According to the Bernoulli equation, at some radius  $r$  the pressure on the external surface of the vent cover,  $p_e(r, t)$ , relative to its value  $p_e(0, t)$  at the centre of external surface of the cover, where the velocity is equal to zero, is

$$p_e(r, t) + \frac{\rho(u_r^e(t))^2}{2} = p_e(0, t). \quad (10-43)$$

For the outside edge of the circular cover the total pressure (static equal to atmospheric plus dynamic) is the same as at the vent cover centre

$$p_a + \frac{\rho(u_{R_0}^e(t))^2}{2} = p_e(0, t). \quad (10-44)$$

Hence, the additional force on external surface of vent cover due to the air cushioning effect is

$$\Delta f_{cushion} = \int_0^{R_0} [p_e(r, t) - p_a] \cdot 2\pi r dr. \quad (10-45)$$

Solving equations (10-43) and (10-44) for  $p_e(r, t)$ , substituting for  $u_r^e(t)$

$$\begin{aligned} p_e(r, t) &= p_a + \frac{\rho}{2} \left( (u_{R_0}^e(t))^2 - (u_r^e(t))^2 \right) = p_a + \frac{\rho}{2} \left( (u_{R_0}^e(t))^2 - (u_{R_0}^e(t))^2 \frac{r^2}{R_0^2} \right) \\ &= p_a + \frac{\rho(u_{R_0}^e(t))^2}{2} \left( 1 - \frac{r^2}{R_0^2} \right) \end{aligned} \quad (10-46)$$

Substitution of equation (10-46) into equation (10-45) and integration gives

$$\begin{aligned} \Delta f_{cushion} &= \int_0^{R_0} \left( \frac{\rho \cdot (u_{R_0}^e(t))^2}{2} \left[ 1 - \frac{r^2}{R_0^2} \right] \right) \cdot 2\pi r dr = \pi \rho \cdot (u_{R_0}^e(t))^2 \left[ \frac{r^2}{2} - \frac{r^4}{4R_0^2} \right]_0^{R_0} \\ &= \pi \rho \cdot (u_{R_0}^e(t))^2 \frac{R_0^2}{4} \end{aligned} \quad (10-47)$$

By substituting equation (10-40) and factoring, one obtains

$$\Delta f_{cushion} = \pi \rho \cdot \frac{R_0^2}{4} \cdot \frac{R_0^2}{4L^2(t)} \cdot u_L^2(t) = (\pi R_0^2) \cdot \left( \frac{\rho u_L^2(t)}{2} \right) \cdot \left( \frac{R_0^2}{8L^2(t)} \right), \quad (10-48)$$

where the first factor is the cover area, the second is the dynamic pressure, and the last could be denoted as a coefficient for air cushioning,  $C_c$ , by analogy to the drag coefficient,  $C_d$ , for the drag force. Substituting for  $L(t)$  in terms of  $R_0$ , the results show that  $C_c \leq 1$  at  $L \geq 0.35R_0$  (approximately). Utilising the value given by equation (10-48) for a gap distance  $L$  of  $0.1R_0$ ,  $C_c$  only reaches 12.5. In fact,  $C_c$  would only reach the sort of values disclosed by the original backfit only for gap distances between cover and damper of  $0.01R_0$  or less, and a value of 100 at approximately  $L = 0.035R_0$ .  $C_c$  only reaches values of 1000 or greater when  $L(t) = 0.011R_0$ , within the last 3% of the total available travel distance. Over most of the vent cover travel distance,  $C_c$  is much lower, only reaching 100 when  $L = 0.035R_0$ . As a result, over most of the vent cover travel path, the drag coefficient associated with the cushioning effect is significantly less than 1000.

Thus, drag and air cushioning effects alone cannot account for the observed behaviour of the vent cover displacement.

### Jet effect

The idea of the jet effect is as follows. The vent cover obstructs gases escaping from the vessel. Some time after a vent release is initiated, a jet forms under the circular cover. As a result, the gas velocity vector changes its direction by  $90^\circ$ . The pressure force acting on the moving cover,  $f(t)$ , can be found by integration

$$f(t) = \int_0^{R_0} [p(r, t) - p_a] \cdot 2\pi r dr, \quad (10-49)$$

where  $p(r, t)$  is a pressure acting on the bottom surface of the vent cover at radius  $r$  at moment  $t$ ,  $p_a$  is the atmospheric pressure,  $R_0$  is vent cover radius.

Using the Bernoulli equation, the total pressure at any point of the internal surface (vessel side) of the vent cover can be written as composed of the static pressure,  $p(r, t)$ , pushing the vent cover, and dynamic pressure,  $\rho u_r^2(t)/2$ , where the vector of  $u_r(t)$  is parallel to the vent cover surface as gases escaping the vessel are turned  $90^\circ$  to form the jet beneath the cover. The total pressure at the centre of the vent cover is equal in our model to the transient pressure in the enclosure,  $p(t)$ , as the velocity at the centre of the vent is equal to zero (stagnation point). The total pressure at any point of bottom surface of the vent cover is constant. Hence, one can write for three points, i.e. at the centre of the vent cover, its edge and at any arbitrary radius  $r$  the following equation

$$p(t) = p_a + \frac{\rho u_{R_0}^2(t)}{2} = p(r, t) + \frac{\rho u_r^2(t)}{2}, \quad (10-50)$$

where  $u_{R_0}(t)$  is the gas velocity at the outermost diameter of the cover, on the interior side of the cover (see Fig. 10-10).

Solving for the static pressure at an arbitrary radius,  $p(r, t)$ , and substituting relationship similar to (10-42) for  $u_r(t)$ , one can get

$$p(r, t) = p(t) - \frac{\rho u_r^2(t)}{2} = p(t) - \frac{\rho u_{R_0}^2(t)}{2} \left( \frac{r}{R_0} \right)^2. \quad (10-51)$$

From equations (10-49) and (10-51)

$$f_p(t) = \int_0^{R_0} \left[ p(t) - p_a - \frac{\rho u_{R_0}^2(t)}{2} \left( \frac{r}{R_0} \right)^2 \right] \cdot 2\pi r dr. \quad (10-52)$$

However, from the Bernoulli equation (10-50)

$$\frac{\rho u_{R_0}^2(t)}{2} = [p(t) - p_a]. \quad (10-53)$$

Substituting equation (10-53) into equation (10-52), and integrating yields (Molkov et al., 2003)

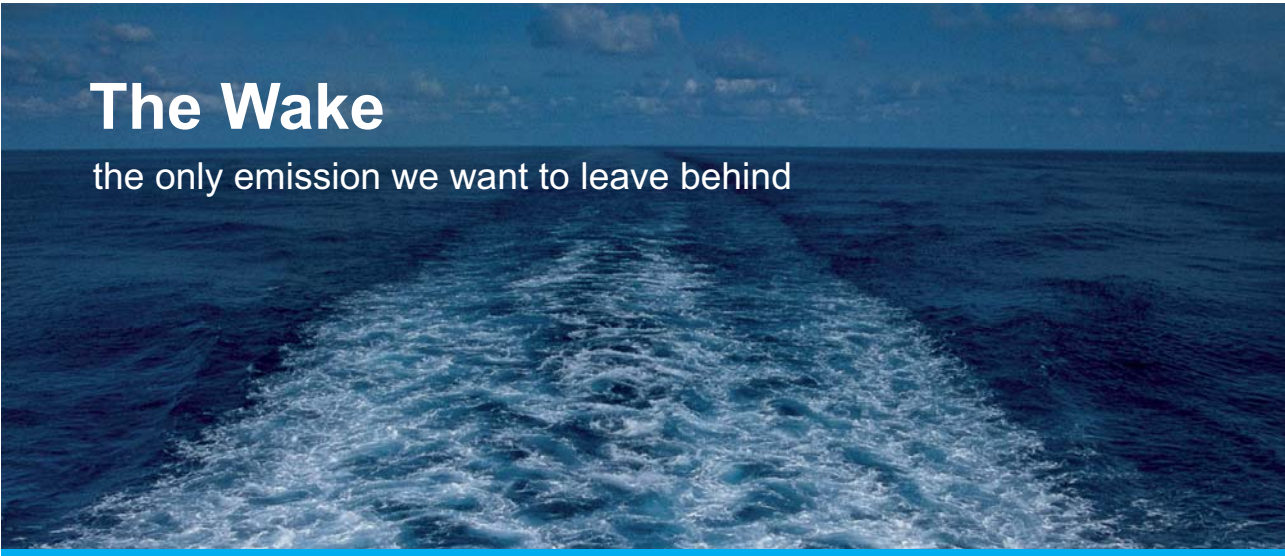
$$f_p(t) = \int_0^{R_0} [p(t) - p_a] \cdot \left[ 1 - \left( \frac{r}{R_0} \right)^2 \right] \cdot 2\pi r dr = [p(t) - p_a] \cdot 2\pi \cdot \left[ \frac{r^2}{2} - \frac{r^4}{4R_0^2} \right]_0^{R_0} =$$

$$= [p(t) - p_a] \cdot 2\pi \cdot \left( \frac{R_0^2}{4} \right) = [p(t) - p_a] \cdot \frac{\pi R_0^2}{2} \quad (10-54)$$

As a result, we see that the pressure force in equation of inertial vent cover motion  $f(t) = [p(t) - p_a]A$ , as follows from the simplified “obvious” consideration, is twice greater than the real pressure force with consideration of the physical nature of jet flow formed under the vent cover. Thus, in assumption of incompressible flow the theoretical pressure force accounting for the jetting effect is found to be

$$f(t) = [p(t) - p_a] \cdot \frac{A}{2} \quad (10-55)$$

As a result one can conclude that the pressure force on cover when jet is formed is only half the pressure force without jet effect, e.g. immediately after vent cover release. This phenomenon has to be accounted for when calculating distance that explosion debris (missiles) could be thrown from an accident scene.



# The Wake


the only emission we want to leave behind

Low-speed Engines Medium-speed Engines Turbochargers Propellers Propulsion Packages PrimeServ

The design of eco-friendly marine power and propulsion solutions is crucial for MAN Diesel & Turbo. Power competencies are offered with the world's largest engine programme – having outputs spanning from 450 to 87,220 kW per engine. Get up front! Find out more at [www.mandieselturbo.com](http://www.mandieselturbo.com)

Engineering the Future – since 1758.

**MAN Diesel & Turbo**



#### 10.3.3.4. Scaling of vent cover inertia

The phenomenon of the double pressure peak in vented gaseous deflagrations with vent opening pressure of relief panel above 7.5 kPa has been well established since the beginning of research at 1950<sup>th</sup>. It seems that Cubbage and Simmonds (1955) were the first who made the statement that inertia of the vent panel, at least over the range of conditions of their tests, had no effect on the second pressure peak. It was demonstrated then by Zalosh (1978), for tests in a 0.19 m<sup>3</sup> vessel with the same vent area but different vent release pressures, that the second peak pressures were almost identical, even though the first peaks differed by a factor of 2.5.

The phenomenon has been explained theoretically in our paper (Molkov, 1999b). The mentioned conclusion by Zalosh (1978) is expected to be correct only in cases when the vent cover is opened fully before the completion of deflagration. Experimental results on vented deflagration in a small-scale duct with ignition at rear wall have shown that the phenomenon of independence of the second pressure peak on the first one does not work always (Ibrahim and Masri, 2001). The case of central ignition in an enclosure with the ratio of the smallest to the largest sizes less than 1:3 is considered here. We will employ the phenomenon of independence of the second pressure peak on the vent cover release pressure in our further calculations.

Cubbage and Marshall (1973) suggested a formula for the maximum explosion pressure at the first pressure peak that appears after the release of the inertial vent cover

$$p_1 = p_v + 0.023 \cdot S_u^2 \cdot K \cdot w / V^{1/3}. \quad (10-56)$$

where  $K$  is the vent area coefficient (ratio of the area of enclosure cross section to the area of relief); and  $w$  is the inertia of vent cover, kg/m<sup>2</sup>. This equation is based on experiments in chambers of volumes up to 30 m<sup>3</sup> using a variety of fuel gases to maximize the range of burning velocity. Unlike the Cubbage and Simmonds (1955) formula for freely lying horizontal relief panels, this latter correlation was devised from the experiments with relief panels that were positively fixed and had to be physically broken by the overpressure in order to create an open vent ( $P_v$  is larger than about 2 kPa).

The fact that the overpressure is proportional to the square  $S_u^2$  of the burning velocity, and not to  $S_u$ , leads to some overestimation of the deflagration pressure for mixtures with  $S_u > 0.5$  m/s. On the basis of experiments with such mixtures, British Gas (1990) recommended that the coefficient in the correlation should be reduced from 0.023 to 0.007. There is even an opinion that this equation (Cubbage and Marshall, 1973) can be applied with confidence to empty rooms of volumes up to 200–300 m<sup>3</sup> (Lautkaski, 1997).

Let us consider enclosures able to withstand internal overpressure not more than 1 bar. It means that the first of the two equations of the vented deflagrations (Molkov, 2001b) can be used to calculate the second pressure peak. Hence, for initial pressure in the enclosure equal to atmospheric we can write

$$P_2 = 1 + 5.65 \cdot P_v^{2.5} \cdot Br_t^{-2.5} (Br_t \geq 2). \quad (10-57)$$

where  $Br_t$  is the turbulent Bradley number (see “Vent sizing technique” section for notations). For the overpressure at the second peak to be less than 1 bar the turbulent Bradley number has to be equal to 2 or greater.

To author's knowledge there is no reasonable relationship that would calculate the upper limit of the cover inertia dependent on the enclosure volume, the vent size, the mixture characteristics and the venting generated turbulence. A cost-efficient design of deflagration mitigation system implies that the vent area is equal to its lower limit and the inertia may be equal to its upper limit. The first pressure peak value, which depends on vent cover inertia, has to be equal to or less than the second peak value, that depends on venting area.

The upper limit for the inertia of a vent cover can be derived from this assumption after simple calculations with two equations above and presented in the form

$$w \leq \frac{V^{1/3} \cdot (F / A_{cs})}{0.023 \cdot S_u^2 \cdot \chi^2} \left[ 1 + P_v \left( \frac{5.65 \cdot (36 \cdot \pi_o)^{5/6}}{Br^{2.5} \cdot (E_i / \gamma_u)^{5/4}} \cdot (\chi / \mu)^{2.5} \cdot P_v^{1.5} - 1 \right) \right], \quad (10-58)$$

where the burning velocity,  $S_u$ , has been multiplied on the turbulence factor,  $\chi$ , as a conservative measure.

Let us calculate the upper limits for the vent cover inertia of enclosures of different volume of 0.1, 10, 100, and 1000 m<sup>3</sup> for the following model conditions. Let us assume for simplicity that enclosures have a cubical form, and a relief panel is mounted in one side only and has an area enough to ensure the reduced pressure 30 kPa. Let us assume further that for all enclosures the vent cover release pressure is equal to  $P_v=1.03$  bar and near-stoichiometric propane-air mixture is used as a fuel ( $S_u=0.31$  m/s;  $E_i=7.9$ ;  $\gamma_u=1.365$ ;  $c_{ui}=335$  m/s).

These values of reduced pressure and vent release pressure have been used to determine the value of the turbulent Bradley number  $Br_t=3.4$  by the first of the two equations of the conservative form of vent sizing correlation (Molkov, 2001b). The turbulent Bradley number is the same for all cases. The DOI numbers,  $\chi/\mu$ , were calculated by the corresponding correlation (see section "Vent sizing technique"). The values for the turbulence factor were calculated from the DOI numbers with a characteristic value of the discharge coefficient  $\mu=0.6$  for all enclosures. The vent areas  $F$ , and hence the respective ratios  $F/A_{cs}$ , were calculated by the application of the conservative form of the vent sizing correlations (Molkov, 2001b) described in detail here in the section "Vent sizing technique". General initial and intermediate data and the results of calculation of the upper limit of the vent cover inertia for different enclosures are given in Table 10–1.

$V, \text{m}^3$	$F, \text{m}^2$	$F/A_{cs}$	$Br$	$\chi/\mu$	$\chi$	$w, \text{kg/m}^2$
0.1	0.04	0.20	31	4.5	2.7	< 0.31
10	1.76	0.38	59	8.6	5.2	< 16
100	11.62	0.54	84	12.3	7.4	< 113
1000	77.70	0.78	122	17.7	10.6	< 782

**Table 10–1.** General initial, intermediate data and upper limits for vent cover inertia for propane-air vented deflagrations in enclosures of different volume and reduced pressure of 30 kPa (conditions applied).



Results of calculations shown in Table 10–1 demonstrate that the upper limit of the vent cover inertia depend strongly on the enclosure volume (for the same reduced deflagration pressure of 30 kPa in this particular case). Nevertheless all vent covers are of 100% “efficiency”, i.e. fully opened before deflagrative combustion within enclosure is finished. The same vent cover material can be “heavy” for small-scale vessels and “light” for large-scale enclosure. For example, the density of glass is about 2470–2560 kg/m<sup>3</sup> and hence the inertia of panes with thickness in the range of 2–5 mm constitutes 5–13 kg/m<sup>2</sup>. Such inertia practically has no influence on the value of the first pressure peak in empty room-size enclosures and enclosures of bigger volume without initial turbulence. However, glass is unacceptable for use as a vent cover material for enclosures with volume of about 0.1 m<sup>3</sup> or less. On the other hand, we have calculated that the upper limit of the inertia for the vent covers in large-scale enclosures of volume about 1000 m<sup>3</sup> is about 800 kg/m<sup>2</sup> even if the estimate is conservative. This value is well above those from 0.5 to 20 kg/m<sup>2</sup> that are under discussions for implementation into international standards.

### 10.3.3.5. Concluding remarks

The theoretical model of vented gaseous deflagration with non-inertial vent covers or initially opened vents by Molkov and Nekrasov (1981) has been extended to include multiple vents that can be either inertial or inertia-free. Modified dimensionless governing equations of explosion dynamics have been derived. Modelling of inertial venting devices motion has been demonstrated for the case of translation panels, spring-loaded covers and hinged doors. Experimental data for hydrocarbon-air vented deflagrations are reproduced well. There is no experimental data on vented hydrogen-air deflagrations with inertial vent covers.

## TURN TO THE EXPERTS FOR SUBSCRIPTION CONSULTANCY

Subscribe is one of the leading companies in Europe when it comes to innovation and business development within subscription businesses.

We innovate new subscription business models or improve existing ones. We do business reviews of existing subscription businesses and we develop acquisition and retention strategies.

Learn more at [linkedin.com/company/subscribe](https://www.linkedin.com/company/subscribe) or contact  
Managing Director Morten Suhr Hansen at [mha@subscribe.dk](mailto:mha@subscribe.dk)

**SUBSCRIBE** - to the future

Vent cover jet effect, originally discovered for translating panels was further confirmed for hinged doors. In all cases the satisfactory model predictions were obtained after taking into account the jet effect of the escaping gases on the vent cover surface. The calculated values of the explosion overpressure transients and the cover displacement transients are in good match with their experimental values published by Höchst and Leuckel (1998) and Wilson (1954). The determined empirical coefficients  $A_{jet}$  and  $C_{jet}$  assume plausible values, thereby confirming that the modelling of vented deflagration dynamics with inertial vent covers is reasonable and the CINDY code could be used as a predictive tool in safety engineering.

#### 10.3.4. Vent sizing technique

Deflagration venting is the most widespread and cost-effective “explosion” mitigation technique. It reduces deflagration-incurred pressure to an acceptable level by venting gases out of an enclosure through a vent or number of vents of sufficient area during the deflagration. Design of explosion vents may be based on the vent sizing correlations or application of the computational fluid dynamics (CFD).

In general, the vent sizing formulas of NFPA 68 standard (2007) and its European version EN 14994 (2007) are not applicable to hydrogen because of its high  $K_G$  index. Indeed, the vent sizing area formulas adopted by NFPA and EN standards are only applicable for a value of  $K_G$  inferior or equal to 550 bar-m/sec. As shown in Fig. C.1 of Annex C of the NFPA 68 (2007), the  $K_G$  index of hydrogen increases with volume. For instance, the  $K_G$  index of hydrogen rises from 550 bar-m/sec for a volume of 0.005 m<sup>3</sup> to 780 bar-m/sec for a volume of 10 m<sup>3</sup>. This simply means that the NFPA 68 (2007) vent sizing approach for hydrogen-air mixtures is not applicable for volumes larger than 5 L.

The dimensionless correlation for vented gaseous deflagrations was suggested for the first time by Molkov (1995) and was updated several times following validation against a wider range of experiments with hydrocarbon-air and hydrogen-air mixtures (Molkov, 1995; Molkov et al., 1997a; Molkov et al., 1997b; Molkov, 1999a; Molkov et al., 1999; Molkov et al., 2000; Molkov, 2001; Molkov, 2002, Molkov et al., 2008a). This list includes the correlation for hydrocarbon-air vented deflagrations at elevated initial pressures (Molkov, 2001a).

The conservative form of the correlation (Molkov, 2001b) created to meet the requirements of the CEN/TC 305 expert group led by Kees van Wingerden who drew up the EN 14994 (2007). Unfortunately, by unknown to author reasons, the novel technique was not included in the final published version of the European standard EN 14994 (2007). Later, the innovative vent sizing methodology for hydrogen-air deflagrations (Molkov et al., 2008a) has been included into the European Installation Permitting Guidance for Hydrogen and Fuel Cells Stationary Applications (HYPER, 2008), and Biennial Report on Hydrogen Safety (BRHS, 2009).

The technique by Molkov et al. (2008a) presented in this book is designed for hydrogen-air vented deflagrations only. In this section the comparison of experimental data on vented hydrogen-air deflagrations with predictions by the innovative vent sizing technique (Molkov et al., 2008a) and NFPA 68 (2007) is presented. The predictions of the NFPA 68 (2007) were calculated using the value  $K_G=550$  bar-m/sec. Experimental configurations included spherical and cylindrical vessels as well as a tunnel. Hydrogen concentrations were in the range 10–30% by volume. The vent sizing methodologies which were previously validated compared against experimental data on vented explosions in enclosures of volumes from 1 m<sup>3</sup> (Pasman et al., 1974) to 6 m<sup>3</sup> (Kumar et al., 1989) were updated to include new experimental data on uniform 40 m<sup>3</sup> volume hydrogen-air deflagrations in a 78.5 m length tunnel (Sato et al., 2006).

#### 10.3.4.1. NFPA 68 (Edition 2007) standard for vent sizing and its limitations

It worth noting that both standards, i.e. NFPA 68 (2007) and EN 14994 (2007), use equations by Bartknecht (1993) that have a limited range of applicability as opposite to the vent sizing technique (Molkov et al., 2008a) that applicable throughout the whole range of possible deflagration conditions.

The equation for high-strength enclosures, i.e. enclosures capable of withstanding reduced pressure (deflagration pressure in vented enclosure minus atmospheric pressure) of more than 0.1 bar, is (Bartknecht, 1993)

$$F = \left\{ \left[ (0.127) \cdot \log_{10} (K_G) - (0.0567) \right] \cdot P_{red}^{-0.582} \right\} \cdot V^{2/3} + \left[ (0.175) \cdot P_{red}^{-0.572} (P_{stat} - 1) \right] \cdot V^{2/3}, \quad (10-59)$$

where  $F$  is the vent area, m<sup>2</sup>;  $K_G$  is the deflagration index, bar-m/sec;  $P_{red}$  is the reduced pressure, bar gauge;  $V$  is the volume of enclosure, m<sup>3</sup>;  $P_{stat}$  is the static vent activation pressure, bar gauge. We use this equation, not equation for low-strength enclosures, as all experimental data available for inter-comparison of different vent sizing techniques have reduced pressure above 0.1 bar.

Bartknecht's equation (10–59) has a very limited application range. It is applicable only for reduced pressures of more than 0.1 bar and less than 2 bar, static vent activation pressures of less than 0.5 bar, initial pressure before ignition of less than 0.2 bar, enclosures with length-to-diameter ratio of less or equal to 2, and a deflagration index  $K_G$  below 550 bar-m/sec. There is no information in NFPA 68 (2007) on how equation (10–59) was validated for volumes of up to 1000 m<sup>3</sup>.

Due to the limitation of  $K_G \leq 550$  bar-m/sec Bartknecht's equation is not, strictly speaking, applicable to hydrogen-air mixtures since all the available values of  $K_G$  for hydrogen are above 550 bar-m/sec (see Figure C.1 in NFPA 68, 2007). The current “consensus” for application of the NFPA 68 (2007) standard to hydrogen is to use Table E1 of NFPA 68 (2007) with a value  $K_G=550$  bar-m/sec for hydrogen in order to calculate the vent area using Bartknecht's equation. It is clear that such an approach ignores the quite strong dependence of  $K_G$  on enclosure volume, and hence does not account for the dependence of vent area on mixture reactivity, i.e. hydrogen concentration. The predictions of vent size or reduced pressures would be significantly overestimated in many situations and would therefore affect the cost of a deflagration mitigation system.

### 10.3.4.2. Innovative vent sizing technique

The conservative form of the universal correlation for vented gaseous deflagrations (Molkov, 2001b) is shown in Fig. 10–11.

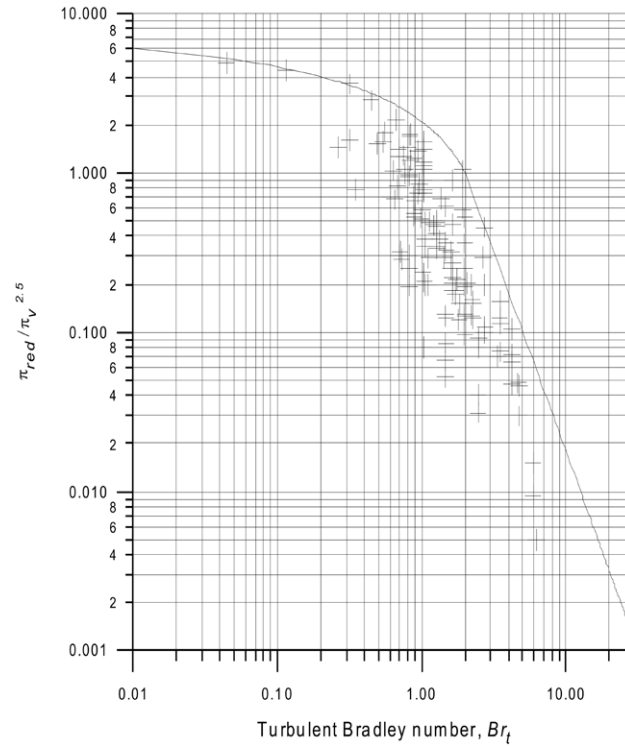


**Figure 10–11.** The conservative form of the correlation for vented gaseous deflagrations (line) and 139 experimental points shown by crosses (Molkov, 2001b).

The correlation (line is Fig. 10–11) is conservative as it is above all experimental points shown. Two equations of the correlation for sub-sonic and sonic vented deflagrations are respectively

$$\frac{\pi_{red}}{\pi_v^{2.5}} = 5.65 \cdot Br_t^{-2.5} \left( \frac{\pi_{red}}{\pi_v^{2.5}} \leq 1; Br_t \geq 2 \right) \quad \text{and} \quad \frac{\pi_{red}}{\pi_v^{2.5}} = 7.9 - 5.8 \cdot Br_t^{0.25} \left( \frac{\pi_{red}}{\pi_v^{2.5}} > 1; Br_t < 2 \right), \quad (10-60)$$

where  $\pi_{red} = P_{red}/P_i$  is the dimensionless reduced pressure;  $P_i$  is the initial pressure in enclosure, Pa;  $\pi_v = (P_{stat} + P_i)/P_i$  is the dimensionless static activation pressure. In formulae (10–60) the turbulent Bradley number is given by the following relationship

$$Br_t = \frac{\sqrt{E_i/\gamma_u}}{\sqrt[3]{36\pi_0}} \cdot \frac{Br}{\chi/\mu}, \quad (10-61)$$

where  $E_i$  is the expansion coefficient of combustion products;  $\gamma_u$  is the specific heats ratio for unburned mixture;  $\pi_0$  is “pi” number;  $\chi/\mu$  is the deflagration-outflow number (see below). The Bradley number is

$$Br = \frac{F}{V^{2/3}} \cdot \frac{c_{ui}}{S_{ui}(E_i - 1)}, \quad (10-62)$$

where  $c_{ui}$  is speed of sound at initial conditions of deflagration, m/s;  $S_{ui}$  is the burning velocity at initial conditions, m/s.

The second constituent part of the innovative vent sizing technique is the correlation for the deflagration-outflow interaction (DOI) number,  $\chi/\mu$ , that can be written for hydrogen-air mixtures at initial atmospheric pressure in the form (Molkov, 2001b)

$$\chi/\mu = \left[ \frac{(1 + e \cdot V_{\#}^g) \cdot (1 + 0.5 \cdot Br^{0.8})}{1 + \pi_v} \right]^{0.4} \quad (10-63)$$

where  $V_{\#}$  is the dimensionless volume,  $V_{\#} = V/(1 \text{ m}^3)$ . The “old” value of empirical coefficients  $e=10$  and  $g=0.33$  were obtained by calibration of the DOI number correlation (10-63) against experimental data on vented hydrogen-air explosions in enclosures of  $1 \text{ m}^3$  (Pasman et al., 1974) and  $6 \text{ m}^3$  (Kumar et al., 1989) volume only (Molkov, 2001b).

Later (Molkov et al., 2008a) the DOI number correlation has been upgraded to apply to further tests by Kumar *et al.* (Kumar et al., 1989) and larger scale tests on deflagrations in a  $37.4 \text{ m}^3$  uniform hydrogen-air mixture  $10 \text{ m}$  long in the center of a  $78.5 \text{ m}$  tunnel (Sato et al., 2006). The inclusion of these new experiments into the validation set has affected the DOI number correlation (10-63) through the modification of two empirical coefficients only, i.e. “new” values  $e=2$  and  $g=0.94$ , to comply with larger scale experiments by Sato et al. (2006).

The procedure for calculating the vent area for an empty enclosure fully filled with a quiescent hydrogen-air or enclosure with insignificant influence of obstacles is as follows:

1. Calculate the dimensionless reduced explosion overpressure  $\pi_{red} = P_{red}/P_i$ ;
2. Determine the dimensionless static activation pressure  $\pi_v = (P_{stat} + P_i)/P_i$ ;
3. Calculate the dimensionless pressure complex  $\pi_{red}/\pi_v^{2.5}$  using data from step1 and 2;
4. Calculate the value of the turbulent Bradley number  $Br_t$  by the use of one of the following two equations depending on the value of the above mentioned dimensionless pressure complex  $\pi_{red}/\pi_v^{2.5}$ :
  - If  $\pi_{red}/\pi_v^{2.5} \leq 1$ , then use equation  $\pi_{red}/\pi_v^{2.5} = 5.65 \cdot Br_t^{-2.5}$ ;
  - If  $\pi_{red}/\pi_v^{2.5} \geq 1$ , then use equation  $\pi_{red}/\pi_v^{2.5} = 7.9 - 5.8 \cdot Br_t^{0.25}$ .

5. Using Fig. 10–12 below, determine the appropriate values of the laminar burning velocity and the expansion ratio for the suitable hydrogen-air mixture (by volumetric fraction of hydrogen in air). For instance, for stoichiometric hydrogen-air mixture at NPT, the following values can be used for the purpose of vent sizing:  $E_i=6.88$ ,  $S_{u0}=1.96$  m/s (Lamoureux et al., 2003; Tse et al., 2000). The influence of the initial temperature on the laminar burning velocity can be extrapolated from the formula  $S_{ui} = S_{u0} \cdot (T_i / 298)^{m_0}$ , where  $m_0$  is the temperature index that can be taken as  $m=1.7$  for near stoichiometric hydrogen-air mixtures (Babkin, 2003); and  $S_{u0}$  is the laminar burning velocity at 298 K and  $T_i$  is the initial temperature in the enclosure.

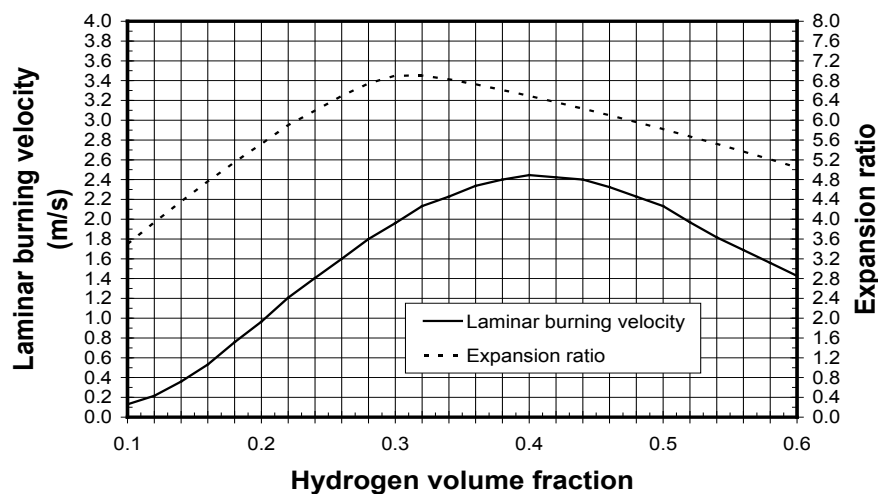


**Figure 10–12.** Laminar burning velocity and expansion ratio of hydrogen-air mixture at NPT as a function of hydrogen volume fraction in air.

6. Determine the vent area by solving numerically the following transcendental equation (by changing area A until the right hand side of the equation is equal to the left hand side)

$$\frac{Br_t \cdot \sqrt[3]{36\pi_0} \cdot V^{2/3}}{c_{ui} \cdot \sqrt{E_i / \gamma_u}} = \frac{F(1 + \pi_v)^{0.4} \cdot \left[ 1 + 0.5 \cdot \left( \frac{F}{V^{2/3}} \cdot \frac{c_{ui}}{S_{ui}(E_i - 1)} \right)^{0.8} \right]^{-0.4}}{(1 + 2 \cdot V^{0.94})^{0.4} \cdot S_{ui} \cdot (E_i - 1)} \quad (10-64)$$

### 10.3.4.3. The innovative vent sizing technique versus Bartknecht's equation

The innovative vent sizing technique (Molkov et al., 2008a) has no inherent limitations compared to the empirical equation by Bartknecht used in NFPA 68 (2007) and EN 14994 (2007). In particular, the reduced pressures can be calculated over a range from close to zero up to the maximum deflagration overpressure in a closed vessel. The technique is applicable to mixtures of different fuel-air compositions.

The prediction capabilities of two vent sizing methodologies are compared against three sets of experimental hydrogen-air deflagrations. The first set of experiments (“K” series in Table 10–2) was carried out by Kumar et al. (1989) in 2.3 m diameter spherical vessel of 6.85 m<sup>3</sup> volume vented through a 3 m long and 45 cm diameter duct. Both the vessel and the duct were filled with a hydrogen-air mixture. An initially closed vent of diameter 15 cm, 25 cm or 45 cm was mounted at the end of the duct to separate the combustible mixture from the atmosphere. The reported vent relief overpressure was less than 10 kPa and this value was accepted for calibration of the correlations. Hydrogen concentration was in the range 6–20% by volume. However, the reproducibility of the experiments was good only at hydrogen concentrations above 10% by volume. The ignition source was located in the centre of the vessel, near or far from the venting duct. Experiments were carried out at an initial pressure near-atmospheric and a temperature of 22 °C.

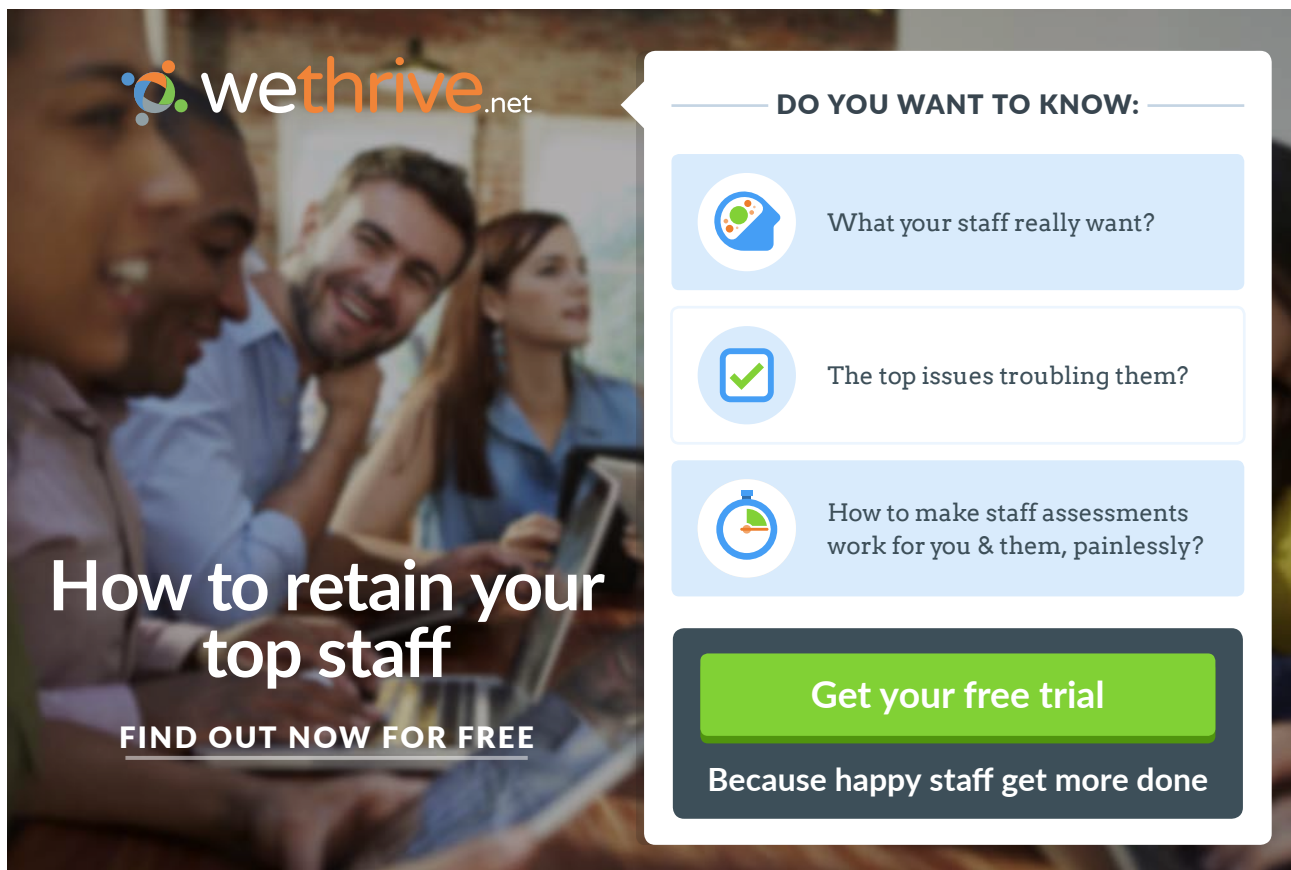
The second set of two experiments (“P” series in Table 10–2) was performed by Pasman et al. (1974) in a 0.95 m<sup>3</sup> cylindrical vessel of 0.97 m diameter and 1.50 m length. A flange was located at the back of the vessel to accommodate a rupture membrane. The hydrogen-air mixture was ignited in the centre of the vessel. Experiments with a stoichiometric (29.6%) hydrogen-air mixture were performed with two different vent areas of 0.3 m<sup>2</sup> (0.62 m diameter) and 0.2 m<sup>2</sup> (0.50 m diameter). The initial pressure in the vessel was equal to 101.8 kPa and the temperature was 281 K.

The third set of experiments (“SRI” series in Table 10–2) was performed in a 78.5 m long tunnel with a height of 1.84 m and horseshoe shape cross section area of 3.74 m<sup>2</sup> (Sato et al., 2006). Uniform 15, 20 and 30% by volume hydrogen-air mixtures of 37.4 m<sup>3</sup> volume (10 m long clouds) were prepared in the middle of the unobstructed tunnel and ignited at the centre of the tunnel at floor level. The quantities of hydrogen in the 30%, 20% and 15% hydrogen-air clouds were equal to 1 kg, 0.667 kg and 0.5 kg respectively.

An additional experiment with obstructions was carried out (Sato et al., 2006) only for the case of a 30% hydrogen-air mixture. Mock “vehicles” of size  $L \times W \times H = 940 \times 362 \times 343$  mm were used as obstacles. The separation distance between the obstacles was equal to a “vehicle” length. The blockage ratio for this type of obstacle is 0.03. Sato et al. (2006) concluded, based on the experimental observations, that there was no difference between the maximum overpressures generated by hydrogen-air explosions in the tunnel without and with obstacles. The uniform mixture deflagrations in the tunnel were considered as vented deflagrations in the following interpretation: the volume of uniform hydrogen-air mixture is taken as the “enclosure volume” and the “vent area” of such a “vented enclosure” is equal to the double cross sectional area of the tunnel.



A comparison between the experiments and the predictions made by the Bartknecht's equation from current standards and the vent sizing technique (Molkov et al., 2008a) is presented in Table 10–2. The innovative vent sizing technique remains conservative across the complete range of experimental data available and predicts vent size and reduced pressure significantly closer to experiments compared to predictions using NFPA 68 (2007) and EN 14994 (2007). Predictions made using Bartknecht's equation occasionally overestimates the experimental data considerably. Indeed, for test K10-15R the vent area is over predicted by a factor of 25 (2435%) and the reduced pressure is significantly over predicted by a factor of 228 (22807%). In other cases, e.g. test P1-C, the methodology applied in standards demonstrates non-conservative character and under predicts by -45% the vent area and by -64% the reduced pressure.



**wethrive.net**

**How to retain your top staff**

**FIND OUT NOW FOR FREE**

**DO YOU WANT TO KNOW:**

- What your staff really want?
- The top issues troubling them?
- How to make staff assessments work for you & them, painlessly?

**Get your free trial**

**Because happy staff get more done**

Test	H <sub>2</sub> , vol. %	V, m <sup>3</sup>	F, m <sup>2</sup>	Vent Area, F (m <sup>2</sup> )				Reduced pressure, P <sub>red</sub>					Use of NFPA <sup>c</sup>	
				VST	% <sup>a</sup>	NFPA	% <sup>a</sup>	Exp <sup>b</sup>	VST <sup>c</sup>	% <sup>a</sup>	NFPA	% <sup>a</sup>		Exp <sup>b</sup>
K10-15-C	10	6.85	0.0177	0.0780	342	0.362	1948	0.0177	3.67	126	260.00	15900	1.625	(+)
K10-15-R	10	6.85	0.0177	0.1070	506	0.448	2435	0.0177	3.67	224	260.00	22807	1.135	(+)
K10-15-N	10	6.85	0.0177	0.0890	405	0.391	2116	0.0177	3.67	158	260.00	18171	1.423	(+)
K10-25-C	10	6.85	0.0191	0.1188	142	0.514	947	0.0491	4.47	396	46.90	5111	0.900	(+)
K10-25-R	10	6.85	0.0191	0.1693	245	0.746	1420	0.0491	4.47	829	46.90	9657	0.481	(+)
K10-25-N	10	6.85	0.0191	0.1555	217	0.682	1291	0.0491	4.47	701	46.90	8305	0.558	(+)
K10-45-C	10	6.85	0.1590	0.2214	39	0.986	521	0.1590	0.54	79	6.49	2063	0.300	(+)
K10-45-R	10	6.85	0.1590	0.3500	120	1.584	897	0.1590	0.54	298	6.49	4707	0.135	(+)
K10-45-N	10	6.85	0.1590	0.4843	205	2.212	1292	0.1590	0.54	598	6.49	8340	0.077	(+)
K15-15-C	15	6.85	0.0177	0.0753	326	0.223	1163	0.0177	5.34	46	260.00	6985	3.670	(-)
K15-25-C	15	6.85	0.0191	0.1002	104	0.238	384	0.0491	4.20	27	46.90	1321	3.300	(-)
K15-45-C	15	6.85	0.1590	0.2378	50	0.311	95	0.1590	2.68	27	6.49	209	2.100	(-)
K15-45-R	15	6.85	0.1590	0.4534	185	0.454	185	0.1590	2.68	141	6.49	485	1.110	(+)
K15-45-N	15	6.85	0.1590	0.4139	160	0.422	165	0.1590	2.68	113	6.49	417	1.255	(+)
K20-15-C	20	6.85	0.0177	0.0536	203	0.185	947	0.0177	6.14	22	260.00	5069	5.030	(-)
K20-25-C	20	6.85	0.0191	0.0819	67	0.196	300	0.0491	5.13	13	46.90	931	4.550	(-)
K20-45-C	20	6.85	0.1590	0.1643	3	0.222	40	0.1590	3.74	1	6.49	75	3.700	(-)
P1-C	29.6	0.95	0.20	0.2132	7	0.110	-45	0.2000	1.35	8	0.45	-64	1.250	(+)
P2-C	29.6	0.95	0.30	0.4176	39	0.233	-22	0.3000	0.74	85	0.26	-35	0.400	(+)
SRI-30F	30	37.4	7.48	11.95	60	1.112	-85	7.48	1.72	33	0.05	-96	1.300	(-)
SRI-20F	20	37.4	7.48	11.82	58	2.434	-67	7.48	0.78	122	0.05	-85	0.280	(-)
SRI-15F	15	37.4	7.48	7.48	0	3.127	-58	7.48	0.23	0	0.05	-77	0.220	(-)

Notes. In column “Test”: C – central ignition, R – rear to vent ignition, N – near vent ignition, F – floor ignition. VST stands for vent sizing technique. <sup>a</sup> - deviation of prediction from corresponding experimental value, calculated by formula:  $100 \times (A_{pred} - A_{exp}) / A_{exp}$ , where  $A$  is reduced pressure or vent area. <sup>b</sup> – experimental data. <sup>c</sup> – applicability of NFPA 68 (2007) to predict particular experiment: (+) in the last column means that the Bartknecht’s equation is applicable, (-) refers to experimental conditions outside the specified range of applicability of the Bartknecht’s equation.

**Table 10–2.** Comparison between experiments and predictions by the vent sizing correlations and Bartknecht’s equation (NFPA 68, 2007).

The vent sizing technique (Molkov et al., 2008a) demonstrates its advanced capability to predict explosion pressure during vented deflagration of uniform initially quiescent hydrogen-air mixture not only in vessels yet in vessels with venting ducts and in large scale tunnels, including in the presence of obstructions with a small blockage ratio. In all cases it predicts experimental data better than the current standards (see Table 10–2).

### 10.3.5. The inverse problem method

In the early studies of vented gaseous deflagrations (Yao, 1974; Pasman et al., 1974) only one parameter, i.e. the turbulence factor  $\chi$ , was used to “tune” theoretical pressure transients in attempt to match experimental pressure-time curves. As a consequence of this “restriction”, the reproduction of experimental data was poor and unexplainable in many cases. This in turn was making impossible the generalisation of experimental data on turbulence generated during vented deflagrations.

Since the first paper of author on vented gaseous deflagrations (Molkov and Nekrasov, 1981) it has been proved that more reasonable agreement between theoretical and experimental pressure transients could be achieved if the second unknown in advance theoretical parameter, i.e. the generalized discharge coefficient  $\mu$ , is “tuned” along with the turbulence factor  $\chi$  during experimental pressure–time curve processing.

The inverse problem method has been applied widely in our research to find two parameters, i.e.  $\chi$  and  $\mu$ , which are characteristic for particular experimental conditions. The inverse problem method is the only available technique for investigation of macro- and micro-scale phenomena that are not accessible for direct assessment. The method was routinely applied by changing parameters  $\chi$  and  $\mu$  until the best reproduction of recorded pressure is achieved. The approximation that both adjustable parameters,  $\chi$  and  $\mu$ , are constants during the course of a particular deflagration usually works well.

The generalized discharge coefficient  $\mu$  is not only the discharge coefficient in a common sense as a part of the standard orifice equations. It has been shown during processing of experimental data on vented deflagrations by that the generalised discharge coefficient  $\mu$  can be more than 1 or less than widely accepted value 0.6 for orifices. The explanation of this “weird” observation is in fact very simple. The standard orifice equations, where the discharge coefficient is applied, are derived in the assumption of zero velocity within the vessel. This is valid for small holes in large vessels, and is not valid when vent area is comparable with cross-section area of vented enclosure. To compensate the use of the orifice equations in conditions when they cannot be strictly applied, the inverse problem method yields higher than usually accepted values of  $\mu$  even higher than 1. Contrary, values less than  $\mu = 0.6$  can be generated by the inverse problem method when for example vent ducts are used in the deflagration mitigation system.

It has been demonstrated that deflagration overpressure correlates not just with turbulence factor,  $\chi$ , yet with the deflagration–outflow interaction (DOI) number,  $\chi/\mu$ . The DOI number can reach a value of about  $\chi/\mu = 20\text{--}30$  for vented hydrocarbon-air deflagration of an initially quiescent mixture in an unobstructed enclosure of volume 4000 m<sup>3</sup> (Molkov et al., 2000).

#### 10.3.6. Le Chatelier-Brown principle analogue for vented deflagrations

The fundamental Le Chatelier-Brown principle analogue for vented deflagrations that was for the first time formulated by Molkov et al. (1993) is discussed in detail in this section. The Le Chatelier-Brown principle analogue for vented deflagration states that the gas dynamics of combustion in a vented vessel responds to external changes in process conditions in such a way as to weaken the effect of the external influence. In spite of differences between the thermodynamic and kinetic parameters of hydrocarbon-air and hydrogen-air systems, they both obey the same general regularities for vented deflagrations, including the Le Chatelier-Brown principle analogue and the form of the deflagration–outflow interaction (DOI) number correlation (Molkov et al., 2000).

The application of the zero isocline method to the system of governing equations describing vented deflagration phenomena, it is easy to obtain a simple formula for the dependence of the dimensionless reduced pressure on burning velocity, turbulence factor, generalized discharge coefficient and vent area in a form

$$\pi_{red} \propto \left[ S_{wi} \cdot \frac{\chi}{\mu} \cdot \frac{1}{F} \right]^2. \quad (10-65)$$

This theoretically derived equation practically reproduces the empirical correlation for vented deflagration with the only difference being the value of exponent “2” not “2.5”. Let us demonstrate that this general principle is applicable for both hydrocarbon-air and hydrogen-air systems and should be taken into account by safety engineers for the design of reliable explosion protection systems and during investigations of accidents with gaseous deflagrations in equipment and buildings.

It seems obvious from equation (10-65) that an increase of the vent area,  $F$ , by two times would decrease the deflagration reduced pressure,  $\pi_{red}$ , by four times. However, the application of equation (10-65) to estimate the deflagration overpressure,  $\pi_{red}$ , is not straight forward as suggested. According to the Le Chatelier-Brown principle analogue, the increase of vent area,  $F$ , is always (!) accompanied by an increase of the deflagration-outflow interaction number,  $\chi/\mu$ , to weaken the effect of the “external influence” (increase of vent area).

For example, for propane-air mixtures in experiments by Pasman et al. (1974), the twofold increase of vent area is accompanied by an increase of 1.57 times in  $\chi/\mu$  (Molkov et al., 2000). For hydrogen-air mixtures in experiments at similar conditions, a 1.5 times increase of the vent area is accompanied by a 1.25 times increase of  $\chi/\mu$ ; in the experiments by Kumar et al. (1989), a ninefold growth of vent area was accompanied by an increase in  $\chi/\mu$  of 2.79 times for a 10% hydrogen-air mixture and 2.93 times for a 20% mixture.

Moreover, in the experiments of Harrison and Eyre (1987) in a 30.4 m<sup>3</sup> enclosure, a 2.06 times increase of vent area was practically compensated by a 1.87 times increase of  $\chi/\mu$ . One likely reason for this is the stronger effect of external deflagration on the internal deflagration turbulence,  $\chi$ , and the generalised discharge coefficient,  $\mu$ , with the increase of vent area in experiments by Harrison and Eyre (1987). As a result of the Le Chatelier-Brown principle analogue, the effective increase of the vent area in this experiment, which is equal to  $F/(\chi/\mu)$ , is often much less than would be expected. In this particular case, the effective increase of vent area is just  $2.06/1.87=1.1$  (10% only), and not as much as 2.06! We believe that this example explains why an increase of vent area is not always effective in engineering practice to mitigate deflagrations to a level of pressure an enclosure can withstand.

Some vented deflagration parameters like position of the ignition source and vent release pressure do not usually have significantly effect, excluding situations when external deflagration has strong influence (coherent deflagrations) or vent cover inertia is important.

Other examples of manifestation of the Le Chatelier-Brown principle analogue are as follows. The large decrease of the generalised discharge coefficient  $\mu$  by 2.25 times with the vent diameter increase from 15 to 45 cm, due to the influence of losses in the vent duct in experiments by Kumar et al. (1989), was accompanied by a 1.12 times decrease in the turbulence factor  $\chi$ . From the other side, a 1.5 times increase of  $\chi$  in experiments by Yao (1974) was compensated partially by a 1.25 times increase of in the generalized discharge coefficient  $\mu$ .

Another example of the universality of the Le Chatelier-Brown principle analogue is related to the burning velocity. A sixfold increase of initial burning velocity  $S_{un}$ , when hydrogen concentration in air changes from 10% to 20% by volume, is accompanied by a slight, but nevertheless a 1.15 times decrease of the turbulence factor  $\chi$ . The important feature of the Le Chatelier-Brown principle analogue for vented deflagrations follows from the examples given above and has to be especially emphasized: the compensation action is always weaker than the primary action.

Very simple general physical ideas underlie the principle being discussed. Indeed, it is easy to imagine that an increase of vent area with all other conditions the same would increase the disturbance of the flame front and hence increase the value of the turbulence factor. It is expected that a growth of the turbulence factor induces an increase of  $\mu$  due to a higher velocity of flow in a vent (it is well known that the discharge coefficient grows with flow velocity). Similarly, a decrease of  $\mu$  could be a reason for a decrease of  $\chi$  due to a relative decrease of the outflow velocity.

It has been demonstrated (Molkov et al., 1997b) that the principle is also valid for obstructed enclosures. This underlines the universality of the Le Chatelier-Brown principle analogue for vented deflagrations.

#### 10.4. Large eddy simulation (LES) of large-scale deflagrations

Considered above lumped parameter models are one-dimensional and have limitations in prediction of gaseous deflagration dynamics compare to three-dimensional computational fluid dynamics (CFD) models. The limitations include deflagrations in enclosures with complex geometry, large length to diameter ratio, internal obstacles, etc. It is very difficult to apply one-dimensional models to simulate deflagration dynamics in a system of enclosures or series of vessels, or coherent deflagrations (Molkov et al., 2006b) when the role of external deflagration cannot be ignored. One-dimensional models also have a limited ability to describe heat losses to enclosure walls, as they don't identify the real flame front position relative to walls and obstacles, especially in complex geometries. Finally, lumped parameter models cannot be used to simulate transitional combustion processes like deflagration-to-detonation transition (DDT).

CFD is the recognised powerful tool to model and simulate fundamental and applied problems of hydrogen safety. This is supported by the ever-increasing performance of hardware and software. However, implementation of CFD into practice requires thorough validation of numerical simulations against experimental data (AIAA, 1998).

LES is promising for deflagration simulation as it avoids time averaging and allows better prediction of highly non-isotropic turbulent flows and large-scale flame-flow interaction at the resolved level (Vervisch and Veynante, 2000; Hawkes and Cant, 2001). Large length-scales and small flame stretch rates are characteristic of accidental gaseous deflagrations, unlike those in many turbulent flames in other engineering applications (Bradley, 1999), e.g. industrial combustors and furnaces, internal combustion engines, *etc.*

The LES model does not assume a priori an isotropic turbulence throughout the whole calculation domain and doesn't require solving additional differential equations for turbulence parameters. The LES model is able to partially resolve the flame front wrinkling at scale of several cells and the rest has to be modelled on the sub-grid scale (SGS) level.

Hydrogen safety engineering requires contemporary tools such as CFD that are able to simulate problems at a real scale of tens of meters and are thoroughly validated against large-scale experiments. The LES technique is generally recognised as fundamentally stronger as compared to Reynolds Averaged Navier-Stokes (RANS), whose vitality is caused mainly by an affordable computational cost for practical flow applications compared to conventional LES. Hundreds of RANS models have been developed, ranging from simple algebraic models to the advanced differential Reynolds Stress Transport Models. Nonetheless, the hopes that a universal, i.e. applicable to arbitrary turbulent flow, RANS turbulence model of whatever complexity will be created sometime are now lower than ever before (Strelets, 2003). This pessimism is caused by realising the crucial importance of the "coherent" structures observed in most turbulent flows of practical interest. In LES of non-reacting flows the transport processes of interest are affected by the resolved, large-scale motions, and there is a cascade of energy, dominantly from the resolved large scales, to the statistically isotropic and universal small scales. LES may provide a more reliable turbulence model than RANS especially if there are large-scale unsteady motions. The quantities of interest and the rate-controlling processes are determined for non-reacting flows by the resolved large scales. In turbulent combustion at high Reynolds and Damkohler numbers, the picture is quite different (Pope, 2004). The essential rate-controlling processes of molecular mixing and chemical reaction occur at the smallest scales which are much thinner than the resolved scales (Peters, 2000). Hence, these processes have to be modelled.

#### 10.4.1. Physical requirements

Depending on fuel and mixture properties, the outward propagating spherical flame front remains laminar up to a radius of the order of some centimetres. Then cellular structure appears on the flame surface. Afterwards flame becomes wrinkled. A wide spectrum of instability wavelengths, from several millimetres to the flame front radius, gives rise to a fractal-like flame wrinkling (Bradley, 1999). The development of the cellular structure leads to an increase of the flame front area, which, in turn, leads to growth of the combustion rate and, eventually, through wrinkled flame to the self-turbulising regime of the flame front propagation. In near stoichiometric initially quiescent hydrogen-air mixture the transition from laminar to self-similar fully developed turbulent regime of flame propagation happens at distance 1.0–1.2 m from the ignition source (Gostintsev et al., 1988). Thus, character and structure of the flame front, propagating in an initially quiescent mixture, changes with flame radius (Bradley, 1999).



Selective diffusion, effects of hydrodynamic and other premixed combustion instabilities on flame propagation velocity usually take place at scales comparable with a laminar flame front thickness of the order of fractions of millimetre. These phenomena cannot be resolved in CFD simulations of large-scale problems of several meters to hundreds of meters due to limitations on mesh size in large calculation domains. The effect of these combustion instabilities has to be modelled rather than resolved. This is done in our case by accounting for these different physical phenomena through the turbulent burning velocity model.

Large eddy simulation (LES) is an approach to numerical simulations of reacting flows which provides the instantaneous resolved field and explicitly computes the large structures of the flow, allowing a better description of the turbulence-combustion interaction (Hawkes and Cant, 1999; Poinso and Veynante, 2001; Chakravarthy and Menon, 2001).

Originally LES was developed for non-reacting flows. It is worth noting that various models for the combustion reaction rate based on Reynolds averaged Navier-Stokes (RANS) approach or sub-grid scale closures for LES feature strong similarities (Vervisch and Veynante, 2000).

A classical spectrum of isotropic flow turbulence decaying with eddy size in non-reacting flow is not strictly speaking applicable to large-scale combustion problems. A number of physical phenomena affecting the turbulent burning velocity, e.g. the turbulence generated by flame front itself and selective diffusion, act at scales much smaller compared to typical for hydrogen safety problems cell size of tens of centimetres. Moreover, this small-scale phenomena drastically affect the growth of the total flame front area and, given a limited computational power of modern computers, cannot be currently resolved at real accident scale of tens and hundreds of meters. The only way is the SGS modelling of the phenomena.

#### 10.4.2. Numerical requirements

There is a numerical requirement to a minimum number of computational cells through the any numerical “front”, e.g. flame or shock wave. The flame front thickness of at least 4 control volumes of rectangular grid was recommended by Catlin et al. (1995). For tetrahedral unstructured grids 4–5 points through the numerical flame front thickness can be “collected” at a distance equal to 2–3 edges of tetrahedral control volume. It means that LES can resolve elements of a flame front structure with a size larger than at least 4–6 edges of the tetrahedron. Smaller sub-grid structures can only be modelled.

The performance of LES on tetrahedral unstructured grids was studied by Jansen (1997), where the simplest filter, i.e. top-hat filter, was found to be the most successful. Kaufmann et al. (2002) recommended unstructured grids for LES applications in complex geometries. The LES model used in Ulster is of numerical type, as defined by Pope (2004) for a case of equivalency between LES filter and cell size. The model does not include an “artificial, i.e. non-physical parameter  $\Delta$ ” (Pope, 2004) applied in some LES models in a source term of the progress variable equation.



Unfortunately, it is not feasible to resolve 80% of scales of turbulent eddies for large-scale problems of tens of meters as usually accepted for “standard” LES, especially for reacting flows. Indeed, a difference of physical scales is at least five orders of magnitude whereas only two-three orders of largest scale resolution is currently feasible in simulations (based on number of equally sized control volumes in a calculation domain  $10^6$ - $10^9$ ).

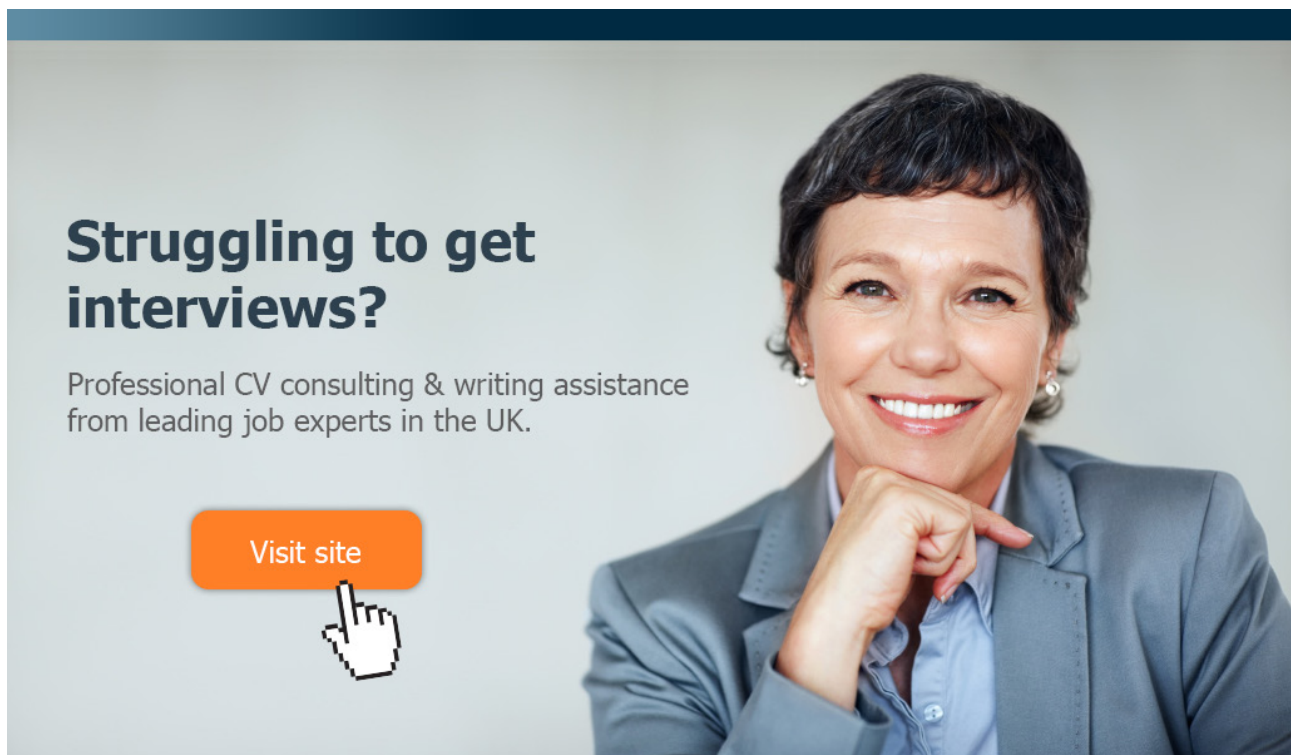
#### 10.4.3. Governing fluid flow equations

The governing equations, employed here for LES, were obtained by filtering the following three-dimensional instantaneous conservation equations for mass, momentum and energy for compressible Newtonian fluid and are described in (Makarov and Molkov, 2004)

$$\frac{\partial \rho}{\partial t} + \frac{\partial}{\partial x_j}(\rho u_j) = 0, \quad (10-66)$$

$$\frac{\partial \rho u_i}{\partial t} + \frac{\partial}{\partial x_j}(\rho u_j u_i) = -\frac{\partial p}{\partial x_i} + \frac{\partial}{\partial x_j} \tau_{ij} + \rho g_i, \quad (10-67)$$

$$\frac{\partial}{\partial t}(\rho E) + \frac{\partial}{\partial x_j}(u_j(\rho E + p)) = \frac{\partial}{\partial x_j} \left( -J_E - \sum_m h_m J_{jm} + u_i \tau_{ij} \right) + S_E. \quad (10-68)$$



**Struggling to get interviews?**

Professional CV consulting & writing assistance from leading job experts in the UK.

[Visit site](#)



Take a short-cut to your next job!  
Improve your interview success rate by 70%.



**TheCVagency**

Visit [thecvagency.co.uk](http://thecvagency.co.uk) for more info.

where  $\rho$  is the density,  $\rho = (pM)/(R_\mu T)$ , where  $M$  is the molecular mass,  $M = \sum_m V_m M_m$ ,  $V_m$  is the volume fraction of  $m$ -th specie,  $p$  – pressure,  $R_\mu$  is the universal gas constant,  $T$  is temperature;  $t$  is time;  $u_{i,j,k}$  are the velocity components;  $x_{i,j,k}$  are the spatial coordinates;  $\tau_{ij}$  is the stress tensor;  $g$  is the vector of gravity acceleration;  $E$  is the total energy,  $E = h - p/\rho + u^2/2$ , where  $h$  is the enthalpy,  $u$  is the velocity;  $J_{jE}$  is the molecular heat flux in  $j$ -th direction,  $J_{jE} = -\left(\frac{\mu c_p}{Pr}\right) \frac{\partial T}{\partial x_j}$ , where  $\mu$  is the dynamic viscosity,  $c_p$  is the specific heat capacity of mixture,  $c_p = \sum_m c_{p_m} Y_m$ ,  $Pr$  is Prandtl number,  $Pr = \mu c_p / k$ ,  $k$  is the molecular heat transfer coefficient;  $J_{jm}$  is the molecular diffusion flux of  $m$ -th specie in  $j$ -th direction,  $J_{jm} = -\left(\frac{\mu}{Sc}\right) \frac{\partial Y_m}{\partial x_j}$ , where  $Y_m$  is the mass fraction of  $m$ -th specie,  $Sc$  is Schmidt number,  $Sc = \mu / \rho D$ , where  $D$  is the diffusion coefficient;  $S_E$  – source term in energy conservation equation;  $i, j, k$  are the spatial coordinate indexes,  $m$  is the specie index

LES filtered (over bar) and mass-weighted (Favre) filtered (tilde) quantities are introduced correspondingly as (Poinso and Veynante, 2001)

$$\bar{\phi}(x, t) = \int_V \phi(x', t) G(x, x') d^3 x', \quad (10-69)$$

$$\bar{\rho}(x, t) \tilde{\phi}(x, t) = \int_V \rho(x', t) \phi(x', t) G(x, x') d^3 x'. \quad (10-70)$$

The filtering operations (10–69), (10–70) decompose a full flow field  $\phi(x, t)$  into a resolved (filtered) components  $\bar{\phi}$ ,  $\tilde{\phi}$ , and a subgrid scale (SGS), unresolved components  $\phi'$ ,  $\phi''$ :  $\phi = \bar{\phi} + \phi'$  and  $\phi = \tilde{\phi} + \phi''$ . Here the LES filter in a physical space is defined as  $G(x, x') = 1/V_{\Delta}^c$  if  $x' \in V_{\Delta}^c$  and  $G(x, x') = 0$  elsewhere and it is implicitly introduced by finite-volume discretization. The filtering of (10–66)–(10–68) leads to the following set of equations

$$\frac{\partial \bar{\rho}}{\partial t} + \frac{\partial}{\partial x_j} (\bar{\rho} \tilde{u}_j) = 0, \quad (10-71)$$

$$\frac{\partial \bar{\rho} \tilde{u}_i}{\partial t} + \frac{\partial}{\partial x_j} (\bar{\rho} \tilde{u}_j \tilde{u}_i) = -\frac{\partial \bar{p}}{\partial x_i} + \frac{\partial}{\partial x_j} (\bar{\tau}_{ij}) - \frac{\partial}{\partial x_j} (\overline{\rho u_j u_i} - \bar{\rho} \tilde{u}_j \tilde{u}_i) + \bar{\rho} g_i, \quad (10-72)$$

$$\begin{aligned} \frac{\partial}{\partial t} (\bar{\rho} \tilde{E}) + \frac{\partial}{\partial x_j} (\tilde{u}_j (\bar{\rho} \tilde{E} + \bar{p})) = \\ = \frac{\partial}{\partial x_j} \left( -\bar{J}_{jE} - \sum_m \overline{h_m J_{jm}} + \overline{u_j \tau_j} \right) - \frac{\partial}{\partial x_j} \left( (\overline{\rho u_j E} - \bar{\rho} \tilde{u}_j \tilde{E}) + (\overline{u_j p} - \tilde{u}_j \bar{p}) \right) + \bar{S}_E \end{aligned} \quad (10-73)$$

Unresolved turbulent SGS momentum fluxes  $\tau_{ij,SGS} = -(\overline{\rho u_j u_i} - \bar{\rho} \tilde{u}_j \tilde{u}_i)$  are expressed similar to standard models for non-reactive flows (Poinso and Veynante, 2001; Chakravarthy and Menon, 2001)

$$\tau_{ij,SGS} = 2\mu_t \tilde{S}_j = \mu_t \left( \frac{\partial \tilde{u}_i}{\partial x_j} + \frac{\partial \tilde{u}_j}{\partial x_i} \right),$$

where  $S_j$  is the rate of strain tensor; index  $t$  stands for turbulent values and SGS – for subgrid scale values. The laminar dilatation term  $-\frac{2}{3}\mu\frac{\partial u_k}{\partial x_k}\delta_j$  ( $\delta_j$  – Kronecker symbol), which is close to zero beyond the flame front and assumed to be small compared to the SGS stress tensor in the flame front area for turbulent flow, was neglected in (Makarov and Molkov, 2004).

Additionally, the numerical flame front thickness, where gas expansion takes place, is wider compared to a real laminar flame front thickness and simulated parameters cannot be realistic inside the numerical flame (laminar or turbulent) front anyway. The effective stress tensor, obtained combining laminar and SGS tensors, is

$$\bar{\tau}_{j,eff} = \bar{\tau}_j + \tau_{j,SGS} = 2(\mu + \mu_t)\tilde{S}_j = 2\mu_{eff}\tilde{S}_j = \mu_{eff}\left(\frac{\partial \tilde{u}_i}{\partial x_j} + \frac{\partial \tilde{u}_j}{\partial x_i}\right).$$

Unresolved SGS and molecular energy fluxes are described using the same approach

$$\bar{J}_{jE,eff} = \bar{J}_{jE} + J_{jE,SGS} = -\frac{\mu_{eff}c_p}{Pr_{eff}}\frac{\partial \tilde{T}}{\partial x_j}.$$

Terms  $\overline{u_i\tau_j}$  and  $-\sum_m \overline{h_m J_{jm}}$  are associated with viscous heating and energy source due to species diffusion and they were modelled assuming

$$\begin{aligned}\overline{u_i\tau_j} &= \tilde{u}_i\bar{\tau}_{j,eff} = \tilde{u}_i\mu_{eff}\left(\frac{\partial \tilde{u}_i}{\partial x_j} + \frac{\partial \tilde{u}_j}{\partial x_i}\right), \\ -\sum_m \overline{h_m J_{jm}} &= -\sum_m \tilde{h}_m\tilde{J}_{jm,eff} = -\sum_m \tilde{h}_m\left(-\frac{\mu_{eff}}{\tilde{Sc}_{eff}}\frac{\partial \tilde{Y}_m}{\partial x_j}\right).\end{aligned}$$

Eventually, the filtered governing fluid flow equations used in this study become

$$\frac{\partial \bar{\rho}}{\partial t} + \frac{\partial}{\partial x_j}(\bar{\rho}\tilde{u}_j) = 0, \quad (10-74)$$

$$\frac{\partial \bar{\rho}\tilde{u}_i}{\partial t} + \frac{\partial}{\partial x_j}(\bar{\rho}\tilde{u}_j\tilde{u}_i) = -\frac{\partial \bar{p}}{\partial x_i} + \frac{\partial}{\partial x_j}\left(\mu_{eff}\left(\frac{\partial \tilde{u}_i}{\partial x_j} + \frac{\partial \tilde{u}_j}{\partial x_i}\right)\right) + \bar{\rho}g_i, \quad (10-75)$$

$$\frac{\partial}{\partial t}(\bar{\rho}\tilde{E}) + \frac{\partial}{\partial x_j}(\tilde{u}_j(\bar{\rho}\tilde{E} + \bar{p})) = \frac{\partial}{\partial x_j}\left(\frac{\mu_{eff}c_p}{Pr_{eff}}\frac{\partial \tilde{T}}{\partial x_j} - \sum_m \tilde{h}_m\left(-\frac{\mu_{eff}}{\tilde{Sc}_{eff}}\frac{\partial \tilde{Y}_m}{\partial x_j}\right) + \tilde{u}_i\mu_{eff}\left(\frac{\partial \tilde{u}_i}{\partial x_j} + \frac{\partial \tilde{u}_j}{\partial x_i}\right)\right) + \bar{S}_E. \quad (10-76)$$

The source term for the energy equation is associated with the chemical reaction rate  $S_E = \Delta H_c \cdot S_c$  and will be considered in the combustion model section.

The effective viscosity was calculated according to renormalization group (RNG) theory, which is capable of modelling fluid flow in limits of both laminar and high Reynolds number flow regimes (Yakhot and Orszag, 1986)

$$\mu_{eff} = \mu \left[ 1 + H \left( \frac{\mu_s^2 \mu_{eff}}{\mu^3} - 100 \right) \right]^{1/3},$$

where  $\mu_s = \bar{\rho} \left( 0.157 V_{CV}^{1/3} \right)^2 \sqrt{2 \tilde{S}_{ij} \tilde{S}_{ij}}$ ,  $H(x)$  is the Heaviside function.

In study by Makarov and Molkov (2004) the molecular Prandtl number was set to  $Pr = 0.7$ . The theoretical equation by Yakhot and Orszag (1986) for effective Prandtl number derived from the RNG theory for non-reactive flows is accepted for modelling

$$\left| \frac{1/Pr_{eff} - 1.3929}{1/Pr - 1.3929} \right|^{0.6321} \left| \frac{1/Pr_{eff} + 2.3929}{1/Pr + 2.3929} \right|^{0.3679} = \frac{\mu}{\mu_{eff}}. \quad (10-77)$$

The RNG model is similar to the Smagorinsky's model (1963), but doesn't contain adjustable or ad hoc parameters and is capable to describe not only turbulent yet transitional and laminar flow regimes: in the laminar flow the Heaviside function argument is negative and the effective viscosity recovers molecular viscosity,  $\mu_{eff} = \mu$ .

#### 10.4.4. The progress variable equation and the gradient method

The species transport equation for the premixed combustion system is usually recast in the form of the progress variable equation (Libby and Williams, 1993)

$$\frac{\partial}{\partial t}(\rho c) + \frac{\partial}{\partial x_j}(\rho u_j c) = \frac{\partial}{\partial x_j} \left( -J_{jc} \right) + S_c, \quad (10-78)$$

**gaiteye**  
Challenge the way we run

**EXPERIENCE THE POWER OF  
FULL ENGAGEMENT...**

**RUN FASTER.  
RUN LONGER..  
RUN EASIER...**

**READ MORE & PRE-ORDER TODAY  
WWW.GAITEYE.COM**

where  $c$  is the progress variable, e.g. normalised product mass fraction,  $c=0$  in unburned mixture and  $c=1.0$  in combustion products,  $J_{jc}$  is the progress variable diffusion flux, and  $S_c$  is the source term.

In the laminar flamelet regime chemical kinetics enters the combustion system only through its influence on the burning velocity  $S_u$ , the flame-turbulence interaction is purely kinematic and modelling of detailed chemistry can be omitted (Bray, 1996).

Various models for the combustion reaction rate feature strong similarities (Vervisch and Veynante, 2000), and the local mass burning rate can be described using the gradient combustion method for the first time suggested by Prudnikov (1967) and widely applied today, e.g. (Oran and Boris, 1987),  $S_c = \rho_u S_u |\text{grad } c|$  (subscript  $u$  stands for unburned mixture). The gradient method ensures that the prescribed mass burning rate,  $\rho_u S_u$ , takes place because the integral of the progress variable gradient in the normal to the flame front direction is always equal to 1 independent of the number and size of cells throughout the numerical flame front thickness

$$\int_V \bar{S}_c dV = \int_V \rho_u S_u |\nabla \tilde{c}| dV = \int_A \rho_u S_u dA \int_{c=0}^{c=1} \frac{\partial c}{\partial x} dx = \int_A \rho_u S_u dA \int_{c=0}^{c=1} dc = \int_A \rho_u S_u dA = \rho_u S_u A.$$

Besides, the method treats the flame front movement and the effect of merging interfaces naturally without additional computational cost.

LES explicitly resolves the flame front wrinkling on a mesh scale. However, unresolved effects of different combustion instabilities affecting turbulent burning rate at the sub-grid scale (SGS) should be accounted using the SGS “turbulence” factor  $\Xi_{SGS}$ , which is a multiplier to the laminar burning velocity and includes by definition effects of different physical mechanisms influencing premixed combustion. Apparently, the smaller the control volume size used the larger the fraction of the flame front wrinkling resolved explicitly in simulations and, thus, the smaller the SGS turbulence factor. In the limit of the fine enough grid and small scale problem the SGS wrinkling factor can be taken as  $\Xi = 1.0$  (direct numerical simulations).

Applying filtering to (10–78) and introducing modelling expression for molecular and SGS diffusion fluxes

$$\bar{J}_{jc} + J_{jc,SGS} = -\frac{\bar{\mu}}{Sc} \frac{\partial \bar{c}}{\partial x_j} + (\overline{\rho u_j c} - \bar{\rho} \tilde{u}_j \tilde{c}) = -\frac{\mu_{eff}}{Sc_{eff}} \frac{\partial \tilde{c}}{\partial x_j},$$

the progress variable equation has a following form

$$\frac{\partial}{\partial t} (\bar{\rho} \tilde{c}) + \frac{\partial}{\partial x_j} (\bar{\rho} \tilde{u}_j \tilde{c}) = \frac{\partial}{\partial x_j} (-\bar{J}_{jc}) - \frac{\partial}{\partial x_j} (\overline{\rho u_j c} - \bar{\rho} \tilde{u}_j \tilde{c}) + \bar{S}_c. \quad (10-79)$$

The molecular Schmidt number was taken in (Makarov and Molkov, 2004) as  $Sc = 0.7$  and the effective Schmidt number was calculated similar to the effective Prandtl number by the RNG theory equation (10–77). The reaction rate was calculated neglecting the difference between  $\tilde{c}$  and  $\bar{c}$  similar to (Weller et al., 1998)

$$\bar{S}_c = \rho_u \cdot S_u \cdot \Xi_{SGS} \cdot |\text{grad } \tilde{c}|.$$

The over-bar  $\bar{\phantom{x}}$  and tilde  $\sim$  will be omitted further, assuming mass-weighted filtered values for all variables except for density and pressure.

To narrow the distribution of the progress variable over grid cells the following modifications of the gradient method and the source terms in the progress variable and energy conservation equations have been suggested

$$S_c = \rho_u S_u \left| \text{grad } c^N \right| \Xi_{SGS}, \quad (10-80)$$

$$S_E = H_c S_c = H_c \rho_u S_u \left| \text{grad } c^N \right| \Xi_{SGS}, \quad (10-81)$$

where  $N$  is chosen from the consideration of the flame front thickness ( $N \geq 1$ ). This approach has a potential to decrease the flame front thickness due to the faster change in the progress variable value and, at the same time, preserving the total mass burning rate, because the integral of  $\text{grad } c^N$  across the flame front thickness is always equal to unity regardless  $N$  value. Choosing the value of  $N$  it needs to keep in mind that too high value of  $N$  can lead to unacceptably thin flame front and numerical instabilities in solution process.

Simulations for two values of  $N$  were carried out and results were compared (Makarov and Molkov, 2004):  $N = 1$  (standard gradient method) and  $N = 2$  (modified gradient method). In all simulations the SGS wrinkling factor was taken as  $\Sigma_{SGS} = 1.0$  because the mixture was initially quiescent and flame front wrinkling was already accounted for in the adopted from lumped parameter model (Molkov et al., 2000) values of  $S_{ui}$  and  $\varepsilon$ .

#### 10.4.5. LES of large-scale closed vessel deflagration

The dynamics of stoichiometric hydrogen-air (29.5% by volume) deflagration in the 6.37 m<sup>3</sup> closed spherical vessel of 2.3 m diameter with central ignition (Kumar et al., 1983) was simulated. Initial temperature and pressure were 373 K and 97 kPa respectively. The burning velocity for this experiment was determined previously by the inverse problem method (Molkov et al., 2000) in the form  $S_u = S_{u0} (p/p_0)^\varepsilon$ , where the initial burning velocity at 373 K was equal  $S_{u0} = 4.15 \text{ m}\cdot\text{s}^{-1}$  and overall thermokinetic index  $\varepsilon = 1.0$ . The molecular masses of hydrogen-air mixture and combustion products were equal to  $M_u = 20.9$  and  $M_b = 20.9 \text{ kg/kmol}$  respectively. Unburned and burned mixture densities at initial pressure were equal to  $\rho_{u0} = 0.65$  and  $\rho_{b0} = 0.12 \text{ kg/m}^3$ , and the expansion coefficient was calculated to be  $E_0 = \rho_{u0}/\rho_{b0} = 5.3$ .



It should be noted that being the result of the processing of experimental pressure-time curve by the lumped parameter model, the burning velocity  $S_{u0}$  and overall thermokinetic index  $\varepsilon$  incorporate all effects of combustion instabilities on the burning velocity. At the same time, the cellular structure (wrinkling) of the flame front will be explicitly partially resolved in LES. It means that the effect of cellular structure on combustion rate will be accounted for with “excess”. Thus, the simulated deflagration dynamics can be expected to be faster than the experimental pressure transient at accepted given values of  $S_u$  and  $\varepsilon$ . Unfortunately, it was impossible to find values of  $S_u$  and  $\varepsilon$  for stoichiometric hydrogen-air mixture for elevated initial temperature of 100°C.

The composition of the burned mixture was calculated using a thermodynamic equilibrium model (Kee et al., 2000) under isohoric conditions, i.e. the internal energy is constant, and taking into account 21 species. The constant value of the heat of reaction, “averaged” through the whole deflagration process, was used in simulations (Makarov and Molkov, 2004). It was determined as a difference of internal energies of unburned mixture and combustion products at initial temperature of experiment,  $\Delta H_c = (e_u - e_b) \Big|_{T_0=373K} = 2.92 \cdot 10^6 \text{ J} \cdot \text{kg}^{-1}$ . Specific heats of mixtures were approximated as piecewise-polynomial functions of temperature with polynomial coefficients calculated according to mass-weighted mixing law of composing species. Molecular viscosities of both fresh and burned mixtures were calculated according to the Sutherland law for air viscosity. In simulations the mixture composition and aforementioned properties were assumed to be independent of pressure.

This e-book  
is made with  
**SetaPDF**



PDF components for PHP developers

[www.setasign.com](http://www.setasign.com)



The simulations were performed using FLUENT software, which is based on a control-volume based finite-difference method. The solver used explicit linearisation of the governing equations with a second order accurate upwind scheme for convection terms and a central-difference second-order accurate scheme for diffusion terms. The Runge-Kutta algorithm was employed for solution of linear equation set. The time step was determined from Courant-Friedrichs-Lewy condition  $\Delta t = (CFL \cdot \Delta) / (a + u)$ , where the CFL number was equal to 0.8 to ensure stability.

The advantage of geometric flexibility of the unstructured tetrahedral grid was used to mesh spherical calculation domain. The average size of tetrahedron edge was  $\Delta = 0.07\text{m}$  (about 33 control volumes along diameter of sphere). This was combined with a hanging-node solution adaptive meshing close to the flame front, where higher spatial resolution is required to reduce the simulated flame front thickness. One level of grid refinement was used, providing cells with a twice smaller average edge size  $\Delta = 0.035\text{ m}$  in the region of high progress variable gradient. Criterion for mesh refinement was  $c \geq 0.001$ . Criterion for de-refinement was specified as combination of  $c \geq 0.090$  and  $S_c \leq 10$ . The cell number during calculations varied from 116,586 (without mesh refinement) to 306,000 (with mesh refinement). The uniform grid with the cell edge  $\Delta = 0.035\text{ m}$  would consist of about one million control volumes.

The data on the cellular structure in the large-scale deflagrations available from experimental observations by Bradley et al. (2001), i.e. cell sizes in a range 15–45 cm were observed for methane-air and propane-air mixtures at radii from 1 to 3m.

At the initial moment,  $\tau = 0\text{ s}$ , fluid was quiescent,  $u = 0\text{ m/s}$ . In our first simulations (Makarov and Molkov, 2004) the combustion was initiated in the centre of sphere using value of the progress variable  $c = 1.0$  in the region with radius  $R \leq 0.04\text{ m}$  and distribution  $c = \exp\left[-(R - 0.04)^2 / 0.08\right]$  everywhere else, which provided a smooth slope of the progress variable profile down to zero, and ensured the numerical stability and the near spherical initial flame kernel. The temperature distribution at the initial moment was  $T = T_{u0} + c \cdot (T_{b0} - T_{u0})$ , where the unburned mixture temperature was equal to experimental  $T_{u0} = 373\text{ K}$ , and the burned mixture temperature, obtained thermodynamically with the accepted heat of reaction  $\Delta H_c$ , was  $T_{b0} = 2280\text{ K}$ .

At the vessel's wall a non-slip boundary condition was used for velocities ( $u = 0$ ). The adiabatic boundary condition was used for the energy equation ( $\partial T / \partial n = 0$ ) and zero flux boundary condition for the progress variable equation ( $\partial c / \partial n = 0$ ).

In this study 4 different cases with two different values of N in the source terms (10–80), (10–81) and with/without mesh refinement were considered

Case 1. $S_c = \rho_u S_u  \text{grad } c $ , no mesh refinement	$N=1$
Case 2. $S_c = \rho_u S_u  \text{grad } c $ , solution adaptive mesh refinement	$N=1$
Case 3. $S_c = \rho_u S_u  \text{grad } c^2 $ , no mesh refinement	$N=2$
Case 4. $S_c = \rho_u S_u  \text{grad } c^2 $ , solution adaptive mesh refinement	$N=2$

#### 10.4.5.1. Simulated flame front structure and thickness

Figure 10–13 shows a cross section of the simulated flame front (Case 4, identified as iso-surface  $c = 0.5$ ) for four moments  $t=9.8, 20.1, 32.7, 44.4$  ms.

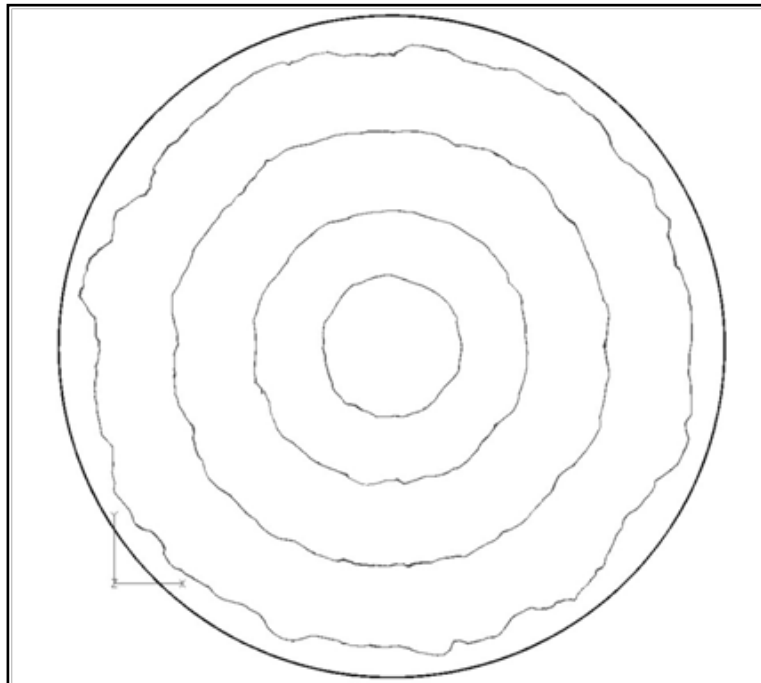


**Figure 10–13.** Simulated flame front profiles in the vessel cross-section: Case 4,  $t=9.8, 20.1, 32.7, 44.4$  ms.

Figure 10–13 demonstrates that the flame front surface has a cellular structure. Similar flame structure was simulated in Cases 1–3. It is seen that buoyancy doesn't affect the flame front shape in spite of large sphere size. This is in agreement with results obtained earlier: the buoyancy affects a spherical propagation of flame when the Froude number becomes less than the critical value  $Fr \leq 0.11$  (Babkin et al., 1984). For the considered experiment the Froude number during the whole deflagration process was more than  $Fr = 21$ .

According to Groff (1982), for stoichiometric propane-air deflagration the onset of cellular structure due to hydrodynamic instability occurs at the flame Reynolds number about  $10^4$  when the flame radius is 0.056 m. If this critical value is accepted as universal and valid for hydrogen-air flame then the cellular structure would onset at the flame front radius  $R_{ff} = (Re \mu_u) / (S_u \rho_u) = 0.084$  m. It should be noted that lean hydrogen-air mixtures can be “wrinkled” earlier by the selective diffusion phenomenon (higher diffusion of hydrogen that results in local redistribution of hydrogen concentration in air close to the wrinkled flame front).

A higher resolved wrinkling factor was obtained in simulations with smaller control volume sizes: Cases 2 and 4 ( $\Delta = 0.035$  m). From analysis of Fig.10–13 it can be concluded that the size of the resolved cells grows with time, which is in agreement with experimental observations (Bradley et al., 2000). A three-dimensional numerical snapshot of the developed cellular structure (Case 4,  $t=44.4$  ms) is shown in Fig. 10–14. At this stage the characteristic size of the resolved cells reached 0.35 m with the average flame front radius of about 1.05 m.



**YOU THINK.  
YOU CAN WORK  
AT RMB**

 **RAND  
MERCHANT  
BANK**  
A division of FirstRand Bank Limited  
Traditional values. Innovative ideas.

Rand Merchant Bank uses good business to create a better world, which is one of the reasons that the country's top talent chooses to work at RMB. For more information visit us at [www.rmb.co.za](http://www.rmb.co.za)

Thinking that can change your world

Rand Merchant Bank is an Authorised Financial Services Provider

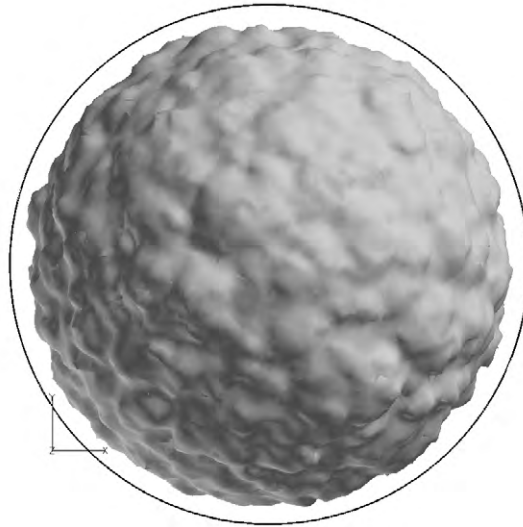


**Figure 10-14.** The numerical snapshot of resolved flame cellular structure: Case 4,  $t=44.4$  ms.

Development of the resolved cellular structure in simulations leads to an increase of the flame front area and, thus, to an increase of the mass burning rate. The resolved wrinkling factor can be calculated as:  $\Xi = F_{C=0.5}/F_b$ , where  $F_{C=0.5}$  is the area of iso-surface  $c=0.5$ , and  $F_b$  is the area of the imaginary sphere of the same volume as the volume inside of simulated iso-surface  $c = 0.5$ . The resolved in simulations flame front wrinkling factor is growing with time and reaches values 1.03 and 1.09 in Case 1 and Case 2 respectively. The higher wrinkling factor for Case 2 in comparison with Case 1 is, apparently, due to the finer grid, which provides a better resolution of the flame front.

The simulated flame thickness  $\Delta_f$  was calculated as the volume between iso-surfaces of the progress variable  $c = 0.01$  and  $c = 0.99$ , divided by the area of the iso-surface  $c = 0.5$ . It is convenient to normalise the simulated flame front thickness using the size of initial cell edge  $\Delta = 0.07\text{m}$ . The variation of the front thickness normalised in such a way, expressed in an equivalent number of the original control volumes, is shown in Fig. 10-15.

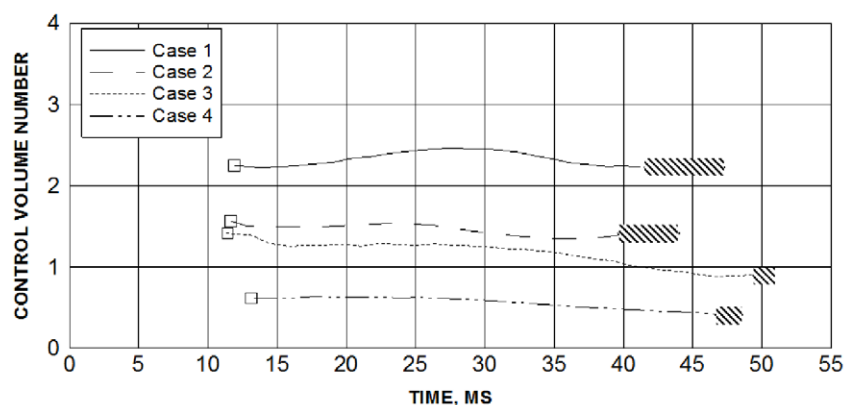


**Figure 10-15.** The normalised by the control volume edge size ( $\Delta=0.07$  m) flame front thickness as a function of time.

□ – moment of stabilisation of flame propagation after ignition, ▨ – period from the moment, when the iso-surface  $c=0.01$  contacts a wall for the first time, to the moment of combustion completion within the vessel.

In simulations the combustion was initiated not from the point ignition source as in experiment, but by near spherical pre-ignited region, which means that the simulation results should be adjusted using the time of flame propagation through the pre-ignited region. Theoretically the flame front radius at the initial moment is zero and at the initial stage of combustion, when the dependence of the burning velocity on pressure rise can be neglected, the flame front velocity is constant and equal to  $S_{u0} E_0$  ( $E_0$  – expansion coefficient,  $E_0 = \rho_u / \rho_b$ ), and the flame front radius grows linearly. The correction times were obtained by imposing the simulated flame front radius with its analytical dependence after the flame separated from the pre-ignited region. As a result, extra time 3.75, 4.0, 3.75 and 4.5 ms were added to the original simulation time in Cases 1–4 respectively.

The analysis of the flame front thickness is meaningful only between the moment when numerical flame propagation is established after the ignition, and the moment when iso-surface  $c = 0.01$  contacts the wall for the first time. Figure 10–15 demonstrates that the use of one level of solution adaptive mesh refinement, i.e. the decrease of characteristic control volume size by two times, reduces the simulated flame front thickness by about two times two as expected. Application of the modified gradient method ( $N=2$ ) decreases the flame front thickness further by about two times, which is close to the size of the original control volume edge size.

There are some consequences of the flame front thickness reduction. In particular, the time between the moment when iso-surface  $c=0.01$  touches the vessel wall and the moment when combustion is completed changes from 5.7 ms (Case 1) and 4.4 ms (Case 2), both  $N=1$ , to 1.5 ms (Case 3) and 1.9 ms (Case 4), both  $N=2$ , respectively.

It is worth mentioning that in unstructured tetrahedral grid the computational cells are oriented randomly and the simulated flame front still occupies about four control volumes even for the modified gradient method ( $N=2$ ). Not less than four computational cells were required for the resolution of the premixed turbulent flame in study by Catlin et al. (1995) also. It can be presumed that if the simulated flame front thickness would decrease below this value, which is in agreement with one of the main numerical requirement to simulation of propagating “discontinuities”, can result in a slower flame front propagation. This can be explained by the fact that for “sharp” numerical front the integral of  $(grad\ c)$  across the numerically flame front will be below 1 due to the insufficient smoothness of  $c$  profile. This is supported by results in Fig. 10–16 and Fig. 10–17.

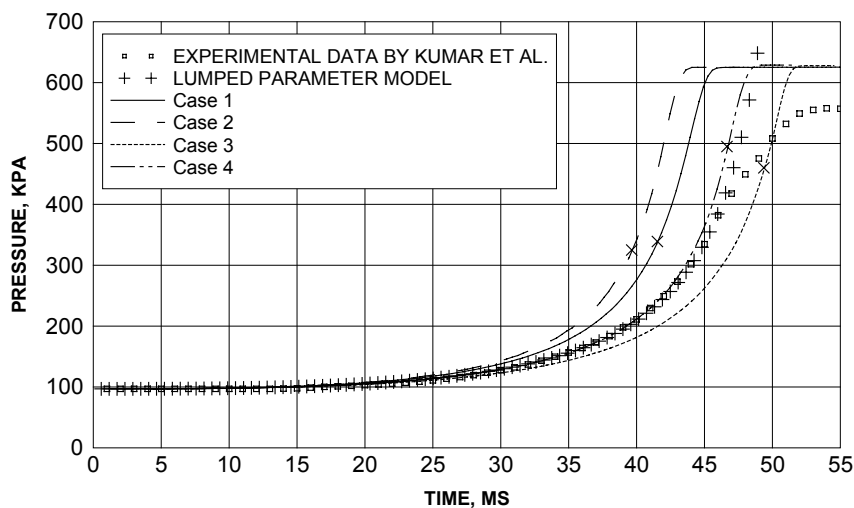


**Figure 10-16.** The comparison of experimental (Kumar et al., 1983) and the simulated pressure dynamics:  
 X – moment, when iso-surface  $c=0.01$  first touches the vessel wall.

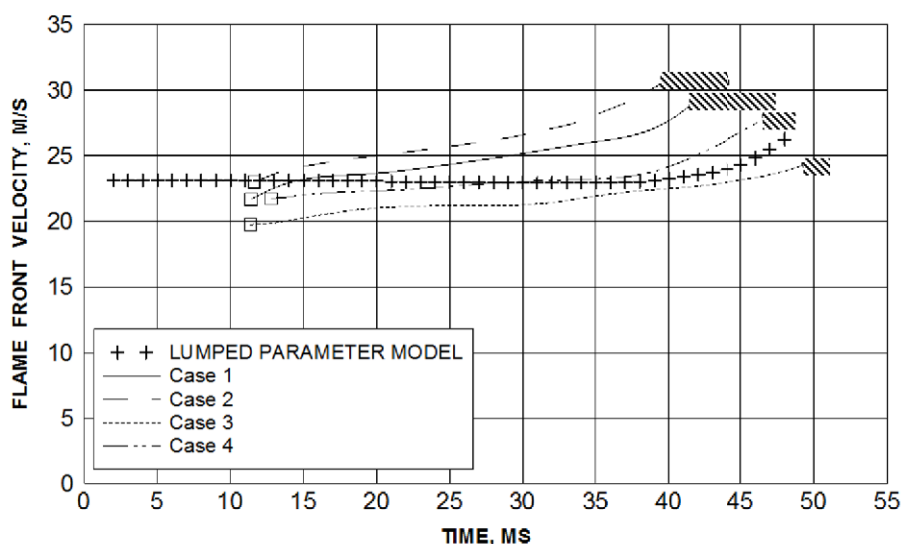


**Figure 10-17.** The simulation results for the flame front propagation velocity: □ - moment of stabilisation of flame propagation after ignition, ▨ - period between the moment, when iso-surface  $c=0.01$  first contacts a wall and the moment of complete mixture burnout

#### 10.4.5.2. Pressure transients

The experimental pressure dynamics (Kumar et al., 1983) and numerical pressure transients along with calculated by the lumped parameter model in study (Molkov et al., 2000) are shown in Fig. 10-16. The lumped parameter model pressure-time curve was obtained by the inverse problem method, i.e. by adjustment of  $S_{ui}$  and  $\varepsilon$  to get the best fit to the experimental pressure transient (Kumar et al., 1983). Thus, it is not a “wonder” that the lumped parameter model provided the best agreement with the experimental pressure-time curve except the final part, where experimental pressure drops due to the heat losses to the vessel walls. This allows us to use data obtained with the lumped parameter model at the interval  $t=0-46$  ms for verification of the LES model against data not measured in experiment.



The maximum explosion pressure, obtained in the LES simulations, is in the range from 625.5 kPa to 627.8 kPa for all considered cases. This is in agreement with the theoretical value of the deflagration pressure calculated according to thermodynamic equilibrium model for closed vessel ( $p=623$  Pa), and slightly lower than the maximum pressure according to the lumped parameter model ( $p=648.4$  Pa). This close agreement is due to the fact that the adopted heat of reaction was calculated at isohoric conditions, which is lower than the heat of reaction for the isobaric process

$$H_c^{p_0} = (h_u - h_b) \Big|_{T_0=373K} = 3.13 \cdot 10^6 \text{ J} \cdot \text{kg}^{-1}.$$

After  $t=46$  ms the second derivative of the experimental pressure transient changes its sign from positive to negative because of heat losses into the vessel walls. In lumped parameter model calculations and LES simulations the heat losses were neglected. This is why the second pressure derivative in the lumped parameter model calculations is always positive. However, in the LES simulations the second pressure derivative changes its sign at the end of combustion. The reason is as follows. Once the leading edge ( $c=0.01$ ) of the thick numerical flame front touches the wall (see Fig. 10–16), its thickness decreases with time. This causes a decrease in the mass burning rate as the integral of ( $grad\ c$ ) over the rest of numerical flame front is now below 1. The decrease of mass burning rate affects the pressure dynamics. The earlier flame front attachment to the vessel walls is observed for the standard gradient method ( $N=1$ ).



Discover the truth at [www.deloitte.ca/careers](http://www.deloitte.ca/careers)

**Deloitte.**

© Deloitte & Touche LLP and affiliated entities.

The best agreement with the experimental pressure dynamics is for Case 4 (see Fig. 10–16). However, as was mentioned earlier, the LES model used the burning velocity at initial conditions and the overall thermokinetic index that were obtained by the inverse problem method from the same experimental data assuming the ideally spherical shape of the flame front. This means that the values of initial burning velocity and overall thermokinetic index implicitly account for the cellular structure developing in the deflagration progress. On the other hand, the LES results have demonstrated that at least a part of cellular flame front structure was explicitly resolved in simulations. Thus, the effect of cellular structure was accounted more than once. This implies that in Fig. 10–16 the LES pressure transient has to be moved to the left of the experimental curve.

The finer grid will provide numerical resolution of smaller and smaller elements of the cellular structure. This will cause faster flame propagation due to larger flame surface and further move of the simulated pressure curve to the left of the experimental pressure record. This statement is supported by simulations: Case 1 and Case 2 (see Fig. 10–16). Unfortunately, investigation of further grid refinement on pressure dynamics and flame front structure was not possible due to the demanding computer resources, required by such simulations in 2004. Finally, the deviation of simulated pressure transients from experimental is less than 10% and can be treated as acceptable.

#### 10.4.5.3. Flame propagation velocity

The flame front propagation velocity was calculated as the propagation velocity of the iso-surface  $c = 0.5$  (Makarov and Molkov, 2004). Data on the flame propagation is not available from the experiment (Kumar et al., 1983). By this reason the simulation results were compared against results of the lumped parameter model (see Fig. 10–17). The initial period of the flame propagation and its final part from the moment when the leading flame edge ( $c = 0.01$ ) touches the vessel wall to the complete burnout of the mixture, are excluded from the analysis.

The lumped parameter model gives nearly constant flame front propagation velocity of  $23 \text{ m}\times\text{s}^{-1}$  during the most of combustion process excluding the final stage of the deflagration. At the end of the deflagration the flame propagation velocity reaches  $26 \text{ m}\times\text{s}^{-1}$  as a result of competition between an increase of laminar burning velocity due to pressure growth and a decrease of propagation velocity when flame approaches wall and the propagation velocity tends to be equal to the burning velocity. The effect of pressure built-up on the burning velocity for near stoichiometric hydrogen-air mixture deflagration in closed vessel is stronger than the effect of flame deceleration close to the vessel wall.

The numerically simulated flame front propagation velocity is in a qualitative agreement with the results of the lumped parameter model, i.e. the flame propagation velocity increases at the final stage of combustion. The faster growth of the LES flame front propagation velocity compared to results obtained from the lumped parameters model (see Fig. 10–17) can be explained by explicit partial resolution of the developing flame cellular structure.

#### 10.4.6. Cellular structure of large-scale premixed flames

The regularities of cellular structure development for initially quiescent stoichiometric hydrogen-air deflagration propagation from a central ignition source in a large-scale 2.3 m diameter spherical vessel (Kumar et al., 1983) are described in this section. The observed in experiments with hydrocarbon-air mixtures growth of cell sizes with flame radius as result of hydrodynamic instability is reproduced numerically for hydrogen-air mixture.

The minimum resolved in the simulations (Molkov et al., 2004c) size of the flame cells is of the order of the simulated flame front thickness that which is about 3 control volume edges. The use of 3.5 cm mesh size in simulations around the flame front allows to resolve cells with sizes as small as about 10 cm. The “resolved” fractal dimension of the wrinkled flame front surface grows and reaches at the end of deflagration a value of 2.15 that is close to the lower limit of the fractal dimension observed in experiments.

For hydrogen-air flames at normal temperature and pressure stable preferential-diffusion conditions are observed at fuel-equivalence ratios above roughly 0.7 (Aung et al., 1997). The neutral preferential-diffusion condition shifts toward fuel-rich conditions with increasing pressure (Aung et al., 1998). It could lead to the development of preferential-diffusion instability at pressures above 4 atm when one could expect that chaotically irregular surfaces will develop. However, a stabilising effect of temperature growth could be assumed as the burning velocity is increasing with temperature. That could compensate for the destabilising influence of the growing pressure.

The influence of preferential diffusion is taken into account in our LES model through the value of burning velocity. The only remaining reason for the developing of the flame front wrinkling in simulations is hydrodynamic instability.

The resolved by LES wrinkled flame front is shown in Fig. 10–18 for four different moments: 6.6, 13.6, 27.3, and 36.6 ms after ignition. The vessel wall is given as an outer thin circle. It is clearly seen that the flame front has an evolving in time cellular structure. At the moment  $t=6.6$  ms the flame front radius is about 26 cm, and cells are not yet pronounced enough. It is easy to observe the appearance and evolution of the fractal structure of the flame surface in time by following the development of two randomly chosen cells, indicated by arrows in Fig. 10–18, to demonstrate that they grow and then split according to theoretical predictions.

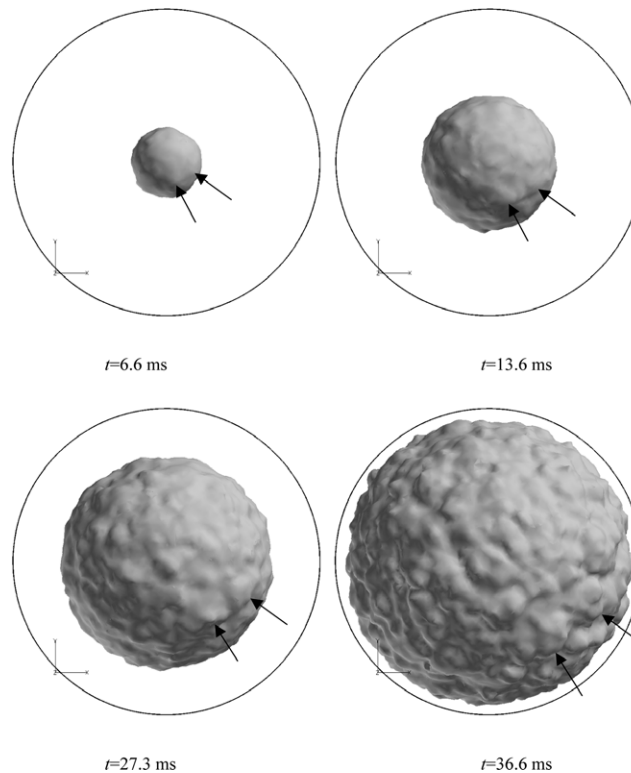


**Figure 10-18.** Development of resolved in LES cellular structure of stoichiometric hydrogen-air flame in 2.3 m diameter sphere in time. Arrows point at two of the evolving cells demonstrating that they grow and then split.

**I WANT TO CHANGE DIRECTION,  
AND THE WORLD.**

**GOT-THE-ENERGY-TO-LEAD.COM**

We believe that energy suppliers should be renewable, too. We are therefore looking for enthusiastic new colleagues with plenty of ideas who want to join RWE in changing the world. Visit us online to find out what we are offering and how we are working together to ensure the energy of the future.

**RWE**  
The energy to lead

Figure 10-18 shows that the cell size grows in time, and along with this growth the further cells of smaller size are created on primary cell surface, giving a rise to a fractal-like flame wrinkling. In spite of the fact that small-scale perturbations of real flame front below LES filter are not resolved, one can identify the cascade of different cell sizes in Fig. 10-18. This numerical result is in agreement with the fractals theory and flame stability analysis by Bradley (1999).

The numerical flame front wrinkling factor is a function of the simulated flame front thickness. The thinner the flame front the smaller resolved wrinkles. Resolved fraction of the cell size spectrum increases with flame front radius and more plausible simulation results can be expected at the end of the deflagration.

The flame front radius at four different moments, the respective values of the resolved flame front wrinkling factor and the fractal dimension are given in Table 1 for simulation results with the average grid size  $\Delta_{CV} = 0.035$  m (adaptive grid). The resolved flame wrinkling factor is growing with time in the time span 6.6-36.6 ms from 1.01 to 1.09. This simulation tendency corresponds to the experimental observation of the self-acceleration of large-scale deflagration flames and conclusions of the fractals theory.

Time index, $i$	Time, ms	Flame radius, $R_{ff}$ m	Flame wrinkling factor, $\Xi$	Fractal dimension, $D$
1	6.6	0.26	1.01	-
2	13.6	0.50	1.025	2.02
3	27.3	0.79	1.04	2.04
4	36.6	1.07	1.09	2.15

**Table 10-3.** Resolved flame front wrinkling factor and fractal dimension.

Due to spherical symmetry of the flame front in this problem the fractal dimension can be calculated through the change of wrinkling factor with radius as (Molkov et al., 2000)

$$D_i = 2 + \left( \ln \left( \frac{\Xi_i}{\Xi_{i-1}} \right) / \ln \left( \frac{R_i}{R_{i-1}} \right) \right), \quad (10-82)$$

where  $i$  is the time index (see Table 10-3). The fractal dimension grows in time and reaches a value about  $D = 2.15$ . This is close to the fractal dimension values  $D=2.14-2.24$  reported for turbulent premixed combustion in Bunsen-type burners by Gulder et al. (2000). A wider range of experimental values of fractal dimension  $D=2.11-2.36$  has been cited for various premixed combustion applications by Gulder (1990). In spite of LES limitation to resolve flame front wrinkling below filter width the obtained values of fractal dimension at the end of combustion are reasonable. Yet, unresolved sub-grid scale flame wrinkling needs to be modelled in the LES SGS combustion sub-model. The observation that simulated fractal dimension is increasing with time, i.e. with the flame front radius, could be related to the growing fraction of the resolved scales of wrinkles with radius rather than a physical phenomenon.

The range of cell sizes resolved in simulations is given in Fig. 10–19. The cell sizes were obtained from the numerical flame front snapshots using 3 independent expert measurements and then weight-averaged. The scatter between the highest and the lowest values of the cell sizes are shown by solid vertical lines. It is easy to see that simulated flame front cellular structure obeys the theoretical conclusion by Bradley (1999) that the size of cells at outer cut-off increases with the flame radius and the size of inner cut-off (about three CV sizes in this case) remains practically constant.

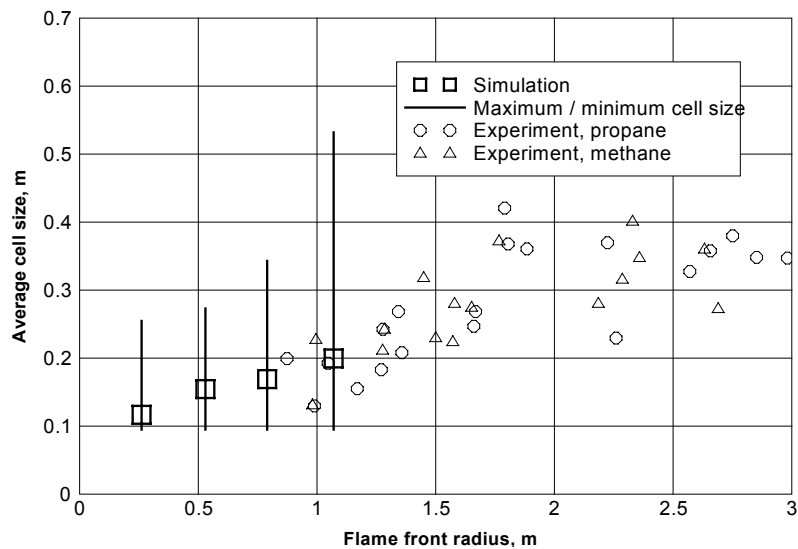


**Figure 10–19.** Experimental (methane-air and propane-air, Bradley et al., 2001) and simulated (hydrogen-air) dependencies of flame front cell sizes on radius. Vertical lines show the range of cell sizes resolved in simulations.

Weight-averaged cell sizes of simulated flame front are indicated by “square” symbols in Fig. 10–19 and grow up to 20 cm at radius of about 1 m. The author is not aware of any large-scale experimental results on hydrogen-air flame propagation, where flame front cell sizes were analysed. Figure 10–19 demonstrates that LES results for hydrogen-air mixture are in quantitative agreement with the experimental data on cell sizes obtained for large-scale hemispherical methane-air and propane-air explosion flames (Bradley et al., 2001). The experiments (Bradley et al., 2001) were part of the SOLVEX (Shell Offshore Large Vented Explosions) research program and were performed in 547 m<sup>3</sup> volume vessel. Experimentally obtained cell sizes for both methane-air and propane-air mixtures at flame radii from 1 to 2.5 m were close to each other and are shown in Fig. 10–19 by triangles and circles respectively. Bradley et al. (2001) commented that when flame front radius reached approximately  $R_{ff}=2.5$  m, the flame front propagation couldn’t be considered as non-vented and hemispherical anymore, and the average cell size decreased drastically.

The fact that cell sizes simulated for hydrogen-air mixture are similar to observed experimentally by Bradley et al. (2001) for mixtures with quite different chemistry and fine flame front structure might be an evidence that the hydrodynamic instability is responsible for self-acceleration of large-scale explosion flames rather than other effects. This conclusion encourages the LES model application to simulation of accidental combustion at larger scales.



#### 10.4.7. The nature of coherent deflagrations

The nature of coherent deflagration phenomena in a vented enclosure-atmosphere system is analysed in this section. The work is based on experimental observations of SOLVEX programme in the empty 547-m<sup>3</sup> vented enclosure and consequent analysis of the test by large eddy simulations (LES). A comparison between simulated and experimental pressure transients and dynamics of flame front propagation inside and outside the enclosure gave an insight into the nature of the complex simultaneous interactions between flow, turbulence and combustion inside and outside the enclosure (coherent deflagrations). It is revealed through LES processing of experimental data that the substantial intensification of premixed combustion occurs only outside the empty SOLVEX enclosure and this leads to steep coherent pressure rise in both internal and external deflagrations. The external highly turbulent premixed combustion does not affect burning rate inside the enclosure. There is only one ad hoc parameter in the LES model, which is used to account for unresolved sub-grid scale (SGS) increase of the flame surface density outside the enclosure. The LES model allows reaching an excellent match between theory and experiment for coherent deflagrations in the empty SOLVEX facility. The hypothetical mechanism of combustion intensification in the atmosphere is discussed and the quantitative estimation of the model ad hoc parameter is given.

CFD simulation of deflagrations is a demanding task due to the non-linearities and range of time scales involved in combustion process in turbulent compressible flows (Hjertager, 2002). One of unresolved questions is the nature of interaction between internal premixed combustion during vented deflagration and so-called “external explosion” of a flammable mixture pushed out of the enclosure after ignition and then partially diluted by atmospheric air on the contact surface (Molkov et al., 2006b).

[bookboon.com](http://bookboon.com)

## Corporate eLibrary

See our Business Solutions for employee learning

Click here



#### 10.4.7.1. “External explosions”

In 1957 Swedish scientists carried out the first experimental study emphasising the important role of the external explosion during vented deflagration (Report of committee for explosion testing, 1958). It was reported that in some cases the maximum explosion pressure outside the 203-m<sup>3</sup> enclosure exceeded the maximum overpressure inside of the enclosure.

Solberg et al. (1980) further highlighted hazards associated with external explosions. They observed that the flame front propagation velocity could reach 100 m/s in the direction perpendicular to the axis normal to the vent during vented deflagration in a 35 m<sup>3</sup> vessel. The flame propagated up to 30 m beyond the vent, even though the vessel was only 4 m long. Cooper et al. (1986) discussed the role and conditions for onset of pressure peak inside an enclosure due to external explosion. Harrison and Eyre (1987) came to the conclusion that for “large vents, where the internally generated pressures are low, the external explosion can be the dominating influence on the internal pressure” and that this influence “could be very important for large volume low strength structures such as buildings or off-shore modules”.

Harrison and Eyre (1987) simultaneously with Swift and Epstein (1987) suggested that the influence of external explosion on the internal pressure dynamics is to decrease the mass flow rate through the vent. Theoretical analysis by Molkov (1997) based on the processing the experimental data by Harrison and Eyre (1987) confirmed that the turbulence factor inside the enclosure was practically not affected by the external explosion. Instead, the substantial decrease of the generalised discharge coefficient in the lumped parameter model, and thus the mass outflow, was found for tests with distinct external combustion. It was concluded that the decrease in a pressure drop on the vent due to combustion outside the enclosure is the main reason for reduced venting of gas outside enclosure.

Catlin (1991) studied the scaling of external explosions. He found that external overpressure increases proportionally to the velocity of combustion products emerging from the vent and igniting the fuel-air mixture in a starting vortex outside the enclosure. Later Catlin with colleagues (1993) developed an engineering model to assess the hazard from external explosion based on the previous study by Catlin (1991) and validated against large scale experiments in enclosures of volumes up to 91 m<sup>3</sup>.

Puttock et al. (1996) observed the external explosions during experiments in the SOLVEX facility with and without internal obstacles. It was reported that “the effect of the external explosion, giving the final peak pressure in pressure transients, is particularly marked in the case of an enclosure without internal obstacles, increasing the internal pressure by about a factor of four above the previous peak”. The effective epicentre of the external explosion, i.e. the centre of the fireball at the moment when the maximum pressure is measured in front of the vent, was only five meters in front of the vent. This is similar to observations by Solberg et al. (1980) and Harrison and Eyre (1987), who found that the centre of the external explosion was very close to the vent.

Former simulations of the SOLVEX test with internal obstacles by means of CFD (Watterson et al., 1998) over predicted the maximum pressure by two orders of magnitude and under predicted the time to the peak pressure by two orders compared to the experimental data. Fairweather et al. (1999) stressed that “improvements in the accuracy with which the combustion process external to the vessel is modelled” are required.

#### 10.4.7.2. SOLVEX methane-air deflagration analysis

The SOLVEX facility (Fig. 10–20) is a large-scale enclosure of 547-m<sup>3</sup> volume with sizes  $H \times W \times L = 6.25 \times 8.75 \times 10.0$  m and a vent  $H \times W = 4.66 \times 5.86$  m located in the centre of the  $H \times W = 6.25 \times 8.75$  m wall. Experiments were performed with initially quiescent 10.5% methane-air mixture inside the enclosure ignited by a point source located at the centre of the wall opposite to the vent (Puttock et al., 1996). There was no special agitation of air in the surrounding atmosphere before ignition. The vent cover was removed just before ignition. The SOLVEX test without obstacles inside the enclosure was chosen for simulations. The repeatability of experiments was excellent that makes them a reliable source of data for validation of the LES model.

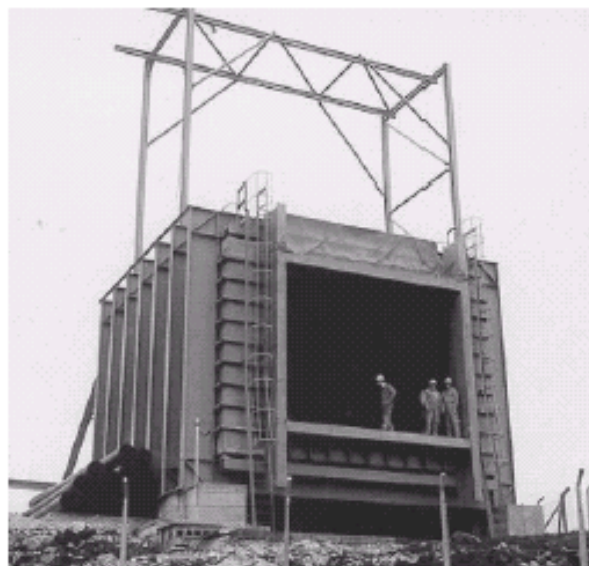


**Figure 10–20.** The SOLVEX facility of 547-m<sup>3</sup> volume for vented deflagrations research.

Figure 10–21 shows the experimental snap-shots of the external explosion, frames A through H. White colour lines outline the enclosure and the vent.

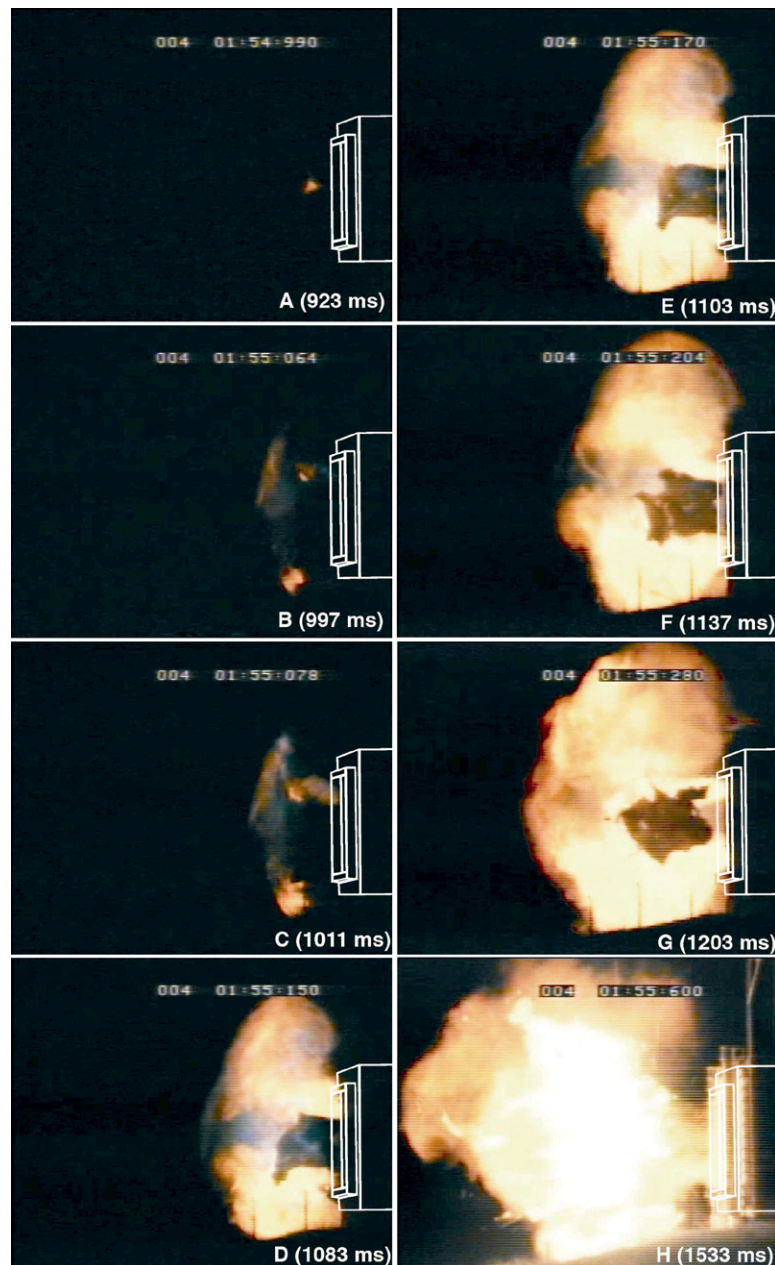


**Figure 10-21.** Snapshots of external deflagration in the SOLVEX facility (Molkov et al., 2006b).

Figure 10-22 shows pressure transients inside and outside the enclosure. Labels on frames A–H in Fig. 10-21 correspond to times after ignition labelled A through G in Fig. 10-21 (label H is not shown in Fig. 10-22 as it is outside abscissa's upper limit). The internal pressure was recorded by a hydrophone, which was installed in 2.2 meters from the rear wall on the bottom of the enclosure. The external pressure was recorded by a hydrophone located at a distance 6.1 m in front of the vent.

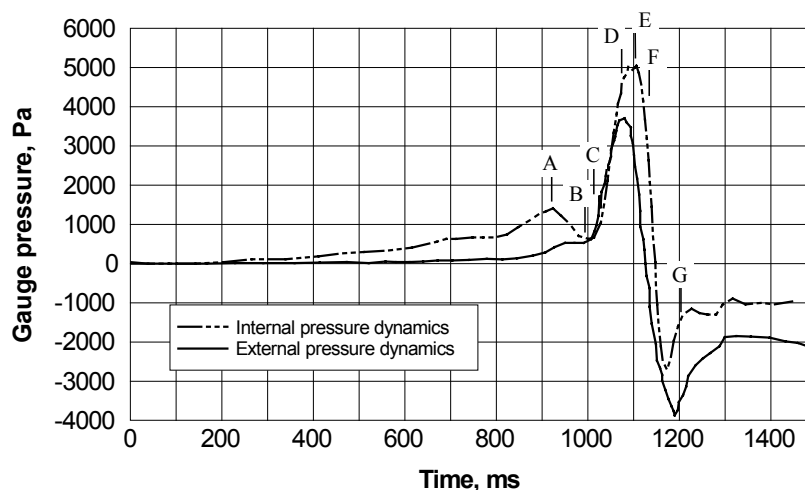


Figure 10-22. Experimental pressure transients inside and outside the enclosure (Molkov et al., 2006b).

To facilitate a comparison between experimental and simulated flame propagation (snapshots) and pressure dynamics it was assumed that the appearance of the flame front in the vent (snap-shot A in Fig. 10-21) corresponds to the first pressure peak on the internal pressure-time curve ( $t=923$  ms). Indeed, it is well known that the first pressure peak inside the enclosure (time A in Fig. 10-22) is caused by the start of venting of combustion products (venting of gases with higher temperature, i.e. combustion products, is more efficient for reduction of pressure compared to venting of gases with lower temperature, i.e. unburned mixture).

# Brain power



By 2020, wind could provide one-tenth of our planet's electricity needs. Already today, SKF's innovative know-how is crucial to running a large proportion of the world's wind turbines.

Up to 25 % of the generating costs relate to maintenance. These can be reduced dramatically thanks to our systems for on-line condition monitoring and automatic lubrication. We help make it more economical to create cleaner, cheaper energy out of thin air.

By sharing our experience, expertise, and creativity, industries can boost performance beyond expectations.

Therefore we need the best employees who can meet this challenge!

The Power of Knowledge Engineering

Plug into The Power of Knowledge Engineering.  
Visit us at [www.skf.com/knowledge](http://www.skf.com/knowledge)





The time of the first flame front appearance in the vent (frame A in Fig. 10–21) was identified approximately. This is because the piece of a plastic sheet, used to cover the vent and removed shortly before ignition, screened the flame. This is why the first flame appearance in Fig. 10–21A is seen at some distance from the vent. The movement of the piece of plastic film can be easily recognised through snapshots in Fig. 10–21.

The combustion outside the enclosure commences in moderate regime between frames A and B in Fig. 10–21. A rapid intensification of combustion starts after the flame emerging from the enclosure reaches the vent edges (the instant between frames B and C). The external pressure reaches a maximum in a short time of about 70 ms after the intensification started (frame D). The maximum pressure inside the enclosure occurs shortly after 1103 ms (frame E). At 1137 ms (frame F) the pressure dynamics is at the decay phase. At 1203 ms (frame G) the pressure is close to its minimum at the negative pressure phase of the deflagration. The experimental video records show that there is still intense turbulent combustion, which proceeds at the top part of the vent. Frame H shows that at the final stage of the process the combustion inside the enclosure continues only at the lower part of the enclosure. This fact was confirmed by numerical simulations.

At the same moment when the pressure inside the enclosure starts to decrease due to more effective venting of combustion products compared to preceding venting of a heavier methane-air mixture (time close to A in Figs. 10–21 and 10–22) the pressure outside the enclosure starts to grow rapidly due to the initiation of turbulent combustion of the flammable mixture outside the enclosure (Fig. 10–22, A to B).

The phenomenon is called coherent deflagrations as the steep rise of pressure inside the enclosure coincides with the pressure rise in the atmosphere. During this period video records demonstrate rapid intensification of combustion in a turbulent wake behind the vent edges outside the enclosure (time C in Fig. 10–22).

There are no video records of what is happening with combustion inside the enclosure at this time. The nature of observed coherent deflagrations inside the vented enclosure and in the atmosphere is not obvious from the analysis of experimental data only. Harrison and Eyre (1987) pointed out that “there is a widely held belief that any increase in internal pressure that is not predicted by simple venting theory should be attributed to an increase in the combustion rate inside the chamber” yet “it is wrong to attempt to represent the peaks caused by external explosions in this way”. This means that Harrison and Eyre (1987) as well as Swift and Epstein (1987) and later Molkov (1997) dealt with experiments when the decrease in pressure drop through the vent was a leading phenomenon. However, Catlin et al. (1993) stated that “the combustion external to the enclosure can provide a source of overpressure and velocity which upon arrival at the vent can interact with the flame inside the enclosure to cause a marked increase in burning rate”.



The main question that remains after the performed analysis of experimental observations is whether the rapid acceleration of combustion in the atmosphere during the empty SOLVEX test affects the burning rate of internal deflagration and if “yes” to what extent?

#### 10.4.7.3. Modelling and LES of SOLVEX methane-air deflagration

The deflagration flame front propagation was simulated using the progress variable equation and the gradient method was used for the model mass burning rate

$$\frac{\partial}{\partial t}(\rho c) + \frac{\partial}{\partial x_j}(\rho u_j c) = \frac{\partial}{\partial x_j} \left( \frac{\mu_{eff}}{Sc_{eff}} \frac{\partial c}{\partial x_j} \right) + \rho_u S_t |grad c|, \quad (10-83)$$

where  $\rho$  is the density,  $\rho_u$  is the unburned methane-air mixture density,  $u_j$  is the velocity component along  $x_j$  coordinate,  $\mu_{eff}$  and  $Sc_{eff}$  are the effective viscosity and effective Schmidt number,  $S_t = S_u \cdot \Xi$  is the turbulent burning velocity that is the product of the laminar burning velocity, which is a function of pressure and temperature,  $S_u = S_u \cdot \pi^\epsilon$ , and the turbulence factor,  $\Xi$ .

To account for the combustion of non-uniform methane-air mixtures outside the enclosure the LES model was extended by an additional conservation equation for air concentration (Molkov et al., 2006b)

$$\frac{\partial}{\partial t}(\rho Y_a) + \frac{\partial}{\partial x_j}(\rho u_j Y_a) = \frac{\partial}{\partial x_j} \left( \frac{\mu_{eff}}{Sc_{eff}} \frac{\partial Y_a}{\partial x_j} \right) - \frac{Y_a}{Y_f + Y_a} \rho_u S_t |grad c|, \quad (10-84)$$

where  $Y_a$  is the air concentration and  $Y_f$  is the initial flammable mixture concentration.

The laminar burning velocity and the heat of reaction in simulations were dependent on the methane concentration in the flammable mixture. The combustion products composition did not vary with the methane concentration and were equal to those of the initial 10.5% methane-air mixture and led to a negligible error in the molecular mass and the specific heat capacity used in the model.

Figure 10–23 shows the calculation domain. It comprised the enclosure itself and a relatively large hemispherical area around the enclosure ( $R=60$  m) to exclude the effects of boundary conditions on the external combustion and to accommodate the diverging pressure wave generated by the coherent deflagrations. The calculation domain was meshed using an unstructured tetrahedral grid, which allows meshing of arbitrary complex calculation domains and concentrating control volumes (CVs) locally in the area of interest reducing the total number of CVs. It does not have preferential directions compared to structured grids. The average edge size of CVs was 0.8 m inside and outside the enclosure where combustion occurred. The characteristic CV size was smoothly increased up to 23 m in the rest of the domain. The total number of CVs was 87,156 that is relatively moderate, keeping in mind the complex geometry and scale of the problem.

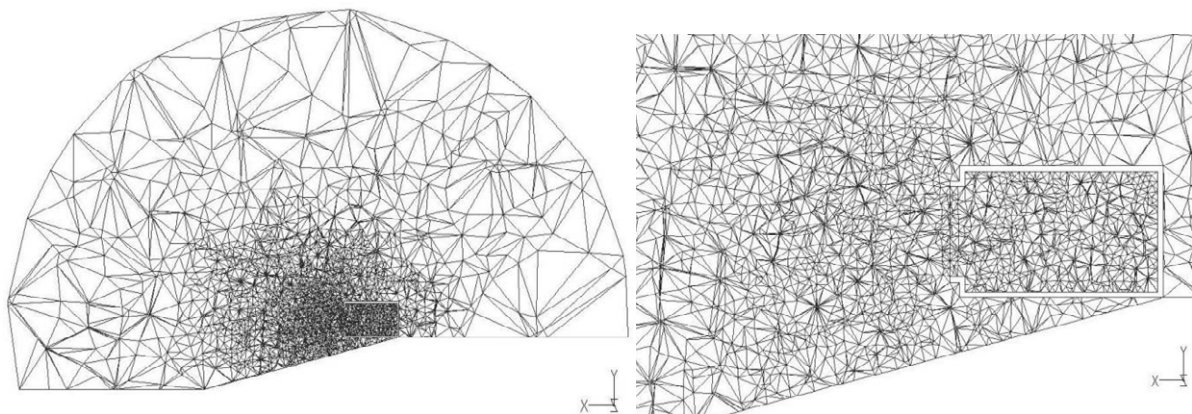


**Figure 10-23.** Calculation domain meshed by unstructured tetrahedral grid:  
general view (left), enlargement of area close to the vessel.

Boundary conditions used for simulations included: no-slip, non-permeable, adiabatic conditions on all walls and ground surfaces and non-reflecting flow conditions at the domain boundary at the atmosphere. At initial conditions the flammable mixture inside the enclosure and air in the atmosphere were quiescent, pressure was equal to atmospheric,  $p=101325$  Pa, and temperature was equal to  $T=285$  K. The initial values  $c=0$ ,  $Y_f=0.061$ ,  $Y_a=0.939$  were used inside the enclosure and  $c=0$ ,  $Y_f=0$ ,  $Y_a=1$  in the atmosphere. Combustion was initiated by a slow increase of the progress variable in one CV at the centre of the rear wall over the first 50 ms.

With us you can  
shape the future.  
Every single day.

For more information go to:  
[www.eon-career.com](http://www.eon-career.com)

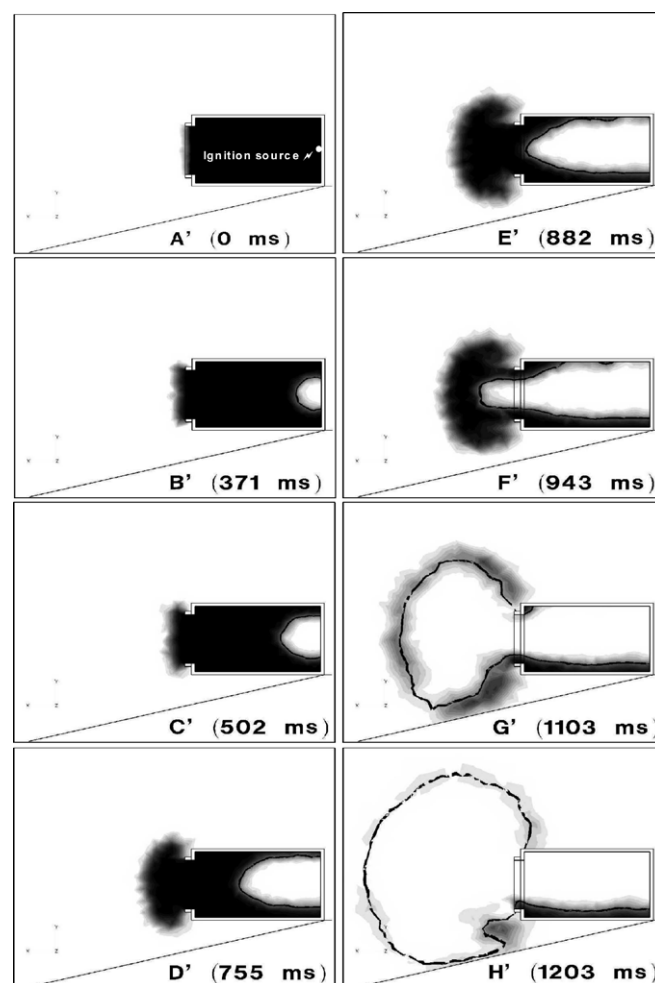
Your energy shapes the future.

**e-on**

The direct application of the LES model to simulate coherent deflagrations in the empty SOLVEX facility, with the turbulence factor  $\Xi=1$ , failed to reproduce experimental pressure dynamics in different locations inside and outside the enclosure. Carried out numerical experiments proved that only introduction of an ad hoc parameter to the model, accounting for unresolved increase of burning rate in the starting vortex region outside the enclosure, enables to reproduce experimental pressure transients of the coherent deflagrations (concurrent premixed combustion inside and outside the enclosure).

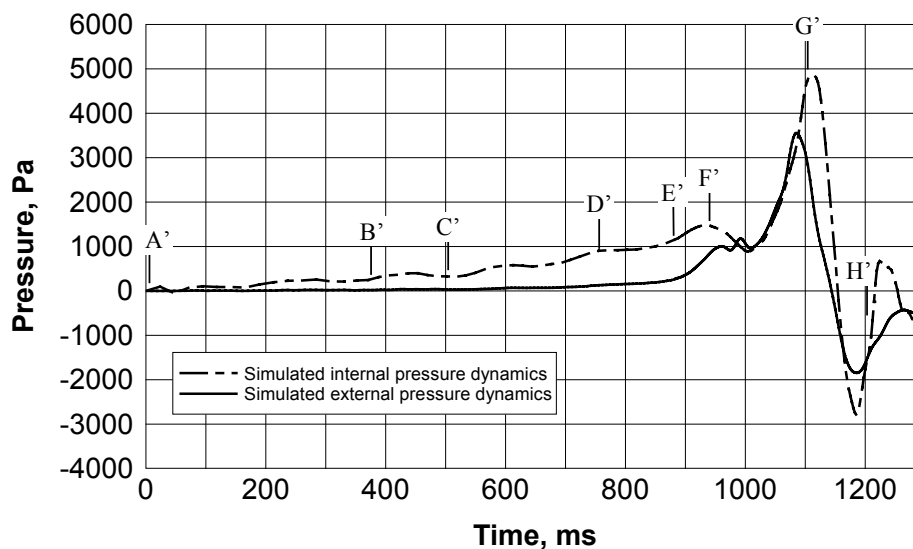
Presented below results of numerical simulations were obtained with the turbulence factor  $\Xi$  linearly growing in the model in the area outside the enclosure from its default value 1 to 2 during the interval of 100 ms following the flame front emerging from the edge of the vent. The reason for the introduction of this ad hoc wrinkling factor in the area of turbulent wake behind the vent edges is apparent: to resolve small-scale swirls generated in this region a much finer grid would be required compared to the applied grid with average cell size in the combustion area of 0.8 m.

Figure 10–24 shows the simulated deflagration flame front propagation and locations of flammable mixture and methane concentrations outside of enclosure.



**Figure 10–24.** Simulated flame front position (black line,  $c=0.5$ ), location of flammable mixture and methane concentration (black/grey scale palette) in the centre-line cross-section.

Simulated pressure transients are obtained at the same locations inside and outside enclosure as in the experiment and are shown in Fig. 10–25. Snapshots A' through H' in Fig. 10–24 corresponds to the times A' through H' in Fig. 10–25.



**Figure 10–25.** Simulated pressure transients of the coherent deflagrations inside and outside the enclosure.

The development of a simulated turbulent combustion zone outside the enclosure (Fig. 10–24) is similar to the experimentally observed (Fig. 10–21). The geometrical centre of the external explosion at the final stage of combustion (Fig. 10–24, frame H') is at a distance of about 5–6 m from the vent, which corresponds to the experimental observations by Puttock et al. (1996). Formation of the vortex structure in the flammable mixture flowing out to the atmosphere through the vent is clearly seen in Fig. 10–24.

Simulated pressure dynamics of coherent deflagrations given in Fig. 10–25 matches experimental pressure transients (Fig. 10–22). Flame arrival time to the vent is very close to the experimental time.

The LES model reproduces the internal deflagration during the whole period of the coherent deflagrations development without introduction of any ad hoc parameter to describe complex interactions of flow, turbulence and combustion inside the enclosure.

The internal pressure dynamics is reproduced in simulations for the whole period of combustion, including the first pressure peak associated with a start of combustion products outflow from the enclosure, the second pressure peak associated with the coherent external/internal deflagrations, and the negative pressure peak related to the momentum of expanding products of the “external explosion”. The amplitude of the negative pressure peak for simulated external explosion at a location 6.1 m outside the enclosure is about half that found in experiment.

Combustion at the top part of the vent at the time 1203 ms (frame G in Fig. 10–21 and frame H' in Fig. 10–24) is not apparent in Fig. 10–24 yet simulations demonstrated that there is still flammable mixture at the top of the vessel at this moment. The explanation could be that Fig. 10–24 shows snapshots of the process in the centre-line vertical cross-section whereas experimental video records show combustion at the upper part of the vent originating from the top corners of the enclosure.

Finally, there is a “residual” combustion at the bottom side of the enclosure (after the time 1203 ms in Fig. 10–24, frame H') that gives rise to somewhat higher pressure in the enclosure compared to the outside pressure following the negative pressure peak.

The development of coherent deflagrations inside and outside the enclosure generates an outward propagating pressure wave. Pressure outside of the SOLVEX enclosure was measured by pressure gauges, installed at distances 6.1, 30.3, 53.9 m far from the vent along the vessel centre-line. Comparison of experimental pressure dynamics at 6.1 m and experimental maximum pressures at 30.3 and 53.9 m with simulated pressure dynamics at the same locations is shown in Fig. 10–26. The simulations provide an excellent agreement with experimental data.

be > your degree

Bring your talent and passion to a global organization at the forefront of business, technology and innovation. Discover how great you can be.

Visit [accenture.com/bookboon](https://www.accenture.com/bookboon)

**Be greater than.**  
consulting | technology | outsourcing

**accenture**  
High performance. Delivered.

© 2013 Accenture  
All rights reserved.

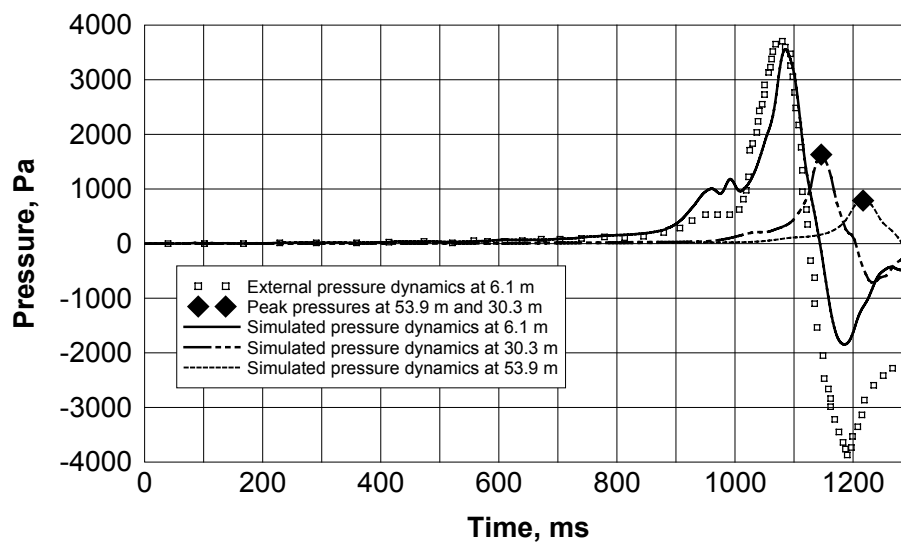


Figure 10–26. Experimental and simulated pressure dynamics and pressure peaks outside the enclosure.

Figure 10–27 shows simulation results for the flame arrival time along the enclosure centre-line axis in comparison with the experimental data reported by Bradley et al. (2001). The flame front position in Fig. 10–27 is associated with value of the progress variable  $c = 0.5$ . During the initial stage of simulations the flame front profile, which requires at least 3-4 computational control volumes, is just forming and is not shown for radii below 1 m. The simulated propagation of the wrinkled flame front beyond 1 m is in a good agreement with both experimental records and theoretical predictions by Bradley et al. (2001).

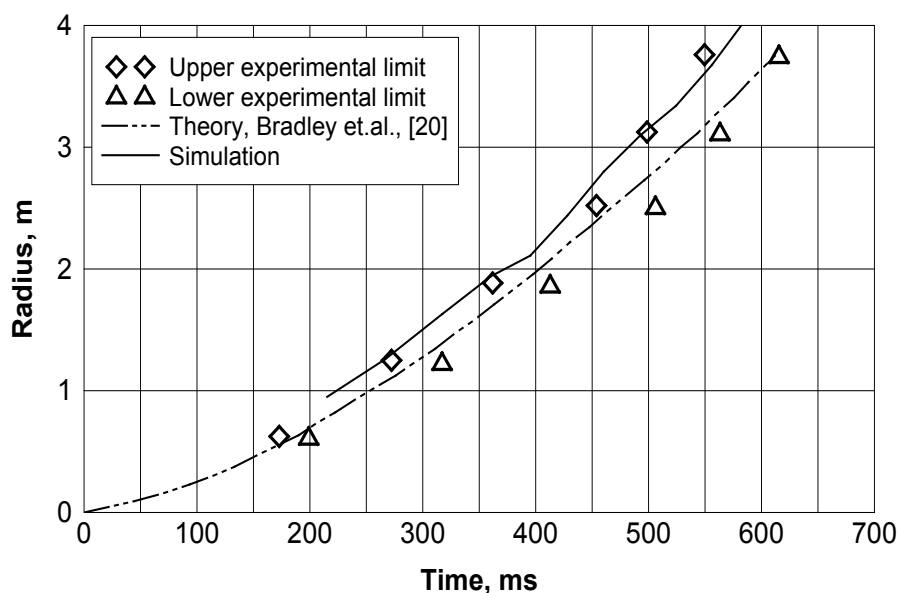


Figure 10–27. Flame front position along a centre-line inside the SOLVEX enclosure (Molkov and Makarov, 2006c).



#### 10.4.7.4. Concluding remarks

The phenomenon of coherent deflagrations in the SOLVEX empty facility-atmosphere system is analysed experimentally and numerically. The processing of experimental pressure transients inside and outside enclosure by the LES deflagration model underpinned important conclusions on the nature of coherent deflagrations. The formation of the starting turbulent vortex in the flammable mixture pushed out of the enclosure during the internal deflagration is a prerequisite for a subsequent intensification of turbulent combustion outside the enclosure.

The rapid increase of the burning rate outside the enclosure commences not at the moment when the flame front emerges from the vent but after the flame front reaches the edges of the vent. The coherent steep pressure rise is observed both inside and outside the enclosure after this instance. The pressure rise in the atmosphere is a direct consequence of the highly turbulent deflagration outside the enclosure. At the same time there is no increase of the burning rate inside the enclosure. The pressure rise inside the enclosure is caused by the decrease of mass flow rate from the enclosure to the atmosphere due to the decrease of pressure drop at the vent as a result of intensive combustion of emerged flammable mixture in the atmosphere in front of the vent.

The ad hoc parameter should be introduced into the LES model to account for increase of the burning rate outside the enclosure due to generation of small-scale swirling structures in the flow downstream the vent edges that is unresolved in the simulations on a quite coarse grid with average control volume edge size in the area of combustion 0.8 m. The LES model correctly reproduces experimental pressures at different locations inside and outside the enclosure and the development of the deflagration in the atmosphere when the ad hoc parameter is gradually increased outside the enclosure from its default value of 1 to 2 in a time equal to the completion of the external combustion. The application of an ad hoc parameter inside the enclosure, or both inside and outside the enclosure, leads to inadequate dynamics of the coherent deflagrations (Molkov and Makarov, 2006c).

#### 10.4.8. Large-scale hydrogen-air deflagrations in the open atmosphere

The emphasis in combustion research for energy applications differs from that in accidental combustion research, e.g. hydrogen safety. Large flow turbulence, high flame strain rates and relatively small scales of inhomogeneous regions are characteristic for most combustion devices. These features can differ radically from that in large-scale unwanted deflagrations. The initial stage of flame propagation at accident often takes place in a quiescent or moderately agitated mixture in a quasi-laminar mode. While combustion research is mainly focused on the aspects of flame behaviour to increase the efficiency of burning, hydrogen safety research is focused on deflagration mitigation. Conventional models, used to design combustion devices, may not be appropriate to analyse large-scale deflagrations as regularities and physical phenomena for freely propagating accidental flames can be different from those for stabilised flames, e.g. burner flames.



Theoretical considerations by Zeldovich et al. (1980) admit deflagration-to-detonation transition (DDT) of free spherical premixed combustion due to flame front instabilities and acceleration. Hydrogen-air deflagrations in unconfined conditions were studied experimentally by Makeev et al. (1983). A spark with energy of 1 J was used to ignite a mixture in the centre of a rubber balloon of initial volume 35 m<sup>3</sup> or 86 m<sup>3</sup> of diameter about 4 m and 5.5 m respectively. Experiments in a 4 m diameter balloon demonstrated that flame front acceleration at the initial stage of combustion ceased and flame propagated with a practically constant velocity of 38 m/s in a mixture with 35% by volume of hydrogen in air. In a 5.5 m diameter balloon test the flame propagation velocity was continuously increasing to 105 m/s for the mixture with the same concentration of hydrogen. The authors (Makeev et al., 1983) concluded that the maximum velocity is increasing with diameter of initial cloud and for volume larger than 500 m<sup>3</sup>, diameter larger than 10 m, DDT is possible. In the same year 1983 experimental studies of large-scale hydrogen-air deflagrations with hemispherical volumes of up to 2094 m<sup>3</sup> were performed in Germany (Pförtner and Schneider, 1983, 1984; Pförtner, 1985; Becker and Ebert, 1985). Tests were conducted with ignition sources of energy within the range from 10 to 1000 J in near stoichiometric hydrogen-air clouds with diameter of hemisphere up to 20 m. No DDT was registered.

Characteristics of a blast wave from unconfined deflagration differ from that of high explosives. For example, in a near-field the overpressure from the positive phase of gaseous explosion is much less compared to high explosives, while the duration of this phase is greater. In a far-field, pressure waves from deflagrations decay slower with distance from a source of initiation and cannot be described by means of the TNT-equivalence concept (Gorev, 1982; Dorofeev et al., 1995b). The TNT-equivalence concept is inadequate to describe the large amplitude of the negative phase of gaseous explosions (Dorofeev et al., 1995b), which is larger than the positive phase amplitude for deflagrations (Gorev, 1982).



"I studied English for 16 years but...  
...I finally learned to speak it in just six lessons"

Jane, Chinese architect

ENGLISH OUT THERE

Click to hear me talking before and after my unique course download

Bradley (1999) suggested that in case of large-scale deflagration flames “the fractal analyses is probably valid because of the large length-scales and small flame stretch rates, unlike turbulent flames in many engineering applications where the flame stretch rate usually reduces the burning rate”. This statement is in line with the results of analysis of 20 unconfined gaseous deflagrations carried out by Gostintsev et al. (1988). They described the behaviour of spherical turbulent premixed flames propagation as a self-similar process in which a total flame front surface area grows  $R^{1/3}$  times faster (theoretical fractal dimension  $D=2.33$ ) than surface of a sphere with the same radius.

According to the fractal theory a ratio of the turbulent flame front area  $A_t$  to the area of the smooth laminar spherical flame  $A_{u0}$  is equal to  $A_t/A_{u0} = S_t/S_u = (\lambda_o/\lambda_i)^{(D-2)}$  (Gouldin, 1987), where  $S_u$  is the laminar and  $S_t$  is the turbulent burning velocities respectively. Bearing in mind, that for freely propagating flames, the outer cut-off  $\lambda_o$  is growing proportionally to the flame front radius  $R$  and the inner cut-off  $\lambda_i$  can be accepted as a constant, the turbulent burning velocity  $S_t$  is a function of the average flame front radius  $R$ :  $S_t/S_{t0} = (R/R_0)^{(D-2)}$ , where  $S_{t0}$  is the turbulent burning velocity at radius  $R_0$ . Gostintsev et al. (1988) reported that for near stoichiometric hydrogen-air mixtures a self-similar regime of flame propagation is established at critical radius of 1.0–1.2 m. After the critical radius the turbulent flame front surface is contorted and thus the fractal theory can be applied.

Different values have been proposed for the fractal dimension,  $D$ . Gouldin (1987) used  $D=2.37$  adopted from Abdel-Gayed et al. (1984). A wide range of experimental values of fractal dimension  $D=2.11$ – $2.36$  was cited for premixed combustion by Gulder (1990). Bradley (1999) suggested to apply the theoretical value  $D=2.33$  for freely propagating flames. Gostintsev et al. (1999) suggested for self-similar freely propagating flames the fractal dimension in the range  $D=2.2$ – $2.33$ . Gulder et al. (2000) reported the fractal dimension within the range  $D=2.14$ – $2.24$  for turbulent premixed combustion in Bunsen-type burners.

This section is devoted to further development of the LES model of large-scale deflagrations and validation of the model. Two combustion sub-models will be tested, one is based on the renormalization group (RNG) theory and another on the fractal theory. Numerical simulations will be compared against the largest ever performed experiment on stoichiometric hydrogen-air deflagration in 20 m diameter hemisphere in the open atmosphere GHT 34 (Pförtner and Schneider, 1983). The comparison will be carried out for flame radius, flame shape and pressure transients at different distances from the ignition source (Molkov et al., 2006a).

#### 10.4.8.1. Largest hydrogen-air deflagration test in atmosphere

A series of experiments with near stoichiometric hydrogen-air deflagrations in unconfined hemispherical volumes was performed by Pförtner and Schneider (1983) in the Fraunhofer Institute for Fuels and Explosive Materials. The experimental conditions and maximum observed flame speed are presented in Table 10–4. The principal aim of these experiments was to investigate the dependency of flame propagation velocity on the hydrogen-air cloud size. Mixtures were ignited at the ground level inside the shell made of thin polyethylene (PE) film to exclude the effect of reflected pressure waves. Burnout of the cloud occurs approximately at two initial diameters that is approximately equal to the cubic root of the products expansion coefficient.

Test No.	$C$ , % vol.	$T_i$ , K	$p_i$ , kPa	$E_{ign}$ , J	$V$ , $m^3$	Hemisphere diameter, m	Maximum flame speed, m/s	$S_{ui}^{exp}$ m/s
GHT 23	29.1	282	98.1	10	7.5	3.06	43	2.31
GHT 26	29.2	281	99.1	1000	7.5	3.06	43	2.32
GHT 39	29.4	279	98.5	1000	50	5.76	50	-
GHT 40*	29.5	279	98.5	150	50	5.76	54	-
GHT 11	31.0	281	100.7	314	262	10.0	60	2.50
GHT 13	25.9	283	100.9	314	262	10.0	48	1.94
GHT 34*	29.7	283	98.9	150	2094	20.0	84	2.39

\* – experiments with rhombus-shaped wire net over the hemispherical balloon (in GHT 34 test the rhombus-wire net was laid over balloon to compensate approximately 7500 N buoyant force).

**Table 10–4.** Experimental conditions and results for different tests (Pförtner and Schneider, 1983).

After burnout the peak deflagration overpressure decays in the form of pressure wave with positive and negative phases. The duration of the positive and the negative phases is independent of the distance for any given size of balloon. The amplitude of negative pressure peak was usually somewhat larger than that of the positive pressure phase and the negative phase being of shorter duration. Pförtner and Schneider (1983) for spherical sonic waves cited a theoretical result derived by Landau that at any distance the integral of overpressure in time should be equal to zero. This theoretical result complies with experimental records of the outward propagating pressure wave outside the combustion area (see pressure transients at distance 35 m and 80 m from the ignition point below).

Processing of visual images of the flame propagation yielded a continuous increase in flame propagation velocity up to a maximum value, which was reached at a distance between the initial radius of the cloud  $R_{hsph}$  and  $1.5 R_{hsph}$ . For initially quiescent stoichiometric hydrogen-air mixture this upper limit was estimated as 125 m/s with a peak overpressure 13 kPa assuming the validity of the approach by Pförtner and Schneider (1983) based on simple turbulent combustion models of Damkohler and Karlovitz. The experimental results indicate that the flame propagation velocity approaches the upper limit with the increase of the cloud size.

In test GHT 34, with 29.7% by volume hydrogen-air mixture in a 20 m diameter hemisphere, the maximum flame propagation velocity was 84 m/s with the initial burning velocity estimated by Pförtner and Schneider (1983) as 2.39 m/s (the expansion coefficient of combustion products was calculated as 7.26 with a density of combustible mixture  $0.8775 \text{ kg/m}^3$  and a speed of sound 397.3 m/s). Errors in velocity measurements were assessed as  $\pm 5\%$  without taking into account certain asymmetries in flame propagation. In the  $2094 \text{ m}^3$  hemisphere experiment, GHT 34, a rhombus-shaped wire net was laid over the hemispherical balloon which was fastened to the ground at 16 points to compensate buoyancy force.

In order to make the hydrogen-air flame visible in daylight finely ground NaCl powder was dispersed inside the balloon at the end of filling process to produce a yellow-coloured flame. Generally 10 to 12 piezo-resistive Kistler pressure sensors (100 kPa range, natural frequency 14 kHz) were used. These were mounted in a steel case having a mass of 20 kg in a way that their pressure-sensitive surfaces were fitted flush with the surface of the ground and covered with a 2 mm thick layer of silicone grease on the membrane to avoid the influence of temperature and heat radiation. In addition a sensor, located at 5-m distance from the ignition source, was protected by means of a laminated plastic plate screwed to the steel casing and having an opening of 4 mm diameter in the middle. For the GHT 34 test an additional pressure sensor was installed at a right angles to the axis with main sensors and mounted on a vertical timber wall 1x1 m<sup>2</sup> (head-on measurement).

The deflagration pressure was measured at distances 2.0, 3.5, 5.0, 6.5, 8.0, 18, 25, 35, 60, and 80 m from the initiation point. The mixture was ignited by pyrotechnical charges with total ignition energy 150 J. The pressure transients of sensors inside the combustion products did not return to zero after the negative pressure phase, except for the sensor installed at 5 m. This can be attributed to the fact that the transducers were thermalized to high temperatures during the explosion. Since they did not remain at the temperature at which they were calibrated, they were no longer calibrated and did not return to the baseline. This is an indication that the protective measures taken by the experimenters to insulate these transducers were insufficient for this large test.



The advertisement features a grey background with a faint world map. In the top left corner is the Duke University logo, which includes the word "DUKE" in a blue box above "THE FUQUA SCHOOL OF BUSINESS". The text "BUSINESS HAPPENS" is written in large, white, sans-serif capital letters. Below it, the website "www.fuqua.duke.edu/globalmba" is shown, with "globalmba" in blue. An orange button with the text "Learn More >" is positioned at the bottom left. On the right side, there is a circular collage of eight diverse individuals' faces, with the word "HERE." in bold black text in the center of the circle.

Figure 10–28 shows that the flame propagated in an almost hemispherical form. The balloon shell first stretched slightly outwards until it burst when the flame had reached about half of the original radius of the balloon  $0.5R_0$ .

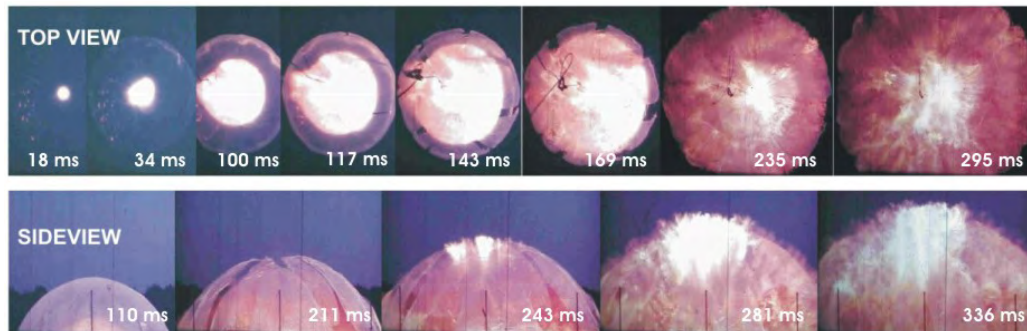


**Figure 10–28.** Snapshots of test GHT 34 in a 20 m diameter hemisphere (Molkov et al., 2006a).

The explosion overpressure of about 6 kPa was practically the same within the cloud distances in GHT 34 test. A sharp overpressure peak  $\Delta p_F$  of about 10 kPa in the pressure transients followed flame propagation. It could be an effect of a high temperature, gas dynamics effect, or it can be assumed that as the flame passed the pressure sensor, it ignited the gas in space between the laminated plastic plate with 4 mm diameter orifice and the sensor so that a partially confined explosion occurs causing the peak pressure  $\Delta p_F$ , similar to pressure peak generation in a vented vessel (mentioned above laminated plastic plates with 4 mm diameter opening could be considered as a vessel wall with a vent).

#### 10.4.8.2. Modelling and LES (RNG-Karlovits and fractal sub-models)

The dilution of hydrogen-air mixture by ambient air on the contact surface of the flammable cloud with the atmosphere was accounted for similar to our previous studies. The propagation of flame was simulated by the progress variable equation with the gradient method applied for the source term  $\bar{S}_c = \rho_u \cdot S_t \cdot |\nabla \tilde{c}|$ . The gradient method allows decoupling between a physical requirement to keep the turbulent mass burning rate equal to  $\rho_u S_t$  and a numerical requirement for a simulated flame front to occupy 4–5 control volumes, independent of a mesh size and a scale of a problem. Indeed, the integral of the source term throughout a numerical flame front thickness always gives a physically correct value for the mass burning rate per unit area, i.e.  $\rho_u S_t$ , independent of the numerical flame front thickness.

As a result of the gradient method use, simulations of flame front propagation and pressure dynamics will not be affected noticeably, regardless of the fact that the structure and size of a numerical flame front are not actual characteristics of the real flame front. Furthermore, tackling problems of practical interest with a scale of tens and hundreds of meters, there is no chance to resolve a structure of real turbulent flame front, where for example the turbulence generated by flame front itself plays a role at scales comparable with thickness of laminar flamelets of the order of millimetre. Nevertheless, the giving up of a fine flame front structure resolution allows one to reproduce reasonably hydrodynamics of flows ahead and behind of the numerical flame front, overall flame propagation and deflagration pressure dynamics because the energy release in the flame front is kept physically correct.



### Dependence of laminar burning velocity on pressure and temperature

The following form of the dependence of the burning velocity on hydrogen concentration,  $Y_{H_2}$ , temperature,  $T$ , and pressure,  $p$ , is applied in the LES model (in the approximation of adiabatic compressions and expansions the thermokinetic index  $\varepsilon = m + n - m / \gamma_u$ )

$$S_u(Y_{H_2}, T, p) = S_{ui}(Y_{H_2}) \cdot \left( \frac{T}{T_{ui}} \right)^{m(Y_{H_2})} \left( \frac{p}{p_i} \right)^{n(Y_{H_2})} = S_{ui}(Y_{H_2}) \cdot \left( \frac{p}{p_i} \right)^{\varepsilon(Y_{H_2})}, \quad (10-85)$$

where  $m$  and  $n$  are the temperature and the baric indices in the dependence of burning velocity on temperature and pressure respectively, and  $S_{ui}$  is the burning velocity at the initial conditions. This equation is a convenient and widely used approximation of the theoretical formula for burning velocity  $S_u \propto k \cdot p^n \cdot \exp(-E/2RT_b)$ , where  $k$  is the pre-exponential factor,  $E$  is the activation energy,  $R$  is the universal gas constant, and  $T_b$  is the temperature of combustion products. In a comparatively narrow range of temperatures between the temperature of combustion products at initial conditions,  $T_{bi}$ , and at the end of combustion,  $T_{be}$ , it was demonstrated that an error of the approximation does not exceed 15% (Babkin et al., 1966).

In former simulations (Molkov et al., 2006b) the dependence of burning velocity on hydrogen concentration was accounted for by using a linear function  $f(Y_{H_2})$ , equal to 1 in stoichiometric mixture (29.7% by volume of hydrogen) and 0 at the lower flammability limit (4% by volume of hydrogen)  $S_{ui}(Y_{H_2}) = S_{ui}^{Stoich} \cdot f(Y_{H_2})$ . The initial value of global (stretched) laminar burning velocity  $S_{ui} = 1.91$  m/s (Lamoureux et al., 2003) was applied here for 29.7% hydrogen-air mixture.

### RNG-Karlovits combustion sub-model

The first model of turbulent burning velocity  $S_t$  applied is based on the RNG premixed turbulent combustion model by Yakhot (1988) and the theoretical analysis of self-turbulized flames by Karlovitz et al. (1951). Based on the analysis by Karlovits et al. (1951) the maximum value of the flame wrinkling factor due to the turbulence generated by flame front itself can be estimated for high levels of flow turbulence, when the assumption  $S_t \approx u'$  is valid, as  $\chi_K^{\max} = (E_i - 1) / \sqrt{3}$ , where  $E_i$  is the expansion coefficient of combustion products that is a function of hydrogen concentration. For stoichiometric hydrogen-air mixture it gives value  $\chi_K^{\max} = 3.6$ .

The following dependence of the SGS flame wrinkling factor on the flame front radius was applied to model a gradual increase of the flame front surface area due to the turbulence generated by flame front itself during transition from laminar to fully developed turbulent flame

$$\chi_K(R) = 1 + (\chi_K^{\max} - 1) \left( 1 - \exp\left(-\frac{R}{R_0}\right) \right), \quad (10-86)$$

where  $R_0$  is the characteristic radius at which transition to the self-similar turbulent regime of flame propagation takes place. Gostintsev et al. (1988) reported that the characteristic radius for onset of a self-similar regime of flame propagation for stoichiometric hydrogen-air mixture is  $R_0 = 1.0 - 1.2$  m and the value  $R_0 = 1.2$  m was adopted here.

The joint effect of the multi-scale flow turbulence and the SGS turbulence generated by flame front itself (this type of turbulence is generated at scales comparable with flame front thickness, i.e. at scales essentially smaller compared to the size of computational mesh used in simulation of large scale problems) on the turbulent burning velocity was accounted for through the implementation of the modified Yakhot's (1988) formula for premixed turbulent combustion, based on the RNG theory of turbulence, into the LES model in the form of transcendental equation

$$S_t = [S_u \cdot \chi_K(R)] \cdot \exp\left(\frac{u'}{S_t}\right)^2. \quad (10-87)$$

The difference with the original Yakhot's formula is the use of SGS turbulent burning velocity  $[S_u \cdot \chi_K(R)]$  instead of the laminar burning velocity  $S_u$ . This is to account for an unresolved in simulations physical phenomenon of turbulence generated by flame front itself, acting at sub-grid scales, in the LES model.

## Join American online LIGS University!

Interactive Online programs  
BBA, MBA, MSc, DBA and PhD

### Special Christmas offer:

- ▶ enroll **by December 18th, 2014**
- ▶ **start studying and paying only in 2015**
- ▶ **save up to \$ 1,200** on the tuition!
- ▶ Interactive Online education
- ▶ visit [ligsuniversity.com](http://ligsuniversity.com) to find out more!

Note: LIGS University is not accredited by any nationally recognized accrediting agency listed by the US Secretary of Education. More info [here](http://ligsuniversity.com).



**Fractal combustion sub-model ( $R > R_0$ )**

The second combustion sub-model, applied at the stage of the LES model development in 2006 to simulate the open atmosphere hydrogen-air deflagration, is based on the fractal analysis of the freely propagating premixed flames, and was described by Makarov et al. (2007a). Following the conclusions of the fractal theory the burning velocity is modelled as

$$S_t = S_t^{R_0} \cdot f(Y_{H_2}) \cdot \left( \frac{R}{R_0} \right)^{D-2}, \quad (10-88)$$

where  $S_t^{R_0}$  is the burning velocity at the critical radius  $R_0$  for the onset of the self-similar (fractal) regime of flame propagation and  $D$  is the fractal dimension. Self-similar (fractal) regime of flame propagation takes place at flame radii above the critical  $R > R_0$ . Hence, the fractal combustion sub-model can be applied with confidence only after that.

It is important to note that the simulations of the transitional stage of the deflagration (flame radii  $R \leq R_0$ ) were performed by the RNG-Karlovits combustion sub-model. The value of burning velocity, extracted from the RNG-Karlovits sub-model at  $R=R_0$  for implementation in formula (10-83) of the fractal sub-model, was calculated as  $S_t^{R_0}=6.44$  m/s by the following procedure. The location of a simulated flame front, at any moment of time, was determined by the averaging of coordinates of all control volumes with values of the progress variable within the range  $c=0.01-0.99$ . At the moment when radius of the flame front became equal to  $R_0$  a total mass burning rate in the flame front was calculated. Then, to obtain the sought burning velocity, the mass burning rate was divided by the product of a combustible mixture density and the area of the hemisphere with radius  $R_0$ . The obtained value  $S_t^{R_0}=6.44$  m/s is by  $\chi=6.44/1.91=3.37$  times larger compared to initial laminar burning velocity of 29.7% by volume hydrogen-air mixture. This augmentation of the burning velocity is due to effects of turbulence generated by flame front itself and flow turbulence. The augmentation of burning velocity for radii  $R > R_0$  was calculated by the fractal combustion sub-model, equation (10-88), instead equations (10-86) and (10-87) in the RNG-Karlovits sub-model.

**Numerical details**

Initial temperature and pressure were taken as in the experiment 283 K and 98.9 kPa respectively. Hydrogen-air mixture and ambient air were quiescent at the moment of ignition,  $u=0$ . The progress variable was set as  $c=0$  all over the domain. Air concentration was equal  $Y_a = 0.9713$  within the hydrogen-air cloud ( $R \leq R_{hsph}$ ) and  $Y_a = 1.0$  beyond it ( $R > R_{hsph}$ ). The no-slip impermeable adiabatic boundary condition was used on the ground. Non-reflecting boundary conditions were used on the boundaries representing far-field in the atmosphere.

Ignition was modelled by increase of the progress variable from  $c=0$  to  $c=1$  in one control volume (CV) during a period  $\Delta t=22$  ms calculated as a time of flame propagation through spherical CV equal by volume to the ignition tetrahedral CV. The value  $c=1$  was kept in the ignition CV until moment 29 ms. No adjustment of simulation results in time (pressure transient shift along the time axis) was required with this procedure.

The calculation domain with sides  $LxWxH=200x200x100$  m was created to simulate both the flame front and the pressure wave propagation. The characteristic size of the tetrahedral CVs in the flame propagation area ( $R \leq 22$  m) was about 1 m and the characteristic size of the hexahedral CVs in the rest of the domain ( $R \leq 30$  m) was 4 m. The transitional area ( $22 < R < 30$  m) was meshed using tetrahedral mesh with CV size changing from 1 to 4 m. The total number of CVs was 294,296.

The grid sensitivity analysis was conducted for the RNG-Karlovits combustion sub-model. Two similar grids with a characteristic CV size in the area of flame propagation 1.0 m and 0.5 m, respectively, were used. The difference in the flame front propagation dynamics, i.e. the growth of the flame front radius in time, was about 5%. This difference is due to better resolution of the flame front wrinkling by the hydrodynamic instability for a finer grid, which provides a larger mass burning rate and, thus, faster flame propagation.

The FLUENT 6.2.16 solver was employed as a platform for the realisation of the LES model. The double precision parallel version of the solver was used with explicit linearisation of the governing equations. The second order upwind scheme was used for convection terms and the central difference scheme for diffusion terms. 4-stage Runge-Kutta scheme was applied for time stepping. The Courant-Friedrichs-Lewy number was equal  $CFL = 0.8$  to ensure stability. Simulation of real time of deflagration and pressure wave propagation up to 0.63 s takes about 6 days on a workstation IBM630 (12GB RAM, 2CPUx1.2GHz Power 4, 1CPU SPECfp=961).

### ***Simulation results: flame shape***

Figure 10-29 shows the simulated flame front propagation for experiment GHT 34. Distinctive large-scale wrinkling of the flame front by the hydrodynamic instability can be seen. The cascade of characteristic wrinkles above a LES filter size, i.e. cell size in the numerical LES approach (Pope, 2004), of 1 m are close in size to experimentally observed hydrogen-air flame wrinkles (Pförtner and Schneider, 1983).

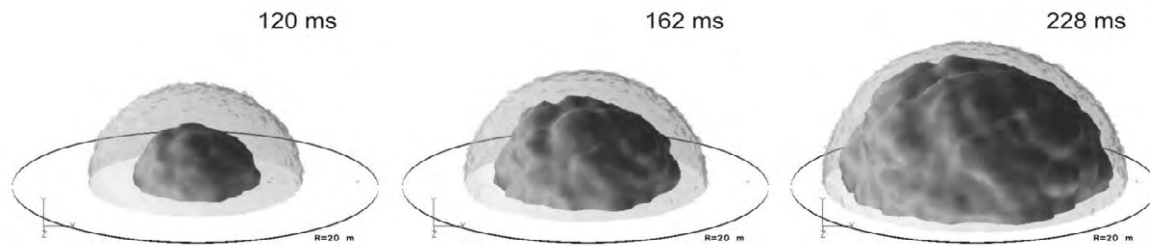


**Figure 10-29.** Snapshots of numerical simulation of flame front propagation in test GHT 34: dark grey – flame front iso-surface  $c=0.5$ , light grey – unburnt hydrogen-air mixture (Molkov et al., 2006).

### *Simulation results: flame front propagation and pressure dynamics*

Figures 10-30, 10-31 and 10-32 show a comparison between experimental results (test GHT 34) and numerical simulations. Experimental data on flame propagation dynamics are represented in Figs. 10-30 and 10-31 as a changing in time position of a leading flame front edge. The thickness of a simulated flame front is shown in Fig. 10-30a by hatched area with the leading flame edge depicted by solid line. At final stages of the deflagration the thickness of the numerical flame front is about 4 m which is close to experimental observations (Molkov et al., 2007a).



**MASTER IN MANAGEMENT**

#1 EUROPEAN BUSINESS SCHOOL  
FINANCIAL TIMES 2013

**#gobeyond**


**Because achieving your dreams is your greatest challenge.** IE Business School's Master in Management taught in English, Spanish or bilingually, trains young high performance professionals at the beginning of their career through an innovative and stimulating program that will help them reach their full potential.

- Choose your area of specialization.
- Customize your master through the different options offered.
- Global Immersion Weeks in locations such as Rio de Janeiro, Shanghai or San Francisco.

*Because you change, we change with you.*

[www.ie.edu/master-management](http://www.ie.edu/master-management)

[mim.admissions@ie.edu](mailto:mim.admissions@ie.edu)







Both considered combustion sub-models reproduce the deceleration of flame at the final stage of the explosion. This deceleration is caused by dilution of the initial hydrogen-air mixture by ambient air and thus the decrease of the burning rate (see Fig. 10–31a). The deceleration of the numerical flame front is more pronounced compared to the experiment. This could be attributed to noticeably large cell sizes used in the simulations in the areas of mixture non-uniformity. Performing simulations on an adaptive grid in the area of large hydrogen concentration gradients could improve predictive capability of the model at final stages of the deflagration.

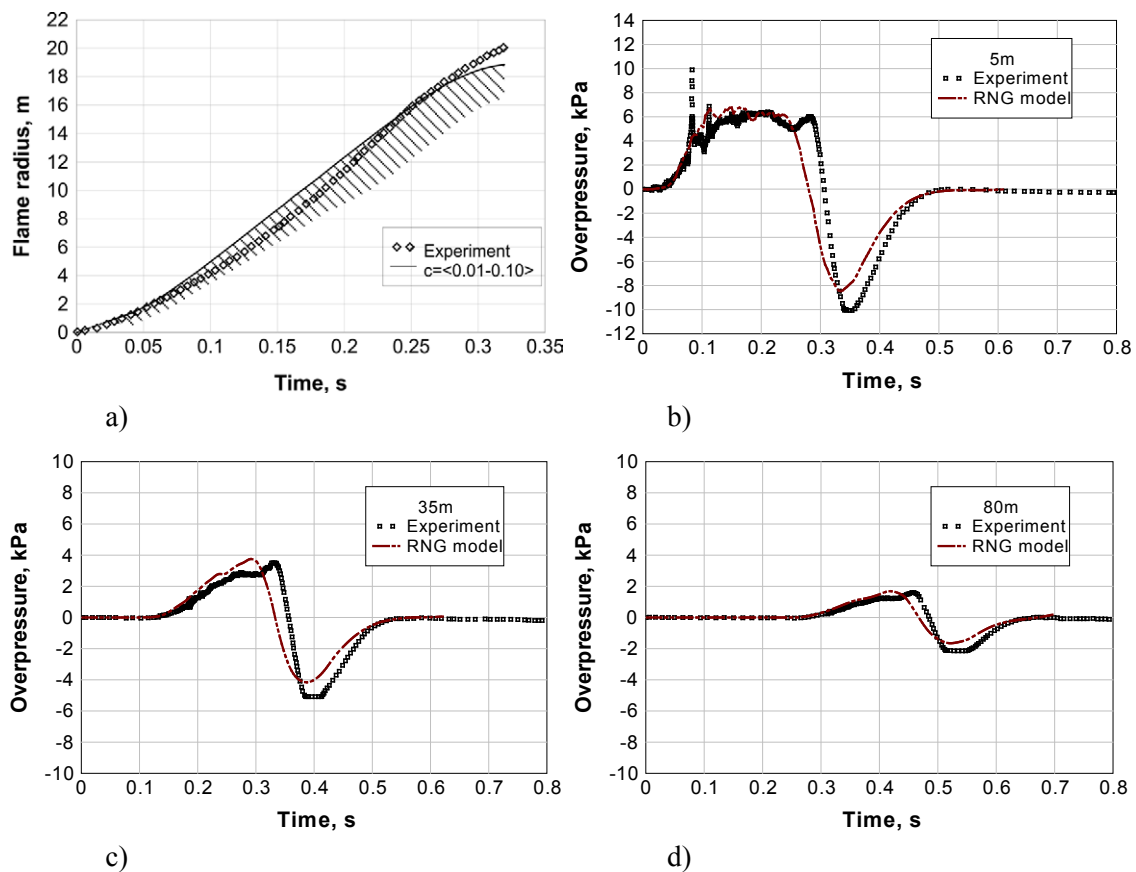


**Figure 10–30.** Comparison between the experiment and simulations by the RNG-Karlovits combustion sub-model:

- a) flame front propagation dynamics: solid line – leading flame front edge (averaging through CVs with the progress variable within the range 0.01 to 0.10), hatched area – numerical flame front thickness;
- b)-d) pressure transients at distances from ignition source  $R=5$  m,  $R=35$  m, and  $R=80$  m respectively.

For the RNG- Karlovits combustion sub-model the maximum deviation of the simulated leading flame front edge from the experimental one does not exceed 1 m. With this obviously “not bad” agreement between the LES model and the experiment, the acceleration of the real flame front is reproduced only in the initial stage of the deflagration. At later stages simulations give practically constant flame propagation velocity (Fig. 10–30a).

The simulated pressure dynamics (Figs. 10–30, b-d) is close to experimental pressure transients at locations of properly functioning transducers at distances 5 m, 35 m, and 80 m. Both positive and negative phases of the pressure wave are reproduced by the numerical experiment, including arrival time, duration and decay of the pressure wave with distance. The amplitude of the positive phase of the pressure wave is reproduced in simulations exactly with a bit faster arrival time in a far-field. However, amplitude of the negative phase is up to 30% less than in experiment. The simulated rear front of the positive phase overpressure wave passes ahead of experimental one due to significantly stronger deceleration of the flame front in simulation at the end of the simulated deflagration compared to the experiment.

Simulation results of the flame front propagation for two cases, with fractal dimensions  $D=2.33$  and  $D=2.22$ , are presented in Fig. 10–31a. The fractal sub-model reproduces the monotonic increase of the flame front propagation velocity similar to the experiment. Deflagration overpressure dynamics is shown in Figs. 10–31, b-d. The simulation with theoretical fractal dimension  $D=2.33$  obviously over predicts both flame propagation and overpressure dynamics. During numerical experiments it was found that a best fit value for the flame propagation dynamics for the fractal sub-model is  $D=2.22$ . This is within the range  $D=2.20$ – $2.33$  reported by Gostintsev et al. (1988). One of possible reasons for the backfitted fractal dimension  $D=2.22$  to be below the theoretical value 2.33 is a partial resolution of the flame front wrinkling structure by LES. Indeed, it was found that for spherical flames the resolved fractal dimension is within the range 2.02–2.15 (Molkov et al., 2004c).

Along with a good agreement in prediction of the amplitude of the negative phase of the pressure wave the fractal sub-model over predicts the amplitude of the positive phase by up to 50%. The reason for over prediction of the positive pressure peak by the fractal model is not clear. This could be due to the effect of PE balloon on the pressure wave. Indeed, segments of a balloon could “consume” part of the energy in the pressure wave in the test. The effect of PE balloon segments is weakened at later stages and as a result the negative phase amplitude could be less affected.

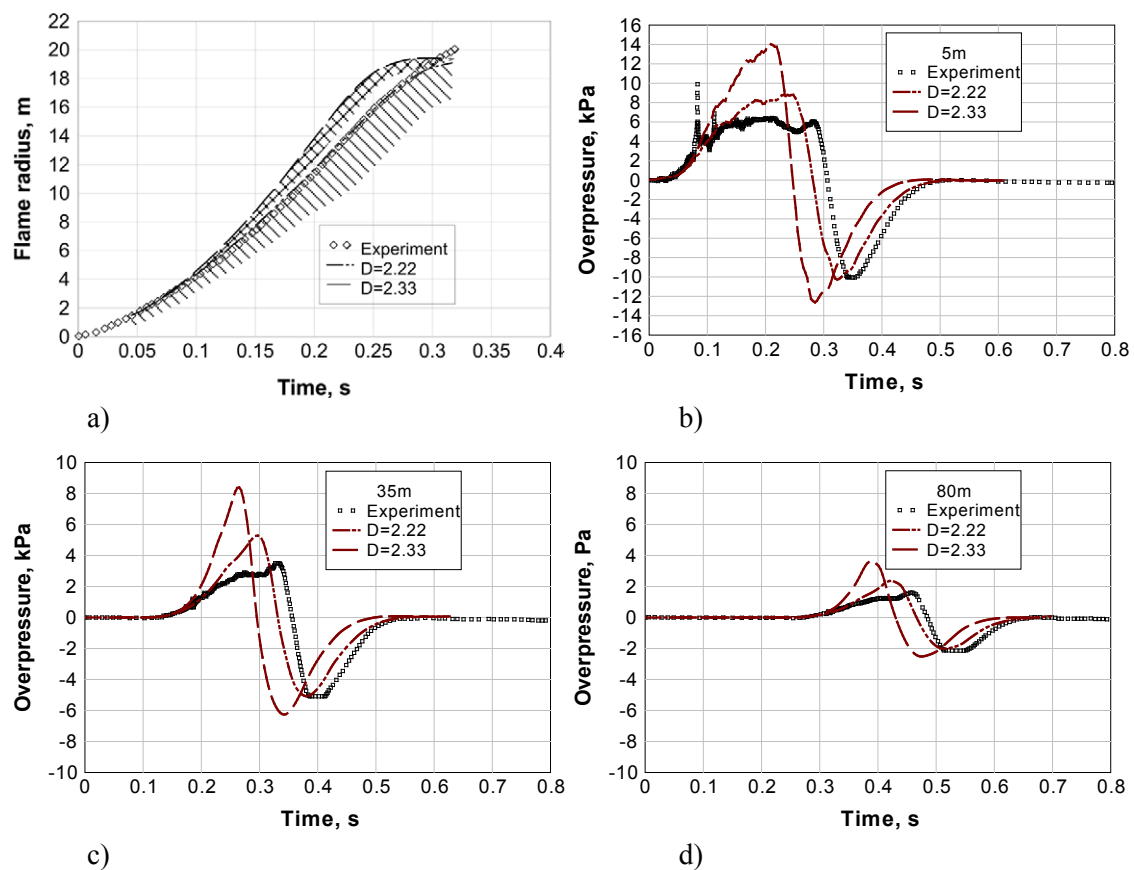


**Figure 10-31.** Comparison between experiment and simulations by the fractal combustion sub-model with two values of the fractal dimension  $D=2.22$  and  $2.33$ : a) flame front propagation dynamics: lines – leading flame edge (averaging through CVs with the progress variable within the range 0.01 to 0.10), hatched area – numerical flame front thickness (only partially reproduced for  $D=2.33$ ); b)-d) pressure dynamics at distance  $R=5$  m,  $R=35$  m, and  $R=80$  m respectively.

The positive phase of the pressure wave at transducer locations inside the combustion zone, i.e. 2 m, 5 m, 8 m, and 18 m, are shown in Fig. 10-32. Transducers located at 2 m, 8 m, and 18 m from the ignition source were affected by the combustion products as their pressure transients didn't return back to atmospheric pressure after the explosion. Still, pressure readings from these transducers may be used for explosion analysis until time of flame arrival.



A distinctive sharp overpressure peak  $\Delta p_F$  of about 10 kPa in the pressure transients followed flame propagation (see Figs. 10–32, b–c). The simulations reproduced an overpressure peak at the moment when the flame front arrived at the sensor's location. Experimental pressure peak appears somewhat earlier compared to simulation results. This is in agreement with experimental data (Pfortner and Schneider, 1983) where it was reported that the flame proliferates along the pressure measurement axis much more rapidly than in other directions. The fact of higher  $\Delta p_F$  at 5 m and 8 m transducers could be explained by the intensification of combustion after the balloon shell had burst when the flame reached about half of the original radius of the balloon  $0.5R_0$ . The underlying physical phenomenon could be Rayleigh-Taylor instability, when flame front is unstable to acceleration from a lighter to a heavier gas.

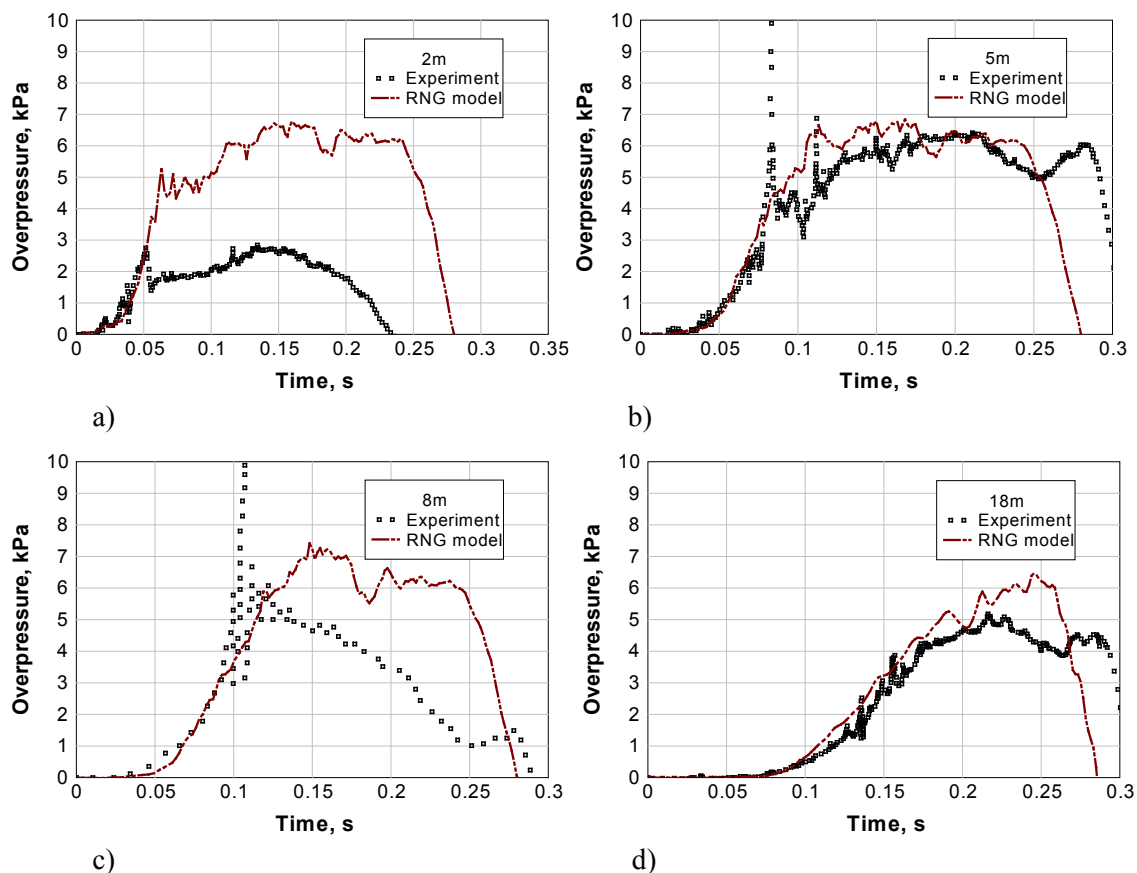


**Figure 10–32.** Comparison between the experiment and simulation by the RGG-Karlovits combustion sub-model for pressure transients at the positive phase of the explosion pressure wave at locations 2 m (a), 5 m (b), 8 m (c), and 18 m (d) from the ignition source.



### **Concluding remarks**

The LES model of large-scale accidental combustion is advanced further and applied to simulate the dynamics of the largest unconfined hydrogen-air deflagration ever performed (Molkov et al., 2006a). Two combustion sub-models were applied to analyse experimental data, one derived from the RNG theory along with findings of Karlovits et al. (1951) and Gostintsev et al. (1988), and another from the fractal theory.

The LES model demonstrates good convergence on different grids. The results of simulations vary by less than 5% for two unstructured tetrahedral grids with a difference in characteristic cell size of 2 times.

Formation and decay of the pressure wave are reproduced in simulations, including the experimental observation that a negative phase has shorter duration and higher amplitude compared to a positive phase.

There is more pronounced deceleration of simulated flame front at the end of the deflagration compared to the experiment. This is thought due to the coarse grid and affects slightly the duration of the positive phase of the pressure wave. Simulations on adaptive grid in the area of hydrogen concentration gradients would better reproduce experimental data.

In the RNG-Karlovits combustion sub-model the effect of flow turbulence on the turbulent burning velocity is taken into account by implementation of the Yakhot's (1988) equation for the turbulent premixed flame propagation velocity, which does not include either adjustable parameters or empirical coefficients. The RNG-Karlovits sub-model reproduces initial flame acceleration yet gives practically constant flame front propagation velocity after that. The RNG-Karlovits sub-model is closer to experimental results in prediction of the positive phase but under predicts by up to 30% the negative phase amplitude.

The fractal combustion sub-model, that exploits the RNG-Karlovits sub-model until the critical radius  $R_0$ , gives the best fit to the experimental flame propagation with a fractal dimension  $D=2.22$ , which is within the range 2.20–2.33 reported by Gostintsev et al. (1999) for large-scale unconfined deflagrations. Simulation with  $D=2.22$  reproduces accurately the experimentally observed flame front acceleration during the whole process of deflagration, the negative phase of the explosion pressure wave and over estimates by up to 50% the positive phase. Higher pressure peak of the positive phase in simulation compared to experiment could be attributed to the effect of PE balloon. Simulations with theoretical value  $D=2.33$  apparently over predicts both the experimental flame propagation and the pressure dynamics.

Numerical simulations partially resolve the flame front wrinkling caused by hydrodynamic instability. This contributes by a factor of the order of 1.1 to the flame propagation velocity. The flow turbulence in the RNG sub-model contributes by an additional factor of the order of 1.15 to the turbulent burning velocity. Fractals increase the flame surface area in the fractal sub-model by a factor of the order of  $(R/1.2)^{0.22}$  depending on the flame front radius, e.g. 1.74 for flame radius  $R=15$  m. Yet, the main contribution to the augmentation of the turbulent burning velocity is the turbulence generated by flame front itself (Karlovits et al., 1951) that is a multiplier of 3.6 to the initial laminar burning velocity for stoichiometric hydrogen-air mixture (Molkov et al., 2006a).

Both sub-models reproduce quite closely the experimental flame front propagation dynamics up to maximum 40 m diameter and pressure dynamics up to maximum available 80 m, i.e. at scales characteristic for hydrogen safety engineering problems. The agreement between numerical simulations and experimental data demonstrates the merits of the LES model for large-scale accidental premixed combustion.

#### 10.4.8.3. A series of deflagrations in the open atmosphere

The updated version of the LES model described above was applied to simulate a series of experiments by Pfortner and Schneider (1983) on near stoichiometric hydrogen-air deflagrations in hemispherical balloons of different radii: 1.53 m, 5.00 m, and 10.00 m. The main features of the LES model applied are published elsewhere (Molkov et al., 2007b).

The effect of flow turbulence on a turbulent burning velocity was modelled by the modified Yakhot's (1988) transcendental equation

$$S_t = S_u^w \cdot \exp\left(\frac{u'}{S_t}\right)^2, \quad (10-89)$$

in which the original laminar burning velocity  $S_u$  was substituted by the SGS wrinkled flame velocity,  $S_u^w$ , to account for unresolved in simulations physical mechanisms affecting turbulent burning velocity such as turbulence generated by flame front itself, fractal structure of turbulent flame front, etc.

# SMS from your computer

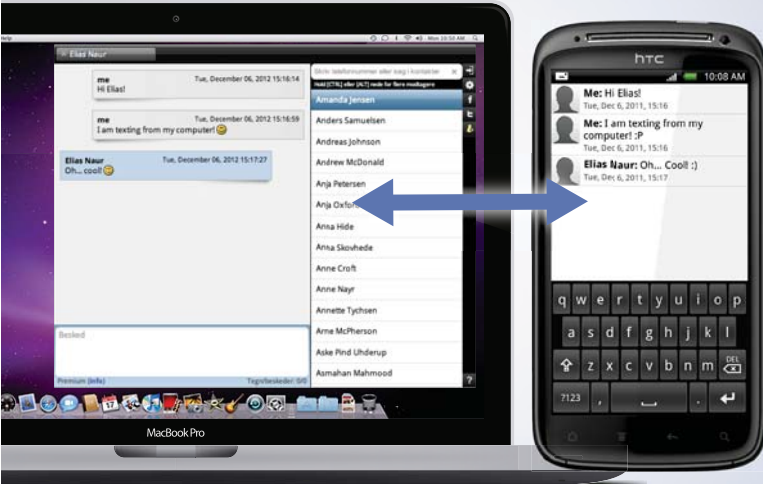
...Sync'd with your Android phone & number


**FREE**  
30 days trial!

Go to

[BrowserTexting.com](http://BrowserTexting.com)

and start texting from your computer!




**BrowserTexting**

The SGS wrinkled flame burning velocity can be written as a product of the laminar burning velocity,  $S_u(Y_{H_2}, T, p)$ , which is a function of hydrogen concentration in air as well as temperature and pressure of the flammable mixture, the Karlovits turbulence factor,  $\chi_K$ , and the factor accounting for flame front surface increase due to its fractal structure,  $\chi_f$

$$S_u^w = S_u \cdot \chi_K \cdot \chi_f. \quad (10-90)$$

To model the unresolved at the SGS level increase of the turbulent burning velocity due to the turbulence generated by flame front itself (Karlovits et al., 1951) the following equation is suggested

$$\chi_K = 1 + (\psi \cdot \chi_K^{Max} - 1) \cdot \left[ 1 - \exp\left(-\frac{R}{R_0}\right) \right], \quad (10-91)$$

where  $\psi$  is the empirical coefficient indicating how close the Karlovits turbulence factor,  $\chi_K$ , could reach its theoretical maximum  $\chi_K^{Max} = (E_i - 1)/\sqrt{3}$ . Simulations with a fine enough mesh, sufficient to resolve flame propagation until the critical radius of the transitional stage  $R_0$ , have demonstrated that value  $\psi=0.7$  is typical for near stoichiometric hydrogen-air mixtures. The transitional period of flame propagation from the ignition source until the critical radius for near stoichiometric hydrogen-air mixtures is accepted as  $R_0=1.2$  m (Gostintsev et al., 1988).

The increase of fractal surface of the turbulent flame with growth of its outer cut-off (flame radius) at assumption of the constant inner cut-off that probably is valid for practically constant pressure combustion in the atmosphere was accounted for as

$$\chi_f = \left( \frac{R}{R_0} \right)^{D-2}. \quad (10-92)$$

So, during the transitional period of flame propagation until the critical radius  $R_0=1.2$  m the following transcendental equation for calculation of the turbulent burning velocity was applied

$$S_t = S_u(Y_{H_2}, T, p) \cdot \chi_K \cdot \exp\left(\frac{u'}{S_t}\right)^2. \quad (10-93)$$

The dependence of laminar burning velocity on hydrogen concentration, pressure and temperature was treated in the same way as before. Dilution of the flammable mixture by ambient air on the contact surface was simulated too.

At the end of transitional stage the Karlovits wrinkling factor was frozen with the value  $\chi_K = \{1 + (\psi \cdot \chi_K^{max} - 1) \cdot [1 - \exp(-1)]\}$ . The fractal combustion model was applied at  $R > R_0$  to simulate further SGS growth of flame surface area and thus the turbulent burning velocity

$$S_t = S_u(Y_{H_2}, T, p) \cdot \{1 + (0.7 \cdot \chi_K^{max} - 1) \cdot [1 - \exp(-1)]\} \cdot \chi_f \cdot \exp\left(\frac{u'}{S_t}\right)^2. \quad (10-94)$$

The difference of this turbulent burning velocity combustion model from the simple fractal model tested above is the application of the fractal model along with the Yakhot's formula accounting for the flow turbulence. This is related to insufficient resolution of the fractal structure of turbulent flame front by the LES model when tackling large-scale problems. As a result the fractal's sub-model becomes the contributor to the SGS level of unresolved physical phenomena, i.e. the term defined by equation (10–92) is a multiplier to the laminar burning velocity in the original transcendental equation for turbulent burning velocity by Yakhot (1988).

### **Experiments**

The LES model described above in this section was applied to simulate the following experiments by Pfortner and Schneider (1983): GHT 23, GHT 26, GHT 11, GHT 13, GHT 34\*. Experimental parameters are given above in Table 10–4. A maximum positive peak pressure was constant within the combustion zone of approximate size  $2R_b$  and decreased inversely proportional with distance outside this zone. In a far field the pressure wave propagated with a form and duration of positive and negative phases independent of the distance for each balloon size.

Three pressure peaks were identified by experimentalists in a positive phase of pressure wave. The balloon shell stretched slightly outwards until it bursted when the flame reached distance  $0.5R_b$ . The first pressure peak  $\Delta p_1$  corresponds to the moment of bursting of the balloon shell. Pressure gauges inside the balloon recorded noticeable peak  $\Delta p_1$  because of pressure relief during bursting. After balloon shell bursting the flame front accelerates. The acceleration of the flame front gives rise to peak pressure  $\Delta p_2$  in outgoing pressure wave. The experimental report suggests that the flame front decelerates approaching shell fragments with subsequent reduction in pressure. After this the flame accelerates again and a pressure peak  $\Delta p_3$  is observed. Analysis of experimental records indicates that the pressure peak  $\Delta p_3$  could be attributed to the combustion of unburnt mixture flown outside the balloon shell fragments. For pressure sensors installed within the combustion area, the additional pressure peak  $\Delta p_p$  corresponding to the moment of flame passing over pressure sensor, is registered. Typical experimentally observed pressure peaks  $\Delta p_p$ ,  $\Delta p_1$ ,  $\Delta p_2$  and  $\Delta p_3$  are shown for test GHT 34 further in this section in Fig. 10–38.

### **Numerical details and ignition procedure**

The area of combustion in calculation domain was meshed by tetrahedral control volumes (CVs), while the area of outgoing pressure wave by hexahedral CVs. A numerical grid for simulation of 1.53 m deflagration is essentially the same as for 5.0 m deflagration and was obtained by scaling with factor 3.268 (Fig. 10–33). Details of calculation domains and meshes used in simulations are given in Table 10–5. Initial temperature and pressure are those in experiments (see Table 10–4). The mixture is initially quiescent,  $u=0$ . Hydrogen mass concentration inside balloon area,  $R \leq R_0$ , is equal  $Y_{H_2}=0.0287$  (corresponds to volume fraction 29.7%) and  $Y_{H_2}=0$  outside,  $R > R_0$ , in all cases. The initial burning velocity 1.91 m/s is accepted for all simulations in this study. The ground boundary is modelled as non-slip, adiabatic, non-permeable surface. Boundary representing atmosphere is modelled by non-reflecting boundary conditions.

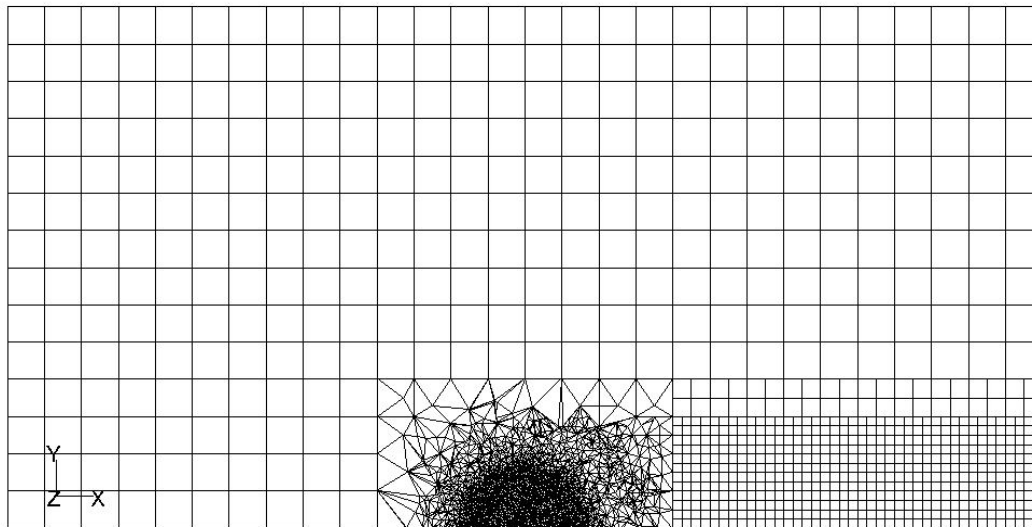


**Figure 10-33.** Calculation domain and numerical grid cross-section for simulation of deflagrations in hemispheres of diameter 1.53 m and 5.0 m.

Parameter	Radius of hemispherical balloon, m			
	1.53	5.0	10.0; coarse grid	10.0; fine grid
Domain size, LxWxH, m	70x70x35	228x228x114	200x200x100	200x200x100
Number of CVs	149,159	149,159	353,422	up to 2M
CV size in combustion area, m	0.25	0.8	0.8	0.4
CV size in external area, m	2.5	8.2	4	4
CV size at ignition location, m	0.253	0.826	0.770	0.385
Numerical ignition time, s	0.009	0.029	0.028	0.014
CPU time, h	10	10	66	192

**Table 10-5.** Details of calculation domains and numerical meshes used in the simulations (Molkov et al., 2007b).

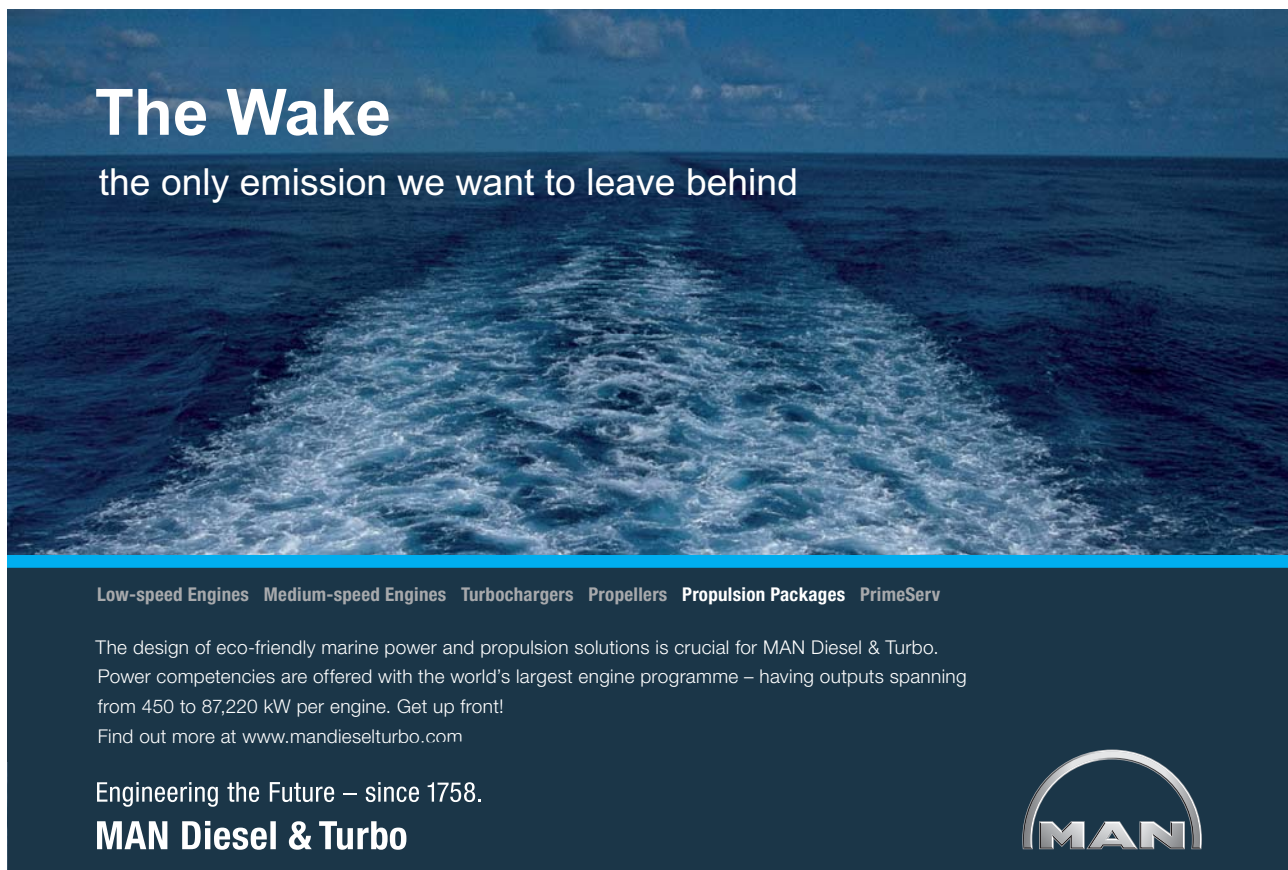
Ignition is modelled using a linear increase of the progress variable from 0 to 1 in one control volume (CV), located at the centre of a hemisphere at ground level. Duration for the increase of the progress variable was calculated as a time of laminar flame propagation over half of the ignition CV edge,  $\Delta t_{ign} = 1/2 \cdot (\Delta_{CV} / (S_u E_0))$ . The size of ignition CV and corresponding ignition time is given in Table 10-5 for each numerical experiment.

Simulated location of the flame front was identified by the leading edge of the flame front by averaging through CVs with values of the progress variable in the range  $c=0.01-0.10$  similar to Molkov et al. (2006a). The simulated flame front radius starts from a size of one cell in which ignition is initiated. All simulations were performed with initial burning velocity 1.91 m/s for stoichiometric hydrogen-air mixture of 29.7% (Lamoureux et al., 2003), and the same fractal dimension  $D=2.20$ .

The model was implemented using FLUENT 6.2 as a CFD engine. Second order upwind scheme was applied for convective terms and central-difference scheme for diffusive terms. Coupled solver with explicit time marching was used. The Courant-Friedrichs-Lewy number was equal  $CFL = 0.8$ . Calculations were carried out on 6-CPU p650 IBM server and a characteristic CPU time required for each simulation is shown in Table 2.

### *Comparison between experiments and simulations*

Experimental and simulated flame front propagation as well as pressure dynamics at locations of gauges at 2.07, 2.87, and 4.95 m from the ignition source for 1.53 m radius hemisphere deflagration at tests GHT 23 and GHT 26 are shown in Fig. 10–34. Under prediction of negative pressure amplitude could be explained for example by fast condensation of a fraction of water vapour in combustion products when mixing with cold air radiation losses from high temperature products. Comparison between experimental (GHT26) and simulated peak pressures  $\Delta p_2$  and  $\Delta p_3$  is shown in Fig. 10–35.




**The Wake**  
the only emission we want to leave behind

Low-speed Engines Medium-speed Engines Turbochargers Propellers Propulsion Packages PrimeServ

The design of eco-friendly marine power and propulsion solutions is crucial for MAN Diesel & Turbo. Power competencies are offered with the world's largest engine programme – having outputs spanning from 450 to 87,220 kW per engine. Get up front! Find out more at [www.mandieselturbo.com](http://www.mandieselturbo.com)

Engineering the Future – since 1758.  
**MAN Diesel & Turbo**





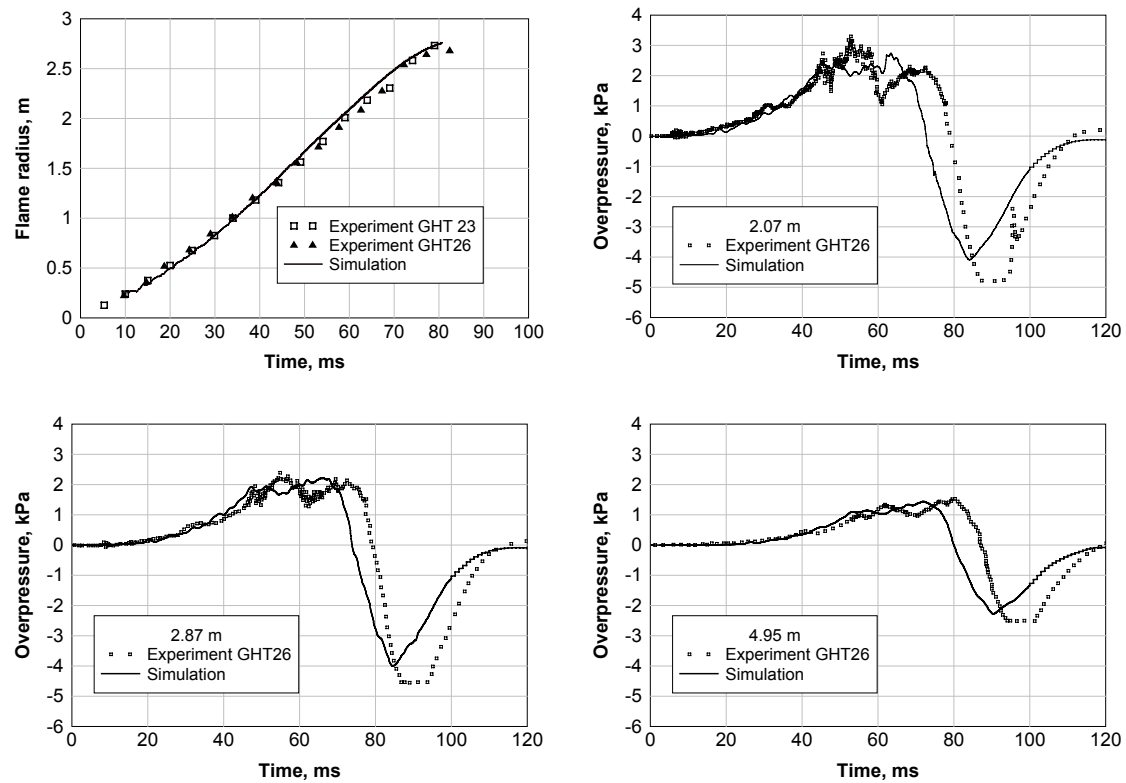


**Figure 10-34.** Comparison between experiment (GHT 23 and GHT 26) and simulations for hemispherical balloon of radius 1.53 m: radius of leading edge of a flame front (top left); pressure dynamics at different distances from the ignition source– 2.07 m (top right), 2.87 m (bottom left), 4.95 m (bottom right).

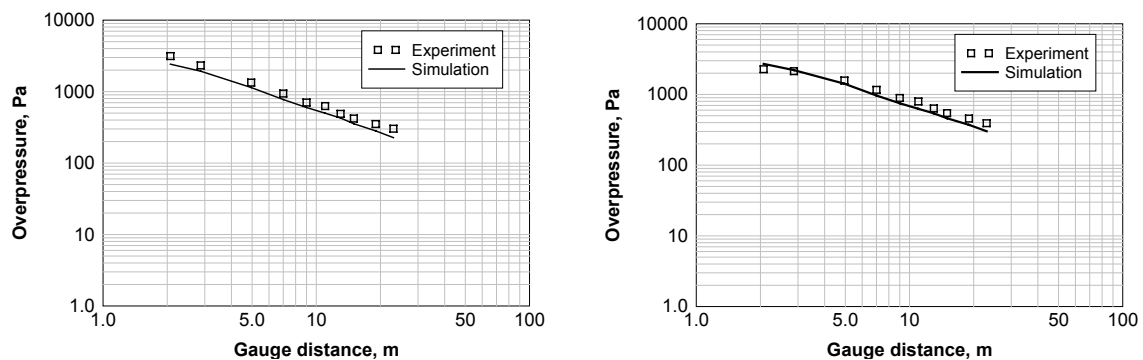


**Figure 10-35.** Experimental (GHT 26) and simulated peak pressures: peak  $\Delta p_2$  (left), peak  $\Delta p_3$  (right).

Figures 10–36 and 10–37 shows experimental and simulated flame propagation and pressure dynamics for test GHT 11 in 5.0 m diameter balloon (experimental flame propagation dynamics for test GHT 13 is shown too). Pressure transients were recorded at 6.85, 8.79, and 10.8 m from the ignition source. A smaller burning velocity in simulations (29.7% hydrogen-air mixture) compared to experiment GHT 11 (31% hydrogen-air mixture) contributed to under prediction of pressure peaks in both positive and negative phases.

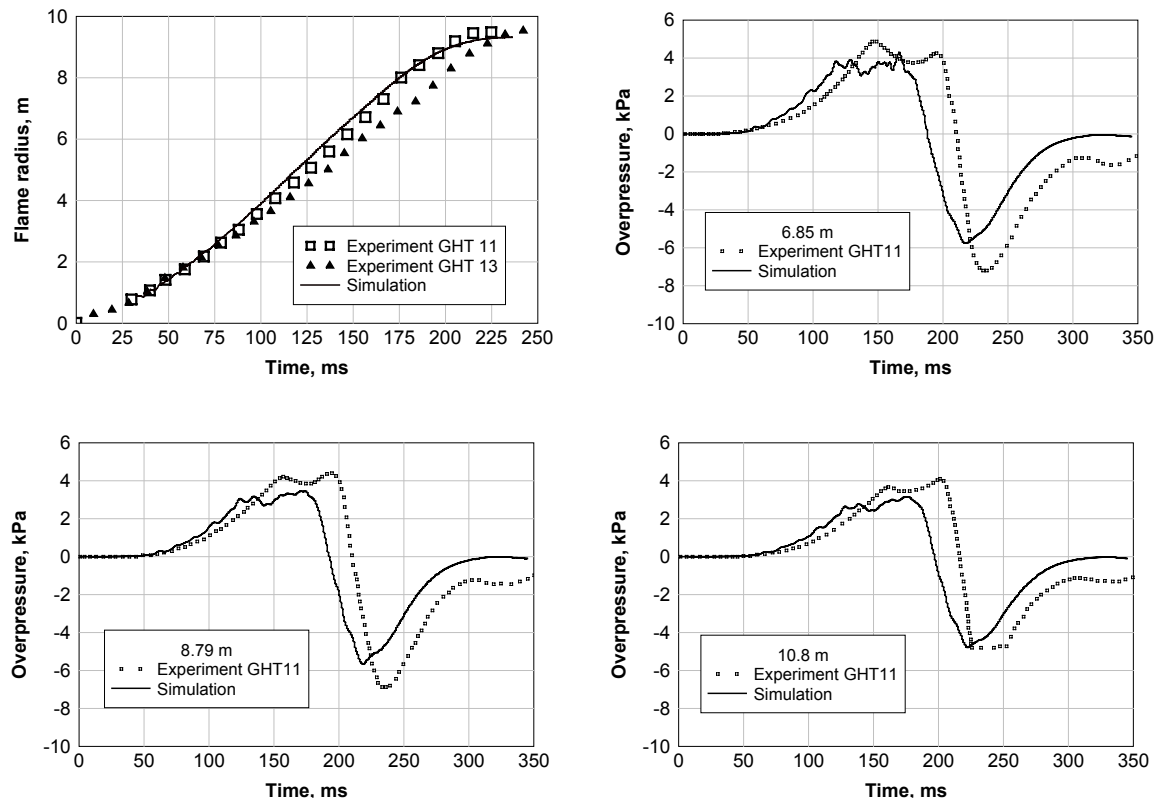


**Figure 10–36.** Comparison between experiment (GHT 11) and simulation for hemispherical balloon of radius 5.0 m: radius of leading edge of a flame front (top left); pressure dynamics at different distances from the ignition source - 6.85 m (top right), 8.79 m (bottom left), 10.8 m (bottom right).

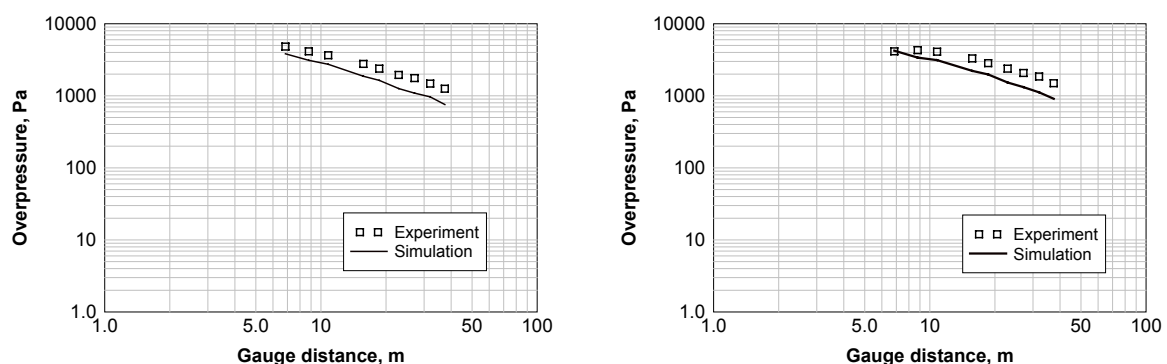


**Figure 10–37.** Experimental (GHT 11) and simulated peak pressures: peak  $\Delta p_2$  (left), peak  $\Delta p_3$  (right).

For the largest known hydrogen-air deflagration (test GHT 34) in 10.0 m diameter hemisphere the comparison between experiment and simulations (Molkov et al., 2007b) is shown in Fig. 10–38 and Fig. 10–39. Pressure dynamics registered at distances 5 m, 35 m and 80 m from the ignition source is presented in Fig. 10–38. The model grid sensitivity was studied for test GHT 34. The original grid (“course” grid of 353,422 CV), used for this simulation, was then adapted in the vicinity of the flame front to decrease CV size twice. The model enables to simulate flame propagation dynamics on two grids with ratio of cell size equal to two with a difference below 10%. This complies with a requirement to LES models performance on different grids (Pope, 2004).

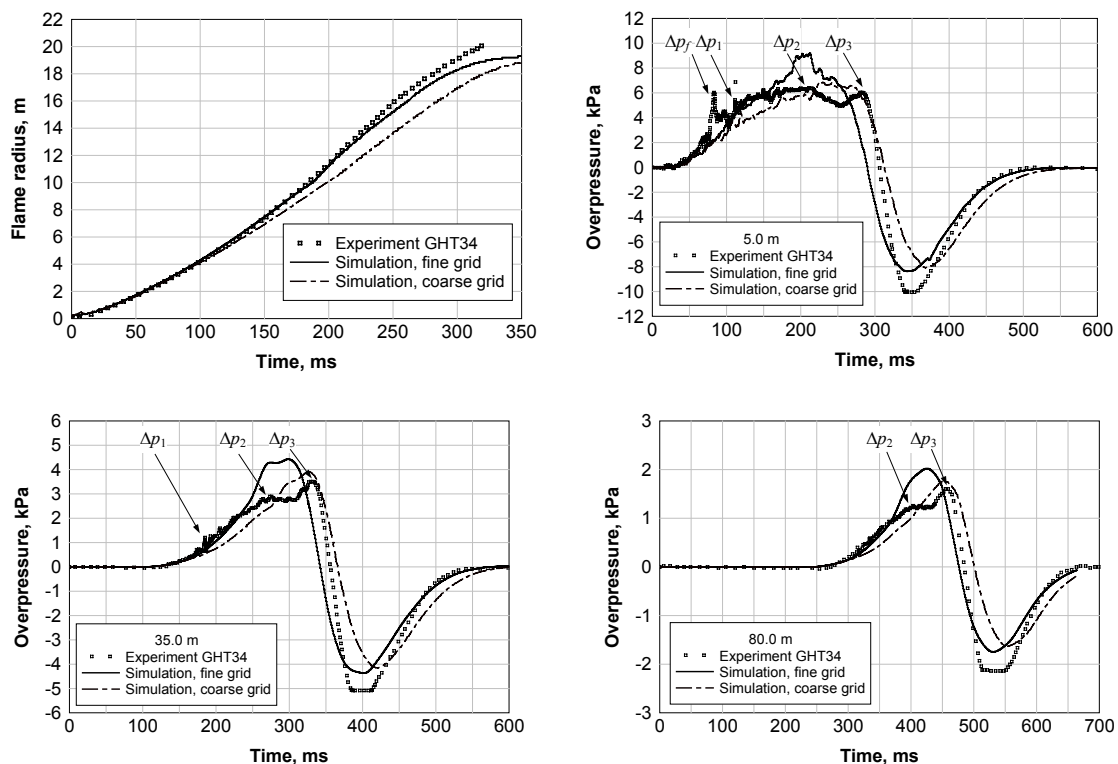


**Figure 10–38.** Comparison between experiment (GHT 34) and simulation for hemispherical balloon of radius 10.0 m: radius of leading edge of a flame front (top left); pressure dynamics at different distances from the ignition source – 5 m (top right), 35 m (bottom left), 80 m (bottom right).

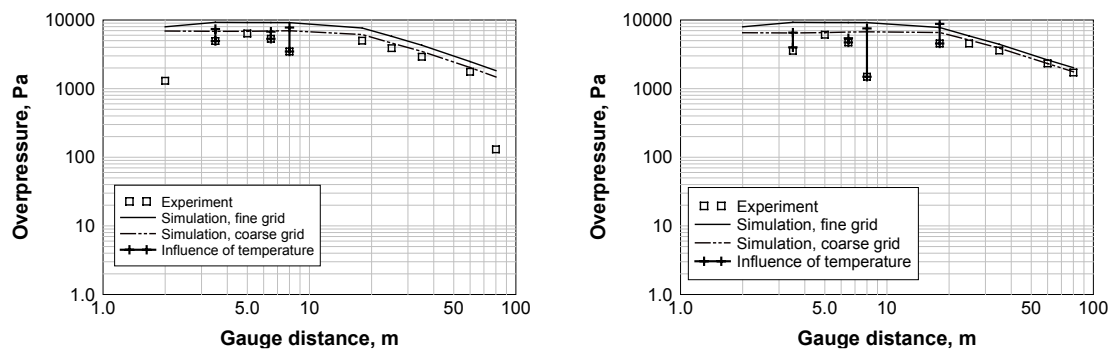


**Figure 10–39.** Experimental (GHT 34) and simulated peak pressures: peak  $\Delta p_2$  (left), peak  $\Delta p_3$  (right).

**Concluding remarks**

The LES model of large-scale gaseous deflagrations (Molkov et al., 2007b) incorporates the turbulent burning velocity combustion sub-model based on interaction of three mechanisms, i.e. the turbulence generated by flame front itself, the fractal growth of turbulent flame surface area with scale, and the flow turbulence. The modified transcendental equation by Yakhot (1988) for the turbulent burning velocity includes the SGS wrinkling velocity instead of the laminar burning velocity, and the fluctuating velocity at the resolved level.

The performance of the LES model has been compared against a series of near stoichiometric hydrogen-air deflagrations in hemispherical polyethylene balloons of radius 1.53, 5.00, and 10.00 m with central ignition. Applied to simulation of all experiments the fractal dimension  $D=2.20$  complies well with reported previously values of the fractal dimension. Taking into account that all simulations were performed with the same values of initial burning velocity 1.91 m/s and fractal dimension 2.20 the LES predictions can be assessed as close to the experimental data.

Simulations reproduced experimentally observed pressure peaks  $\Delta p_2$  and  $\Delta p_3$ , which were attributed to effect of PE balloon by the experimentalists (Pförtner and Schneider, 1983). Indeed, experimental peak  $\Delta p_2$  is somewhat larger than simulated that confirms an influence of PE shell burst on the flame acceleration. Still, the presence of  $\Delta p_2$  in simulations should be understood.

## TURN TO THE EXPERTS FOR SUBSCRIPTION CONSULTANCY

Subsrybe is one of the leading companies in Europe when it comes to innovation and business development within subscription businesses.

We innovate new subscription business models or improve existing ones. We do business reviews of existing subscription businesses and we develop acquisition and retention strategies.

Learn more at [linkedin.com/company/subsrybe](https://www.linkedin.com/company/subsrybe) or contact  
Managing Director Morten Suhr Hansen at [mha@subsrybe.dk](mailto:mha@subsrybe.dk)

**SUBSCR**✓**BE** - to the future

#### 10.4.8.4. Blast wave overpressure in the atmosphere

Gaseous deflagrations in the open atmosphere generate outgoing pressure waves. The acoustic theory can be applied for deflagration generated pressure waves. Pressure in a blast wave can be estimated as (Gorev et al., 1980)

$$\frac{p(t, R_w) - p_i}{p_i} = \frac{\gamma(E_i - 1)}{[1 + r_b(t)/c_0 t] E_i c_0^2} \frac{r_b(t)}{R_w} \left[ 2w^2 + r_b(t) \frac{dw}{dt} \right], \quad (10-95)$$

where  $r_b(t)$  is the flame radius at moment  $t$ , m;  $R_w$  is the distance at which pressure  $p$  is estimated, m;  $c_0$  is the speed of sound, m/s;  $w$  is the flame front propagation velocity, m/s. The key conclusion from this formula is that the pressure wave peak depends on both the flame propagation velocity and the flame acceleration, especially at large radii. Deceleration of the flame front results in a pressure drop in the pressure wave. This formula states as well that the pressure wave decays inversely proportional to the distance from the ignition source. Author leaves the validation of this formula by the GHT34 experiment to a reader.

#### 10.4.9. LES of hydrogen-air deflagrations in a 78.5 m tunnel

The LES model previously validated against a series of deflagrations in the open atmosphere, including the largest known 20-m diameter deflagration, is applied in this section to reproduce experimental data on 20% and 30% hydrogen-air deflagrations in a central part of a 78.5-m long tunnel (Groethe et al., 2005). The model enables the transient modelling of deflagration dynamics with a laminar flamelet burning velocity which alters with mixture composition, pressure, and temperature. The turbulent burning velocity is computed using Yakhot's transcendental equation for premixed combustion. Yakhot's equation is essentially modified to account for the transitional phenomena of turbulence generated by the flame front itself and the fractal structure of the turbulent flame surface at unresolved sub-grid scale (SGS) level.

The LES model (Molkov et al., 2008b) reproduced experimental data for both mixtures in an unobstructed and an obstructed tunnel. The simulations gave insight into the dynamics of flame propagation and the pressure build up within and outside of the tunnel. The LES model enabled the analysis of phenomena which were not reported in the experimental study. For example, a significant increase in the maximum explosion overpressure was observed in the vicinity of obstacles due to obstacle side-on pressure wave reflection in later stages of the event.

The hydrogen economy has become a part of our everyday life. Characteristic hazards, associated with different kinds of hydrogen applications, have to be first understood in order to prevent or mitigate accidents. Hydrogen fuelled buses and cars are already on the roads. The safety of hydrogen automotive applications and the related infrastructure, including garages, maintenance workshops, parking, and tunnels is one area of concern. A typical amount of on-board stored hydrogen in a passenger car is about 6 kg and in a bus is up to 40 kg. The release of several kilograms of hydrogen from a hydrogen powered vehicle during an accident in a tunnel followed by an ignition and thus deflagration is a possible accident scenario. The pressure and impulse generated by such deflagrations should be calculated with reasonable accuracy for hazards and risk assessment. The role of obstacles, i.e. vehicles, on deflagration dynamics in a tunnel has to be clarified. A recent numerical study by Gamezo et al. (2007) of the deflagration-to-detonation transition (DDT) in an obstructed small-scale tube containing a hydrogen-air mixture gave an insight into the physics of the phenomenon. The authors demonstrated that the reflection of a developing shock on repeated obstacles is a reason for shock-to-detonation transition, including through the role of Richtmayer-Meshkov instability.

#### 10.4.9.1. Overview of experiments

Large-scale experiments on hydrogen-air deflagrations were performed in a 1/5th real scale tunnel 78.5 m in length, 1.84 m in height, with a horseshoe shape cross sectional area of 3.74 m<sup>2</sup> by Groethe et al. (2005). Uniform 20% and 30% hydrogen-air mixtures of 37.4 m<sup>3</sup> volume (10 m long cloud) were prepared in the middle of the unobstructed tunnel and ignited at the centre of the tunnel at floor level. The amount of hydrogen in near stoichiometric 30% hydrogen-air cloud was equal to 1 kg. An additional experiment with obstructions was carried out only for a 30% hydrogen-air mixture. Mock vehicles of size  $L \times W \times H = 940 \times 362 \times 343$  mm were used as obstacles. The separation distance between the obstacles was equal to a “vehicle” length. A blockage ratio for this type of obstacle is 0.03.

Maximum overpressures along the tunnel for all three tests, one transient pressure measurement and impulse at a distance 34 m from the ignition source for 30% hydrogen-air mixture in the unobstructed tunnel test were the only experimental data reported (Groethe et al., 2005). There is no information reported on the exact location of the pressure transducers used in the experiments, other than their distance from the ignition source. The experimentalists concluded that there was no difference between the maximum overpressures generated by hydrogen-air explosion in the tunnel without and with obstacles.



#### 10.4.9.2. The LES model and numerical details

The LES model used for the tunnel deflagration (Molkov et al., 2008b) is exactly the same as in our recent study (Molkov et al., 2007b) with one exception, i.e. the theoretical fractal dimension  $D = 2.33$  was accepted in circumstances of absence of any preliminary information on  $D$  in geometries like tunnels.

The calculation domain dimensions were  $L \times W \times H = 300 \times 150 \times 75$  m. The domain included both the tunnel and the surroundings in order to minimize the effect of boundary conditions and to simulate a pressure wave propagating out of the tunnel into the open atmosphere. An unstructured tetrahedral mesh with an average control volume (CV) size of about 0.3 m was used inside the tunnel. External to the tunnel, part of the calculation domain was meshed using a structured hexahedral mesh with a CV size of 4.0 m in order to minimize computational time. One grid was generated for the unobstructed tunnel with a total number of 166502 CVs, and another for the tunnel with obstacles comprising 125884 CVs. The grid for the unobstructed tunnel was partially refined to increase the accuracy of simulation of the blast wave propagating outside of the tunnel. The numerical grid for the whole calculation domain and the part inside the tunnel with obstacles is shown in Fig. 10–40.

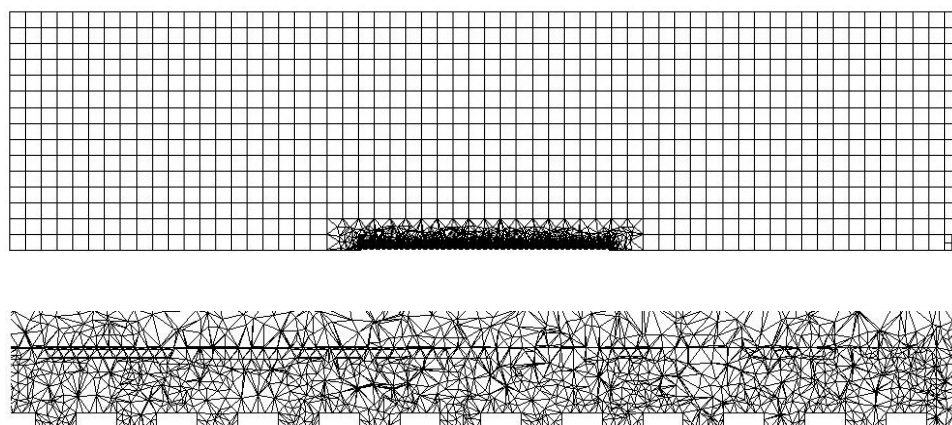


**Figure 10–40.** The numerical grid of the calculation domain (top) and its part inside the obstructed tunnel section (bottom).

The grid sensitivity of the LES model was studied previously and it was demonstrated that the decrease of CV size twice results in maximum 5–10% increase of the maximum pressure at particular time, which arise from a better resolved flame front wrinkling and, thus, higher mass burning rate.

The initial pressure and temperature were equal to those recorded in the experiments:  $T = 295$  K,  $p = 101.325$  kPa. All walls and surfaces were modelled as adiabatic impermeable surfaces. Non-reflecting pressure-far-field boundary conditions were used on the boundaries representing the atmosphere. FLUENT 6.2 software was used as a CFD engine to realize the LES model. A coupled compressible solver with explicit linearization of the equation set was used with  $CFL = 0.8$ . A second-order upwind scheme was used for discretization of the convection terms and a second-order central difference scheme was applied for the diffusion terms. The thermodynamic properties of hydrogen-air mixture and combustion products were calculated using the CHEMKIN software (Kee et al., 2000).

### 10.4.9.3. Results and discussion

A comparison between maximum experimental and simulated overpressures along the tunnel is presented in Fig. 10–41 for all three experiments. Side-on obstacle overpressure is available for numerical simulations only. There is good agreement for all cases with insignificant under prediction of the maximum overpressures in simulations. This result is very positive for the LES model validation bearing in mind that the model was “calibrated” for very different conditions of unconfined deflagrations.

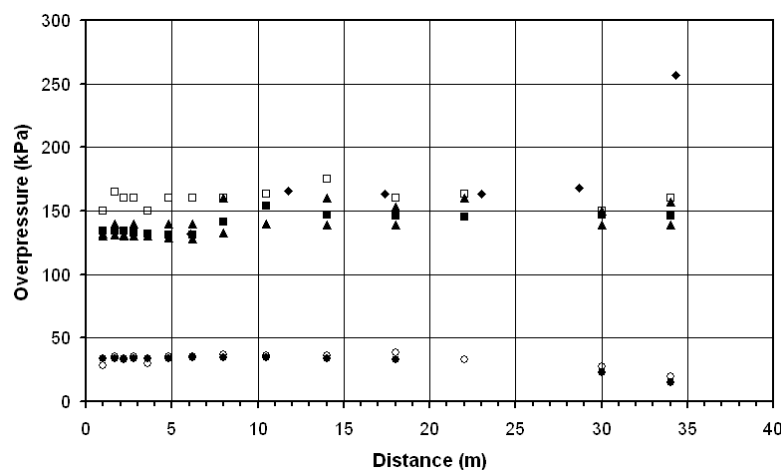


**Figure 10–41.** Maximum deflagration overpressures along the tunnel (distance is given from the tunnel centre): 20% hydrogen-air mixture (○ – experiment; ● – simulations); 30% hydrogen-air mixture, unobstructed tunnel (△ – experiment; ▲ – simulations); 30% hydrogen-air mixture, obstructed tunnel (□ – experiment; ■ – simulations, ceiling; ◆ – simulations, obstacle).

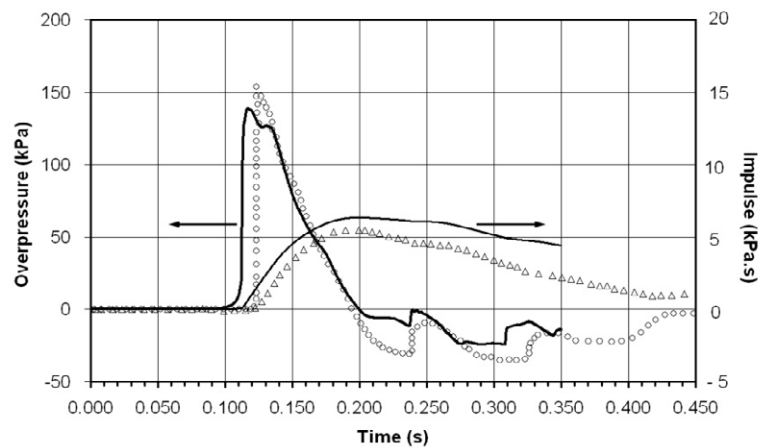
The LES analysis of cases without and with obstructions inside the tunnel demonstrated significantly higher deflagration generated overpressures on the obstacle surfaces (◆ in Fig. 10–41) compared to overpressures measured at the ceiling level (■ in Fig. 10–41). Indeed, in the agreement with experimental data the maximum overpressures simulated above the obstacle level are practically the same as those measured experimentally for the cases with and without obstacles. However, with increasing distance from the ignition source, the difference between static side-on obstacle overpressure and the static overpressure on the ceiling increases. This is an indication that the initial pressure wave from combustion forms a shock, which reflects from the rigid “vehicle” surface, thus increasing the static pressure at the stagnation area.

The pressure in the reflected shock,  $p_3$ , can be estimated from values of the initial pressure,  $p_1$ , and the incident shock,  $p_2$ , using the formula (Landau and Lifshits, 1988)


$$\frac{p_3}{p_2} = \frac{(3\gamma - 1)p_2 - (\gamma - 1)p_1}{(\gamma - 1)p_2 + (\gamma + 1)p_1}. \quad (10-96)$$

For a specific heat ratio of  $\gamma=1.4$ ,  $p_1=1$  bar and  $p_2=2.5$  bar the ratio is about  $p_3/p_2=2.2$ . Because the formation of the shock is not yet finished and the reflection is not exactly normal the simulated ratio is lower than theoretical and only about  $p_3/p_2=1.5$ . The numerical requirement to have 3-5 control volumes through any “discontinuity” in simulations could contribute to this difference too.




The simulated shock wave structure at a distance of 34 m from the ignition source reproduced transient pressures and impulse quite close to those measured in the experiments (Fig. 10–42). The simulated arrival time of the shock practically coincides with the experimental value. Somewhat faster arrival times of simulated oscillating pressure waves can be observed in Fig. 10–42. This could be explained by the higher speed of sound in the combustion products in the simulations. Indeed, the model does not include heat losses from combustion products. This would reduce the temperature and hence the speed of sound.



**Figure 10–42.** Comparison between experimental and simulated pressure dynamics and impulses at a distance of 34 m from the ignition source: experimental pressure dynamics (circles) and impulse (triangles), simulated pressure dynamics and impulse (solid lines).



**DO YOU WANT TO KNOW:**

-  What your staff really want?
-  The top issues troubling them?
-  How to make staff assessments work for you & them, painlessly?

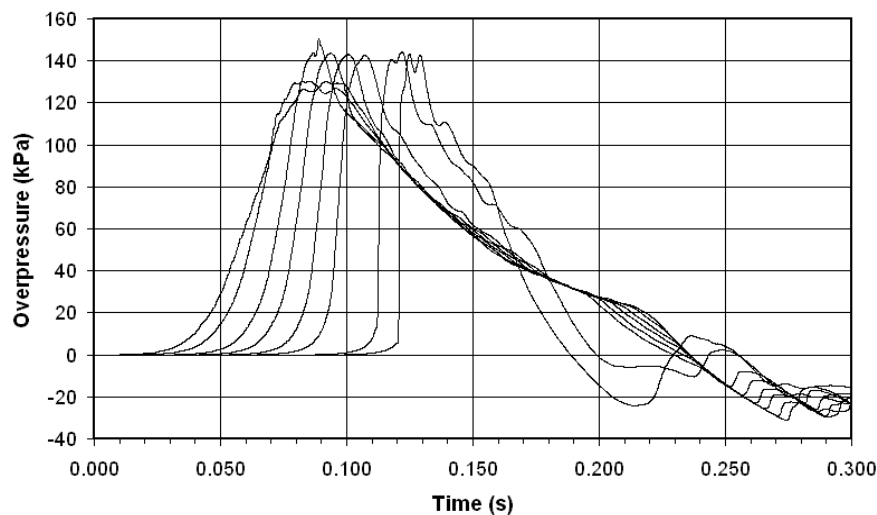
**Get your free trial**

Because happy staff get more done

## How to retain your top staff

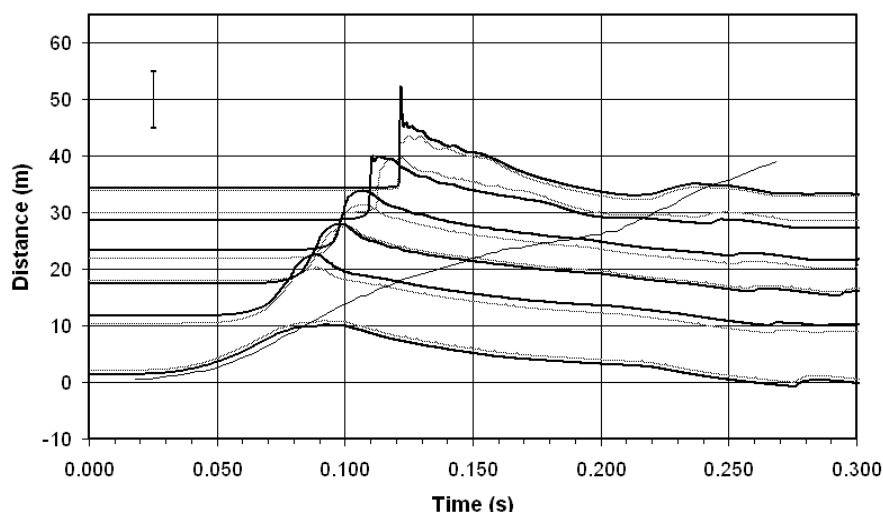
FIND OUT NOW FOR FREE

Figure 10–43 shows simulated pressure dynamics at different distances from the ignition source along the tunnel. The formation of the shock wave with a steep leading edge from the initial sloping shape pressure wave during deflagration progression is seen. The maximum overpressure is practically the same along the tunnel. Bearing in mind a level of overpressure observed in experiments and reproduced in simulations, a serious damage to life and property inside the tunnel can be expected for the considered scenario for the whole duration of a tunnel as a shock wave does not indicate the tendency to decay with distance.



**Figure 10–43.** The formation of shock wave during pressure wave propagation along the tunnel (ceiling level).  
Simulated pressure transients at distances 2.8, 6.2, 10.5, 14, 18, 22, 30, and 34 m from the ignition source.

The difference in dynamics of the overpressure at ceiling level and side-on obstacle overpressure along the tunnel is shown in Fig. 10–44. The shock is formed at the end of the tunnel. Pressure transients have similar dynamics at various locations along the tunnel cross section. An exception is a part of the pressure-time curve close to the maximum overpressure which is affected by the absence (ceiling) or presence (obstacle's side) of the blast wave reflection. There is no experimental data available on the flame propagation inside the tunnel. There are distinctive phases of the leading edge of the flame front acceleration and deceleration in simulations (Fig. 10–44). The flame front reaches the end of the right part of the tunnel about 270 ms after ignition.



**Figure 10-44.** Simulated static overpressure dynamics (dotted (gray) lines – ceiling overpressures; solid lines – side-on obstacle overpressures; location of the computational pressure gauges can be read from the ordinate axis) and flame propagation dynamics (position of flame on tunnel's centre line in time).

In order to understand the dynamics of the deflagration in the tunnel in more detail the simulation results have been analysed. This analysis is presented in Fig. 10-45 (left), along with data on hydrogen concentration in air which is presented in Fig. 10-45 (right).

Computational visualization of the overpressure field in the tunnel, overlapped with locations of the turbulent flame front brush ( $c=0.1-0.9$ ), for a series of consequent moments is shown in Fig. 10-45 (left). This confirms the flame acceleration at initial stage, then deceleration and acceleration again up to almost the moment when the flame front exits the tunnel approximately 270 ms after ignition. The formation of the shock with time is clearly seen. Areas of high side-on obstacle pressure can be identified. The shock leaves the tunnel at approximately 131 ms, at this time the flame has only passed half way along the tunnel. The rarefaction wave is seen in Fig. 10-45 (left), this propagates inside the tunnel after the shock wave leaves the tunnel. This rarefaction wave, and the resulting flow induced, is responsible for the second acceleration of the flame.

Fig. 10-45 (right) shows the movement of the flammable hydrogen-air mixture in a range of concentrations relative to the flame position; from an initial concentration of 30% down to the lower flammability limit of 4% of hydrogen in air. The dilution with time of the initially uniform near stoichiometric 30% hydrogen-air mixture (black colour in Fig. 10-45, right) by the air at the contact surface is seen. There is an essential decrease in the volume of flammable mixture present at approximately 140 ms. The flammable cloud at this time is above the level of the obstacles. Slow combustion of the hydrogen-air mixture with concentrations close to the lower flammability limit continues up to  $t=350$  ms. After 140 ms combustion no longer has a significant effect on the flow dynamics, to the contrary the flow induced by the pressure waves is responsible for the second flame “acceleration” and the reverse movement of the flame back to the centre of the tunnel after 290 ms.

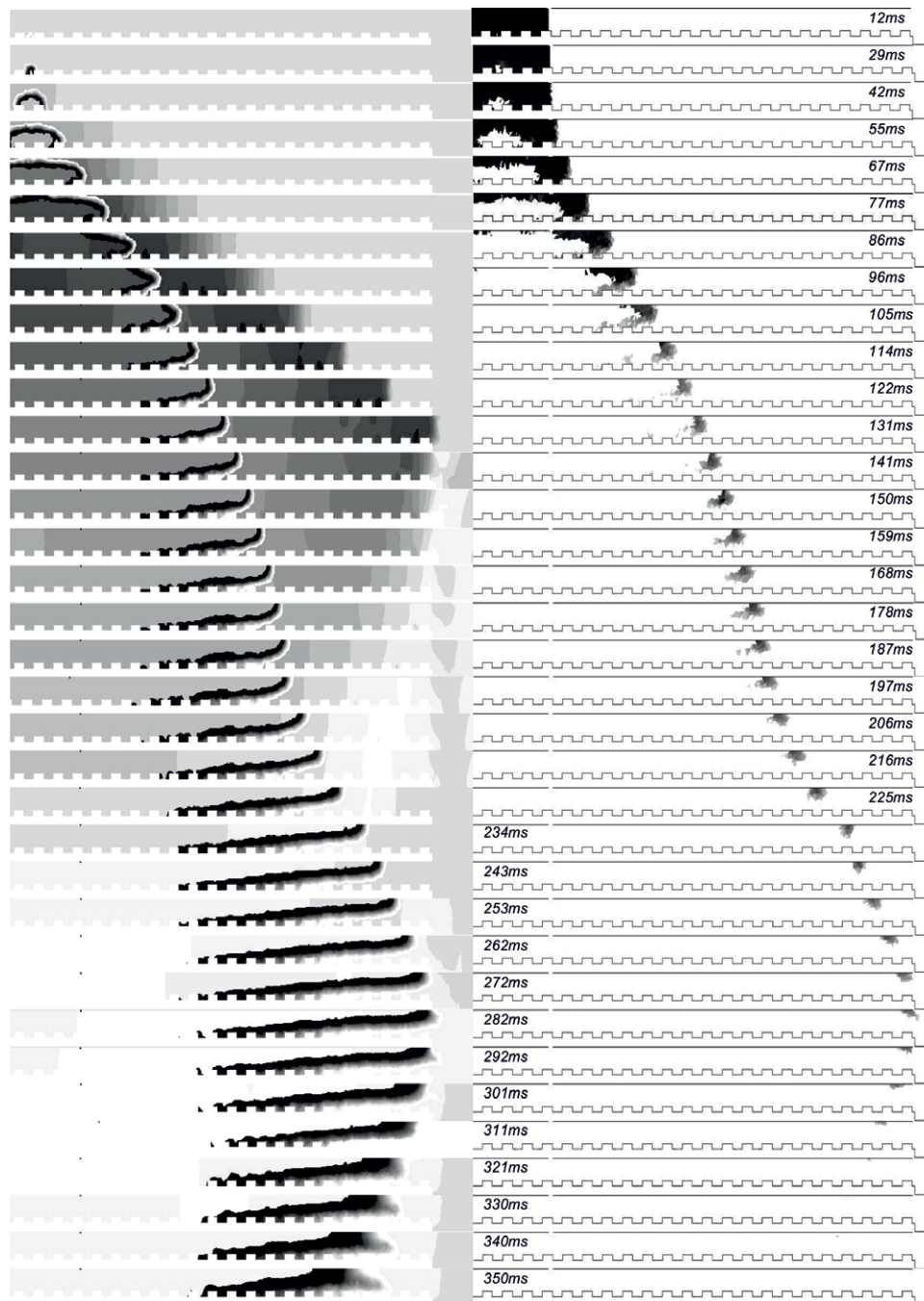


**Figure 10-45.** Left column: pressure and rarefaction waves, flame front ( $c=0.1-0.9$ ,  $t<270$  ms), and combustion products ( $c=0.1-0.9$ ,  $t>270$  ms). Right column: flammable hydrogen-air mixture propagation in the tunnel (black colour refers to 30% by volume of hydrogen in air, grey colour corresponds to 4% of hydrogen). Time after ignition refers to both columns.


From the analysis of Fig. 10-45 (left) and Fig. 10-45 (right) it follows that approximately 140 ms after ignition the premixed combustion proceeds in the upper part of the tunnel above the obstacles and a large mixing layer of combustion products and air develops. This can assist in the assessment of a thermal hazard inside the tunnel.



From Fig. 10–44 it is seen that the deceleration of flame is started at approximately 80–90 ms. There can be two main reasons for the flame deceleration. The first is a reduction in the transient total flame front area and the second is a decrease in the laminar burning velocity in the flamelets. Indeed, at approximately 85 ms the flame reached the ceiling and the flame surface area begins to reduce.

Let us analyse the temporal behaviour of the laminar burning velocity,  $S_u(Y_{H_2}, T, p)$ , during the deflagration. A value of  $S_{ui}=1.96$  m/s is accepted in this study as an initial value for the laminar burning velocity for a 30% hydrogen-air mixture (Lamoureux et al., 2003). Fig. 10–46 shows the scattering of values of the laminar burning velocity in the cells of the numerical flame brush for the duration of the deflagration. It can be seen from Fig. 10–46 that up to approximately 50 ms after ignition the laminar burning velocity is practically the same in the different cells of the flame front brush, i.e. there is no scattering.


The laminar burning velocity increases slightly due to adiabatic compression according to the equation  $S_u(Y_{H_2}, T, p) = S_{ui}(Y_{H_2}) \cdot (T/T_i)^{m(Y_{H_2})} \cdot (p/p_i)^{n(Y_{H_2})} = S_{ui}(Y_{H_2}) \cdot (p/p_i)^{\varepsilon(Y_{H_2})}$ , where  $S_{ui}=1.96$  m/s is the initial value of the laminar burning velocity for 30% hydrogen-air mixture,  $T_i$  and  $p_i$  are the initial temperature and pressure respectively,  $T$  and  $p$  are the transient temperature of unburned mixture and pressure respectively,  $m$  and  $n$  are temperature and baric indices in dependence of burning velocity on temperature and pressure respectively, and  $\varepsilon=0.565$  is the thermokinetic index. Values of the thermokinetic index  $\varepsilon$  (Babkin, 2003), temperature index  $m$  (Drell and Belles, 1958), and baric index  $n$ , (Manton and Milliken, 1956) are shown in Table 10–6 along with temperature index,  $m$ , calculated from  $\varepsilon$  and  $n$  by the formula  $m=[(\varepsilon-n)\gamma_u]/(\gamma_u-1)$  and shown in parenthesis (Verbecke, 2009).



**Struggling to get interviews?**

Professional CV consulting & writing assistance from leading job experts in the UK.

[Visit site](#)

 Take a short-cut to your next job!  
Improve your interview success rate by 70%.

 **TheCVagency**  
Visit [theagency.co.uk](http://theagency.co.uk) for more info.

H <sub>2</sub> , %	15	20	25	29.5	35	40	43	45	50	55	60	65	70
$m^*$	(2.6)	(2.2)	(1.9)	1.7	(1.5)	(1.45)	1.4	(1.4)	(1.45)	(1.5)	1.7	(1.9)	(2.2)
$n^{**}$	-0.05	0.01	0.05	0.09	0.1	0.1	0.1	0.1	0.1	0.08	0.06	0.03	0
$\varepsilon^{***}$	0.68	0.63	0.58	0.57	0.52	0.51	0.49	0.49	0.51	0.50	0.54	0.56	0.61

Notes: \* – Drell and Belles (1958); \*\* – Manton and Milliken (1956); \*\*\* – Babkin (2003); values in parenthesis are interpolated or extrapolated (Verbeke, 2009).

**Table 10–6.** Temperature, baric, and thermokinetic indices for hydrogen-air laminar burning velocity as a function of hydrogen concentration at NTP.

Approximately 60 ms after ignition a scattering in the values of laminar burning velocity in different flame front locations can be observed. The scattering reaches a maximum at a time approximately 85 ms after ignition. At this time both the pressure effect associated with a maximum value of laminar burning velocity, and the dilution effect, associated with a minimum value in the scattered data, are pronounced. Beyond this point the dilution of the hydrogen-air mixture by the surrounding air on the contact surface dominates and the laminar burning velocity decreases monotonically to zero at a time of approximately 350 ms. At this time there is no hydrogen-air mixture remaining in the tunnel at concentrations above the lower flammability limit (see Fig. 10–45, right).

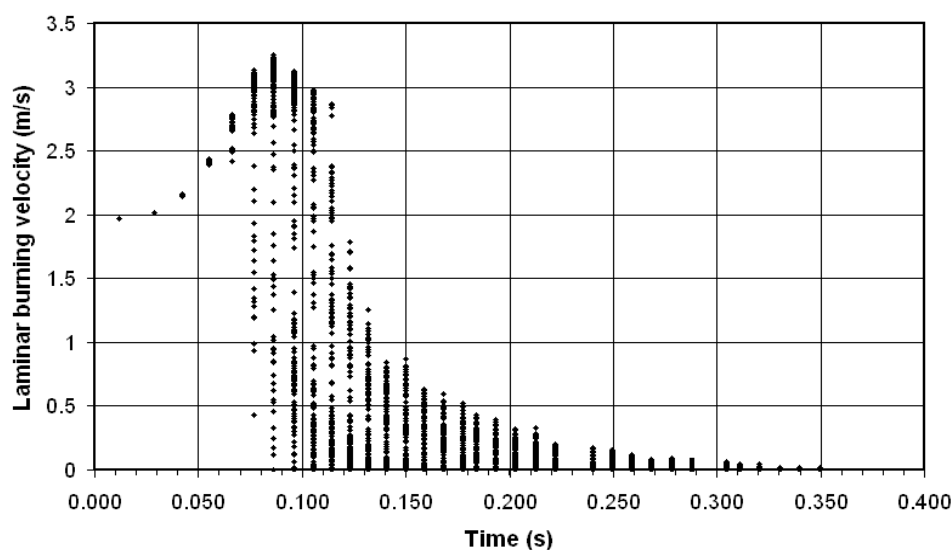


**Figure 10–46.** Scattering of the laminar burning velocity within the flame front brush ( $c=0.1$ – $0.9$ ) as a function of time after ignition.

The pressure transients at two locations at the end of the tunnel and two just outside the tunnel are shown in Fig. 10–47. The pressure drops quite fast to achieve a value of approximately 5 kPa at a distance approximately 1 diameter outside the tunnel.

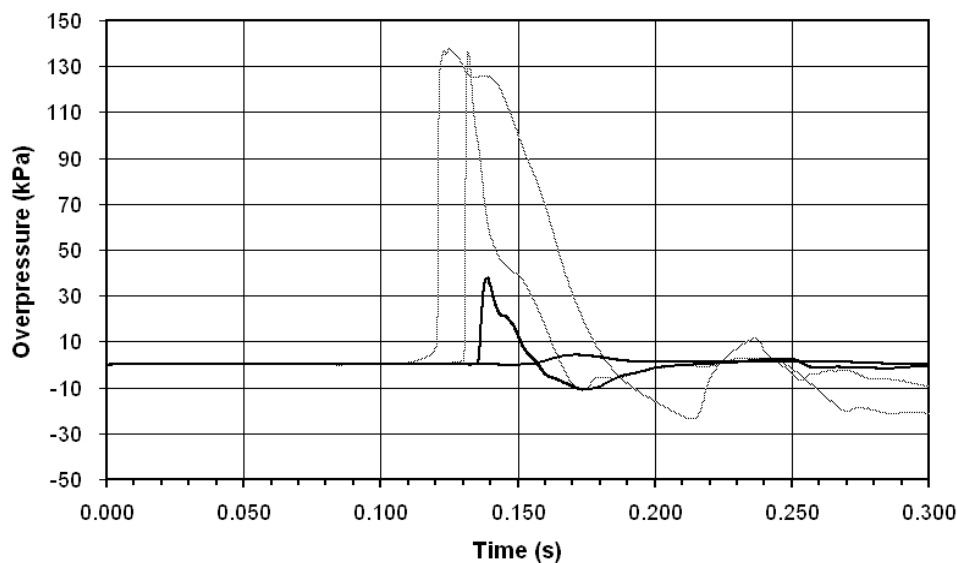


**Figure 10-47.** Simulated pressure dynamics: dotted (gray) lines – ceiling overpressure inside the tunnel at 34 m and 39 m from ignition source (inside the tunnel, 5.25 m and 0.25 m from the end of the tunnel respectively); solid lines – 40 m and 42 m from the ignition source (outside the tunnel, 0.75 m and 2.75 m respectively) at 1.2 m and 1.5 m from the ground level respectively.

#### 10.4.9.4. Concluding remarks

The LES model, calibrated previously to predict the dynamics of large-scale hydrogen-air deflagrations in the open atmosphere, is validated against experimental hydrogen-air explosions in a quite different environment of a 78.5-m long tunnel. The simulation reproduced the experimental results for both 20% and 30% hydrogen-air deflagrations, and included deflagrations in an unobstructed tunnel and a tunnel with obstacles.

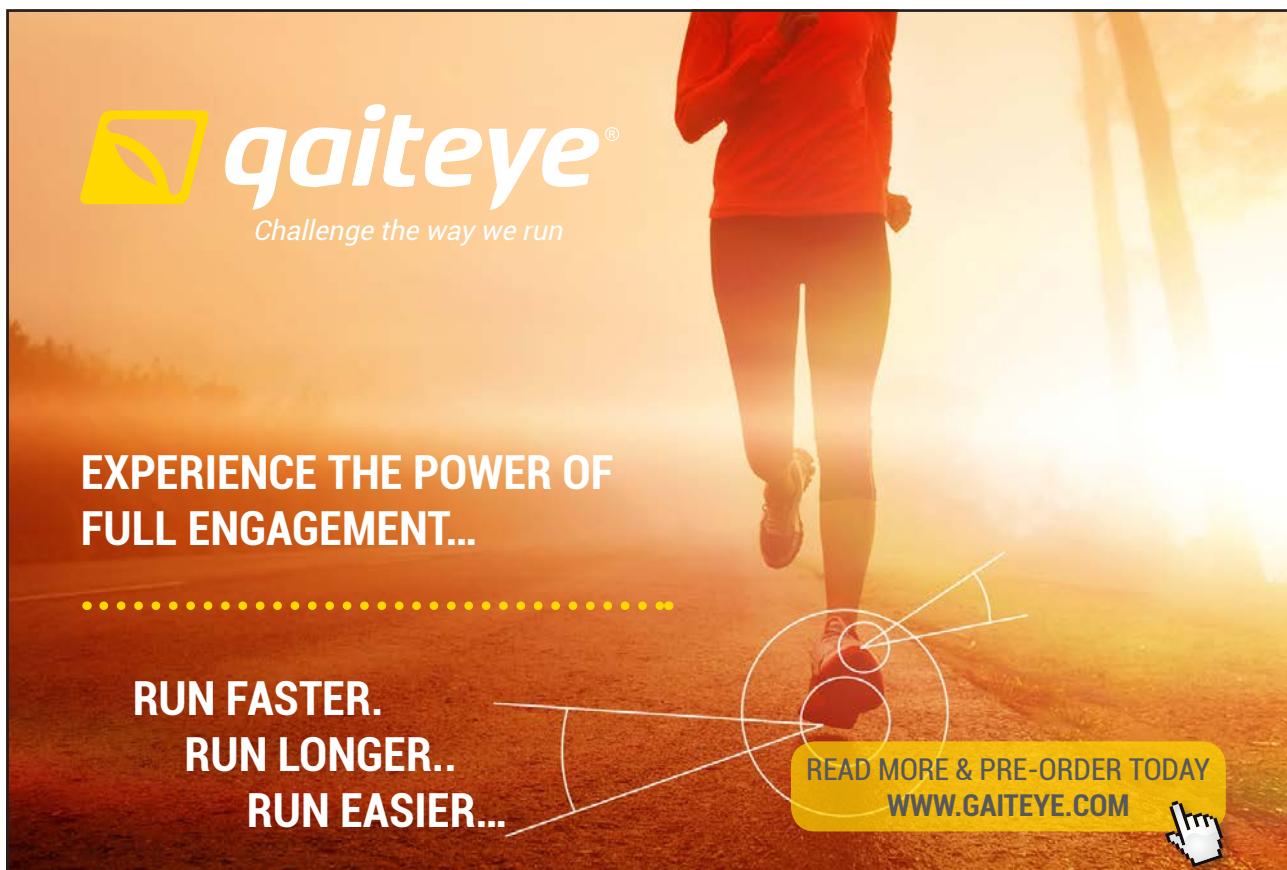
Hydrogen-air deflagrations in confined spaces present more severe hazards and associated risks compared to deflagrations in the open atmosphere. Indeed, overpressures registered during the near stoichiometric hydrogen-air deflagration of 1 kg of hydrogen in the tunnel are in the range 150–175 kPa (Groethe et al., 2005). This is essentially higher than overpressures of the order of only 6–10 kPa that were recorded during the stoichiometric hydrogen-air deflagration of significantly larger amounts of hydrogen of 55.5 kg in the open atmosphere (Pfortner and Schneider, 1983).

The simulations confirmed experimental observations that obstacles with a blockage ratio of 0.03, as per the tested configuration, have no significant effect on the maximum explosion pressure in the tunnel beyond the immediate vicinity of the obstacles. Both experiment and numerical simulations show small variance in maximum pressure along the tunnel. Based on the LES analysis it is demonstrated that side-on obstacle overpressure can increase significantly due to reflection of the shock wave formed in the tunnel during the deflagration.

Numerical experiments should be undertaken to apply the validated LES models to assess the consequences of realistic releases of hydrogen in the real scale tunnels. “Optimisation” of potential accidental releases has to be undertaken to exclude formation of hydrogen-air clouds that able to jeopardise life. For example, most of released hydrogen should be mixed with air below or close to the lower flammability limit. The possibility of shock-to-detonation transition should be estimated to assess the potential risk associated with an accident involving a hydrogen fuelled vehicle in a tunnel. Following this, a scenario of non-uniform mixture deflagration, created by realistic hydrogen release and dispersion, should be simulated to access realistic hazards.

#### 10.4.10. Lean hydrogen-air mixture combustion and non-uniform deflagrations

Most of numerical studies are devoted to uniform gaseous deflagrations. Hydrogen safety engineering requires prediction of pressure loads for realistic scenarios which are practically always include formation and consequent combustion of non-uniform flammable mixture. To be considered as a reliable predictive tool CFD models have to be validated against large-scale experiments which reproduce real life conditions. For non-reacting flows, the quantities of interest in LES are determined by the resolved large scales. In turbulent combustion, the essential rate-controlling processes of molecular mixing and chemical reaction occur at the scales which are much smaller than the resolved ones (Pope, 2004). Hence, these SGS processes have to be modelled. It is generally agreed that if more than 20% of turbulent scales are not resolved and have to be modelled then the method is called very large eddy simulations (VLES) rather than LES. However, we will continue to use the term LES.



**gaiteye**  
Challenge the way we run

**EXPERIENCE THE POWER OF  
FULL ENGAGEMENT...**

**RUN FASTER.  
RUN LONGER..  
RUN EASIER...**

**READ MORE & PRE-ORDER TODAY  
WWW.GAITEYE.COM**

The LES model previously applied for prediction of large scale unconfined stoichiometric hydrogen-air deflagrations, and 20–30% hydrogen-air deflagrations in a 78.5 m long tunnel, has been developed further to reproduce dynamics of lean uniform and non-uniform (gradient) hydrogen-air premixed combustion in a 5.7 m height and 1.5 m diameter cylindrical vessel (Molkov, 2009c; Verbecke et al., 2009).

Similar to previous studies the turbulent burning velocity model includes three interacting mechanisms: flow turbulence that is computed by Yakhot's (1988) equation for premixed turbulent combustion; evolution of the turbulence generated by flame front itself with the maximum value calculated from the Karlovitz et al. (1951) theory; and change of a total flame front area with the integral flame scale (outer cut-off) and the flame front thickness (inner cut-off) following the fractal theory.

An additional mechanism based on the leading point concept as formulated by Kuznetsov and Sabel'nikov and implemented by Zimont and Lipatnikov is introduced into the LES model. The results of numerical simulations reproduced experimental data on flame propagation in the uniform 12.8%, 14%, 16% and 20% by volume hydrogen-air mixtures in the large-scale vessel. The model is further applied to simulate non-uniform hydrogen-air deflagration: a mixture with concentration gradient (27% by volume of hydrogen at the top of the vessel and 2.5% at the bottom, average concentration 12.6%). Good agreement is achieved between simulations and experimental data for dynamics of both pressure and flame propagation only when the fourth mechanism, i.e. the leading point concept based on the selective diffusion phenomenon, is introduced to the LES model. The fractal sub-model was modified as well. Instead of a constant fractal dimension a fractal dimension as a function of burning velocity and r.m.s. velocity is introduced to make the fractal sub-model more universal (North and Santavicca, 1990).

#### 10.4.10.1. Overview of experiments

Experiments were carried out in a hermetically sealed 5.7 m height and 1.5 m internal diameter cylindrical vessel. All experiments were performed with dry hydrogen-air mixtures at  $25^{\circ}\text{C} \pm 3^{\circ}\text{C}$ . Ignition source was located 15 cm beneath the top of the vessel. Several fine-wire (75 micron diameter) thermocouples were located on both sides along the vessel's axis to detect the flame position in the vessel. The thermocouples were spaced 0.55 m apart vertically in a plane passing through the axis. Several piezoelectric transducers were installed at different intervals along the axis of the cylinder.

For uniform hydrogen-air mixtures, three fans were used to homogenise the mixture. For 12.8%, 14%, 16%, and 20% uniform hydrogen-air mixtures only data on flame propagations along the cylinder axis are available (Kumar and Bowles, 1990).

To establish concentration gradients, the hydrogen and air were first premixed in a small chamber prior to entering the top of the cylinder, then hydrogen was introduced continually by increased hydrogen concentration in the vessel. The rate of hydrogen increase was pre-determined on the test by test basis to create the desired gradient. After the concentration gradient was established, hydrogen concentrations were measured at the vertical sampling locations (Whitehouse et al., 1996). For a non-uniform mixture with 12.6% by volume average concentration the hydrogen distribution along the vessel axis is reported in (Whitehouse et al., 1996): 27% at the top of the vessel, and decaying to 2.5% at the bottom. Pressure dynamics and flame propagation in the 12.6% by volume gradient hydrogen-air mixture were compared with those in a well-mixed uniform 12.8% by volume mixture containing equivalent amount of hydrogen (Kumar and Bowles, 1990).

#### 10.4.10.2. The LES model (2009 version)

##### *Selective diffusion and leading point concept*

Combustion instabilities, including preferential-diffusive-thermal and hydrodynamic, cause perturbations of the laminar flame triggering formation of a cellular flame structure and then flame wrinkling, e.g. (Bradley, 1999; Bradley et al., 2001; Lipatnikov and Chomiak, 2005; Lipatnikov, 2007; Dorofeev, 2008; Ciccarelli and Dorofeev, 2008).

The selective diffusion phenomenon destabilises flat laminar flame front of lean hydrogen-air mixtures. Protruded (convex) into unburned mixture wrinkles propagate with higher velocity compared to concave wrinkles due to redistribution of hydrogen close to these wrinkles. Indeed, due to higher diffusivity of hydrogen its concentration at convex wrinkles will grow and at concave will decrease. Consequently, the burning velocity will increase or decrease respectively. This will lead to the increase of wrinkles amplitude. The selective diffusion effect depends on wrinkle curvature, i.e. reciprocal to radius.

There is a curvature of wrinkle at which the effect of selective diffusion on mass burning rate is maximum. Because a real flame has a spectrum of wrinkles of different curvature, the flame will be led by those wrinkles that have this optimum from a point of view of maximum burning rate curvature. These wrinkles will be responsible for propagation of a leading edge of flame front and called “leading points”. The concept of leading points was first suggested by Zeldovich and then developed further. Thus, an increase in the flame speed results from the development of the cellular structure in combination with formation of leading flamelet structures, i.e. leading points (Kuznetsov and Sabelnikov, 1990; Bradley, 1999; Bradley et al., 2001).

Kuznetsov and Sabelnikov (1990) stated that the turbulent flame speed is controlled by the burning velocity of these leading point flamelets, where the mixture composition is locally altered due to different diffusivity of fuel and oxidiser, i.e. preferential diffusion. Based on the assumption of a critically strained structure for the leading point and different diffusivities of fuel and oxidiser, they derived the model for a local change in the mixture composition within the leading point combustion zone as follows



$$\text{If } \alpha_{lp} \geq 1 \text{ then } \alpha_{lp} = \frac{\alpha_0(1 + C_{st}) \cdot d + d - 1}{d + C_{st}}; \text{ if } \alpha_{lp} < 1 \text{ then } \alpha_{lp} = \frac{\alpha_0(C_{st} + d)}{1 + \alpha_0 \cdot C_{st} + C_{st} \cdot (1 - \alpha_0 \cdot d)}, \quad (10-97)$$

where  $\alpha_p = 1/\phi_p$  is the reciprocal of the equivalence ratio  $\phi_p$  at the leading point;  $\alpha_0$  is the reciprocal of the equivalent ratio  $\phi$  in the original mixture;  $d = \sqrt{D_{ox}/D_f}$ , where  $D_{ox}$  and  $D_f$  are the molecular diffusion coefficients of oxidant and fuel respectively; and  $C_{st}$  is the mass stoichiometric coefficient.

To account for preferential diffusion effects for curved hydrogen flames the leading point concept as proposed by Kuznetsov and Sabel'nikov (1990) and implemented by Zimont and Lipatnikov (1995), who determined the hydrogen concentration at the leading points and found their corresponding burning velocities by linear interpolation of the experimental data provided by Karpov and Severin, was applied in the LES model (Verbeke, 2009). Figure 10–48 shows the augmentation of burning velocity by the leading point phenomenon,  $\chi_{lp}$ . Lean mixtures are all affected by this mechanism. For example, for 10% hydrogen-air mixture the laminar burning velocity has to be multiplied by the factor 2.4.

This e-book  
is made with  
**SetaPDF**



PDF components for PHP developers

[www.setasign.com](http://www.setasign.com)

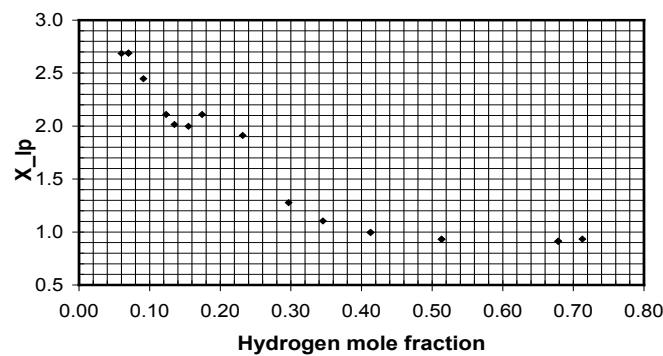


Figure 10-48. Leading point factor as a function to hydrogen mole fraction.

The preferential diffusion effect coupled with flame curvature is pronounced for lean hydrogen-air mixtures and has to be accounted for in the premixed combustion model through an additional “leading point” turbulence factor. This fourth mechanism of the turbulent burning velocity enhancement causes flamelet perturbations in the proximity of these leading flamelets cannot be resolved on meshes applied for large-scale problems and thus has to be modelled at SGS level. The leading point flame wrinkling factor  $\chi_p$  is introduced in the combustion model to correct the SGS burning velocity. It is assumed that the leading point turbulence coefficient develops linearly with radius to reach the maximum (see Fig. 10-48) at half of the critical radius  $R_0$ . It remains constant after that  $\chi_p = \chi_p^{\max}$ .

#### Update of the fractal sub-model (2009)

As the flame propagates, the Peclet number  $Pe$  (ratio of flame radius to flame thickness) increases beyond the second critical Peclet number,  $Pe_{cl}$ , from which the flame becomes self-similar, self-turbulized (Bradley, 1999; Bradley et al., 2001). The nature of combustion in the regime for  $Pe \geq Pe_{cl}$  is referred as fractal-like flame wrinkling and is responsible for a further increase of the turbulent burning velocity. Gostintsev et al. (1988) suggested that there is a transition from a cellular flame to a self-similar flame propagation regime at critical radius 1.0–1.2 m for near stoichiometric hydrogen-air mixtures, i.e. at the critical Peclet number of about 100,000 when a flame thickness is estimated as  $a/S_u$  where  $a$  stands for the thermal diffusivity. Bradley (1997) reported that in every case the burning velocity was about three times the laminar burning velocity just after the suggested transition.

According to the fractal theory the measured area of a surface in volume of size  $R$  (outer cut-off) depends on the area measurement scale  $\varepsilon^2$  as by  $A_l \approx \varepsilon^{2-D} R^D$ , where  $D$  is the fractal dimension, and  $\varepsilon$  is the inner cut-off (Gouldin, 1987). In the flamelet regime a ratio of turbulent to laminar burning velocity  $S_t/S_u$  is equal to a ratio of turbulent flame front area to laminar one  $A_t/A_l$  (Damkolher, 1940). For spherical flame the laminar flame front area is  $A_l \propto R^2$ . From the above it follows that  $S_t/S_u = A_t/A_l \propto (R/\varepsilon)^{D-2}$ . Then, to apply the fractal theory within its validity range, i.e. when the surface is contorted like in turbulent not laminar flame, and exclude problems with finding the proportionality coefficient, one could easily get  $S_{t1}/S_{t2} = (R_1 \cdot \varepsilon_2 / R_2 \varepsilon_1)^{D-2}$ .

The fractal theory was developed to provide a tool for description of highly contorted surfaces. Fully developed turbulent flame in the flamelet regime can be considered as such kind of surface. If  $R_0$  is a critical radius of a spherical flame at which the transition from laminar to turbulent self-similar regime of flame propagation is accomplished ( $R_0=1.0-1.2$  m for near stoichiometric hydrogen-air mixtures according to Gostintsev et al., 1988) then the following formula is applied to calculate the growth of turbulent burning velocity at radius  $R$  due to fractal structure of turbulent flame

$$S_t / S_{R_0} = (R \cdot \varepsilon_{R_0} / R_0 \cdot \varepsilon)^{D-2}, \quad (10-98)$$

where  $S_{R_0}$  is the turbulent burning velocity at radius  $R_0$ , and  $\varepsilon_{R_0}$  and  $\varepsilon$  are inner cut-off scales at  $R_0$  and  $R$  respectively.

A wide range of experimental values were suggested for the fractal dimension of flames. Gouldin (1988) argued that for low intensity turbulence the fractal dimension is lower than 7/3, and found  $D=2.11$  for very low turbulent flow intensities. Murayama and Takeno (1988), obtained fractal dimension data varying in a range  $D=2.2-2.35$ , with an average value around 2.26 for open atmosphere turbulent flames. Similar values  $D=2.2-2.33$  were reported by Gostintsev et al. (1999) for freely propagating premixed flames. Bradley (1999) suggested a theoretical value of  $D=2.33$ . Gülder et al. (2000) reported fractal dimensions within a range  $D=2.14-2.24$ .

The choice of the fractal dimension from the wide range of mentioned values is ambiguous. To make the LES model more universal the fractal sub-model has to exclude as much as possible adjustable by user parameters. North and Santavicca (1990) defined the fractal dimension by an empirical parameterization as a function of the ratio of the fluctuating velocity to the laminar burning velocity,  $u'/S_u$ ,

$$D = \frac{2.05}{u'/S_u + 1} + \frac{2.35}{S_u/u' + 1}, \quad (10-99)$$

where  $D=2.05$  in a limit of low flow intensities and  $D=2.35$  for highly turbulent flow.

Verbeke et al. (2009) assumed that the inner cut-off scale,  $\varepsilon$ , is proportional to the laminar flame thickness  $\varepsilon \approx \delta_L$  similar to Fureby (2005). Assuming  $\delta_L = \nu/S_u = \mu/(\rho \cdot S_u)$ , one can calculate:  $\varepsilon_{R_0}/\varepsilon = (\rho \cdot S_u \cdot \mu_{R_0})/(\rho_{R_0} \cdot S_{u_{R_0}} \cdot \mu)$ . Combining with the assumption of adiabatic compression and expansion  $S_u/S_{R_0} = (p/p_{R_0})^\varepsilon$ ,  $\rho/\rho_{R_0} = (p/p_{R_0})^{1/\gamma}$ ,  $T/T_{R_0} = (p/p_{R_0})^{(\gamma-1)/\gamma}$ , and Sutherland's viscosity equation  $\mu/\mu_{R_0} = (T/T_{R_0})^{3/2} \cdot (T_{R_0} + S)/(T + S)$ , yields

$$\frac{\varepsilon_{R_0}}{\varepsilon} = \left( (p/p_{R_0})^{\frac{5}{2\gamma} + \varepsilon - \frac{3}{2}} \cdot \left( T_{R_0} \cdot (p/p_{R_0})^{\left(\frac{\gamma-1}{\gamma}\right)} + S \right) / (T_{R_0} + S) \right), \quad (10-100)$$

where  $S=110.56K$  is the Sutherland's constant for air in temperature range 293 to 473 K.

***The turbulent burning velocity model***

The turbulent burning velocity model can be summarized as follows. For the transitional stage of flame propagation from laminar to fully turbulent ( $0 < R < R_0$ ), the model includes effects of the flow turbulence (Yakhot's transcendental equation), the turbulence generated by flame front itself (Karlovitz turbulence), and the leading point mechanism

$$S_t = S_u \cdot \chi_p \cdot \chi_K \cdot \exp\left(\frac{u'}{S_t}\right)^2. \quad (10-101)$$

For the self-similar fully developed turbulent combustion regime ( $R > R_0$ )

$$S_t = S_u \cdot \chi_p \cdot \chi_K \cdot \left(\frac{\varepsilon_{R_0}}{\varepsilon} \cdot \frac{R}{R_0}\right)^{D-2} \cdot \exp\left(\frac{u'}{S_t}\right)^2. \quad (10-102)$$

It is worth noting that the Karlovitz turbulence was modelled throughout the whole duration of flame propagation that is different from previous versions of the LES model

$$\chi_K = 1 + \left(\psi \cdot \chi_K^{\max} - 1\right) \cdot \left[1 - \exp\left(-\frac{R}{R_0}\right)\right]. \quad (10-103)$$



**YOU THINK.  
YOU CAN WORK  
AT RMB**

 **RAND  
MERCHANT  
BANK**  
A division of FirstRand Bank Limited  
Traditional values. Innovative ideas.

Rand Merchant Bank uses good business to create a better world, which is one of the reasons that the country's top talent chooses to work at RMB. For more information visit us at [www.rmb.co.za](http://www.rmb.co.za)

Thinking that can change your world

Rand Merchant Bank is an Authorised Financial Services Provider

The empirical parameterization by North and Santavicca (1990) for the fractal dimension is applied, see equation (10–99). There is only one empirical constant, i.e.  $\psi$ , available for a calibration of the LES model. There is a reservation for value of the critical diameter  $R_0$  for lean and rich mixtures.

### Numerical details

The calculation domain was designed according to the specification of the facility description (Kumar and Bowles, 1990; Whitehouse et al., 1996; AECL, 2008) and meshed by tetrahedral control volumes (CVs) of average size  $\Delta_{\mathcal{C}} = 0.8 \text{ m}$  with a total number 157,352 CVs. The general view of the domain, its dimensions and the surface mesh are shown in Fig. 10–49.

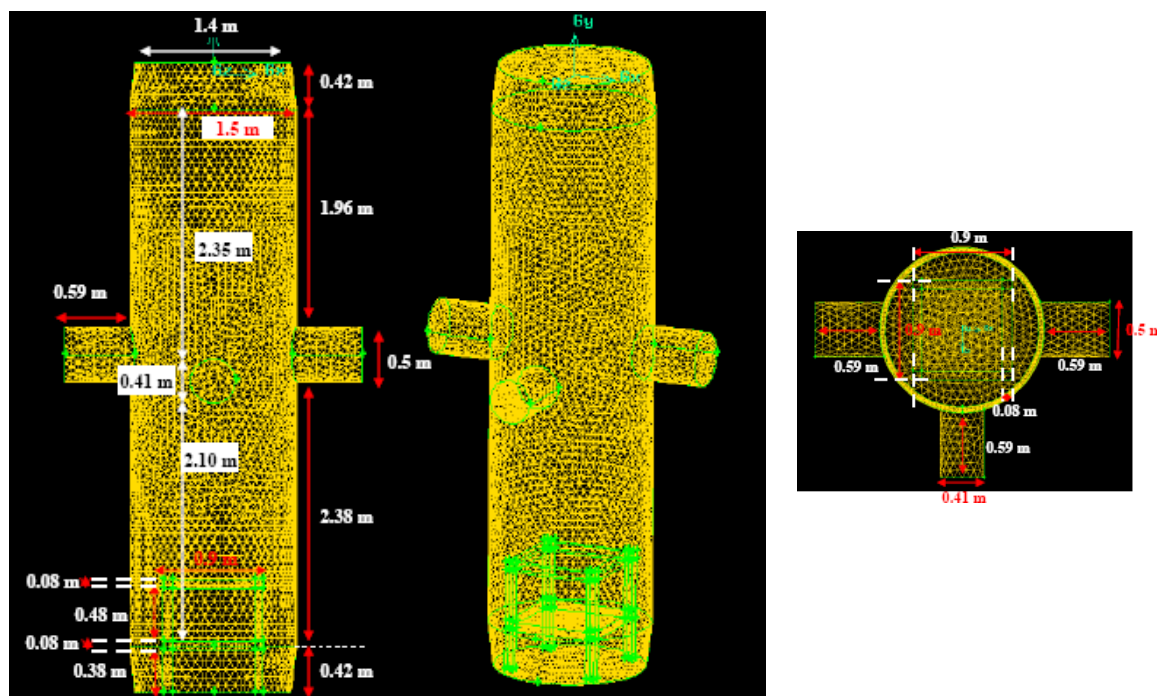


Figure 10–49. The calculation domain and the surface mesh.

The initial pressure and temperature were equal to those in the experiments:  $T=295 \text{ K}$ ,  $p=101.325 \text{ kPa}$ . Walls were modelled as non-slip, adiabatic, impermeable boundaries. Ignition was simulated by linear increase of the progress variable from 0 to 1 in one CV during a time equal to laminar flame propagation over half of the edge of the ignition control volume:  $\Delta t_{ign} = 1/2 \cdot (\Delta_{\mathcal{C}}^v / (S_u E_0))$ .

FLUENT 6.3 has been used as a CFD engine to realize the LES model. A coupled compressible solver with explicit linearization of the equation set was used with a Courant-Friedrichs-Lewy number equal to 0.8. A second-order upwind difference scheme was applied for discretization of convection terms and a second-order central scheme for diffusion terms.

## Results and discussion

A comparison between experimental and simulated flame propagation along the vessel axis for uniform 12.8%, 14%, 16% and 20% hydrogen-air mixtures is presented in Fig. 10–50. There is a reasonably good agreement for all mixtures with a calibration constant  $\psi = 1$ . It is worth noting that using exactly the same LES model as described in this section for large-scale unconfined near stoichiometric hydrogen-air deflagrations, and 20% and 30% hydrogen-air deflagrations in a 78.5 m long tunnel, the best agreement with experiments was achieved with  $\psi = 0.5$  (Verbecke, 2009). This may be attributed to instabilities, e.g. flame front interaction with acoustic waves, which are not resolved for this large-scale vessel and are not yet modelled at SGS level. Flame propagation in enclosure generates acoustic waves that, after reflections from the walls, interact with the flame front and develop flame perturbations, see for example (Dorofeev, 2008; Ciccarelli and Dorofeev, 2008).

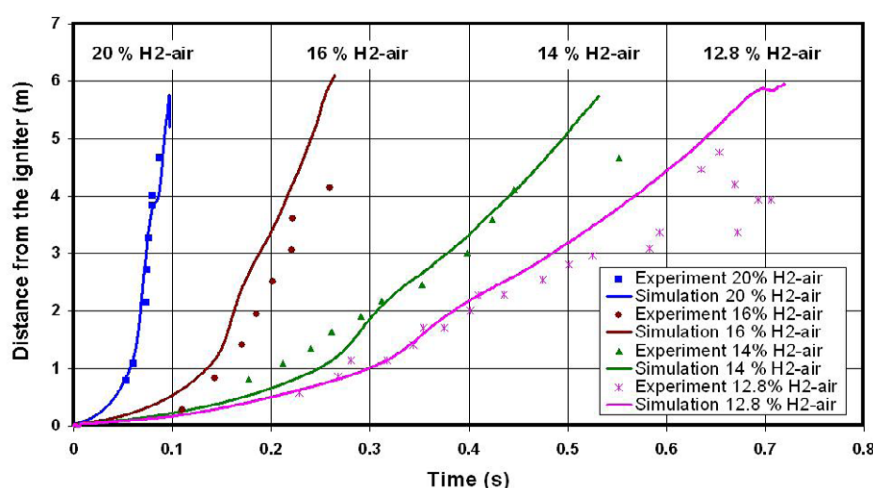


**Figure 10–50.** Experimental and simulated flame propagation dynamics along the vessel axis for 20%, 16%, 14%, and 12.8% hydrogen-air mixtures (Verbecke et al., 2009).

Modelling studies confirmed experimental findings that the enhancement of flame front wrinkling in a changing pressure field is associated with generation of vorticity through baroclinic effects (Liu et al., 1993; Batley et al., 1996). Bradley and Harper (1994) showed that Rayleigh–Taylor instability is the most probable source of turbulence arising from the baroclinic term  $\nabla p \times \nabla \rho / \rho^2$  in the vorticity equation. In its turn, the vorticity generation is promoted by flame-acoustic interaction, distorting the flame and further increasing the flame surface area. This mechanism is not yet resolved or modelled in the LES model.

Another possible reason for the increase of  $\psi$  from 0.5 for near stoichiometric to 1 for lean hydrogen-air mixtures is approaching a theoretical maximum for the turbulence generated by flame front itself in lean slowly burning mixtures, when “closing” of wrinkles is slower due to smaller burning velocity.



The leading point mechanism is essential for modelling lean hydrogen-air deflagrations as seen in Fig. 10–51. Without the implementation of leading point factor into the turbulent burning velocity model, the flame propagation is significantly underestimated compared to the experimental data. Indeed, for 20% hydrogen-air mixture the flame propagation velocity is equal to 44 m/s at distance 1 m from the ignition source and 162 m/s at distance 3 m with the turbulent burning velocity corrected by the leading point factor, and it is only 22 m/s and 50 m/s at 1 m and 3 m respectively without the correction. In the case of uniform 12.8% hydrogen-air mixture, the flame speed is 7.7 m/s at 1 m with correction and only 2.95 m/s without correction.

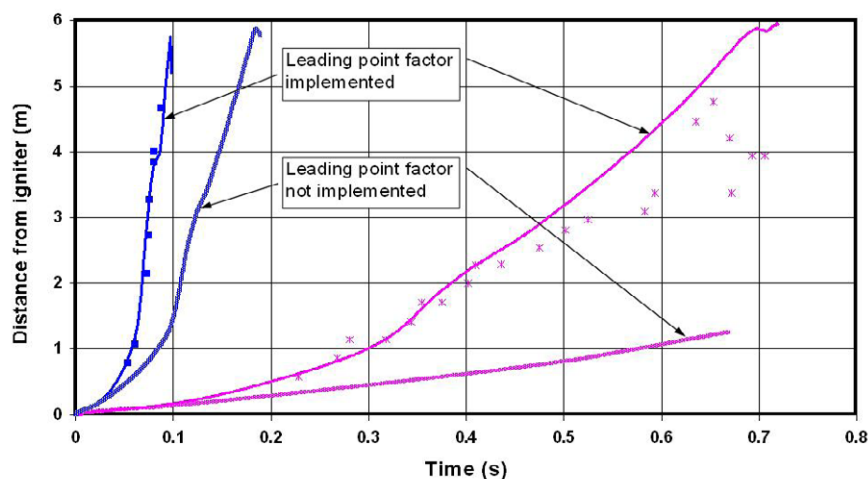


**Figure 10–51.** Experimental and simulated flame propagation with/without implementation of the leading point correction for uniform 12.8% and 20% hydrogen-air mixtures.

Figure 10–52 shows flame propagation dynamics for the uniform (12.8% vol.) and the gradient (average 12.6% vol.) hydrogen-air mixtures. For a scenario with practically the same amount of hydrogen released, flame propagates much faster in the mixture with concentration gradient. This can be explained by higher hydrogen concentration at location of the ignition source, i.e. 27% by volume hydrogen that is close to the stoichiometry. It can be estimated that for the gradient hydrogen-air mixture the flame speed reaches 57 m/s and 209 m/s at 1 m and 3 m from the ignition source respectively. For the uniform 12.8% hydrogen-air mixture the flame speed at the same locations reaches only 7.7 m/s and 9 m/s respectively.

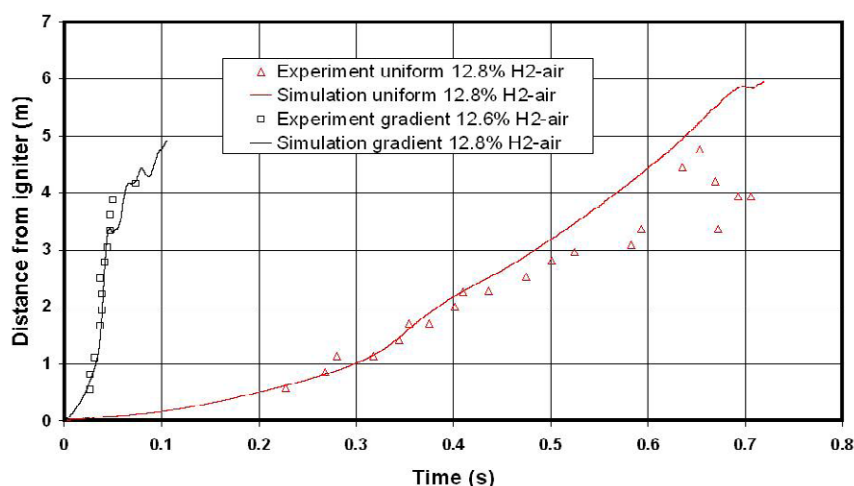


**Figure 10-52.** Experimental and simulated flame propagation for 12.8% uniform hydrogen-air mixture and 12.6% (averaged) gradient hydrogen-air mixture.

Comparison of experimental and simulated pressure dynamics for 12.8% uniform hydrogen-air mixture and 12.6% gradient hydrogen-air mixture is shown in Fig. 10-53. The pressure rise is much steeper in the mixture with the hydrogen concentration gradient compared to the uniform 12.8% hydrogen-air mixture. This is consistent with observed flame speeds and conclusions of the experimental study (Whitehouse et al., 1996) for top ignition: mixtures with hydrogen concentration gradient have much shorter times to peak overpressure than uniform mixtures with the same quantity of hydrogen because of higher hydrogen concentration at the ignition point.



Discover the truth at [www.deloitte.ca/careers](http://www.deloitte.ca/careers)

**Deloitte.**

© Deloitte & Touche LLP and affiliated entities.

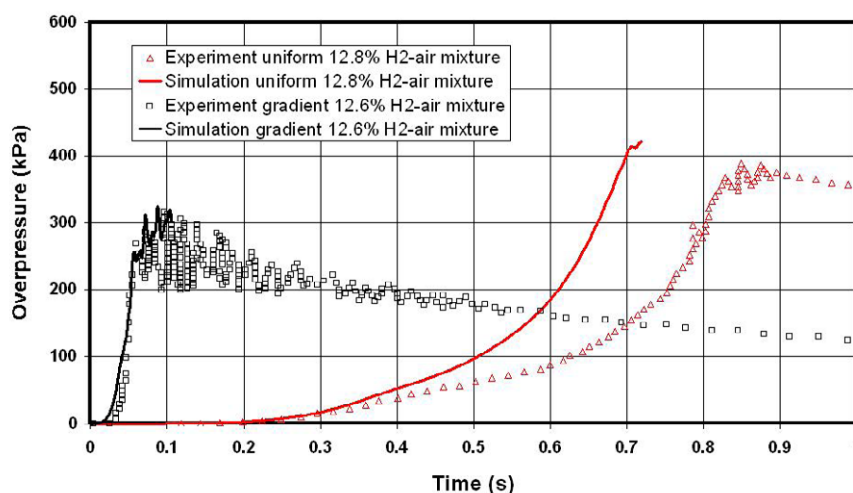


**Figure 10-53.** Experimental and simulated pressure dynamics for uniform 12.8% hydrogen-air mixture and non-uniform (12.6% averaged) gradient hydrogen-air mixture.

It is worth noting that the best fit simulation for the gradient (average 12.6% vol.) hydrogen-air mixture deflagration was obtained with  $\psi = 0.7$  as compared to  $\psi = 1$  for all uniform lean hydrogen-air mixtures in a range of concentrations 12.8-20.0% by volume. The possible reason may be the fact that in the gradient mixture the hydrogen concentration in the ignition region is near stoichiometric (27% vol.) with typically lower value of  $\psi$ . This is probably due to more pronounced intrinsic feature of lean flames to generate Karlovitz turbulence closer to its theoretical maximum.

The simulated pressure for non-uniform mixture is close to experiment. Contrary, simulated pressure develops faster than experimental pressure transients for the uniform mixture. This can be explained by absence of heat losses from hot combustion products to walls in the simulations. Heat losses have to grow with time.

### **Concluding remarks**

The LES model, calibrated previously to predict dynamics of large-scale hydrogen-air deflagrations in the open atmosphere and in a 78.5 m length tunnel, is developed further to reproduce experimental data on dynamics of lean uniform and non-uniform hydrogen-air deflagrations in 5.7 m height and 1.5 m diameter closed vessel.

The turbulent burning velocity model accounts for four mechanisms affecting turbulent burning velocity. In addition to three mechanisms applied in the previous versions of the model, i.e. flow turbulence, turbulence generated by the flame front itself, and fractal increase of flame front area with an integral flame scale, the model is amended by the fourth so-called leading point mechanism, affecting the mass burning rate through the synergy of preferential diffusion instability and spectrum of flamelets of different curvature (Kuznetsov and Sabelnikov, 1990; Zimont and Lipatnikov, 1995). The fractal sub-model is modified by the introduction of the inner cut-off dependence of deflagration pressure and temperature, which is taken as the flame front thickness, and the “universal” equation for the fractal dimension by North and Santavicca (1990).

The LES model update enables to reproduce the experimental flame propagation and pressure dynamics of lean uniform hydrogen-air mixtures in the range from 12.8% to 20% by volume of hydrogen in air. It is demonstrated that without correction of turbulent burning velocity by the preferential diffusion factor the flame propagation dynamics in lean hydrogen-air mixtures (12.8–20% vol.) is significantly under predicted.

Experimental data on flame propagation and deflagration pressure dynamics in the gradient (average 12.6% vol.) hydrogen-air mixture are reproduced by the LES model. In full agreement with experiment the pressure build up and flame propagation are much faster in the gradient mixture compared to the uniform mixture with practically the same amount of hydrogen.

The role of Rayleigh-Taylor instability, enhanced by flame-acoustic interaction within closed cylinder geometry, on the increase of the only calibration parameter of the model coefficient  $\psi$  is discussed briefly. It is suggested that the turbulence generated by slower burning lean hydrogen-air flames is closer to the theoretical maximum of the Karlovitz's turbulence compared to near stoichiometric mixtures. However, more research is needed to understand the dependence of  $\psi$  on deflagration parameters.

#### 10.4.11. Multi-phenomena turbulent burning velocity model of deflagrations

The multi-phenomena turbulent burning velocity model for LES of large-scale deflagrations is being continuously developed at the University of Ulster since 2002. The model is summarised in this section. There was no adjustment of any model parameters compared to the last version of the model published (Molkov, 2009c; Verbecke et al., 2009). Recently the model has been successfully applied to simulated distorted tulip flame in a small-scale closed duct (Xiao et al., 2012).

The compressible LES governing equations are obtained by filtering the three-dimensional conservation equations of mass, momentum, energy and the progress variable equation. The sub-grid scale (SGS) turbulence model derived from the renormalization group (RNG) theory by Yakhot and Orszag (1986) is adopted. The RNG model is purely theoretical and does not contain any empirical parameters. It is able to reproduce laminar, transitional and turbulent flows.

The progress variable equation is used to model the flame front propagation. The mass burning rate is described by the gradient method (Prudnikov, 1967). The gradient method ensures that the prescribed mass burning rate  $\rho_u S_t$  takes place in the simulations independent of the grid resolution. The numerical requirement to the gradient method is that a simulated flame thickness spreads over 4-5 control volumes.

The model is based on the assumption of a flamelet regime of premixed turbulent combustion that is thought to be valid for accidental combustion with comparatively large scales and moderate turbulence. In the model, the mass burning rate is determined in general as a product of the local burning velocity in a flamelet and the surface area of flamelets both being affected by different instabilities, etc.

#### 10.4.11.1. Effect pressure, temperature and concentration on the burning velocity

The values of laminar burning velocity for the whole hydrogen flammable range can be found in the literatures (Zimont and Lipatnikov, 1995; Tse et al., 2000; Lamoureux et al., 2003). The dependence of laminar burning velocity on temperature and pressure during deflagration simulations uses the assumption of adiabatic compression or expansion similar to previous studies (Molkov and Nekrasov, 1981)

$$S_u = S_{ui} \cdot \left( \frac{T}{T_{ui}} \right)^m \left( \frac{p}{p_i} \right)^n = S_{ui} \cdot \left( \frac{p}{p_i} \right)^\varepsilon \quad (10-104)$$

where  $S_{ui}$  is the burning velocity at initial temperature  $T_{ui}$  and pressure  $p_i$ ,  $\varepsilon = m + n - m/\gamma_u$  is the overall thermokinetic index, and  $\gamma_u$  is the adiabatic index of unburned mixture. The effect of hydrogen concentration on the burning velocity is included into a value of the initial laminar burning velocity  $S_{ui}$ , and indices  $m$  and  $n$  when it is needed.

#### 10.4.11.2. Effect of flow turbulence on the burning rate

When turbulence occurs in the flow during combustion wave propagation the flame front would be distorted and the burning rate will be enhanced consequently. The flame thickness is normally a fraction of a millimeter (Aung et al., 1997) and it is impractical to resolve in simulations the three-dimensional real flame thickness and the flow turbulence at all scales, i.e. it is impossible to perform DNS at comparatively large scales characteristic for most of hydrogen safety problems.

**I WANT TO CHANGE DIRECTION,  
AND THE WORLD.**

**GOT-THE-ENERGY-TO-LEAD.COM**

We believe that energy suppliers should be renewable, too. We are therefore looking for enthusiastic new colleagues with plenty of ideas who want to join RWE in changing the world. Visit us online to find out what we are offering and how we are working together to ensure the energy of the future.

**RWE**  
The energy to lead

The effect of flow turbulence on the flame front wrinkling is partially resolved by LES at scales comparable to applied mesh. The effect of unresolved SGS flow turbulence is modeled following the Yakhot's (1988) transcendental equation for the turbulent burning velocity of premixed turbulent combustion  $S_t = S_u \cdot \exp(u'/S_t)^2$ , where  $u'$  is the SGS residual velocity. This equation is derived from the first principles and does not include any empirical coefficients. For the laminar flow with  $u' = 0$ , the equation yields  $S_t = S_u$ .

However, the Yakhot's equation cannot be used in its original form in the LES of large-scale deflagrations as the mesh size is large compared to the flame front thickness and thus phenomena affecting the turbulent burning rate at scales of flame thickness cannot be resolved in simulations. In order to account for various mechanisms enhancing turbulent burning velocity and unresolved on a comparatively large mesh, i.e. selective diffusion and flamelet curvature as well as turbulence generated by flame front itself and fractals structure of the flame front, the laminar burning velocity in the original Yakhot's equation is substituted by a SGS wrinkling velocity in the model

$$S_t = S_w^{SGS} \cdot \exp(u'/S_t)^2. \quad (10-105)$$

This is the principle difference in the application of the Yakhot's equation compared to other studies. As the SGS physical mechanisms cannot be resolved directly, the methods used to account for these mechanisms are overviewed below.

#### 10.4.11.3 Effect of turbulence generated by flame front itself

The wrinkled or turbulent flame front generates additional turbulence in the near-field region (Karlovits et al., 1951). The increase of surface area of the flame front due to the turbulence generated by the flame front itself cannot be resolved with current computing power even for moderate scale practical problems. The upper limit for a flame wrinkling factor due to the self-induced turbulence can be derived for high Reynolds number flows as (Molkov et al., 1984)

$$\chi_K^{\max} = (E - 1) / \sqrt{3}, \quad (10-106)$$

where  $E$  is the expansion coefficient of combustion products, i.e. the ratio of densities of the unburned mixture and the burned gases. For a flame propagating in an initially quiescent mixture, this wrinkling factor gradually increases from 1 at the ignition point to the maximum value of  $\chi_K^{\max}$  for a fully developed turbulence. Gostintsev et al. (1988) reported that the critical radius for the onset of self-similar flame propagation (fully developed turbulence) for near-stoichiometric hydrogen–air mixtures is about  $R_0 = 1.0\text{--}1.2$  m. In order to take into account these transitional effects, the following equation is applied for SGS modeling of the unresolved self-induced by flame turbulence

$$\Xi_K = 1 + (\psi \cdot \chi_K^{\max} - 1) \cdot [1 - \exp(-R/R_0)], \quad (10-107)$$



where  $R$  is the distance from the ignition point to the flame front, and  $\psi \leq 1$  is a model constant. This constant to current knowledge is about  $\psi = 0.5-0.6$  for near stoichiometric and moderately rich hydrogen-air mixture, and it grows to maximum value  $\psi = 1$  for lean hydrogen-air mixtures (Molkov et al., (2008b)). Therefore, with the consideration of physical phenomenon of the turbulence generated by flame front itself the following expansion for the SGS wrinkling burning velocity is obtained  $S_w^{SGS} = S_u \cdot \chi_K$ .

#### 10.4.11.4. Effect of preferential diffusion coupled with flamelet curvature (leading point)

The hydrogen flame with a Lewis number less than unity is affected by the preferential diffusion effect. For a given mixture composition, there exists a flame curvature radius which corresponds to the maximum mass burning rate. According to Zeldovich's idea the flamelets of such curvature will lead the turbulent premixed flame propagation. Zimont and Lipatnikov (1995), based on the work of Kuznetsov and Sabelnikov (1990), calculated a leading point coefficient  $\chi_p^{\max}$  associated with this mechanism as a correction to the laminar burning velocity dependent on mixture composition. In the present model, it is assumed that the diffusive-thermal instability  $\chi_p$  develops linearly to the maximum value  $\chi_p^{\max}$  at half of the critical radius  $R_0$

$$\chi_p = \left\{ 1 + \frac{(\chi_p^{\max} - 1) \cdot 2R}{R_0} \right\}, \quad (10-108)$$

For distances from the ignition source above the critical radius  $R > R_0$ ,  $\chi_p = \chi_p^{\max}$ . Taking into account the leading point mechanism, the equation for the SGS wrinkling burning velocity to be changed to  $S_w^{SGS} = S_u \cdot \chi_K \cdot \chi_p$ .

#### 10.4.11.5. Effect of fractal surface of turbulent flame front

Turbulent flame has a contorted surface. Thus, the conclusions of the fractal theory are applied to model change of fractal surface area of a turbulent flame as a function of the outer cut-off that is usually the flame size, and the inner cut-off that is currently chosen as the flame front thickness. The enhancement of turbulent burning velocity by this physical phenomenon is calculated in the model as

$$\chi_f = \left( R \cdot \varepsilon_{R_0} / R_0 \cdot \varepsilon \right)^{D-2}, \quad (10-109)$$

where  $R_0$  is the critical radius for establishment of fully developed turbulent flame, from which the fractal sub-model is applied;  $R$  is distance from the ignition source (outer cut-off);  $\varepsilon_{R_0}$  and  $\varepsilon$  are inner cut-off scales at  $R_0$  and  $R$  respectively; and  $D$  is the fractal dimension.

The choice of the fractal dimension from the wide range of mentioned values is ambiguous. To make the LES model more universal the fractal sub-model has to exclude as much as possible adjustable by user parameters. defined the fractal dimension by.

The empirical parameterization of the fractal dimension,  $D$ , as a function of the ratio of the fluctuating velocity,  $u'$ , to the laminar burning velocity,  $S_u$ , is applied (North and Santavicca, 1990)

$$D = \frac{2.05}{u'/S_u + 1} + \frac{2.35}{S_u/u' + 1} \quad (10-110)$$

The equation for the SGS wrinkling burning velocity has to be changed to  $S_w^{SGS} = S_u \cdot \chi_K \cdot \chi_p \cdot \chi_f$  to account for unresolved in simulations the fractal structure of turbulent flame front.

#### 10.4.11.6. The equation for turbulent burning velocity

Finally, the multi-phenomena combustion model includes currently five different physical mechanisms affecting the turbulent burning velocity, i.e. the effects of transient hydrogen concentration, temperature and pressure on laminar burning velocity, the flow turbulence in the incoming unburned mixture, the turbulence generated by flame front itself, the leading point mechanisms, and the fractal increase of turbulent flame front area. The turbulent burning velocity is modeled as

$$S_t = S_u \cdot \chi_K \cdot \chi_p \cdot \chi_f \cdot \exp\left(\frac{u'}{S_t}\right)^2 \quad (10-111)$$

The advantage of the turbulent burning velocity model for LES is its flexibility to include new mechanisms affecting the burning rate. Currently research continues at the HySAFER centre on inclusion of Rayleigh-Taylor instability to the model.

[bookboon.com](http://bookboon.com)

## Corporate eLibrary

See our Business Solutions for employee learning

[Click here](#)



# 11 Detonations

## 11.1. Direct initiation of detonation

The ability of a hydrogen-air mixture to direct initiation of detonation is greater than that of hydrocarbons. The direct initiation of hydrogen-air mixture detonation is possible by 1.1 g of high explosive tetryl (BRHS, 2009). Only 1.86 g of high explosive TNT (trinitrotoluene) is needed to initiate detonation in 34.7% hydrogen-air mixture in the open atmosphere. However, for 20% hydrogen-air mixture the critical TNT charge increases significantly to 190 g.

For comparison, release of energy during explosive reaction of 1 g TNT is arbitrarily standardized as 4.184 kJ (a gram of TNT releases 4.1–4.602 kJ upon explosion, see Wikipedia), and the lower heat of combustion of 1 g of hydrogen is equal to  $(241.7 \text{ kJ/mol} / 2.016 \text{ g/mol}) = 119.89 \text{ kJ}$ . Thus, the TNT equivalent of hydrogen is high: 28.65, i.e. 28.65 g of TNT is energetic equivalent of 1 g of hydrogen.

## 11.2. LES of hydrogen-air detonations

The large eddy simulation (LES) model of hydrogen-air detonation at very large scales, which doesn't require Arrhenius chemistry, is presented in this section (Zbikowski et al., 2008). The progress variable equation is applied for the first time to simulate propagation of a reaction front following and coupled with a leading shock. The gradient method, based on a product of pre-shock mixture density and detonation velocity, is employed as a source term in the progress variable equation. Chemical kinetics enters the combustion model only through its influence on the detonation velocity and modelling of detailed chemistry is omitted.

The LES model is verified against theoretical solution by the Zeldovich-von Neumann-Döring (ZND) theory for a case of planar 29.05% hydrogen-air detonation in elongated  $3 \times 3 \times 100 \text{ m}$  calculation domain. Thermodynamically calculated values of the specific heats ratio for burned mixture  $\gamma=1.22$  and the standard heat of combustion  $\Delta H_c=3.2 \text{ MJ/kg}$  are applied without any adjustment often applied in other models to achieve better reproduction of experimental data.

Numerical simulation reproduced theoretical values of von Neumann spike, Chapman-Jouguet pressure, Taylor wave and prescribed detonation propagation velocity. There are no adjustable parameters in the model. Practically no grid sensitivity for the planar detonation wave is demonstrated by this LES model. Detonation velocity and pressures are shown to be nearly independent of the computational cell size in a wide range of cell sizes 0.1–1.0 m. Impulse depends to some extent on a cell size. There is no intention to use this oriented on large-scale applications LES model to reproduce fine structure of the detonation wave.

### 11.2.1. Introduction to detonation modelling

Detonation is a worst case scenario for accidents with unscheduled hydrogen release. Higher propensity of hydrogen-air mixtures to deflagration-to-detonation transition (DDT) compared to hydrocarbon-air mixtures, along with lower ignition energy and wider detonability limits, require special technical and organizational measures to guarantee the same level of safety for emerging hydrogen-powered technologies as for today's fossil-fuelled economy. Contemporary engineering tools are needed to simulate pressure effects of hydrogen explosions in the open atmosphere and complex geometries at practical scales. Prediction of detonation pressure effects, i.e. pressure and impulse, as well as blast parameters beyond the detonation zone are important for hydrogen safety engineering, particularly for hazard and risk assessment through realistic safety distance assessment for hydrogen infrastructure and development of mitigation techniques.

The Zeldovich – von Neumann – Döring (ZND) theory, developed by Zeldovich (1940), von Neumann (1942) and Döring (1943) following the analysis of one-dimensional shock with energy feeding performed earlier independently by Chapman (1899) and Jouguet (1905–1906), implies that detonation is a complex of precursor shock and combustion wave. This shock compresses the fresh mixture and enables it to react. The end of reaction zone is defined by the Chapman-Jouguet (CJ) condition (sonic plane).

Expansion of the combustion products in the reaction zone creates the thrust supporting the leading shock (Lee, 2008a). An ideal detonation travels at a near constant supersonic speed of von Neumann shock 1.5–3 km/s with a propagation Mach number between 4.5 and 9 (Fickett and Davis, 2000). The reacting flow is subsonic relative to the shock, and the local Mach number  $M$  ( $M < 1$ ) increases with the distance from the leading shock due to the heat release by the chemical reaction (Clavin, 2004).

Detonation front thickness is a distance from the precursor shock to the end of reaction zone where the CJ condition is reached. Each wave of the ZND type has a minimum sustainable detonation speed known as the CJ speed in which a sonic plane (relative to the detonation shock speed) arises at the CJ point. The reaction zone in detonation is usually less than 10 mm for most stoichiometric fuel-air mixtures and less than 0.1 mm for fuel-oxygen mixtures (Bauwens, 2006), which is due to the fact that in detonation a material is consumed  $10^3$  to  $10^8$  times faster than in an ordinary premixed flame making detonation “easily distinguishable from other combustion processes” (Fickett and Davis, 2000).

Combustion energy released in reaction front feeds the leading shock by sonic waves. The speed of detonation wave and the thermodynamic state at the CJ point are determined by the initial upstream shock state and by the equation of state for the reaction products alone. Rapid combustion occurs in the detonation as a result of the exponential dependence of the chemical reaction rate on temperature which in consequence supports the shock (Lee, 1984; Oran, 1999). The particular form of the reaction rate law and the equation of state for partially reacted material affect only the interior structure of the reaction zone (Fickett and Davis, 2000; Short, 2005).

Downstream of the sonic plane is a region where an expansion wave, i.e. Taylor wave, connects the state at the CJ plane to the rear boundary. The Taylor wave does not have to be attached to the final point, i.e. CJ point (Fickett and Davis, 2000; Short, 2005). The expansion fan is not strictly a part of either the CJ or ZND models. The products beyond the CJ plane continue to accelerate as they expand and their temperature and pressure continue to drop. Taylor (1950) was the first to examine the distribution of velocity in this region. Gas velocity at the CJ plane is about  $\frac{1}{3}$  of  $D$  (Nettleton, 1987). The pressure gradient in the expansion wave for particular pressure depends only on the distance of the front from the detonation origin. At the end of the Taylor wave for planar detonation the pressure is about 0.375 of  $P_{CJ}$  (Nettleton, 1987).

Euler equations with Arrhenius chemistry are commonly used for numerical simulation of detonations. The application of Navier-Stokes (NS) equations is more promising approach (Sharpe, 2001) enabling DDT modelling and simulation. However, as mentioned by Fujiwara and Fukiba (2001) the unsteadiness in multidimensional detonation makes it extremely difficult to use NS equations, because of a number of unsteady shear layers existing not only on the tube walls but also down-stream of the curved and intersecting shock waves.



**Brain power**

By 2020, wind could provide one-tenth of our planet's electricity needs. Already today, SKF's innovative know-how is crucial to running a large proportion of the world's wind turbines.

Up to 25 % of the generating costs relate to maintenance. These can be reduced dramatically thanks to our systems for on-line condition monitoring and automatic lubrication. We help make it more economical to create cleaner, cheaper energy out of thin air.

By sharing our experience, expertise, and creativity, industries can boost performance beyond expectations.

Therefore we need the best employees who can meet this challenge!

**The Power of Knowledge Engineering**

Plug into The Power of Knowledge Engineering.  
Visit us at [www.skf.com/knowledge](http://www.skf.com/knowledge)

**SKF**

Real detonation wave structure is far more complex than in the ZND model of planar detonation, and involves interactions between incident shocks, Mach stems, transverse waves, and boundary layers through which detonation is moving (Lee, 2008b). At the interaction of a transverse wave, Mach stem and incident shock, triple points are formed and create patterns called detonation cells, which size depends on the mixture composition and the chemical reaction mechanism (Oran, 1999). Resolution of these three-dimensional structures would require grid size of the order of few microns. Such resolution has to be naturally given up in tackling large-scale industrial problems.

Over 100 points are required in the half-reaction length of steady planar detonation to obtain a truly converged solution when Arrhenius chemistry is applied (Sharpe, 2000). Resolutions of less than about 20 points per half-reaction length give very poor or else entirely spurious solutions. Short and Quirk (1997) have shown that for pulsating detonations with realistic chain-branching reactions, a few hundred points per half-reaction length may be required to obtain even the qualitatively correct solutions. The resolution required to obtain converged solutions in multi-dimensional cellular detonation simulations is likely to be higher than that for the simpler pulsating detonations.

Generation of high-accuracy solution-adaptive grids resolving all such highly-unsteady shear layers is impossible within the present computational capabilities as a required mesh of 1 micron necessitates  $2 \times 10^{10}$  grid points for a 2D domain of only 10x20 cm which is far too small for accident scales of tens and hundreds of meters. Increase of cell size makes even one step irreversible Arrhenius chemistry incapable of reproduction of experimental explosion characteristics without “recalibration” for each particular grid.

An important feature of the Arrhenius reaction rate detonation models at large scales is that numerical mesh doesn't allow to resolve the detonation front and its simulated thickness is much larger than the physical one, hence the reaction rate is grid-sensitive. As a result the application of Arrhenius reaction rate equation to large-scale detonation modelling requires calibration of grid-dependent pre-exponential factor and activation energy, as well as calibration of a value of the heat of combustion in some cases, to provide CJ detonation propagation speed. Modelling of the planar ZND detonation using CFD and Arrhenius reaction rate chemistry would require resolution of the reaction zone with a grid size of the order of microns, otherwise, “tuning” of constants in the Arrhenius equation with the grid size is necessary. This makes detonation simulations with Arrhenius chemistry on large grids “loose”. Thus, Arrhenius chemistry approach can hardly be suggested as a grid independent tool for hydrogen safety engineering to tackle large-scale problems. Alternative methods of detonation modelling should be developed, verified by recognised theories and validated against large-scale experiments.

A few publications on simulation of comparatively large-scale hydrogen-air detonations can be found in literature (Breitung et al., 1996; Armand et al., 1997; Ng et al., 2007; Vaagsaether et al., 2007; Bedard-Tremblay et al., 2009; Heidari et al., 2009). Some details of these studies are overviewed below.



The simulations of hydrogen-air detonation experiment in the RUT facility using Euler equations were presented by Breitung et al. (1996). The authors used one-step Arrhenius chemical reaction and the uniform cubic mesh size of 1 cm. Simulation of 25% hydrogen-air mixture detonation demonstrated a close agreement between the simulated and the observed pressure peak arrival time. Difference between the experimental and the simulated pressure impulse was within 10%. However, the simulation of 16% hydrogen-air mixture detonation required introduction of two-step reaction chemistry on the 1 cm size mesh.

Reduced chemistry with five reactions was used in (Armand et al., 1997) to model detonations, including the hydrogen-air detonation experiments in the RUT facility. The authors performed 3D simulations, but 1D and 2D calibration studies were used prior to detonation simulations to find suitable pre-exponential factor and activation energy which would reproduce the experimentally observed detonation pressures and propagation velocity.

The detonation simulations by Heidari et al. (2009) were based on the Euler equation set and single step chemistry with grid resolution of the order of 5 cm. The constants of the Arrhenius reaction, i.e. pre-exponential factor and activation energy, had to be adjusted to ensure that CJ pressure and velocity are reproduced. The authors paid special attention to shock capturing and used Van Leer (TVD family) scheme.

Detonation of non-uniform hydrogen-air mixture, resulted from accidental hydrogen release in the electrolyser facility with sizes 4.0x2.54 m and the reformer facilities with sizes 2.9x2.1 m, was simulated by Bedard-Tremblay et al. (2009) using 2D formulation. The authors used one step Arrhenius reaction rate chemistry and Euler equations. A flux limiter scheme was used close to the shock for the better shock capturing and second order accurate in space and time schemes were used in the rest of the domain. 2D formulation allowed to use the numerical mesh size as small as 1.4 mm.

Comprehensive review of detonation modelling and numerical simulations may be found elsewhere (Gamezo and Oran, 2005). Detonation models were used to solve combustion and detonation problems including shock-flame interactions and predictive DDT (Oran et al., 2008). A review of an alternative method for detonation/DDT simulations to Arrhenius chemistry can be found in (Cant et al., 2004).

Numerical simulations are performed sometimes not only with different Arrhenius constants yet with thermodynamic parameters different from actual ones to achieve better agreement with experiment. These can include increased heat of combustion or reduced ratio of specific heats for combustion products of hydrogen-air mixtures, e.g.  $\gamma=1.16-1.17$  instead of 1.24 for stoichiometric hydrogen-air mixture, etc. The LES detonation model developed at Ulster is free from such adjustments.

The DDT phenomenon includes both deflagration, i.e. subsonic propagation of combustion wave, and detonation, i.e. supersonic propagation of coupled shock and reaction front structure, as well as their interaction with shocks, shock reflections, boundary layers, etc. (Oran et al., 2008). Contrary to detonation, where effects of viscosity play negligible role and which may be modelled using inviscid Euler equations, a DDT model requires solution of Navier-Stokes equations as viscosity and turbulence are important part of the DDT process. Thus, DDT simulations (Gamezo et al., 2008) were based on solution of the Navier-Stokes equation set, one-step Arrhenius reaction mechanism; the calculation domain was  $2 \times 128$  cm only. It is worth to mention that the required resolution in this simulation was of the order 4.8 microns. Simulations of DDT at larger scale pipe of  $0.107 \times 4$  m was attempted in (Vaagsaether et al., 2007). The authors also solved Navier-Stokes equations and used two-step Arrhenius reaction rate mechanism on 2 mm grid.

In this section we test the LES model to reproduce parameters of hydrogen-air detonation without Arrhenius chemistry. The objective is verification of a new LES methodology to simulate planar hydrogen-air detonation at scales of hundred of meters against a solution by the ZND theory.

The LES model will be applied in this section to simulate detonation of near stoichiometric 29.05% hydrogen-air mixture at initial conditions of 0.099 MPa and 304 K, that travels at 1954 m/s with a propagation Mach number  $M=4.8$  and the detonation front thickness 5.21 mm according to the ZND theory (Brown and Shepherd, 2006).

With us you can  
shape the future.  
Every single day.

For more information go to:  
[www.eon-career.com](http://www.eon-career.com)

Your energy shapes the future.

**e-on**

### 11.2.2. The LES model of detonation and its verification against the ZND theory

The LES models of deflagration and detonation exhibit similarities. The underlying idea of this approach is a transient simulation of deflagration through the DDT to detonation in the future using the same model and software.

The governing equations are the same as for the LES deflagration model described in the previous chapter, and include the continuity equation for mass conservation, the Navier-Stokes equations for momentum conservation, and the energy conservation equation. The progress variable equation for detonation propagation has the same form as for gaseous deflagrations with only one difference, i.e. the turbulent burning velocity being substituted by the detonation velocity in the source term. The renormalization group (RNG) model is applied for sub-grid scale (SGS) modelling of turbulence.

#### ***Combustion model***

The extent of reaction in the detonation wave can be measured in terms of the progress variable, which has zero value  $c=0$  immediately behind the leading shock and  $c=1$  at the CJ plane at which reaction is complete (Nettleton, 1987). Chemical kinetics enters the combustion model only through its influence on the detonation velocity and modelling of detailed chemistry is omitted in this approach. This creates conditions for grid independency of the numerical methodology when the gradient method is applied.

The combustion model applied for detonation front tracking is based on the same progress variable equation as for the LES model of deflagration, with the gradient method for a source term,  $S_c = \rho_u \cdot D \cdot |\nabla \tilde{c}|$ . The only difference between deflagration and detonation mathematical models, as mentioned above, is the substitution of turbulent burning velocity by detonation velocity. Integration of the source term through the numerical reaction front thickness reproduces independent on an actual numerical thickness of the front a physically correct mass consumption rate per unit area of the planar detonation wave, i.e.  $\rho_u \cdot D$ . The mass flow rate of mixture entering the unit area of the planar shock is equal to the mixture mass consumed at time unit per unit area of reaction front following the shock.

Detonation velocity,  $D$ , is pre-calculated for each mixture composition, e.g. with use of the Shock and Detonation Toolbox ([http://www.galcit.caltech.edu/EDL/public/cantera/html/SD\\_Toolbox/index.html](http://www.galcit.caltech.edu/EDL/public/cantera/html/SD_Toolbox/index.html)).

The source term in the energy conservation equation is  $S_e = \Delta H_c \cdot S_c$ , where  $\Delta H_c$  is the standard heat of combustion. Integration of this source term through the thickness of the numerical reaction zone reproduces correct value of energy released during combustion of mixture passing unit area of reaction front in unit of time. Thermodynamically calculated by CANTERA the lower heat of combustion of 29.05% hydrogen-air mixture  $\Delta H_c = 3.2$  MJ/kg is applied. Similar to the heat of combustion, the specific heats ratios for unburned and burnt mixtures calculated thermodynamically without any adjustment were adopted. Specific heats of unburned and burnt mixtures throughout the calculation domain were approximated as piecewise-polynomial functions of temperature with polynomial coefficients calculated according to mass-weighted mixing law of composing species. The ratios of specific heats for fresh and burnt mixture were calculated as  $\gamma_u = 1.4$  and  $\gamma_b = 1.22$  respectively. The ratio of specific heats for burnt mixture was determined for isobaric conditions at CJ plane.

The gradient method does not define the exact location of the reaction front as an interface in a computational cell or between cells, but represents it as a monotonous change of the progress variable through a number of control volumes (CV) as underlined by Oran and Boris (2001). The numerical requirement for a flame front thickness simulated by the gradient method is about 4–5 CVs (Hawkes and Cant, 2001). Bearing in mind that a real reacting zone thickness in detonation wave is a few millimetres, there is a full understanding that a simulated reaction zone for large-scale problems could occupy up to a few meters, e.g. in case of 1 m mesh, and simulation of a fine structure of the detonation wave has to be given up.

This requirement of 4-5 cells is valid not for reaction front yet for the shock resolution too. It is worth noting that simulated shock is essentially thickened compared to real von Neumann shock of a few free path distances. This numerical requirement to simulated “fronts” should be correctly addressed in the numerical realisation of the model to keep reaction front behind the shock without their non-physical overlap. This numerical peculiarity could lead to “loss” of a part of released combustion energy out of feeding the leading shock and as a result to “not resolving” von Neumann spike and other non-physical simulated parameters.

It is clear that the fine structure of detonation wave cannot be resolved by this methodology at large scale like by other techniques. However, as demonstrated later, the method reproduces overall detonation parameters needed for explosion safety engineering, i.e. pressure, impulse and propagation velocity, quite well.

### ***Calculation domain, initial and boundary conditions***

Numerical experiments with LES of planar detonation wave propagation were performed in elongated calculation domain of 3x3x100 m with one closed end. Three hexahedral grids were built of control volumes with sizes 0.5x0.5x1 m (3600 CVs), 0.5x0.5x0.25 m (14400 CVs), 0.5x0.5x0.5 m (7200 CVs), and 0.5x0.5x0.1 m (36000 CVs). Detonation was initiated at the closed end of the calculation domain. The symmetry conditions were defined on the “walls” and on the “ground” to simulate the planar detonation propagation in a 3D geometry.

Initial conditions are taken as in the experiment by Pförtner and Schneider (1984), temperature 304 K and pressure 99.9 kPa. Mixture is initially quiescent,  $u=0$  m/s. Hydrogen and air concentrations are equal to  $Y_{H_2}=0.02789$  and  $Y_a=0.9721$  respectively. The progress variable is  $c=0$  in the whole domain except the area of detonation initiation. Initiation of detonation is simulated by defining the following initial conditions in one slice of control volume at the closed end of the channel: pressure 10 MPa, temperature 3000 K and the progress variable  $c=1$ .

### ***Numerical scheme***

The Fluent 6.3 solver was employed as a platform for the realization of the LES model of detonation. The double precision parallel version of the solver was used with explicit linearization of the governing equations. To compute the convective fluxes the Advection Upstream Splitting Method (AUSM+) was used (Liou, 1996) and the central difference scheme for diffusion terms. The 4-order Runge–Kutt scheme was applied for time stepping.

The Courant-Friedrichs-Lewy (CFL) number was equal to  $CFL=0.05$ . This number was found to provide solution stability and convergence for simulation as the detonation speed is higher than the speed of sound used in the CFL definition. Sensitivity of numerical simulations to CFL number was tested. For CFL between 0.05 and 0.2 the numerical solution was converging and stable with no noticeable difference in detonation overpressure. For larger CFL values numerical instabilities occur and theoretical pressure peak was not reproduced. The physical explanation of small CFL numbers is quite obvious. Indeed, the original CFL number definition for compressible flows is reciprocal to the sum of a flow velocity and the speed of sound in a computational cell. However, the characteristic velocity for detonation process is larger than the speed of sound. Hence, a smaller CFL number is needed to provide a time step in explicit solver at which, for example, von Neumann spike propagates through a cell in a few steps rather than “jumps” through a number of cells in one time step.

### ***Results and discussion***

The simulation results are compared against solution by the ZND theory for a planar detonation wave. The theoretical parameters of planar detonation are calculated by methods (Brown and Shepherd, 2005 and 2006; [http://www.galcit.caltech.edu/EDL/public/cantera/html/SD\\_Toolbox/index.html](http://www.galcit.caltech.edu/EDL/public/cantera/html/SD_Toolbox/index.html)) built on the one-dimensional detonation theory and presented in Table 11–1 along with results of LES for four grids applied with longitudinal cell size 0.1 m, 0.25 m, 0.5 m, and 1.0 m. The LES model is slightly conservative relative to the theoretical predictions for 29.05% hydrogen-air mixture.

Parameter	ZND	LES mesh size			
		0.1 m	0.25 m	0.5 m	1.0 m
$P_{vN}$ , MPa	2.69	2.73	2.69	2.90	2.77
$P_{CJ}$ , MPa	1.45	1.52	1.46	1.71	1.49
$T_{CJ}$ , K	2960	3118	3090	3310	3200
$V$ , m/s	1956	1960	1956	2015	1961

Notes:  $P_{vN}$  is the von Neumann pressure spike;  $P_{CJ}$  is the pressure in the CJ plane,  $T_{CJ}$  is the temperature in the CJ plane,  $V$  is the detonation velocity.

**Table 11-1.** Comparison between detonation parameters calculated by the ZND theory and simulated by the LES model for three different cell sizes.

A typical profile of simulated pressure and the progress variable are shown in Fig.11-1. The LES model reproduced closely the amplitude of von Neumann pressure spike, CJ pressure, and the Taylor wave. There is a small secondary shock propagating after the leading shock (see Figs. 11-1 and 11-4). This shock is created by expanding driver gas (Edwards et al., 1975) and can be affected by numerical procedure of detonation initiation.

be > your degree

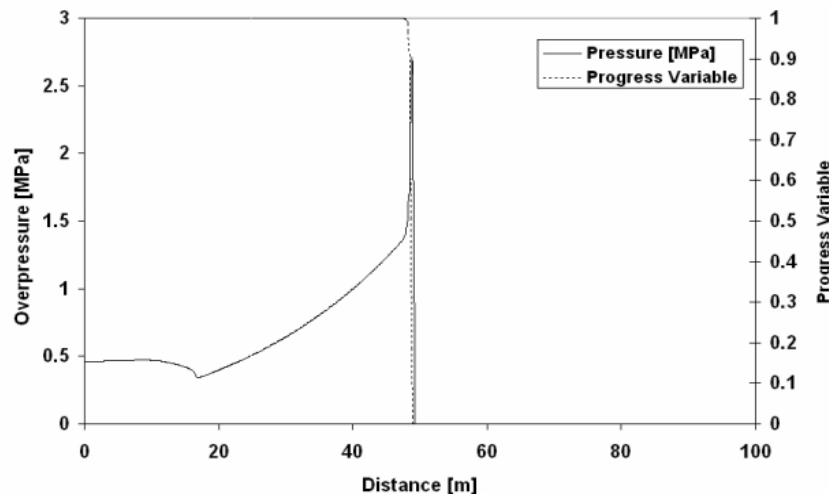
Bring your talent and passion to a global organization at the forefront of business, technology and innovation. Discover how great you can be. Visit [accenture.com/bookboon](https://www.accenture.com/bookboon)

Be greater than.  
consulting | technology | outsourcing

accenture  
High performance. Delivered.

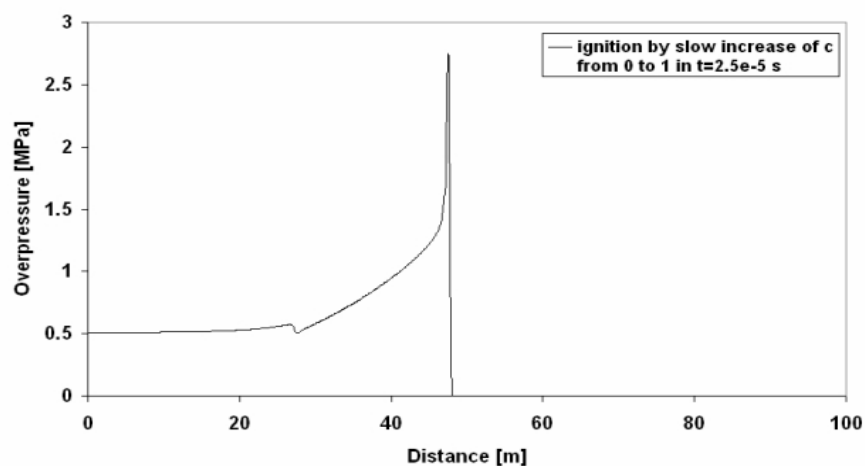
© 2013 Accenture. All rights reserved.





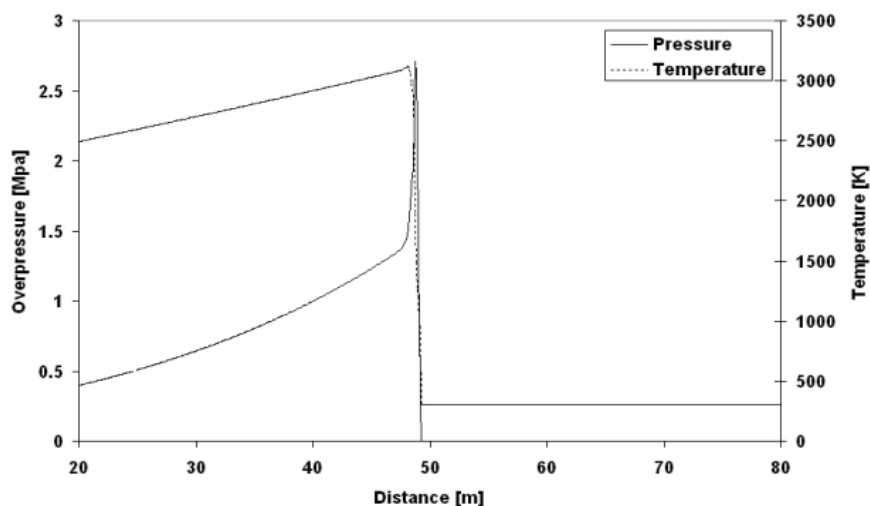
**Figure 11-1.** Pressure and the progress variable profiles in the detonation wave at time 24.8 ms (shock is at 49 m),  $\Delta=0.1$  m (Zbikowski et al., 2008).

Figure 11-2 demonstrates the pressure distribution in space when detonation was initiated differently. The progress variable was “slowly” increased (linearly) from 0 to 1 during 25 ms in one slice of CVs with initial conditions as in the rest of domain. The secondary pressure wave moves with sonic velocity away from the ignition point and finally evolves into a weak shock. In the experimental investigations only a short period of the pressure time history is recorded during the passage of the detonation for each probe position. Therefore, no further information on the waves following the detonation is available from the experiments (Bielert and Sichel, 1998).



**Figure 11-2.** Pressure profile of the detonation wave simulated by the LES model at time 24.8 ms (shock is at 48 m). Ignition in slice of CV by slow increase of  $c$  from 0 to 1 in  $t=2.5E-5$  s. CV size  $\Delta=0.1$  m.

The maximum temperature in the detonation wave (CJ plane) simulated by the LES model is 3118 K (cell size  $\Delta=0.1$  m). It is about 5% over the ZND theory value of 2960 K. Typical profiles of pressure and temperature in the detonation wave are shown in Fig. 11-3.



**Figure 11-3.** Typical profiles of pressure and temperature in the detonation wave.

The simulated von Neumann spike is 2.73 MPa for a grid with CV size 0.5x0.5x0.1 m. This is very close to the theoretical value 2.69 MPa calculated by the ZND theory. The LES results are practically independent of mesh size as seen from Table 11-1 (see Fig. 11-6 also). In the numerical experiment the detonation wave propagates with velocity 1960 m/s (grid 0.5x0.5x0.1 m) despite the fact that it is a pre-defined constant equal to 1956 m/s according to calculation by the ZND theory. This is a numerical error which can be caused, in particular, by a fact that the integral of the source term (gradient of the progress variable) through the thickness of the numerical flame front is not equal to 1 on the grid applied. However, the accuracy of the order of 0.2% in this particular case of the numerical simulation of a strong shock followed by a reaction front on quite coarse grid can be treated as satisfactory.

At CJ plane that corresponds to the end of the reaction zone and where the progress variable is equal  $c=1$  the simulated pressure in detonation wave equals to its theoretical ZND value of 1.45 MPa. Simulated temperature at von Neumann spike is 1650 K (ZND predicts 1528 K). Spatial distribution of pressure at different moments of time is shown in Fig. 11-4. Pressure at the end of the Taylor wave predicted by the LES model is 0.48-0.51 MPa and the theoretical (Taylor, 1950; Nettleton, 1987) estimate is 5.4 MPa.

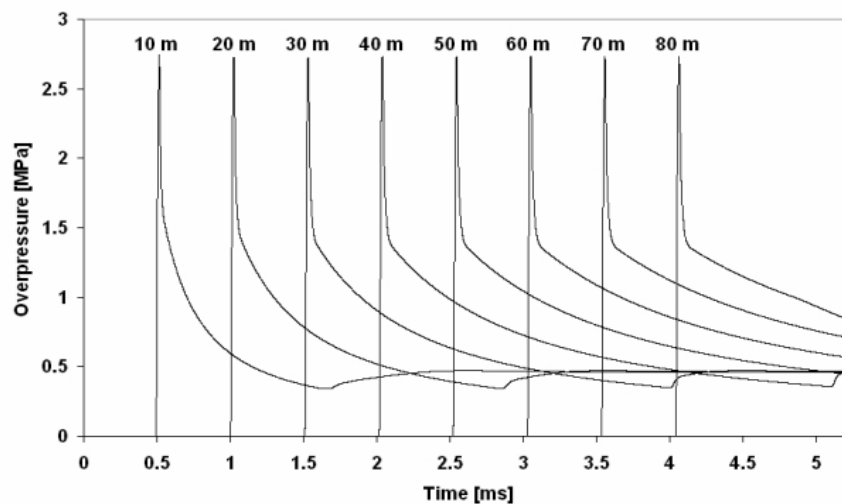


**Figure 11-4.** Pressure dynamics of 29.05% planar hydrogen-air detonation along 100 m channel,  $\Delta=0.1$  m.

The combustion energy has to be released behind the maximum peak of pressure to feed it (Fig. 11-5). In the ZND theory detonation speed depends on a value of heat release only when real thermodynamic parameters of the mixture are adopted. The correct value of the heat of combustion 3.2 MJ/kg applied in this study assures a proper value of the numerical detonation velocity of 1960 m/s.

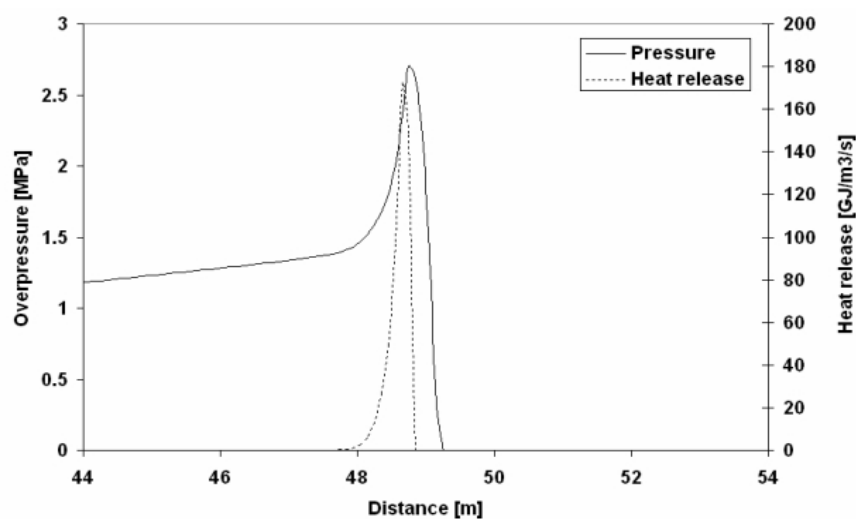


**Figure 11-5.** Spatial distribution of detonation pressure and heat release rate at time 24.8 ms (shock is at 49 m),  $\Delta=0.1$  m.

It is worth noting that the simulation results were obtained using extremely large size of numerical mesh in a range  $\Delta=0.1$ –1.0 m. In spite of the fact that numerical shock and reaction zone are extremely thickened on applied grid the general laws of the ZND theory and physical mechanism of detonation propagation are conserved in the numerical simulations.

Graphical presentation of grid sensitivity of the LES model of detonation is given in Fig. 11–6 for the maximum overpressure in the detonation wave and the detonation propagation velocity. Detonation parameters exhibit non-monotonic change with CV size. Tenfold increase of a cell size doesn't change the detonation parameters on more than about  $\pm 5\%$ .

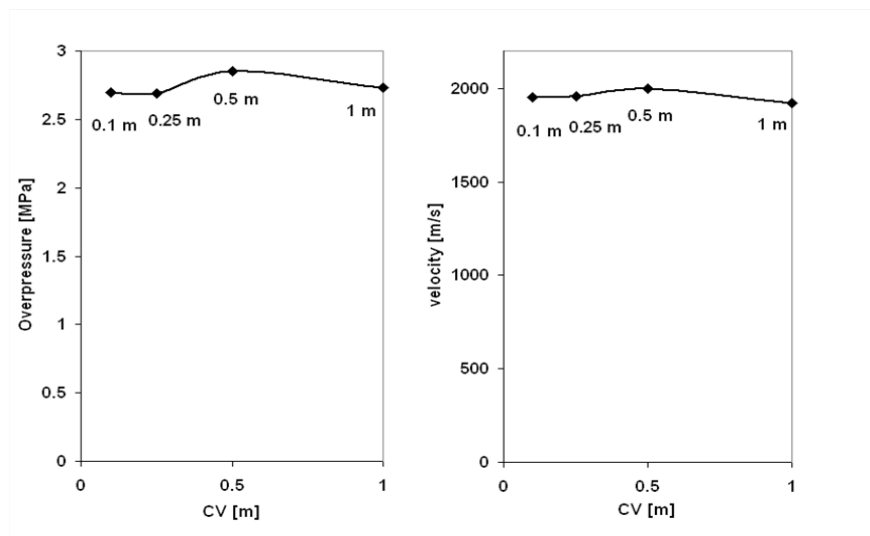


**Figure 11–6.** Grid sensitivity of the LES model for the von Neumann spike (left) and detonation velocity (right), cell sizes:  $\Delta=0.1, 0.25, 0.5, 1$  m.

"I studied English for 16 years but...  
...I finally learned to speak it in just six lessons"

Jane, Chinese architect

ENGLISH OUT THERE

Click to hear me talking before and after my unique course download

Impulse is another important parameter for explosion safety engineering along with maximum overpressure (Baker et al., 1983). For instance, it is of importance when predicting the extent of building destruction. Figure 11–7 demonstrates temporal change of simulated overpressure dynamics and impulse as a function of mesh size. Simulated impulse is more sensitive to mesh size compared to the maximum pressure because of thickening of the numerical shock with cell size. Indeed, the von Neumann pressure spike magnitude in our approach is independent of mesh while the thickness of detonation front increases proportional to CV size (4–5 CVs).

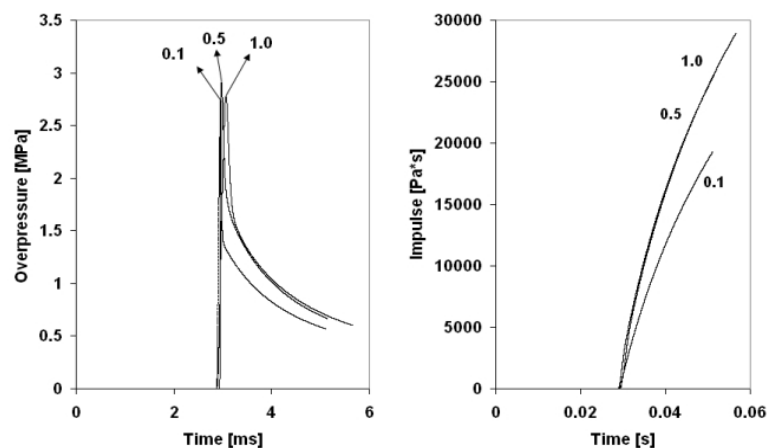


**Figure 11–7.** Simulated detonation overpressure and impulse dynamics for different control volumes:  $\Delta=0.1, 0.5, 1$  m.

The most common numerical schemes used to model detonation front are the second order Godunov scheme with Flux Corrected Transport method (Oran and Boris, 2001), or the MUSCL scheme with TVD method (Eto et al., 2005). Accurate simulation of detonations requires sophisticated numerical methods. These methods must be able to capture strong shocks and accurately compute the turbulent shear flows which arise as a result of the explosion. Genin et al. (2005) states that shock capturing methods have significant numerical dissipation to prevent generating unphysical oscillations near the shock, but this dissipation tends to smear out fine-scale turbulent structures in the flow. On the other hand, highly accurate numerical schemes developed to simulate smooth flow tend to produce unphysical oscillations in regions of strong gradients and/or discontinuities. In numerical studies of detonation with inclusion of Arrhenius chemistry it was pointed out that the physical phenomena obtained from calculation are highly dependent on grid resolution and numerical scheme (Fryxell et al., 2005).

Numerical models, schemes and codes need to be thoroughly tested and for this a Riemann problem (RP) is commonly used. It gives an exact solution to non-linear equations like the Euler equations. The solution consists of constant regions separated by waves. For the Euler equations the exact solution of the RP is well-known, self-similar, and consists of a combination of three wave types: shocks, rarefaction waves, and contact discontinuities. In our simulations AUSM+ numerical scheme is used which gives a proper solution of the strong shocks (Liou, 1996). High pressure region of 10 MPa was set as an initial condition at the distance of 2 m from the closed end. On the right hand side overpressure was equal 0. The CFL number in this numerical experiment was 0.05. 3D calculation domain of  $1 \times 1 \times 10$  m consists of hexahedral CVs of  $0.1 \times 0.1 \times 0.1$  m with the symmetry conditions at walls, ground and ceiling.

Figure 11–8 shows the comparison between analytical solution and numerical simulation of the Riemann problem on the grid with longitudinal CV size 0.1 m. It can be seen that the LES model of planar detonation and the numerical scheme applied are able to reproduce pressure levels in a shock and a rarefaction wave. However, they give up the resolution of the shock leading front compared to physical reality and the analytical solution. The increased thickness of a leading front of the numerical shock should be properly addressed by any model to keep the physics of the phenomenon right.

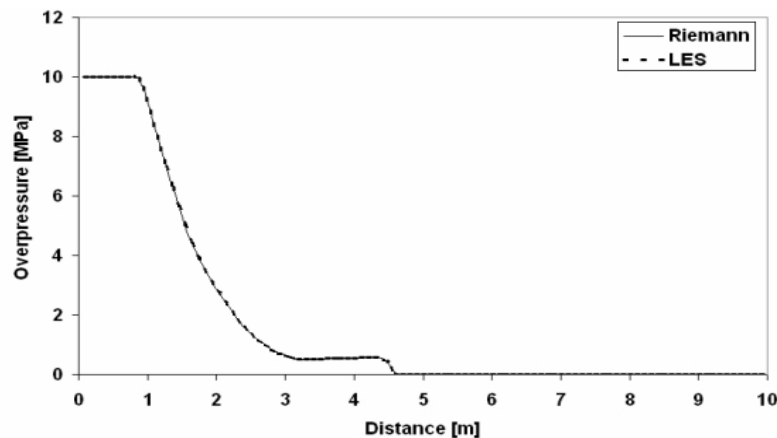


**Figure 11–8.** Comparison between analytical solution and numerical simulation of the Riemann problem for cbb 10 MPa discontinuity decay, time 2.58 ms.

Similar result is observed in LES of the detonation wave. Indeed, in spite of the fact that a leading front of the detonation shock is located over 3–5 CVs the simulated pressure peak is equal to the von Neumann spike in the ZND theory. In the ZND theory detonation propagates with velocity of the leading precursor shock, i.e. von Neumann spike. The LES model requirement to reproduce the von Neumann pressure peak provides physically correct detonation propagation velocity. The model is realised in a way that all combustion energy is released behind the shock to feed the shock peak rather than disperse released energy among parts of numerical leading front of the shock when pressure and reaction fronts are collapsed into one non-physical complex (or partially overlap).

Many of recent numerical studies of detonation were focused on resolving of detonation wave fine structure and modelling of detailed chemistry. They require fine mesh of few microns (Tsuboi, 2007). For hydrogen safety engineering such mesh is impractical and the resolution of the fine structure of detonation wave has to be given up. It is more important to reproduce with reasonable accuracy the overall parameters of detonation such as maximum pressure, impulse and propagation velocity.

From the physical point of view it is very important to reproduce von Neumann peak in numerical simulations. Indeed, it will provide correct value of detonation propagation velocity and arrival times. From the engineering point of view the influence of von Neumann pressure spike on the structural response is usually neglected since the spike thickness is of such a short length compared to typical length of structural element, that an influence on the structural response is small in comparison with the effects of the main loading produced by the Taylor-Zeldovich pressure profile behind the detonation front (Shepherd, 2006).



In the open atmosphere or semi confined geometries any consideration of detonation pressure effect and its decay with distance should be carried out with taking into account the fact that total destruction of buildings occur at pressures above 70100 Pa and impulse above 770 Pa×s (Baker et al., 1983; Dorofeev, 2005). For life safety considerations a maximum pressure in a shock or decaying blast wave plays an important role.

Figure 11–9 shows comparison between the LES model predictions and the ZND theory overpressures for lean hydrogen-air mixtures down to 20% of hydrogen concentration by volume. The discrepancy is within acceptable for engineering purposes 5%.

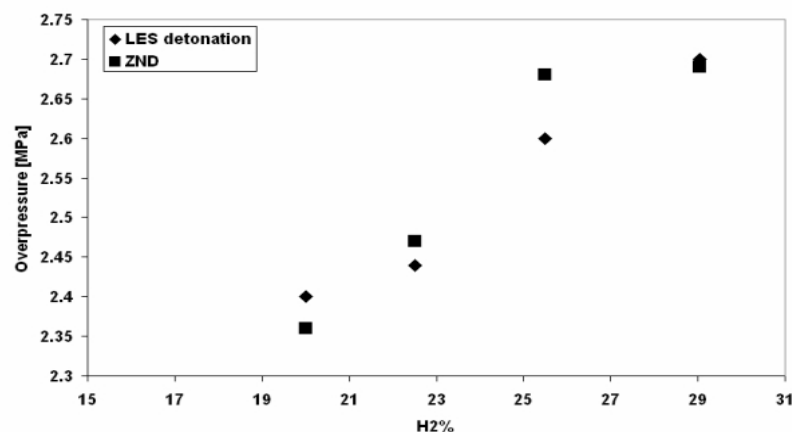


**Figure 11–9.** Comparison between the maximum detonation overpressure predicted by the ZND theory and simulated by the LES model for different concentrations of hydrogen in air,  $\Delta=0.1$  m.



**BUSINESS HAPPENS**

[www.fuqua.duke.edu/globalmba](http://www.fuqua.duke.edu/globalmba)

**Learn More >**



**HERE.**

Screening simulation is performed on a tetrahedral mesh of characteristic size of 0.5 m in a calculation domain 6x6x25 m. Simulated overpressure is less than obtained on the hexahedral mesh in longer calculation domain. The von Neumann pressure peak is 25.5 MPa, i.e. 5% below the ZND theory. Propagation velocity as well is slightly under predicted by about 5% with value 1850 m/s. The effect of tetrahedral grid on the overall detonation parameters should be studied further in more detail.

### ***Concluding remarks***

The LES model of large scale planar detonation is proposed for prediction of pressure effects at large scale accidents. The combustion model is based on the progress variable equation with the gradient method for the source term modelling and doesn't require Arrhenius chemistry. The LES model is verified against solutions of the ZND theory. Simulated detonation velocity, von Neumann spike pressure, Chapman-Jouguet pressure and Taylor wave parameters are in good agreement with theoretical values. There is some over prediction of impulse with increase of cell size. The model is practically grid independent in the range of tested cell sizes 0.1-1.0 m and doesn't require any "calibration" of the heat of combustion and the ratio of specific heats. This original approach to detonation simulation is proved to work successfully for the planar case. The next step is application of this methodology to LES of spherical large scale hydrogen-air detonation.

### **11.2.3. LES of spherical detonation**

#### **11.2.3.1. Detonation of 30% hydrogen-air mixture in 5.23 m hemisphere**

The LES model was applied to simulate a hemispherical detonation of 30% hydrogen-air mixture in a polyethylene balloon of radius 5.23 m propagating through unobstructed environment (Groethe et al., 2005). Direct initiation of the detonation was at the ground level. Figure 11–10 gives snapshots of the experiment. Blast wave overpressure dynamics was recorded at distance 15.6 m and the corresponding blast wave impulse was calculated.

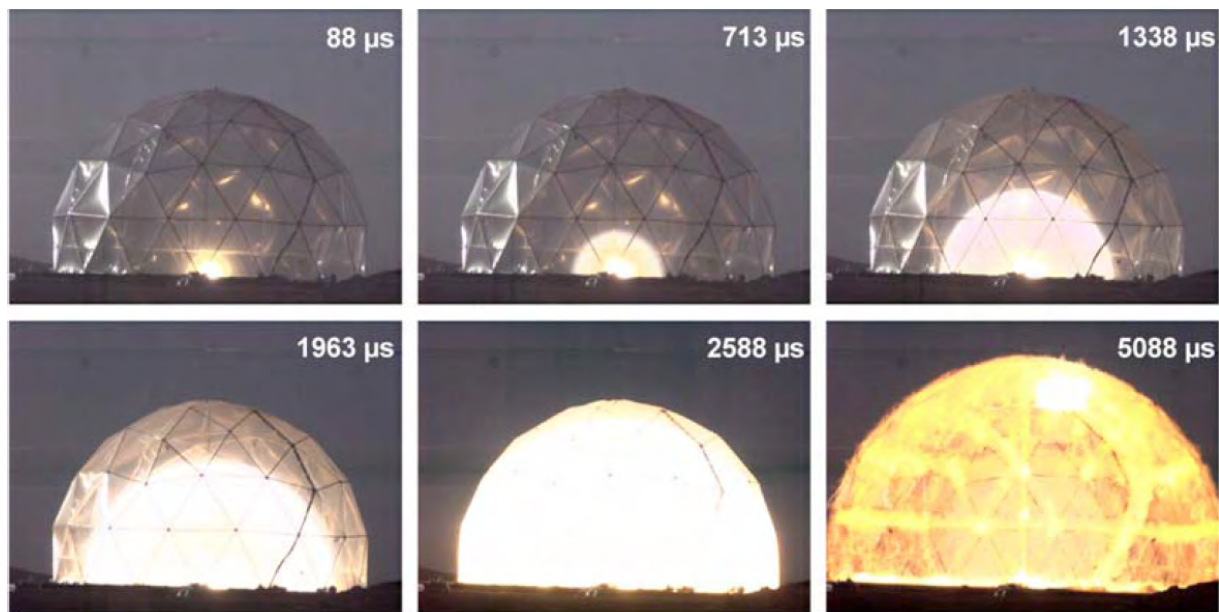


**Figure 11-10.** Hemispherical detonation of 30% hydrogen-air mixture in a polyethylene balloon of radius 5.23 m (Groethe, 2005).

The detonation was initiated in the same way as in deflagration simulation, i.e. by the increase of the progress variable from 0 to 1 in one control volume, corresponding to position of the ignition source. The duration of numerical initiation corresponds to the detonation wave propagation through half of the ignition control volume. Calculation domain was meshed using tetrahedral control volumes close to ignition area and hexahedral control volumes everywhere else.

The detonation (Chapman-Jouguet) velocity for 30% hydrogen-air mixture determined according to (Brown and Shepherd, 2004) is  $D=1977$  m/s. The simulated combustion wave propagation velocity, smoothed through oscillations, is shown in Fig. 11-11 (Makarov et al., 2007b). The simulated velocity is in good agreement with theoretical value. There are higher values of the detonation wave propagation velocity immediately after initiation and at the end of the process (probably due to the decrease of a number of control volumes in numerical combustion front at the end of the process).

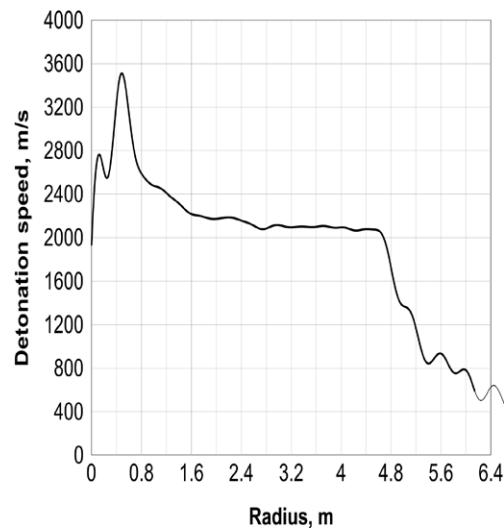


Figure 11-11. Smoothed simulated detonation propagation velocity.

Neither von Neumann (2.85 MPa) no Chapmen-Jouguet (1.53 MPa) pressures for planar detonation were achieved in this simulation of spherical detonation. The maximum simulated detonation overpressure is about 0.9 MPa. Unfortunately, experimental data on the maximum detonation pressure is absent. Pressure distribution within combustion area is an agreement with theoretically expected solution (Nettleton, 1987): Tailor expansion wave occupies about 50% of the burnt mixture radius with the pressure at the end of the expansion wave about 0.4 MPa.

## Join American online LIGS University!

Interactive Online programs  
BBA, MBA, MSc, DBA and PhD

### Special Christmas offer:

- ▶ enroll **by December 18th, 2014**
- ▶ **start studying and paying only in 2015**
- ▶ **save up to \$ 1,200** on the tuition!
- ▶ Interactive Online education
- ▶ visit [ligsuniversity.com](http://ligsuniversity.com) to find out more!

Note: LIGS University is not accredited by any nationally recognized accrediting agency listed by the US Secretary of Education. More info [here](#).

Experimental and simulated dynamics of a blast wave from detonation at distance 15.61 m from the ignition point is given in Fig. 11–12. The agreement is in general acceptable, with 25% under prediction of the blast pressure in the simulations.

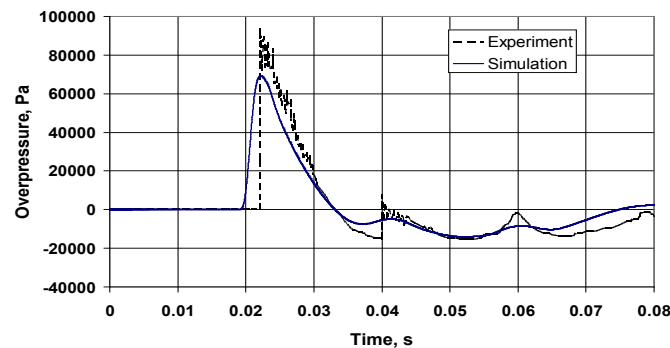


**Figure 11–12.** Experimental and simulated blast wave overpressure dynamics at distance 15.61 m.

Contrary to the blast wave pressure dynamics, the calculated impulse is in good agreement with experiment (Fig. 11–13). This is thought due to correct energy balance provided by the model.

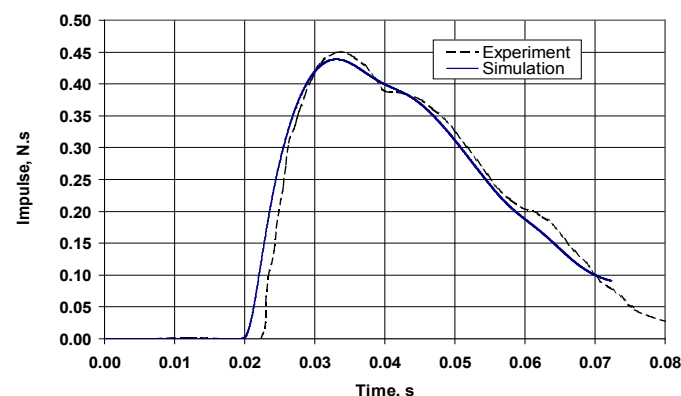


**Figure 11–13.** Experimental and simulated blast wave impulse at distance 15.61 m.

### 11.2.3.2 Detonation of 29.05% hydrogen-air mixture in 2.95 m radius balloon

Here results of a simulation of spherical detonation in a 2.95 m radius balloon are presented (Zbikowski, 2010).

#### *Experiment*

In experiment by Pfortner and Schneider (1984) hemispherical balloon with radius 2.95 m was filled with 29.05% hydrogen-air mixture. Measurements of pressure inside the balloon were carried out with piezoelectric transducers of frequency 450 kHz (PBC) and in the far field piezoresistive transducers with frequency 70 kHz (Kistler). Detonation was initiated by the 50 g of high explosive charge which was located in the middle of the balloon. Detonation velocity measured in the experiment was 1956 m/s. Initial temperature 304K.

### Numerical details

The calculation domain was created according to the experimental description (Pförtner and Schneider, 1984) and meshed using uniform hexahedral mesh targeting uniform control volumes with size  $0.1 \times 0.1 \times 0.1$  m, in the area of hydrogen-air mixture. In the volume defined as a far field (only air) tetrahedral CVs are used with the size of 1 m. Numerical detonation was initiated by defining pressure 20 MPa, temperature 6000 K and progress variable  $c = 1$  in one CV. Non-slip boundary conditions for the momentum equations, adiabatic boundary conditions for the energy equation, and zero flux boundary conditions for the progress variable equation were imposed at all walls. At the moment of ignition mixture was quiescent,  $u = 0$  m/s. Hydrogen and air mass fractions were  $Y_{H_2} = 0.0278$  and  $Y_a = 0.9721$  respectively. The progress variable was set to  $c = 0$  in the whole domain except the area of detonation initiation.

The Fluent 6.3 software was used as an engine for the LES model simulations. The combustion model was implemented through the User Defined Function in Fluent. The double precision parallel version of the solver was used with explicit linearization of the governing equations. To compute the convective fluxes the Advection Upstream Splitting Method (AUSM+) by Liou (1996) and the central difference scheme for diffusion terms were applied. The 4<sup>th</sup>-order Runge-Kutta scheme was used for time stepping. The Courant-Friedrichs-Lewy (CFL) number was equal to 0.1. In the area of pressure gradient adaptive mesh was used with 2 levels of adaptation. Model was normalized by scaling and adaptation was initiated dynamically every 5<sup>th</sup> iteration. Coarsen Threshold was 0.4 and Refine Threshold 0.8.

### Results

Results of 3D simulation of detonation are presented below. Records were taken by the pressure gauges  $P1$ ,  $P2$ ,  $P3$  located at a distances 0.75, 1.5, 1.75 m from the ignition point respectively (all inside the balloon). Data from three pressure transducers was used to compare results of the simulation with experiments.

Figure 11–14 shows the pressure dynamics of the detonation front at the distance 0.75 m from the ignition source. Simulated detonation velocity is reproduced the experimental velocity (1954 m/s). Maximum experimental pressure peak is 2.85 MPa yet in simulation it is only 1.45 MPa (theoretical von Neumann spike for planar detonation is  $P_{vN} = 2.69$  MPa, i.e. the detonation was overdriven). Another reason for the lower simulated overpressure is overlapping of numerical reaction front and shock front in the vicinity of the initiation point.



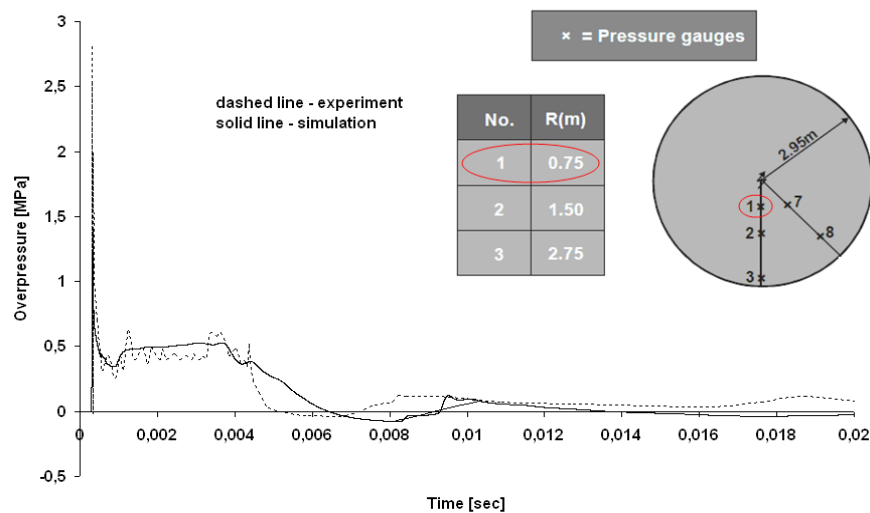


Figure 11-14. Overpressure at location 0.75 m from the ignition source (sensor P1).

Detonation pressure was registered by the gauge positioned at half of the balloon radius, i.e. 1.5 m (see Fig. 11-15). At this location the experimental detonation is stabilized and propagates with the CJ detonation velocity of 1954 m/s. The maximum pressure peak for spherical detonation is practically the same for both the experiment and simulations, i.e. 1.9 MPa. This is below  $P_{vN}$  for the planar detonation, and above  $P_{CJ}=1.45$  MPa.



**MASTER IN MANAGEMENT**

#1 EUROPEAN BUSINESS SCHOOL  
FINANCIAL TIMES 2013

#gobeyond


**Because achieving your dreams is your greatest challenge.** IE Business School's Master in Management taught in English, Spanish or bilingually, trains young high performance professionals at the beginning of their career through an innovative and stimulating program that will help them reach their full potential.

- Choose your area of specialization.
- Customize your master through the different options offered.
- Global Immersion Weeks in locations such as Rio de Janeiro, Shanghai or San Francisco.

*Because you change, we change with you.*

[www.ie.edu/master-management](http://www.ie.edu/master-management)

[mim.admissions@ie.edu](mailto:mim.admissions@ie.edu)



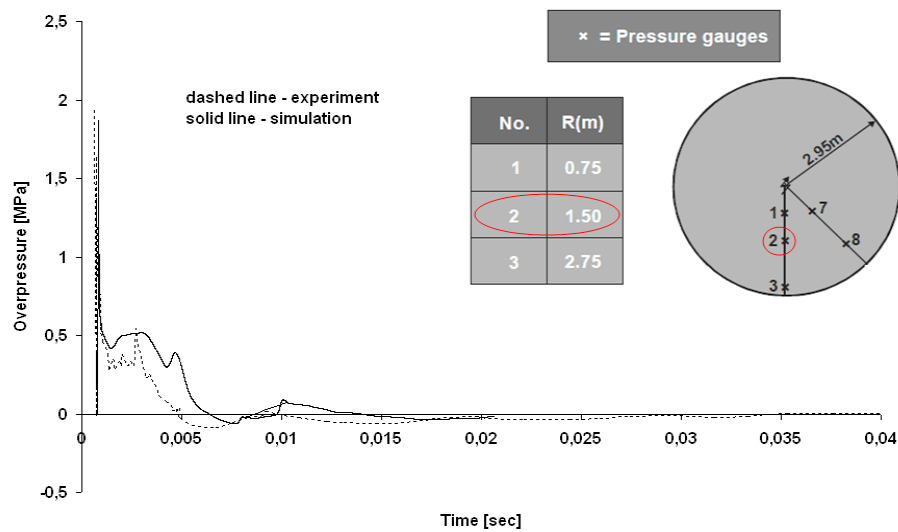


**Figure 11-15.** Overpressure at location 1.5 m from the ignition source (sensor P2).

Pressure sensor *P3* is the last in the spherical balloon located close to the border at the distance of 2.75 m from the ignition point. Figure 11-16 shows that numerical detonation maximum peak of pressure and velocity under-predict by about 10% the experimental observations. The experimental maximum peak of pressure at the distance 2.75 m is 1.93 MPa while the LES model gives 1.85 MPa.

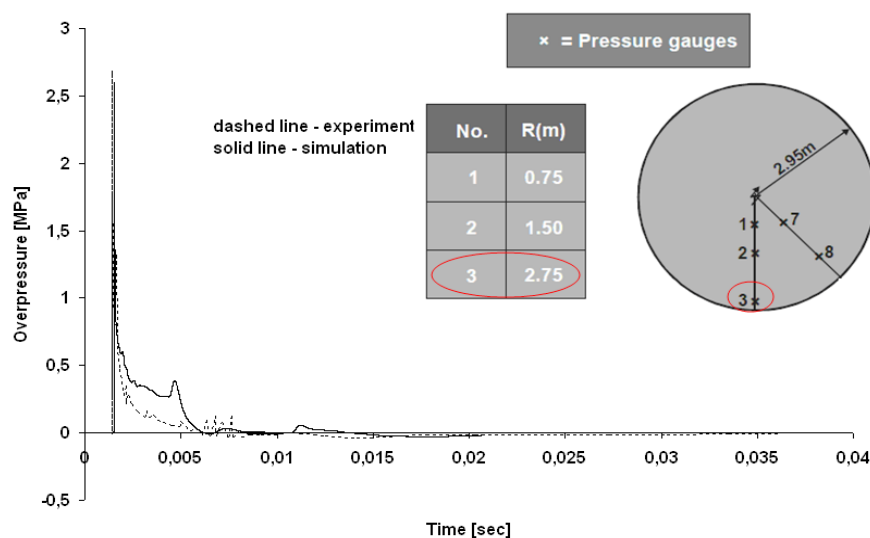


**Figure 11-16.** Overpressure at location 2.75 m from the ignition source (sensor P3).

Simulations showed similar results for pressure decay in the Taylor wave at different locations. However, there is some delay of pressure in the numerical Taylor wave. This could be explained by thickened numerical reaction zone and leading shock front when solving large-scale problems.

Figures 11–17 and 11–18 present the dynamics of decaying blast wave from the detonation at the distance of 3.25 m and 5 m from the ignition source respectively. Velocity of the blast wave is well resolved due to a proper simulation of the energy release. Maximum peak of pressure for the first location (3.25m) is under predicted by 30% (Fig. 11–17), probably due to the coarse mesh. Simulated blast wave pressure dynamics at distance 5 m from the ignition source (Fig. 11–18) is in good agreement with the experimental pressure transient.

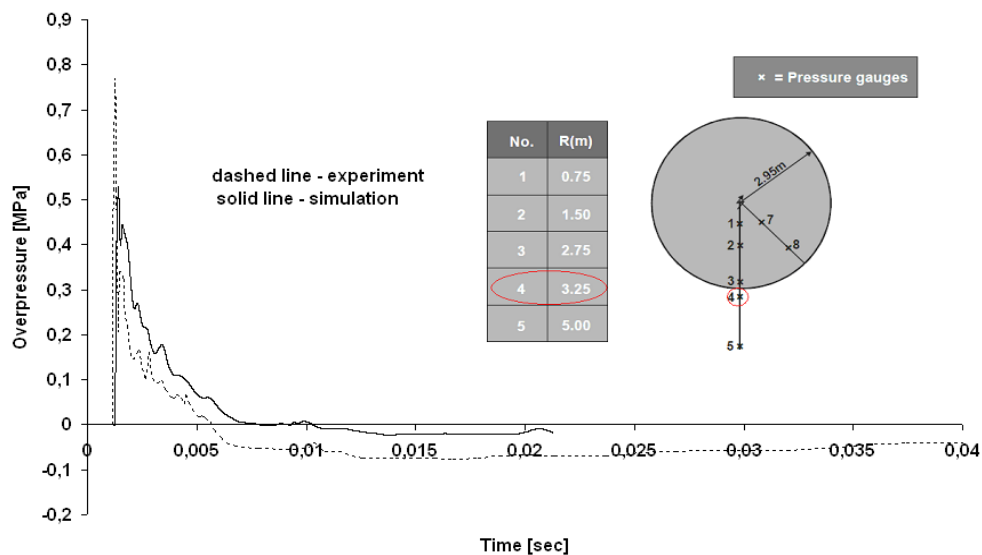


**Figure 11–17.** Pressure in the blast wave at distance of 3.25 m from the ignition source.

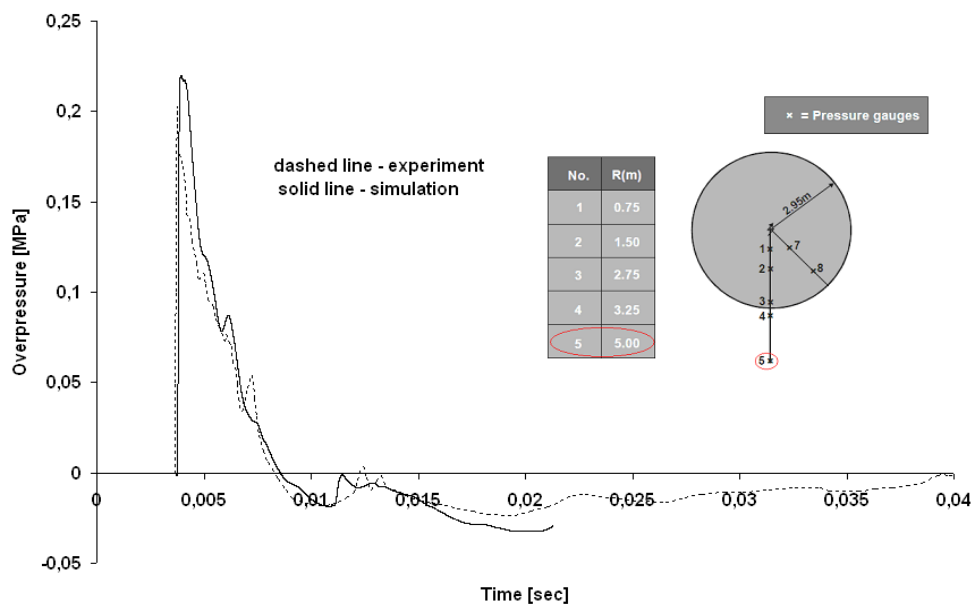


**Figure 11–18.** Pressure in the blast wave at distance of 5 m from the ignition source.

#### 11.2.4. LES of detonation in the RUT facility

The LES model was tested against two large-scale experiments in the RUT facility (Zbikowski et al., 2010). The facility was  $27.6 \times 6.3 \times 6.55$  m compartment with complex three-dimensional geometry. Experiments with 20% and 25.5% hydrogen-air mixture and different location of direct detonation initiation were simulated. Sensitivity of 3D simulations to control volume size and type were tested and found to be stringent compared to the planar detonation case. The maximum simulated pressure peak was found to be lower than the theoretical von Neumann spike value for the planar detonation and larger than the Chapman-Jouguet pressure thus indicating that it is more challenging to keep numerical reaction zone behind a leading front of numerical shock for curved fronts. The simulations demonstrated agreement with the experimental data.

##### 11.2.4.1. Experiments

Large scale hydrogen-air detonation experiments were carried out in the RUT facility and described in (Breitung et al., 1996) and later in more detail in (Efimenko and Gavrikov, 2007). The RUT facility is a steel-lined reinforced concrete structure shown in Fig. 11–19.

# SMS from your computer

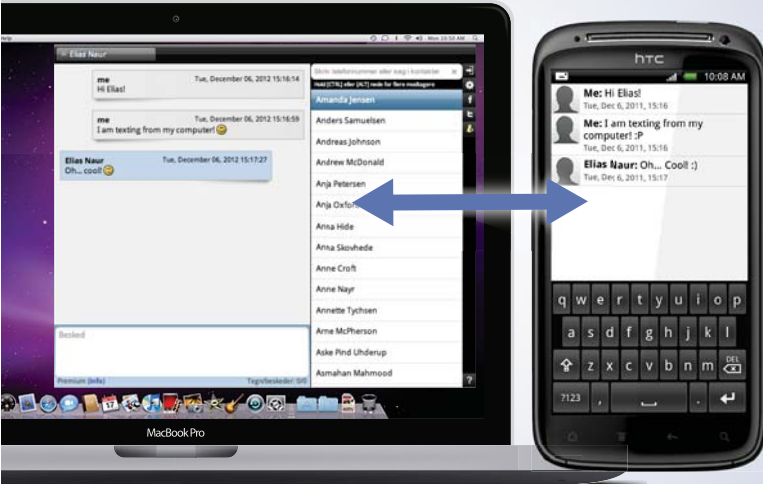
...Sync'd with your Android phone & number

**FREE**  
30 days trial!

Go to

[BrowserTexting.com](http://BrowserTexting.com)

and start texting from  
your computer!




**BrowserTexting**

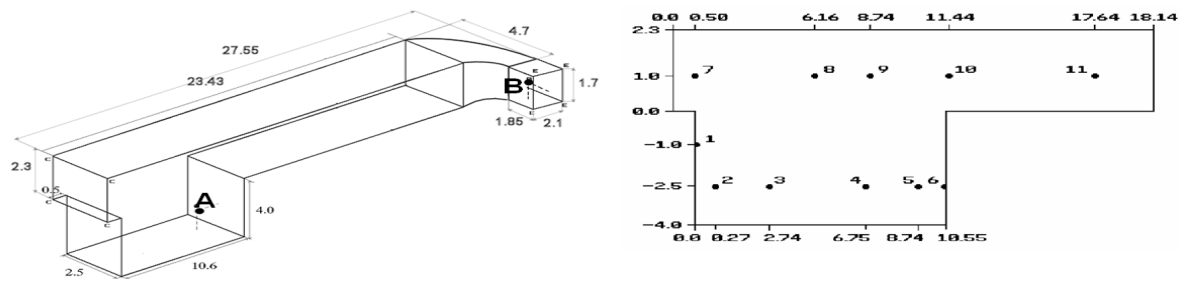


**Figure 11-19.** The RUT facility scheme: left – isometric view and locations of detonation initiator (A and B); right – location of the pressure sensors, side view.

The experimental section of the RUT facility maximum dimensions are: 27.6 m long, 6.3 m deep and 6.55 m wide. The volume of the facility is 263 m<sup>3</sup>. Two tests were carried out to investigate the effect of the detonation initiator location and hydrogen concentration in 3D large-scale geometry. The first test was detonation of 20% hydrogen-air mixture initiated at point A (see Fig. 11-19). The second test was detonation of 25.5% hydrogen-air mixture initiated at point B. High-frequency measurement system, including piezoelectric pressure transducers Kistler, models 701 and 7031, tenso-resistive pressure transducers ENDEVCO, models 8511A-5K and 8530B-1000, signal amplifiers, cables, digital transient recorder DL-2800 and computer for data processing and storage were used. Signal was recorded with the DL-2800 register with a sample rate of 5  $\mu$ s.

Two lines of pressure transducers were arranged inside the experimental volume. The first one was placed in the canyon (lower part of the facility) and included transducers 1-6 (line 1). The second one was placed in the channel with transducers 7-11 (line 2). The pressure transducers number 2 to 5 were located on the longitudinal wall of the canyon, and the transducers 7 to 11 on the opposite wall of the channel as depicted in Fig. 11-19 (right). Transducers 1, 6, 11 were placed in the middle of the transversal walls.

High explosive charges of 200 g were used as initiators being located at distance 80 cm from the floor and 50 cm from the wall. The initial mixture temperature and pressure were 20°C and 0.1 MPa respectively in both tests. Mixing of hydrogen and air was assured by fans. Hydrogen concentration and mixture uniformity were checked taking samples from two different points of the flammable volume. The non-uniformity was less than 0.5% by volume of hydrogen.

#### 11.2.4.2. Modelling and numerical details

The applied LES detonation model was verified previously against analytical solution of the ZND theory for the planar detonation wave and provided an excellent agreement for von Neumann spike pressure, detonation propagation velocity, etc. The LES detonation model demonstrated the capability to capture strong shocks and reproduce major detonation parameters. The model was found to be grid independent for planar detonation in a wide range of CV sizes from 10 cm to 1 m.

The aim of these simulations is a validation of the LES detonation model, which is fully compatible with the LES deflagration model described above, in a complex geometry. The detonation model is paired to the LES multi-phenomena deflagration model. The gradient method for the source term in the progress variable equation is applied. It does not resolve real reaction front, but represents it as a monotonous change of the progress variable through a number of CVs (Laskey et al., 1988). The numerical requirement is that the flame front thickness simulated by the gradient method is about 4-5 CVs. It is clear that the real detonation wave thickness is given up when large control volumes are used to tackle industrial scale problems without any adjustment of simulation parameters.

The chemical kinetics is incorporated within the detonation velocity value, which was pre-calculated using the Shock and Detonation (SD) Toolbox ([http://www.galcit.caltech.edu/EDL/public/cantera/html/SD\\_Toolbox/index.html](http://www.galcit.caltech.edu/EDL/public/cantera/html/SD_Toolbox/index.html)) built on the CANTERA software (Goodwin, 2005). Thermodynamic and thermokinetic data used in the simulations are presented in Table 11–2 along with near stoichiometric 29.05% hydrogen-air mixture data.

Hydrogen concentration, % by volume	$\Delta H_c$ , J/kg	$D$ , m/s	$\rho_u$ , kg/m <sup>3</sup>	$\gamma_u$	$\gamma_b$
20.00	2.04E+6	1704	0.976	1.4	1.27
25.50	2.73E+6	1874	0.915	1.4	1.25
29.05	3.15E+6	1954	0.832	1.4	1.22

Notes:  $\Delta H_c$  is the heat of combustion;  $D$  is the detonation velocity;  $\rho_u$  is the density of unburned mixture;  $\gamma_u$  and  $\gamma_b$  are the specific heat ratio for unburned and burned mixture respectively.

**Table 11–2.** Thermodynamic parameters for 20%, 25.5% and 29.05% of hydrogen-air mixtures.

To make the heat release in the numerical reaction zone able to feed the leading shock one should keep the simulated reaction (heat release) zone behind the peak of the leading shock without their numerical “non-physical” overlapping that “kills” the von Neumann spike in numerical simulations when this physics is ignored. Failure to address it results in under-prediction of maximum pressure in the von Neumann spike. To achieve this in simulations the source term for the progress variable is kept equal to zero when the pressure derivative with time in the considered CV is positive (before the pressure peak), and is “switched on” only when the pressure derivative with time becomes negative (close or after the pressure peak).

The calculation domain was designed according to the experimental description and meshed using hexahedral CVs targeting uniform grid with the mesh size 0.1x0.1x0.1 m totalling 237,005 CVs. In simulations the detonation was initiated by defining pressure 20 MPa, temperature 6000 K and progress variable  $c=1$  in the region of 0.2x0.2x0.2m (2x2x2 CVs) at the ignition source location. Such initiation allows creation of the strong shock which is then supported by the heat release in the reaction front. Model itself is not sensitive to ignition parameters like it is in Arrhenius chemistry based codes. Pressure and temperature are needed to create strong shock wave which is then supported by the reaction heat release. Otherwise value of the source term in the energy equation is too small to support decaying leading shock on a course mesh. This phenomenon can be explained by numerical diffusion which cannot be avoided when shock is curved.



The non-slip boundary condition for the momentum equations, adiabatic boundary conditions for the energy equation, and zero flux boundary condition for the progress variable equation were imposed at the walls. The mixture is initially quiescent,  $u=0$  m/s. Hydrogen and air mass fractions for 20% and 25.5% are  $Y_{20\%H_2} = 0.017$  and  $Y_a = 0.983$ , and  $Y_{25.5\%H_2} = 0.024$  and  $Y_a = 0.976$  respectively. The progress variable is set to  $c=0$  in the whole domain except the area of detonation initiation. Heat release is kept behind the maximum peak of pressure by defining condition that the source term in the progress variable equation in front of this peak is equal to zero and allowed to grow in cells behind the peak.

The Fluent 6.3 software was used as a CFD engine for the LES model realisation. The double precision parallel version of the solver was used with explicit linearization of the governing equations. To compute the convective fluxes the AUSM+ (Liou, 1996) and the central difference scheme for diffusion terms were applied. The 4<sup>th</sup>-order Runge–Kutta scheme was used for time stepping. The CFL number was equal to 0.05. The so low number was chosen to guarantee stability and converging solution in situation when the characteristic speed in the problem is the detonation speed, which is higher than the speed of sound used by default in the CFL number.

#### 11.2.4.3. Results

Important conclusions of the study (Zbikowski et al., 2008) are: the LES model of detonation is practically grid independent for planar detonation simulations in the range of cell sizes 0.1–1.0 m; and it doesn't require any "calibration" of the heat of combustion and the ratio of specific heats (no Arrhenius chemistry parameters dependence either due to use of pre-calculated detonation velocity), which are often applied in other models to better reproduce experimental data.

The profiles of numerical detonation wave structure for the planar detonation of near stoichiometric 29.05% hydrogen-air mixture at different distances from the initiation plane (calculation domain 100 m, mesh size 0.1 m) is shown in Fig. 11–20. It is seen that simulated structure of the detonation wave is practically the same at different locations of the 1000 CVs calculation domain. This demonstrates that there is no "numerical diffusion" in simulations that could be attributed as very useful inherent feature to the gradient method coupled with the progress variable equation.

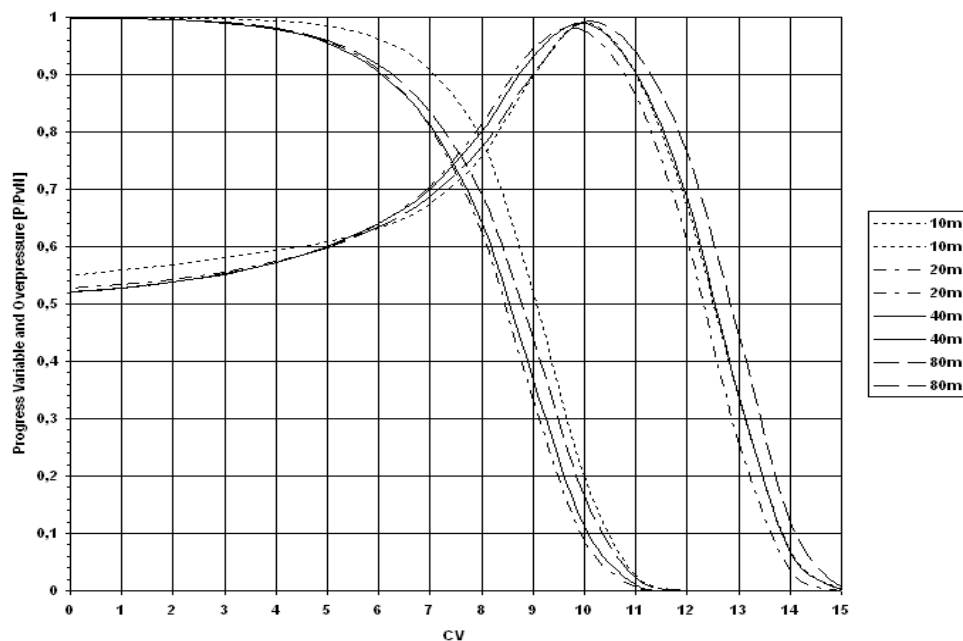


**Figure 11–20.** Simulated detonation wave profiles (monotonic curves – progress variable; curves with maximum – pressures) at different locations for 29.05% planar hydrogen-air mixture in 100 m long calculation domain with control volume size 0.1 m as a function of CV number (relative).

# The Wake

the only emission we want to leave behind

Low-speed Engines Medium-speed Engines Turbochargers Propellers Propulsion Packages PrimeServ

The design of eco-friendly marine power and propulsion solutions is crucial for MAN Diesel & Turbo. Power competencies are offered with the world's largest engine programme – having outputs spanning from 450 to 87,220 kW per engine. Get up front! Find out more at [www.mandieselturbo.com](http://www.mandieselturbo.com)

Engineering the Future – since 1758.

**MAN Diesel & Turbo**



The progress variable graphs in Fig. 11–20 demonstrate that the number of CVs in the combustion front is about 10. The maximum pressure peak is located at CV number 10 where the progress variable is just between 0.1 and 0.2. This behaviour does not have any influence on the propagation of detonation wave while heat release is located between values 0.45 and 0.6 of the progress variable  $c$ . The physics behind this arrangement is to keep the heat release behind the maximum peak of pressure (von Neumann spike) to overcome the numerical requirement for any numerical front (here the shock front) to be spread at least through 4–5 cells and thus allow released heat to feed the leading numerical shock.

The verification procedure used previously for the stoichiometric hydrogen-air planar detonation was applied in this study for 20% and 25.5% hydrogen-air planar detonations before proceeding to the simulations in the RUT facility. Simulations of planar detonations were performed in the calculation domain of 3x3x100 m with one closed end and hexahedral mesh with CV size 0.5x0.5x0.1 m (36,000 CVs) for both 20% and 25.5% of hydrogen-air mixtures. Simulated detonation velocity, von Neumann spike pressure, Chapman-Jouguet pressure and Taylor wave parameters (0.375 of  $P_{CJ}$ ) are in a good agreement with the theoretical values (see Table 11–3).

Parameter	20% hydrogen		25.5% hydrogen		29.05% hydrogen	
	ZND	LES	ZND	LES	ZND	LES
$P_{vN}$ MPa	2.36	2.51	2.67	2.7	2.69	2.73
$P_{CJ}$ MPa	1.28	1.35	1.45	1.51	1.45	1.52
$T_{CJ}$ K	2400	2570	2761.5	2900	2960	3118
$V_{CJ}$ m/s	1703.7	1800	1873.3	1905	1956	1960
$P_{Taylor}$	0.48	0.46	0.54	0.49	0.54	0.5

Notes:  $P_{vN}$  is the von Neumann pressure spike;  $P_{CJ}$  is the pressure in the CJ plane;  $T_{CJ}$  is the temperature in the CJ plane;  $V_{CJ}$  is the CJ detonation velocity;  $P_{Taylor}$  is the pressure in the Taylor wave.

**Table 11–3.** Comparison between planar detonation parameters calculated by the ZND theory and simulated by the LES detonation model for 20%, 25.5%, 29.05% hydrogen-air mixture.

A profile of simulated pressure and the progress variable for the planar detonation is shown in Fig. 11–21. The thickness of the simulated detonation wave is of the order of one meter due to the large cell size of 0.1 m used and the requirement of the model to keep the reaction zone (area of changing progress variable) behind the von Neumann spike. Yet, the maximum peak of pressure (von Neumann spike), temperature and detonation velocity in CJ plane are grid independent for this model in case of planar detonation (Zbikowski, 2008). It is also seen that the progress variable profile starts to change after the pressure peak, giving rise to the heat release behind the leading shock, which is a key element of the model realisation as only with such model arrangements the heat released in the reaction front feeds the leading shock.

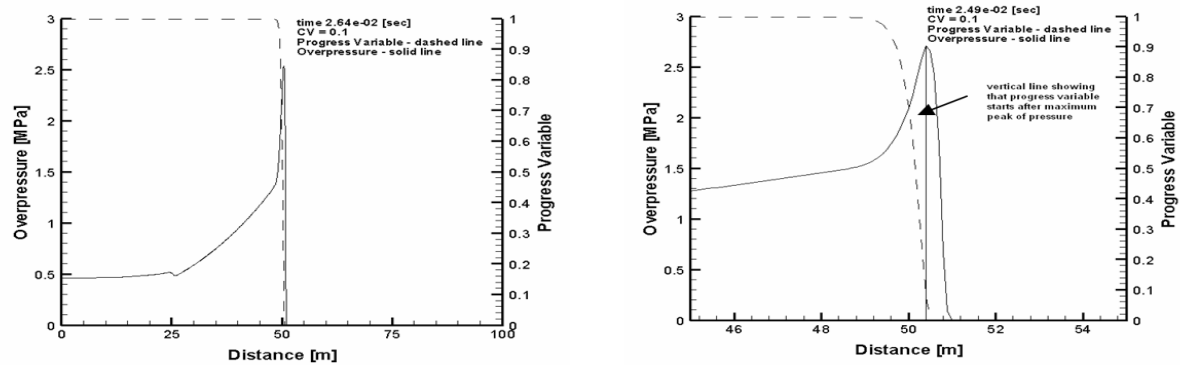


**Figure 11-21.** Simulated overpressure and the progress variable profile (CV size is 0.1 m): left – 20.0% hydrogen-air mixture (whole calculation domain), right – 25.5% hydrogen-air mixture (enlargement around the shock wave area).

The experimental pressure transients and the simulated pressure dynamics obtained in 3D simulation of 20% hydrogen-air mixture detonation in the RUT facility are shown in Fig. 11-22. Pressure gauges 2, 3, 4 and 5 have been selected for comparison of simulation results and experimental data. Pressure transducers are located along the side wall in the canyon section (encircled in Fig. 11-22 insert). In this experiment (ignition at point A, close to the sensor 6 in Fig. 11-22 insert) the pressure transients from sensors 7–11 are distorted by multiple reflections and are not of interest for the comparison.

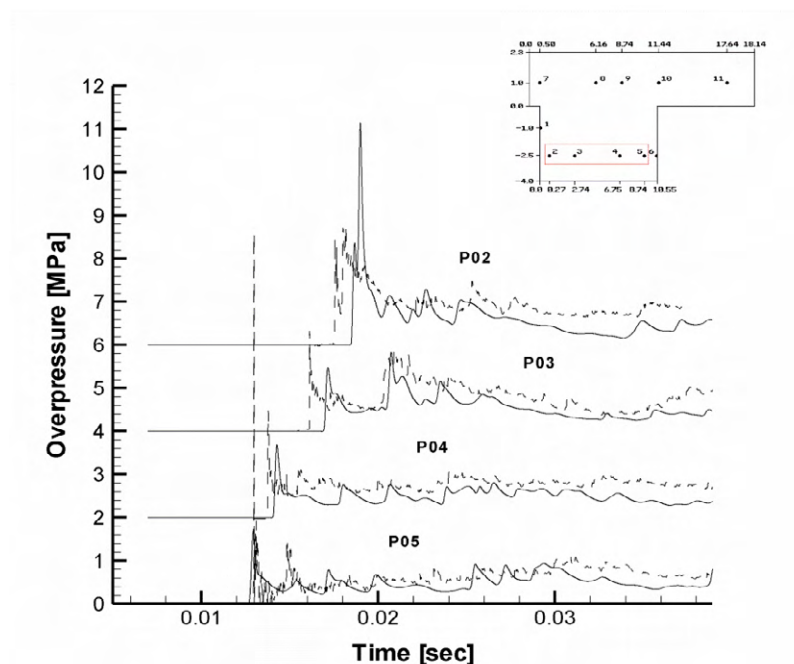


**Figure 11-22.** Pressure transients in the canyon along the side wall from the gauges 5 to 2, 20% hydrogen-air mixture (dotted line – experiment, solid line – simulation).

The simulated pressure profile for each pressure transducer is in a reasonably good agreement with the experiment if the strong initiation pressure peak is taken into account. Velocity of the numerical detonation is somewhat under predicted (6%). This could be caused by the overlapping to some extent of the numerical reaction zone and the numerical shock in 3D simulations and/or quite large difference in numerical shock and reaction zone radii in the beginning of the process especially when control volume size is as large as 10 cm. Another possible reason is the behaviour of the detonation wave in the experiment. The experimental results show overdriven detonation in the pressure gauge 5, affected by the spherical detonation blast created by the initiator in the experiment. Then the detonation wave decays to the theoretical value of CJ detonation velocity (1703 m/s) as it is in the experiment.

Looking into detailed structure of the pressure dynamics we may see that when the detonation wave is reflected from the wall (second pressure peak on the pressure dynamics of gauge 2, Fig. 11–22) simulation results over predict the maximum peak of the experimental reflected pressure wave. This is probably caused by thickened numerical shock when CV size of 0.1 m is applied and related increase of density of the unburned mixture in location of numerical gauge 2. Thus, simulations with shock reflections might require finer mesh for better reproduction of pressure transients with this model.

In the second simulated experiment with 25.5% hydrogen-air mixture the detonation was initiated at location “B” (see Fig. 11–19, right). Figure 11–23 shows comparison of simulated and experimental pressure dynamics for sensors 7, 8, 9, 10 and 11, located at the wall of the channel along the main way of the experimental detonation wave propagation. The detonation wave propagates from the right to

## TURN TO THE EXPERTS FOR SUBSCRIPTION CONSULTANCY

Subscribe is one of the leading companies in Europe when it comes to innovation and business development within subscription businesses.

We innovate new subscription business models or improve existing ones. We do business reviews of existing subscription businesses and we develop acquisition and retention strategies.

Learn more at [linkedin.com/company/subscribe](https://www.linkedin.com/company/subscribe) or contact  
Managing Director Morten Suhr Hansen at [mha@subscribe.dk](mailto:mha@subscribe.dk)

**SUBSCRIBE** - to the future

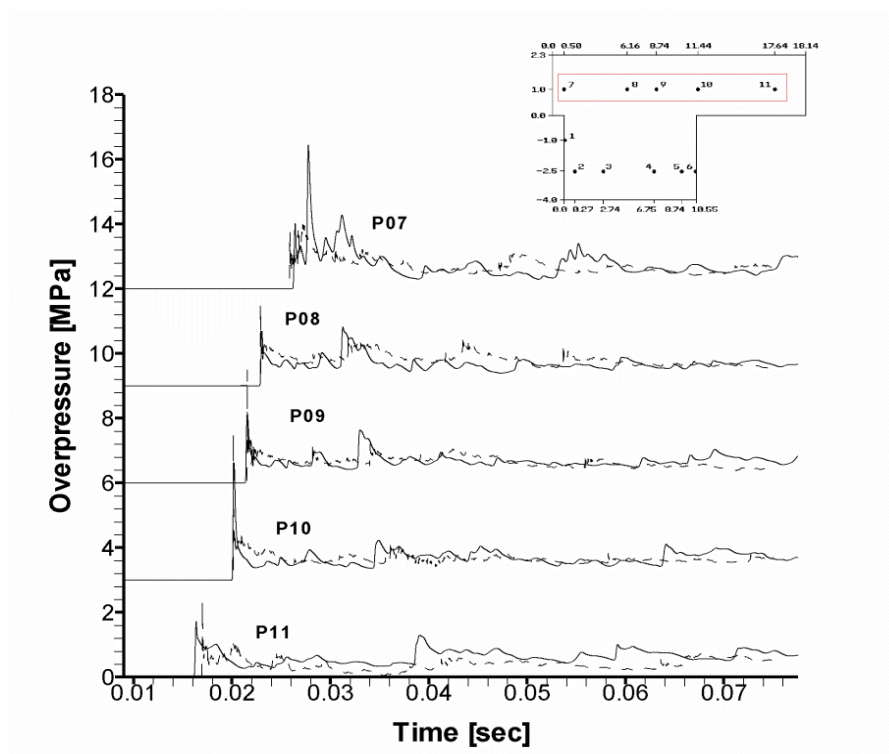


**Figure 11-23.** Pressure transients in the channel along the side wall from the gauges 11 to 7, 25.5% hydrogen-air mixture (dotted line – experiment, solid line – simulation).



Figure 11–23 shows that the pressure signal of the simulated detonation and rarefaction waves are close to the experimental transients with all major experimental peaks having their simulated pairs. Over-predicted detonation velocity, observed in pressure gauge 11, in the authors opinion is due to behaviour of the detonation wave in the channel bend. According to the experimental results in a laboratory scale (Frolov et al., 2007) a detonation front propagating in a bend tube is subjected to temporary attenuation with the velocity drop of about 15%, which is then followed by the recovery of the propagation velocity in the straight tube section downstream from the bend. This seems to be the case in the considered experiment: arrival of the detonation to gauge 11, located after the bend, is “delayed”, though the detonation velocity during its further propagation along the straight part of the channel is close to the theoretical value. Experimental and simulated pressure peak arrival time in location of pressure transducers 10, 9, 8, 7 are in a perfect agreement, which means the simulated propagation velocity is in the agreement with the experimental one. Maximum peak of pressure in the leading front is somewhat under predicted. This is particularly pronounced in the pressure gauge 11, 9, and 7 (leading peak pressure 1.7, 2.1 and 2.1 MPa respectively), and in a less degree in sensor 8 (leading peak pressure 2.4 MPa). In location of sensor 10 the simulated leading peak pressure reached value is 3.6 MPa, i.e. higher than the theoretical von Neumann pressure 2.67 MPa. This is thought due to reflection effect of thickened numerical detonation wave.

The instantaneous simulated pressure, progress variable and temperature profiles for 25.5% hydrogen-air mixture detonation between gauges 10 and 11 are shown in Fig. 11–24.

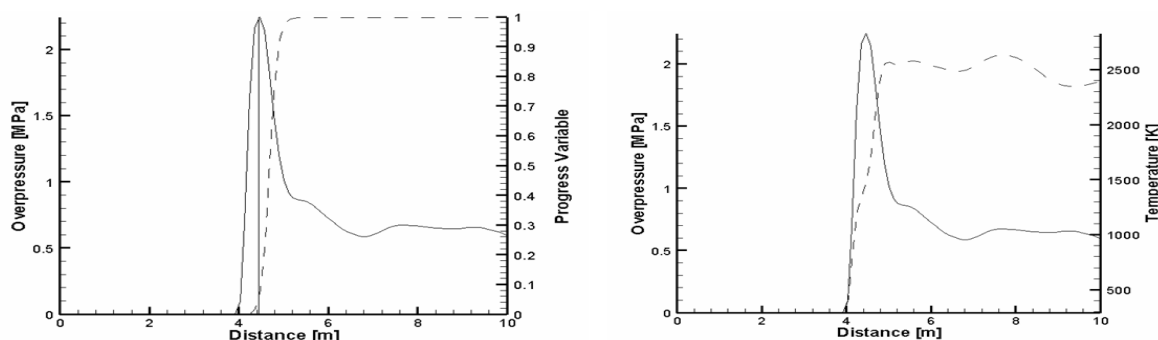


**Figure 11–24.** Detonation parameter profile in 3D simulations (25.5% hydrogen-air mixture, CV size 0.1 m, hexahedral grid): left – overpressure (vertical line identifies the pressure peak) and the progress variable, right – overpressure and temperature.

Figure 11–24 shows that the leading shock wave smoothly increases to the maximum value due to 3D effects, which start to affect the detonation wave propagation in this experimental geometry. Yet the model is capable to handle discontinuities on the large control volumes. This result is achieved due to the proper amount of the released energy, calculated using the gradient method, and the proper location of the energy release within the detonation wave structure, i.e. behind the leading shock wave. It is also seen that the mentioned above requirement for the numerical reaction front thickness resolution by at least 4–5 CVs is valid for the leading shock front too.

Maximum pressure peak differs for each pressure gauge located along the wall for both experiment and simulations in two processed tests (see Fig. 11–25). Simulated pressures follow the experimental trend with some under-prediction except pressure gauge 7 where computed pressure peak is slightly higher. There is a noticeable under-prediction in location of gauge 5 that is easy to explain by the vicinity of the initiating charge to this pressure gauge.

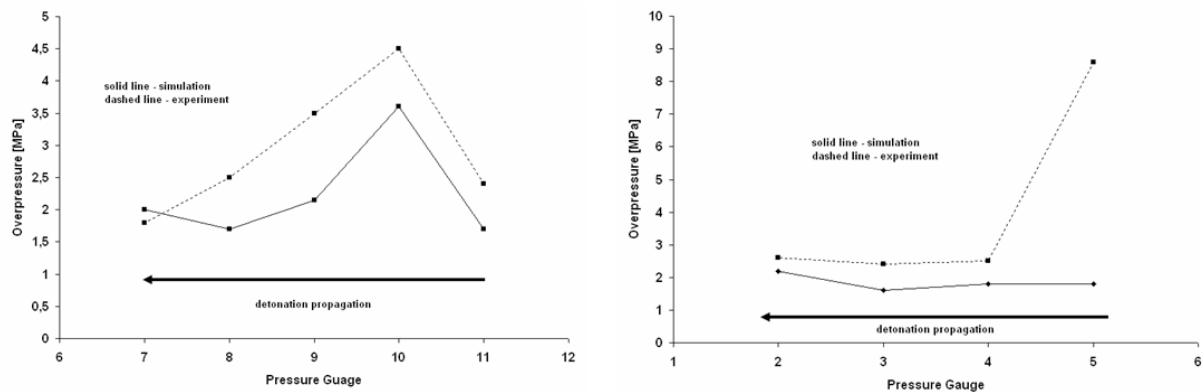


**Figure 11–25.** Maximum peak of pressure for pressure gauges: left – gauges 11–7 (25.5% hydrogen-air mixture); right – gauges 5–1 (20% hydrogen-air mixture).

Sensitivity of the LES model in 3D simulations to the CV size and mesh type was tested using 25.5% hydrogen-air mixture detonation. CV size varied between 0.05 and 0.5 m, and hexahedral and tetrahedral meshes were used in simulations. The simulations were unstable for CV size bigger than 0.1 m. The same situation is for the tetrahedral mesh with CV size in the range 0.1–0.5 m. The grid sensitivity analysis showed that for CV size larger than 0.1 m numerical diffusion starts to play a dominant role in 3D complex geometries when the model is applied. This behaviour can be clearly seen during the shock wave diffraction. Computational cost of simulations with CV size less than 0.1 m for both hexahedral and tetrahedral meshes was prohibitively high.

The sensitivity of the model was tested with one level of adaptive to the pressure gradient mesh refinement (CV size in refinement 0.05 m). The pressure and temperature profiles obtained with the refined grid are shown in Fig. 11–26. Measurement of the numerical pressure and temperature were obtained in pressure gauge number 10. The general shape of the pressure profiles is similar to those obtained without grid refinement (see Fig. 11–24). The simulated von Neumann pressure peak is equal to its theoretical value.

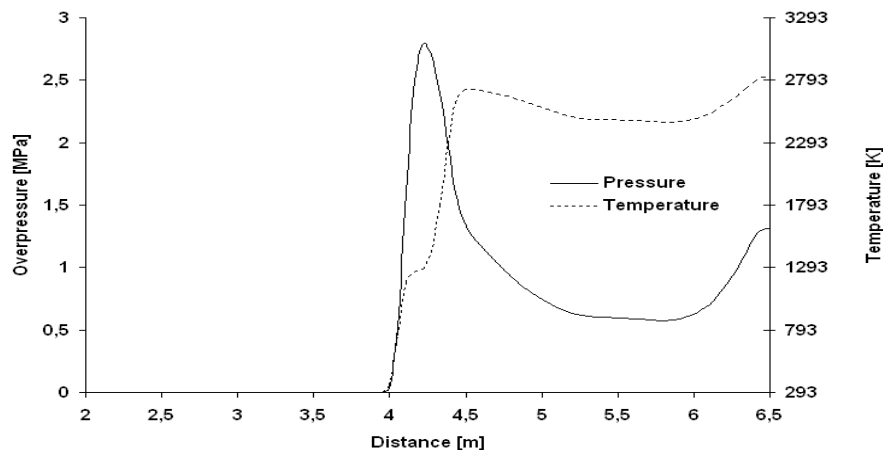


**Figure 11–26.** Pressure and temperature profiles for hexahedral grid (CV size 0.05 m) with one level of the grid refinement (25.5% hydrogen-air mixture).

#### 11.2.4.4. Concluding remarks

The LES detonation model, developed and verified earlier against the ZND theory of planar detonation has been tested against two large scale detonation experiment in the RUT facility with uniform hydrogen-air mixtures of 20% and 25.5% by volume of hydrogen in air and different location of detonation initiation. The LES model of detonation is based on the progress variable equation coupled with the gradient method where chemical kinetics is incorporated into the value of the detonation velocity. Simulations are in good agreement with experimental pressure transients in different locations within the experimental facility for both mixtures and ignition locations.

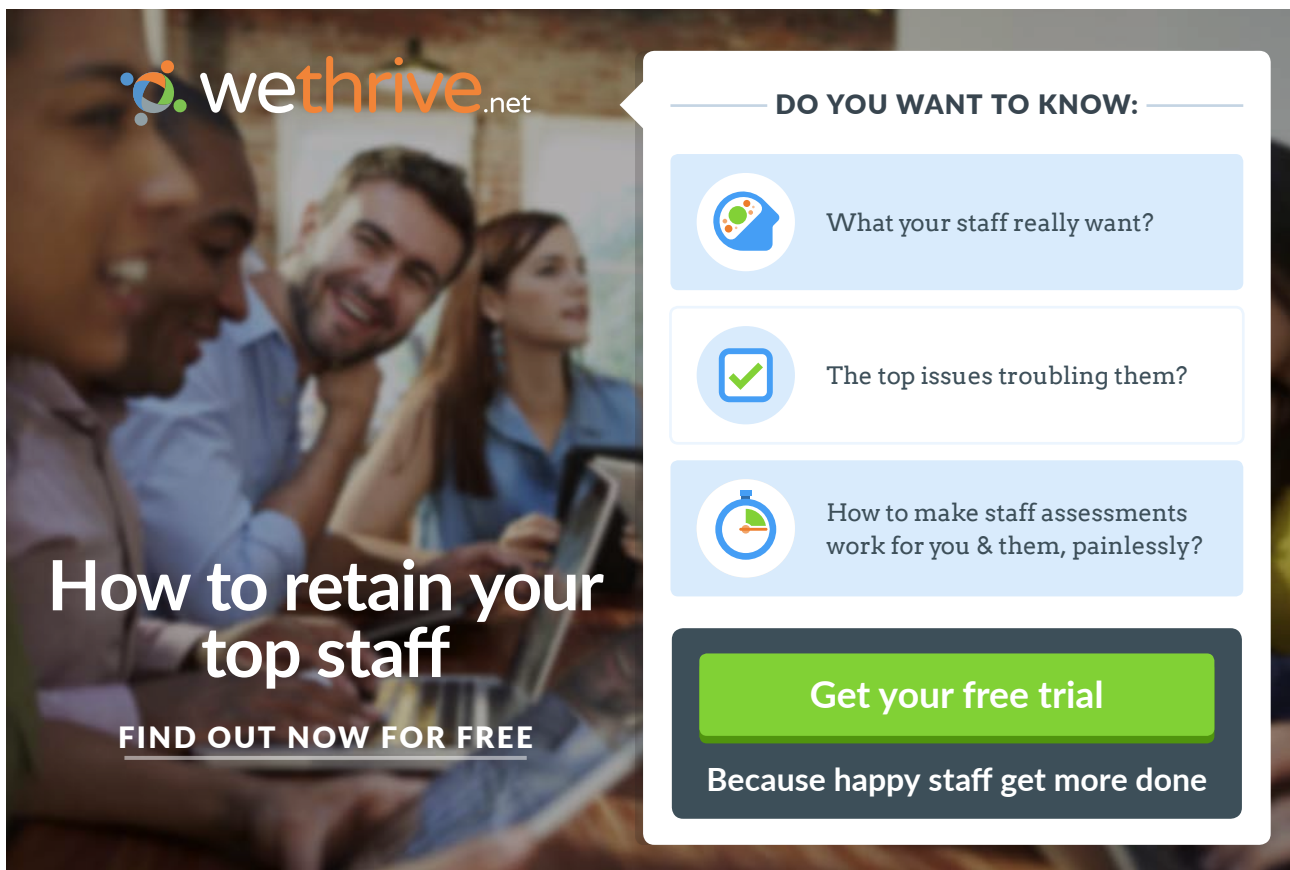
Detonation velocity in simulations is not constant that could be attributed to the effect of walls on the solution of the progress variable equation. Differently to the planar detonation simulations, the LES model demonstrates a degree of grid dependency for the 3D detonation propagation in the complex geometry with reflections: maximum size of CV for simulation stability was equal 0.1 m using hexahedral CVs. The grid adaptation improves results of large scale detonation simulations without significant increase of the computational effort. The presented LES detonation model is considered as a platform for a future DDT model development and as a contemporary tool for hydrogen safety engineering.

## 12 Safety strategies and mitigation techniques

The main general safety strategy to deal with hydrogen leaks is to minimize its mass flow rate and piping diameter, and “let it go” to prevent its accumulation to a hazardous level when a flammable hydrogen-air mixture represents unacceptable hazards and risks. This chapter gives some examples of hydrogen safety engineering.

The standard “Basic considerations for the safety of hydrogen systems” (ISO/TR 15916:2004) gives some general recommendations to minimize the severity of the consequences of a potential mishap:

- Minimize the quantity of hydrogen that is stored and involved in an operation;
- Isolate hydrogen from oxidizers, hazardous materials and dangerous equipment;
- Identify and, if possible, separate or eliminate potential ignition sources;
- Separate people and facilities from the potential effects of fire, deflagration, or detonation originating from the failure of hydrogen equipment or storage systems;
- Elevate hydrogen systems or vent them above other facilities;
- Prevent hydrogen-oxidizer mixtures from accumulating in confined spaces (under the eaves of roofs, in equipment racks or cabinets, or within equipment covers or cowlings);






**wethrive.net**

### How to retain your top staff

**FIND OUT NOW FOR FREE**

**DO YOU WANT TO KNOW:**

-  What your staff really want?
-  The top issues troubling them?
-  How to make staff assessments work for you & them, painlessly?

**Get your free trial**

**Because happy staff get more done**

- Minimize personnel exposure by limiting the number of people exposed, the time that the personnel are exposed;
- Use of personal protective equipment;
- Use of alarms and warning devices (including hydrogen and fire detectors), and area control around a hydrogen system;
- Practice good housekeeping, such as keeping access and evacuation routes clear and keeping weeds and other debris away from hydrogen systems;
- Observe safe operational requirements, such as working in pairs when operating in a hazardous situation.

Design of buildings and rooms in which hydrogen is stored or used should address safety issues such as the following, in order to minimize the hydrogen hazards: pressure relief systems to mitigate deflagrations by venting technique (ISO/TR 15916:2004). Explosion-proof equipment should be used in all locations described above unless it can be shown that it is not necessary, or required by local, regional or national regulations (ISO/TR 15916:2004).

### 12.1. Inherently safer design of fuel cell systems

Inherently safer design is an approach that focuses on reducing or eliminating hazards associated with the product or the process. Consider how a fuel cell (FC) safety system could be improved by reducing hazards without interfering the technology itself. Unfortunately, current fuel cell systems are often designed using piping diameters of 5–15 mm and pressures of 0.5–1.5 MPa without consideration of hazards. The mass flow through a 5 mm diameter orifice at storage pressure of 0.5 MPa can be calculated using the under-expanded jet theory, and is about 6 g/s. For a pipe of 15 mm diameter and pressure 1.5 MPa the mass flow rate is 170 g/s.

Now let us estimate the mass flow rate for a 50 kW FC system for providing energy for large facilities such as hotels, hospitals, office buildings, and multi-family dwellings. Assuming that an electrical efficiency of FC is 45%, and the upper heat of reaction (combustion) of hydrogen with air is  $[(286.1 \text{ kJ/mol}) / (2.016 \text{ g/mol})] = 141.92 \text{ kJ/g}$ , the mass flow rate for the FC functioning at maximum power can be calculated as  $(50 \text{ kW}) / (0.45 / (141.92 \text{ kJ/g})) = 0.78 \text{ g/s}$ . For example, this mass flow rate can be provided at a pressure 0.5 MPa through a restrictor in the storage or piping system with an orifice diameter of only about 1.8 mm, or at pressure 0.2 MPa through a diameter orifice of about 2.9 mm.

The separation distance for unignited release can be estimated as proportional to a nozzle diameter and square root from a storage pressure. Thus, decrease of pipe diameter from 15 mm to 2.9 mm and pressure from 1.5 MPa to 0.2 MPa could decrease separation distance by more than 14 times!

Further analysis can be performed to compare separation distances for these two options: option 1 – pressure 0.5 MPa and pipe diameter 1.8 mm; option 2 – 0.2 MPa and 2.9 mm. The ratio of separation distances for unignited releases in option 1 and 2 in assumption of full bore rupture can be estimated as 0.98, i.e. they are practically the same. These examples clearly demonstrate advantages of the science-informed safety design of hydrogen and fuel cell systems to essentially reduce separation distances without affecting the performance parameters of FC.

## 12.2. Mitigation of release consequences

The similarity law (5–21) with substitution of hydrogen density in the real nozzle exit is a simple and thoroughly validated tool for hydrogen safety engineering for both expanded and under-expanded round jets. For example, let us calculate a diameter of a pressure relief device (PRD) for a forklift onboard storage to obey the following safety strategy. In the case of an upward release from the onboard storage at 35 MPa we would like to exclude formation of a flammable layer under a ceiling which is 10 m above the PRD.

To realize this strategy the concentration on the jet axis at distance 10 m should be equal or below 4% by volume (corresponding mass fraction of hydrogen is  $C_{ax}=0.00288$ ). The density of hydrogen in the nozzle exit, calculated by the under-expanded jet theory for the storage pressure of 35 MPa, is  $\rho_N=14.6$  kg/m<sup>3</sup>. Thus, the diameter of the PRD can be calculated straight forward from the similarity law (5–21) as equal or less than 1.5 mm

$$D = \frac{C_{ax}}{5.4} \sqrt{\frac{\rho_S}{\rho_N}} x = \frac{0.00288}{5.4} \sqrt{\frac{1.204}{14.6}} 10 = 0.0015 \text{ m.}$$

To finalize this safety strategy for use of hydrogen-powered forklifts in the warehouse a requirement to fire-resistance rating of the onboard storage tank must be formulated and testing carried out. Indeed, the fire-resistance rating should be greater than the blowdown time (the time to empty the storage vessel) of the storage tank to exclude its catastrophic failure in the case of external fire. It is clear that the use of a PRD with a larger diameter would create a flammable cloud or a jet flame with higher hazards, e.g. dangerous overpressure during “delayed ignition” or deflagration of initial cloud, and associated risks.

## 12.3. Reduction of separation distances for high debit pipes

Since 1969 Air Products operates in Houston (Texas, USA) 232 km of hydrogen pipelines of diameter 11.4 cm to 22 cm at a pressure of 5.8 MPa. For these parameters the under-expanded jet theory gives the maximum notional nozzle exit diameter 120 cm and mass flow rate 133.2 kg/s (for a scenario of full bore rupture of pipe with 22 cm internal diameter at 5.8 MPa).

Distance to 4% by volume of hydrogen in the horizontal jet, if it is assumed to be in the momentum-controlled regime, can be calculated graphically directly from the nomogram in Fig. 5–6 or by the following simple equation (assuming for air  $\rho_s=1.204$  kg/m<sup>3</sup>)

$$x_{4\%} = 1574 \cdot \sqrt{\rho_N} \cdot D ,$$



where  $D$  is the maximum actual diameter of the release (0.22 m). The density in the nozzle at storage pressure of 5.8 MPa can be calculated by the under-expanded jet theory, e.g. from the lower graph in Fig. 5–6, and is equal to  $\rho_N=2.87 \text{ kg/m}^3$ . Thus, the distance to 4% by volume calculated by the above equation, i.e. in the assumption of momentum-dominated jet, is 587 m!

Fortunately, the jet is not momentum-controlled at the range of concentration of interest. Indeed, the Froude number calculated by flow parameters at the notional nozzle exit is  $Fr=5.1$ . Analysis of Fig. 5–8 with  $Fr=5.1$  gives that the jet becomes buoyancy-controlled (intersection of vertical line from  $Fr=5.1$  with the curve denoted “Downward”) at  $\text{Log}(x/D)=2$  (notional nozzle is applied to use Fig. 5–8), i.e. at distance  $x=100D=120 \text{ m}$ ! This distance is 4.9 times shorter compared to the safety distance determined without accounting for the effect of hydrogen buoyancy.

## 12.4. Mitigation by barriers

Sandia National Laboratories performed a series of experimental and numerical studies in order to assess the effectiveness of barriers to reduce the hazard from unintended releases of hydrogen, including within the HYPER project international collaboration. For the conditions investigated, i.e. 13.79 MPa source pressure and 3.175 mm diameter round leak, the barrier configurations studied were found to reduce horizontal jet flame impingement hazard by deflecting the jet flame, reduce radiation hazard distances for horizontal jet flames and reduce horizontal unignited jet flammability hazard distances.

For the 1-wall vertical barrier and 3-wall barrier configurations the simulations of the peak overpressures from ignition were found to be approximately 40 kPa on the release side of the barrier while approximately 3–5 kPa on downstream backside of the barrier.

## 12.5. Mitigation of deflagration-to-detonation transition (DDT)

Strategies to minimize the potential for flame acceleration or detonation include (ISO/TR 15916:2004):

- Avoiding confinement and congestion where flammable hydrogen-air mixtures might form;
- Using flame arrestors, small orifices, or channels to prevent deflagration and detonation from propagating within a system;
- Using diluents, like steam or carbon dioxide, or oxygen depletion techniques where possible and water spray or mist systems to retard flame acceleration. This recommendation of the standard (ISO/TR 15916:2004) should be taken with care as hydrogen-air flames are difficult to quench and they can burn or even accelerate around the droplets in heavy sprays of water (Shebeko et al., 1990);
- Reduce size of a system where possible to narrow detonability limits.

A low carbon economy will more and more exploit fuels with addition of hydrogen. Knowing that hydrogen combustion is prone to DDT, especially at large scales, there are serious concerns on how technologies could be made safer. For such kind of applications, the safety strategy can be, in the author's opinion, to organize and control the process of combustion of a hydrogen-contained mixture in a way that the mixture supplied to the burner is between the lower flammability limit and the lower detonability limit.

## 12.6. Prevention of DDT within a fuel cell

In experiments of Pro-Science (Friedrich et al., 2009) in a mock up of fuel cell (FC), a significant flame acceleration was recorded leading to a high overpressure, for the total injected mass of 15 g and 25 g, sufficient for complete demolition of the experimental rig. Both experimental and numerical studies of the FC mock up suggest that the total injected mass should be less than 6 g for the configuration studied in order to keep overpressures below 10 to 20 kPa. Missile effects could be still possible for this 6 g inventory. So, an inventory of 1 g seems a good target for safety for accidental release within this FC mock up. This research result can be used to formulate requirements to a shut down safety system for fuel cells.

The feed line pressure and diameter of a pipe and restrictor orifice should, by design, limit the mass flow rate of hydrogen to a technological level that is required for the FC to function. The release duration, due to the time required to detect the leak and operate the valve should be reduced as much as possible to exclude release of more than 1 g of hydrogen. An estimate shows that for a 50 kW fuel cell, that needs consumption rate of hydrogen just below 1 g/s, a leak detection time and time of shutting down supply line should be together less than 1 s. Any reduction of this time would have a positive impact on safety.

This requirement is difficult to achieve for currently available sensors. Innovative systems of leak detection, e.g. based on supply pressure fluctuation analysis, have to be developed and implemented to provide acceptable level of safety. The grid obstacle, used in the Pro-Science experiments to mimic the congestion within real fuel cell, led to strong flame acceleration (Friedrich et al., 2009). The congestion of internal space of the FC enclosure should be avoided as much as possible by a careful design.

## 12.7. Detection and hydrogen sensors

The addition of an odorant to hydrogen would ease the detection of small leaks. However, this is not practicable in most situations, e.g. this would poison an expensive catalyst in fuel cells. Moreover, this is not feasible for liquefied hydrogen as any added substance would be in a solid state at the temperature of liquefied hydrogen of 20 K. Hydrogen fire detection can be based on registration of infrared radiation of flames which are not seen in a day light.

In 2009 INERIS (France) conducted a test program within the HYPER (2008) project based on the international standard parts IEC 61779-1&4 (1998) and aimed at assessing the performance of commercially available hydrogen detectors. These devices were of electrochemical and catalytic types, i.e. the two types most often used in industry. The catalytic sensor was 5 times faster than the electrochemical one to respond to a sudden exposure of hydrogen. However, the response time was approximately 10 s for the catalytic sensor and 50 s for the electrochemical sensor. These figures also apply for the recovery time. In many practical scenarios this long time is hardly acceptable.

Catalytic detectors studied within the HYPER (2008) project were also prone to loss of sensitivity and drift of zero after a prolonged exposure to hydrogen. This emphasizes the need to regularly calibrate these devices. Higher humidity tended to increase the reading of the catalytic detector for constant hydrogen content. The catalytic detector was very sensitive to the presence of carbon monoxide but the interfering was only temporary, i.e. when the CO exposure ceases the detector behaves in an ordinary way.

Research by Joint Research Centre, Institute for Energy, The European Commission within the HYPER (2008) project demonstrated that the time required by the electrochemical sensor to respond to hydrogen exposure of known concentration becomes longer when the gas flow rate is reduced, i.e. it could be twice longer by solely reducing the flow rate from 100 to 30 ml/min. This finding is particularly important when the sensor is intended to control the formation of an explosive atmosphere within a FC cabinet.

There is another issue related to faster catalytic sensors that is not yet sufficiently addressed in literature. This is a potential to ignite hydrogen-air mixture with high concentrations of hydrogen by the sensor. The ignition of hydrogen-air mixtures with high content of hydrogen by recombiners was already observed (Blanchat and Malliakos, 1998).

A variety of methods and sensor types are commercially available to detect the presence of hydrogen (ISO/TR 15916:2004). Many of these detectors are suitable for use in automatic warning and operating systems, see for example ISO 26142:2010 for details concerning stationary systems.

# Concluding remarks

We tend to treat our current fuels, notably petrol and natural gas, quite ‘casually’ due to familiarity with them, whereas hydrogen is viewed with some trepidation as it is ‘unknown’ and wrongly linked as a reason to past ‘catastrophic’ events like Hindenburg dirigible. The inevitability of the hydrogen economy and the important role of hydrogen safety, especially the hydrogen safety engineering, in its underpinning are introduced. Hydrogen safety engineering is defined as an application of scientific and engineering principles to the protection of life, property and environment from adverse effects of incidents/accidents involving hydrogen. These principles have to be formulated and tools to carry out hydrogen safety engineering developed and validated against experimental data

Hydrogen is not more dangerous or safer than other energy carriers. Hydrogen is different and requires professional safety knowledge and skills at all stages starting from design of hydrogen and fuel cell (HFC) systems through their certification, permitting and commissioning to new safety culture in use of these technologies by public.

Safety of HFC systems and infrastructure is a paramount for their commercial competitiveness and public acceptance. The activities of the European Network of Excellence HySafe (2004–2009) and currently of the International Association for Hydrogen Safety (IA HySafe) along with national and international programs, e.g. funded by European Fuel Cell and Hydrogen Joint Undertaking and US Department of Energy, are a firm guarantee of the progress in closing numerous knowledge gaps, development of innovative safety strategies and breakthrough engineering solutions. The progress achieved so far cannot be interpreted as a closure of safety issues. New processes of hydrogen production, storage, transportation and use in HFC systems will appear that will require both basic and applied research.

Hazards and associated risks have to be fully understood and addressed. The role of risk assessment methods should not be overestimated in the absence of reliable statistics on probable potential benefits for the business and in no way at the cost of public safety. Car manufacturers carrying out own competitive research on hydrogen-powered vehicles should be more open and cooperative in solving common for all safety problems. The opinion “there are no safety issues” for HFC technologies should be considered as not professional and misleading public.

The examples of innovative safety strategies and inherently safer engineered systems should be disseminated as wide as possible instead. The test results of safety performance of hydrogen-fuelled vehicles should be publicly available and activities on improvement of safety characteristics should be continuously reported to public to prevent rumours and non-professional interpretations.

Conclusion is drawn that onboard storage and pressure relief devices (PRDs) currently available for hydrogen-powered vehicles should be redesigned to mitigate potential accidents especially in confined spaces as garages, car parks, maintenance shops, tunnels, etc. This requires at least reduction of mass flow rate during release through the PRD and increase of fire resistance rating of the onboard storage from current 1–6 minutes by an order of magnitude. The underestimation of the role of safety for HFC products and following accidents, which will happen as for any other technology, would have catastrophic consequences and thus imply further delays for the commercialization. That is what no one working in the field of hydrogen and fuel cell technologies wants to happen.

Inherently safer design of HFC systems has to be the primary goal of developers. For example, parameters of piping system, i.e. pressure and internal diameter, have to be minimized to provide technological requirements on mass flow rate but not more. It is demonstrate that separation distances could be reduced by more than order of magnitude if system developers are educated in carrying out hydrogen safety engineering. Another example of inherently safer design is as follows. The safety strategy for burners and turbines using mixtures of hydrogen with other gases could be a provision that the mixture supplied to the combustion device is between the lower flammability limit and the lower detonability limit to sustain combustion yet to prevent detonation.

## Struggling to get interviews?

Professional CV consulting & writing assistance from leading job experts in the UK.

Visit site



Take a short-cut to your next job!  
Improve your interview success rate by 70%.



TheCVagency

Visit [theagency.co.uk](https://theagency.co.uk) for more info.

There is a clear need in the development of an overarching performance-based standard for carrying out hydrogen safety engineering of HFC applications and infrastructure that is scientifically informed. Indeed, current RCS in the field are fragmented, are far from being complete, have grown in number, are prepared mainly by the industry and for the industry, are difficult to interpret, and are sometimes contradicting available knowledge being by definition at least 3 years old. This novel for hydrogen safety standard should have organizational and technical frameworks on how to carry out hydrogen safety engineering and gather together in one place description of technical sub-systems, e.g. through so-called “published documents” similar to British standard BS 7974 approach for fire safety engineering (BSI, 2001). The concept of the standard and the structure of technical sub-systems allow for their continuous update by research results and are convenient for new people to get rapidly into the emerging profession of hydrogen safety engineering.

Professional workforce having a higher education degree to lead hydrogen safety activities in industry, regulatory bodies, research organizations and academia is another important element in securing the safe introduction of HFC technologies to the market.

The main progress in closing knowledge gaps in hydrogen safety science and engineering can be briefly summarized, based on the research results presented in this book, as follows.

For non-reacting hydrogen releases:

- The under-expanded jet theory is developed for prediction of flow parameters at the actual nozzle and notional nozzle exits. The theory accounts for non-ideal behaviour of hydrogen at high pressures by the Abel-Noble equation. For example, the use of the ideal gas law will overestimate the hydrogen mass released from 70 MPa storage tank by about 45%.
- The similarity law for hydrogen concentration decay in both expanded and under-expanded momentum-controlled jets is proposed and validated.
- A methodology to define where a jet transition from momentum- to buoyancy-controlled regime takes place is developed. This is of importance to essentially reduce separation distance, e.g. for high debit jets from pipelines.



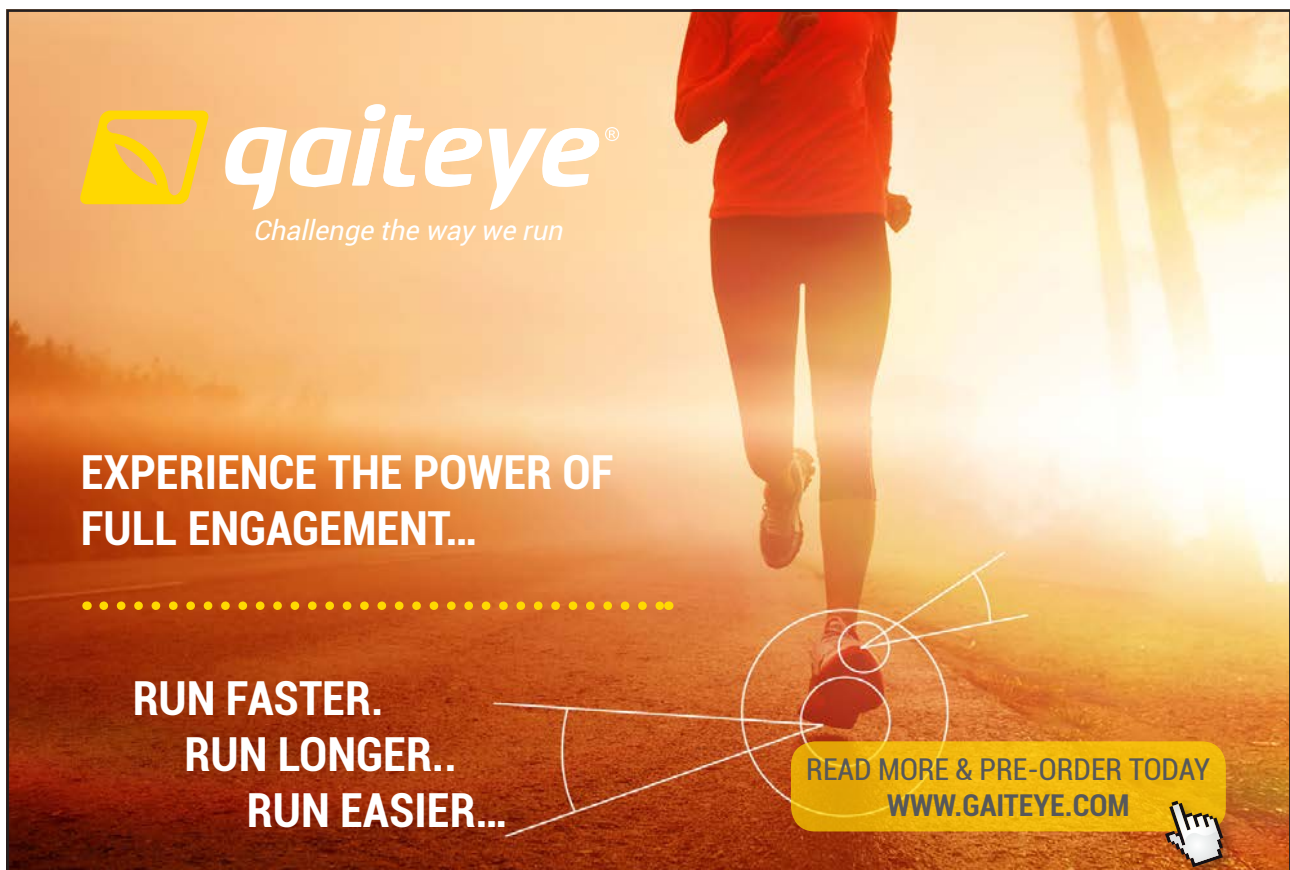
For ignitions and hydrogen fires:

- The dimensional correlation for hydrogen jet flame length is developed. The conservative estimate of the flame length is 50% longer than the best fit curve.
- The novel dimensionless correlation for a jet flame length accounting for dependence on  $Fr$ ,  $Re$ ,  $M$  numbers and covering the full spectrum of hydrogen releases, including laminar and turbulent flows, buoyancy- and momentum-controlled leaks, expanded and under-expanded jets is developed. There are three distinguishable parts in this innovative correlation: traditional ascending buoyancy-controlled, traditional momentum-dominated plateau for expanded jets, and a new third ascending part that represents under-expanded momentum-controlled jet fires. The dimensionless flame length in the last part of correlation depends on Reynolds rather than Froude number. There is no saturation of the dimensionless flame length at value  $L_f/D=230$  observed in previous studies with expanded jets, instead reported experiments demonstrate values up to  $L_f/D=3000$ .
- The contradictory statements available in combustion literature about the location of a turbulent non-premixed flame tip are clarified. It is established that the flame tip is located for momentum-controlled jets (both expanded and under-expanded) at the distance from the leak source where the axial concentration of hydrogen in an unignited jet is 11% by volume (in the range from 8% to 16%). This is far below the stoichiometric concentration of 29.5% by volume as was stated previously.
- The potential of sensors to ignite mixture at high concentration of hydrogen has to be addressed from the beginning of hydrogen detector development. Relevant testing methods have to be developed and included into RCS.
- The LES model of hydrogen ignition during sudden releases, including to complex geometries like T-shaped channel, is validated against experimental observations.

For hydrogen deflagrations and detonations:

- Delayed ignition of hydrogen releases produces highly turbulent deflagration. It has been demonstrated in experiments by HSL that with the ignition delay of 0.8 s the release from 20.5 MPa storage through 9.5 mm orifice generates overpressure of 16.5 kPa for free jet, 42 kPa if 90° barrier wall is installed, and 57 kPa if 60° barrier is applied. This is comparable with the moderate level of damage to structures by overpressure (17 kPa), severe damage (above 35 kPa), and total structure destruction (above 83 kPa). At the same series of experiments no overpressure was observed for nozzle diameter of 1.5 mm.
- Mitigation by barriers study performed by Sandia National Laboratories for 13.79 MPa release through 3.175 mm diameter round leak demonstrated that for different barrier configurations the peak overpressure to be approximately 40 kPa on the release side of the barrier and only 3–5 kPa on downstream backside of the barrier.

- Experimental and numerical studies show that turbulence of mixture during sudden release of high pressure hydrogen to the atmosphere has a greater effect on the deflagration overpressure than the total amount of released gas or the volume of flammable mixture.
- Deflagration-to-detonation transition (DDT) phenomenon is not yet studied enough to have predictive contemporary models and tools for solving large-scale engineering problems. Detonation is the worst case scenario for an accident involving hydrogen and all measures should be undertaken to prevent it. Indeed, the energetic equivalent of 1 g of hydrogen is quite high, i.e. 28.65 g of TNT.
- Results obtained by Pro-Science during the FP6 HYPER project indicate that the accidental release of no more than 1 g of hydrogen inside the fuel cell is a good target for hydrogen safety engineers to prevent DDT.
- The LES models of deflagrations and detonations are being developed and validated. They can be used as contemporary tools for hydrogen safety engineering.



**gaiteye**  
*Challenge the way we run*

**EXPERIENCE THE POWER OF  
FULL ENGAGEMENT...**

**RUN FASTER.  
RUN LONGER..  
RUN EASIER...**

**READ MORE & PRE-ORDER TODAY  
[WWW.GAITEYE.COM](http://WWW.GAITEYE.COM)**

# Acknowledgements

Author is grateful to colleagues from the HySAFER Centre at the University of Ulster and partners from all over the globe for their collaboration and devotion to hydrogen safety research, education and outreach. Financial support of the European Commission and the Fuel Cell and Hydrogen Joint Undertaking to hydrogen safety research at HySAFER is highly appreciated.

# Appendix 1. Glossary

**Accident** is an unforeseen and unplanned event or circumstance causing loss or injury.

**Auto-ignition temperature** is the minimum temperature required to initiate combustion reaction of fuel-oxidiser mixture in the absence of an external source of ignition.

**Boiling point** is the temperature to which a fuel must be cooled in order to store and use it as a liquid. The *normal boiling point* (NBP) of a liquid is the case in which the vapor pressure of the liquid equals the defined atmospheric pressure at sea level (1 atmosphere or 101,325 Pa). The *standard boiling point* (SBP) is defined as the temperature at which boiling occurs under a pressure of 1 bar (100,000 Pa).

**Deflagration** and **detonation** are propagation of a combustion zone at a velocity that is respectively less than and greater than the speed of sound in the unreacted mixture.

**Equivalence ratio** is the ratio of the fuel-to-oxidizer ratio to the stoichiometric fuel-to-oxidizer ratio.

**Fire-resistance rating** is a measure of time for which a passive fire protection system can withstand a standard fire resistance test.

**Flammability range** is the range of concentrations between the lower and the upper flammability limits. The *lower flammability limit* (LFL) is the lowest concentration of a combustible substance in a gaseous oxidizer that will propagate a flame. The *upper flammability limit* (UFL) is the highest concentration of a combustible substance in a gaseous oxidizer that will propagate a flame.

**Flashpoint** is the lowest temperature at which the fuel produces enough vapours to form a flammable mixture with air at its surface.

**Hazard** is a chemical or physical condition that has the potential for causing damage to people, property and the environment.

**Hydrogen safety engineering** (HSE) is application of scientific and engineering principles to the protection of life, property and environment from adverse effects of incidents/accidents involving hydrogen.

**Incident** is something that occurs casually in connection with something else.

**Laminar burning velocity** is the rate of flame propagation relative to the velocity of the unburned gas that is ahead of it, under stated conditions of composition, temperature, and pressure of the unburned gas.

**Limiting oxygen index** is the minimum concentration of oxygen that will support flame propagation in a mixture of fuel, air, and nitrogen.

**Mach disk** is a strong shock normal to the under-expanded jet flow direction.

**Maximum experimental safe gap** (MESG) of flammable gases and vapours is the lowest value of the safe gap measured according to IEC 60079-1-1 (2002) by varying the composition of the mixture. The safe gap is the gap width (determined with a gap length of 25 mm) at which in the case of a given mixture composition, a flashback just fails to occur.

**Minimum ignition energy** (MIE) of flammable gases and vapours is the minimum value of the electric energy, stored in the discharge circuit with as small a loss in the leads as possible, which (upon discharge across a spark gap) just ignites the quiescent mixture in the most ignitable composition. For a given mixture composition the following parameters of the discharge circuit must be varied to get the optimum conditions: capacitance, inductivity, charging voltage, as well as shape and dimensions of the electrodes and the distance between electrodes.

**Normal Temperature and Pressure** (NTP) conditions are: temperature 293.15 K and pressure 101.325 kPa.

**Quenching distance** is the maximum distance between two parallel plates that will extinguish a flame passing between the plates.

**Quenching gap** is the spark gap between two flat parallel-plate electrodes at which ignition of combustible fuel-air mixtures is suppressed. The quenching gap is the passage gap dimension requirement to prevent propagation of an open flame through a flammable fuel-air mixture that fills the passage.

**Permeation** is the movement of atoms, molecules, or ions into or through a porous or permeable substance.

**Separation distance** is the minimum separation between a hazard source and an object (human, equipment or environment) which will mitigate the effect of a likely foreseeable incident and prevent a minor incident escalating into a larger incident.

**Specific gravity** is the ratio of the density of a substance to the density of a reference substance, both at the same temperature and pressure.

**Sublimation** is the change directly from solid to vapour or vice versa without going through the liquid phase.

**Reynolds number** is a dimensionless number that gives a measure of the ratio of inertial to viscous forces.

**Risk** is the combination of the probability of an event and its consequence.

**Under-expanded jet** is a jet with a pressure at the nozzle exit which is above atmospheric pressure.

This e-book  
*is made with*  
**SetaPDF**



PDF components for PHP developers

[www.setasign.com](http://www.setasign.com)



# References

- Abdel-Gayed, RG, Al-Khishali, KJ and Bradley, D (1984) Turbulent burning velocities and flame straining in explosions. *Proc. Roy. Soc. Lond. A*:391, pp. 393–414.
- Ackroyd, GP and Newton, SG (2003) An investigation of the electrostatic ignition risks associated with a plastic coated metal. *J Electrostatics*, vol. 59, pp. 143–51.
- Adams, P, Bengaouer, A, Cariteau, B, Molkov, V and Venetsanos, AG (2011) Allowable hydrogen permeation rate from road vehicles. *International Journal of Hydrogen Energy*, vol. 36, pp. 2742–2749.
- AECL (2008) Private communication, Atomic Energy of Canada Limited.
- Ahrens, M (2009) Structure Fires Originating in vehicle storage areas, garages or carports of one- or two-family homes excluding fires in properties coded as detached garages. National Fire Protection Association, Quincy, MA, September 2009.
- Ahrens, M (2006) Structure and vehicle fires in general vehicle parking garages. National Fire Protection Association, Quincy, MA, January 2006.
- AIAA (1998) Guide for the Verification and Validation of Computational Fluid Dynamics Simulations, American Institute of Aeronautics and Astronautics. AIAA G-077-1998, ISBN 1563472856.
- Alcock, JL, Shirvill, LC and Cracknell, RF (2001) Compilation of existing safety data on hydrogen and comparative fuels. *Deliverable Report of European FP5 project EIHP2, May 2001*. Available from: [http://www.eihp.org/public/documents/CompilationExistingSafetyData\\_on\\_H2\\_and\\_ComparativeFuels\\_S..pdf](http://www.eihp.org/public/documents/CompilationExistingSafetyData_on_H2_and_ComparativeFuels_S..pdf). [Accessed 25.12.11].
- Armand, P, Vendel, J and Galon, P (1997) Physical analysis of combustion tests in the RUT facility and simulation of the detonation. *Transactions of the 14th Int. Conf. on Structural Mech. in Reactor Tech. (SMiRT 14)*, Lyon, France, August 17–22, 1997.
- Astbury, GR and Hawksworth, SJ (2007) Spontaneous ignition of hydrogen leaks: A review of postulated mechanisms. *International Journal of Hydrogen Energy*, vol. 32, pp. 2178–2185.
- Aung, KT, Hassan, MI and Faeth, GM (1997) Flame stretch interactions of laminar premixed hydrogen/air flames at normal temperature and pressure. *Combustion and Flame*, vol. 109, pp. 1–24.

- Aung, KT, Hassan, MI and Faeth, GM (1998) Effects of pressure and nitrogen dilution on flame/stretch interactions of laminar premixed  $H_2/O_2/N_2$  flames. *Combustion and Flame*, vol. 112, pp. 1–15.
- Azatyany, VV, Shebeko, YuN, Bolodian, IA, Shebeko, AYU, Navzenya, VYu and Tomilin, AV (2009) Combustion characteristics of mixtures  $H_2-(O_2-N_2)$ -diluent at various oxygen contents in oxydizers. *Proceedings of the 5th International Seminar on Fire and Explosion Hazards*. Edinburgh: Scotland, 23–27 April 2007, pp. 273–281.
- Babkin, VS (2003) Private communication. Institute of Chemical Kinetics and Combustion, Siberian Branch, Russian Academy of Science, Novosibirsk, Russia.
- Babkin, VS, Viun, AV and Kozachenko, LS (1966) The investigation of pressure dependence of burning velocity by the constant volume bomb method. *Combustion, Explosion and Shock Waves*, vol. 2(2), pp. 52–60.
- Babkin, VS and Kononenko, YuG (1967) Equations for burning velocity determination in spherical constant volume bomb. *Fizika Goreniya i Vzryva*, vol. 3(2), pp. 268–275 (in Russian).
- Babkin, VS, Vykhristyuk, AY, Krivulin, VN and Kudryavcev, EA (1984) Convection instability of spherical flames. *Archivum Combustionis*, vol. 4, pp. 321–327 (in Russian).
- Baev, VK, Kuznetsov, PP, Mogil'nyi, IA, Tret'yakov, PK and Yasakov, VA (1974a) Length of diffusion flames. *Combustion, Explosion and Shock Waves*, vol. 10, pp. 420–427.
- Baev, VK and Yasakov, VA (1974b) Effect of lifting forces on the length of diffusion flames. *Combustion, Explosion and Shock Waves*, vol. 10, pp. 752–758.
- Bain, A and Van Vorst, WD (1999) The *Hindenburg* tragedy revisited: the fatal flaw found, *International Journal of Hydrogen Energy*, vol. 24, pp. 399–403.
- Baker, WE, Cox, PA, Westine, PS, Kulesz, JJ and Strehlow, RA (1983) *Explosion Hazards and Evaluation*, Elsevier Scientific Publishing Co., Amsterdam, The Netherlands.
- Baker, J, Calvert, ME and Murphy, DW (2002) Structure and dynamics of laminar jet micro-slot diffusion flames. *Journal of Heat Transfer*, vol. 124, pp. 783–790.

Baraldi, D, Papanikolaou, E, Heitsch, M, Moretto, P, Cant, RS, Roekaerts, D, Dorofeev, S, Koutchourko, A, Middha, P, Tchouvelev, AV, Ledin, S, Wen, J, Venetsanos, A and Molkov, VV (2010) Report: Gap Analysis of CFD Modelling of Accidental Hydrogen Release and Combustion, JRC, Institute for Energy, Petten, The Netherlands, EUR 24399 EN, ISBN 978-92-79-15992-3, ISSN 1018-5593, doi:10.2790/2090, European Commission, 60 pp.

Baratov, AN, Korolchenko, AY and Kravchuk, GN (eds) – (1990) *Fire and explosion hazards of substances and materials*. Moscow, Khimiya. 496 p., ISBN 5-7245-0603-3 part 1, ISBN 5-7245-0408-1 part 2. (In Russian).

Barlow, RS and Carter, CD (1996) Relationships among Nitric Oxide, Temperature, and Mixture Fraction in Hydrogen Jet Flames. *Combustion and Flame*, vol. 104, pp. 288-299.

Barry, TF (2003) Fire exposure profile modeling: some threshold damage limit (TDL) data.

Barthélémy, H (2009) Private communication, Air Liquide.

Bartknecht, W (1978) *Explosionen*. Springer-Verlag, Berlin, Heidelberg, New York.

Bartknecht, W (1993) *Explosions-Schutz: Grundlagen und Anwendung*, Springer-Verlag.



**YOU THINK.  
YOU CAN WORK  
AT RMB**

**RAND  
MERCHANT  
BANK**  
A division of FirstRand Bank Limited  
Traditional values. Innovative ideas.

Rand Merchant Bank uses good business to create a better world, which is one of the reasons that the country's top talent chooses to work at RMB. For more information visit us at [www.rmb.co.za](http://www.rmb.co.za)

Thinking that can change your world

Rand Merchant Bank is an Authorised Financial Services Provider

- Batley, GA, McIntosh, AC and Brindley, J (1996) Phil. Trans. R. Soc. Lond. A, vol. 45, pp. 2199–2221.
- Bauwens, L (2006) Numerical simulation of hydrogen detonations and application in enclosed environments, Lecture presented at the 1<sup>st</sup> European Summer School on Hydrogen Safety, Belfast 2006.
- Bazhenova, TV, Bragin, MV, Golub, VV and Ivanov, MF (2006) Self-ignition of a fuel gas upon pulsed efflux into an oxidative medium, *Technical Physics Letters*, vol. 32(3), pp. 269–271.
- Becker, HA and Liang, D (1978) Visible Length of Vertical Free Turbulent Diffusion Flames. *Combustion and Flame*, vol. 32, pp. 115–137.
- Becker, Th and Ebert, F (1985) Vergleich zwischen Experiment und Theorie der Explosion grosser, freier Gaswolken. *Chem.-Ing.-Tech.*, vol. 57(1), pp. 42–5.
- Bedard-Tremblay, L, Fang, L, Melguizo-Gavilanes, J, Bauwens, L, Finstad, PHE, Cheng, Z and Tchouvelev, AV (2009) Simulation of detonation after an accidental hydrogen release in enclosed environments. *Int J Hydrogen Energy*, vol. 34(14), pp. 5894–5901.
- Bielert, U and Sichel, M (1998) Numerical Simulation of Premixed Combustion Processes in Closed Tubes. *Combustion and Flame*, vol. 114, pp. 397–419.
- Bilger, RW (1976) Turbulent Jet Diffusion Flames. *Prog. Energy Combustion Sci.*, vol. 1, pp. 87–109.
- Bilger, RW and Beck, RE (1975) Further experiments on turbulent jet diffusion flames. *Fifteenth International Symposium on Combustion*, pp. 541–552.
- Birch, AD, Brown, DR, Dodson, MG and Swaffield, F (1984) The structure and concentration decay of high pressure jets of natural gas. *Combustion Science and Technology*, vol. 36, pp. 249–261.
- Birch, AD, Hughes, DJ and Swaffield, F (1987) Velocity decay of high pressure jets. *Combustion Science and Technology*, vol. 52, pp. 161–171.
- Blake, TR and McDonald, M (1993) An examination of flame length data from vertical turbulent diffusion flames. *Combustion and Flame*, vol. 94, pp. 426–432.
- Blanchard, DC (1963) Electrification of the atmosphere by particles from bubbles in the sea. *Prog Oceanogr*, vol. 1, pp. 71–202.
- Blanchat, TK and Malliakos, A (1998) Performance testing of passive autocatalytic recombiners, NUREG/CR-6580, SAND97-2632.

- Blinov, VI and Khudyakov, GN (1957) Certain Laws Governing Diffusion Burning of Liquids. *Dokl. Acad. Nauk USSR*, vol. 113, pp. 1094–1098, in Russian (reviewed by Hottell HC, A Review of Blinov VI and Khudyakov GN, *Fire Res. Abst. Rev.*, 1959; vol. 1, pp. 41–43).
- Bond, J (1991) Sources of ignition: flammability characteristics of chemicals and products. Oxford: Butterworth Heinemann.
- Bradley, D (1997) Evolution of flame propagation in large diameter explosions. *Proceedings of the 2nd International Seminar on Fire and Explosion Hazard of Substances and Venting of Deflagrations*, Moscow, All-Russian Research Institute for Fire Protection.
- Bradley, D (1999) Instabilities and flame speeds in large-scale premixed gaseous explosions. *Phil. Trans. R. Soc. Lond. A*, vol. 357, pp. 3567–3581.
- Bradley, D and Mitcheson, A (1978) The venting of gaseous explosions in spherical vessels. *Combustion and Flame*, vol. 32, pp. 221–236 and 237–255.
- Bradley, D and Harper, CM (1994) The development of instabilities in laminar explosion flames. *Combustion and Flame*, vol. 99, pp. 562–572.
- Bradley, D, Cresswell, TM and Puttock, JS (2001) Flame acceleration due to flame-induced instabilities in large-scale explosions. *Combustion and Flame*, vol. 124, pp. 551–559.
- Bragin, M and Molkov, V (2009) Physics of spontaneous ignition of high-pressure hydrogen release and transition to jet fire, *Proceedings of the 3<sup>rd</sup> International Conference on Hydrogen Safety*, 16–18 September 2009, Ajaccio, France. (Bragin, MV and Molkov, VV (2011) Physics of spontaneous ignition of high-pressure hydrogen release and transition to jet fire, *International Journal of Hydrogen Energy*, vol. 36, pp. 2589–2596).
- Bragin, MV, Makarov, DV and Molkov, VV (2011) Pressure limit of hydrogen spontaneous ignition in a T-shaped channel. *Proceedings of the 4<sup>th</sup> International Conference on Hydrogen Safety*, 12–14 September 2011, San Francisco, USA.
- Brown, S and Shepherd, JE (2005) Numerical Solution Methods for Control Volume Explosions and ZND Structure. GALCIT Report, July 2005.
- Brown, S and Shepherd, JE (2006) Numerical solution methods for shock and detonation jump conditions. GALCIT Report FM 2006.006, [www.galcit.caltech.edu/~stbrowne/.\(2004\).](http://www.galcit.caltech.edu/~stbrowne/.(2004).)
- Bray, KNC (1996) The challenge of turbulent combustion. 26th Symp. (Int.) on Combustion, pp. 1–26.

Breitung, W, Dorofeev, SB, Efimenko, AA, Kochurko, AS, Redlinger, R and Sidorov, VP (1996) Large Scale confined hydrogen-air detonation experiments and their numerical simulation. *Proc. 20th ISSW*, Singapore: World Scientific Publishing Co 1996, pp. 1101–1106.

Breitung, W, Chan, CK, Dorofeev, SB, Eder, A, Gelfand, BE, Heitsch M, Klein, R, Malliakos, A, Shepherd, JE, Studer, E and Thibault, P (2000) Flame acceleration and deflagration-to-detonation transition in nuclear safety. State-of-the-art report. Nea/CSNI/R(2000)7. Paris: OECD Nuclear Energy Agency.

Brennan, S, Makarov, D and Molkov, V (2009) LES of high pressure hydrogen jet fire, *Journal of Loss Prevention in the Process Industries*, vol. 22 (3), pp. 353–359.

Brennan, S, Makarov, D and Molkov, V (2010) Dynamics of flammable hydrogen-air mixture formation in an enclosure with a single vent. *Proceedings of the 6<sup>th</sup> International Seminar on Fire and Explosion Hazards*, Leeds, April 2010.

Brennan, S and Molkov, V (2011) Safety assessment of unignited hydrogen discharge from onboard storage in garages with low levels of natural ventilation. *Proceedings of the 4<sup>th</sup> International Conference on Hydrogen Safety*, 12–14 September 2011, San Francisco, USA.

BRHS, Biennial Report on Hydrogen Safety (2009) The European Network of Excellence “Safety of Hydrogen as an Energy Carrier” (NoE HySafe). Available from: [www.hysafe.org](http://www.hysafe.org). [Accessed 28.12.11].



Discover the truth at [www.deloitte.ca/careers](http://www.deloitte.ca/careers)

**Deloitte.**

© Deloitte & Touche LLP and affiliated entities.



British Gas (1990) Review of the applicability of predictive methods to gas explosions in offshore modules. London: Department of Energy. Offshore Technology Report OTH 89 312, ISBN 0-11-413314-X, 175 p.

Bryan, JL (1986) Damageability of buildings, contents and personnel from exposure to fire. *Fire Safety Journal*, vol. 11, pp. 15–31.

BSI (1997) British Standard 7899-2:1997. Code of practice for assessment of hazard to life and health from fire. Guidance on methods for the quantification of hazards to life and health and estimation of time to incapacitation and death in fires. British Standards Institution.

BSI (2001) British standard BS7974:2001 “Application of fire safety engineering to the design of buildings – Code of Practice”. Published Document PD 7974–0:2002 (2002) Application of fire safety engineering principles to the design of buildings – Part 0: Guide to design framework and fire safety engineering procedures, British Standard Institution.

BSI (2004) Published Document PD 7974-6:2004. The application of fire safety engineering principles to fire safety design of buildings – Part 6: Human factors: Life safety strategies – Occupants evacuation, behaviour and condition (Sub-system 6). British Standards Institution.

Bulewicz, EM, et al.(1977) Zapłon mieszaniny wodorowo-tlenowej od gorącej powierzchni [The ignition of hydrogen-oxygen mixtures from a hot surface]. *Archiwum Termodynamiki i Spalania*, vol. 8(1), pp. 85–93.

Buncefield Investigation (2010) The Buncefield Major Incident Investigation Board. Available from: <http://www.buncefieldinvestigation.gov.uk/index.htm>. [Accessed 26.12.11].

Butler, MS, Moran, CW, Suderland, PB and Axelbaum, RL (2009) Limits for hydrogen leaks that can support stable flames. *International Journal of Hydrogen Energy*, vo. 34, pp. 5174–5182.

Butlin, RN (1975) A review of information on experiments concerning the venting of gas explosions in buildings, *Fire Research Note No. 1026*, 19 p.

Cain, TM (1997) Autoignition of hydrogen at high pressure. *Combust Flame*, vol. 111, pp. 124–32.

Canada Mortgage and Housing Corporation (2001) Air Infiltration from Attached Garages in Canadian Houses, Technical Series 01–122.

Canada Mortgage and Housing Corporation (2004) Garage Performance Testing”, Technical Series 04–108.

- Cant, RS, Dawes, WN and Savill, AM (2004) Advanced CFD and modelling of accidental explosions. *Annual Rev. Fluid Mech.*, vol. 36, pp. 97–119.
- Cariteau, B, Brinster, J and Tkatschenko I (2011) Experiments on the distribution of concentration due to buoyant gas low flow rate release in an enclosure. *Int J Hydrogen Energy*, vol. 36(3), pp. 2505–2512.
- Cassutt, L, Biron, D and Vonnegut B (1962) Electrostatic hazards associated with the transfer and storage of liquid hydrogen. *Adv Cryog Eng*, vol. 7, pp. 327–35.
- Catlin, CA (1991) Scale effects on the external combustion caused by venting of a confined explosions. *Combustion and Flame*, vol. 83, pp. 399–411.
- Catlin, CA, Manos, A and Tite, JP (1993) Mathematical modelling of confined explosions in empty cube and duct shaped enclosures: effects of scale and geometry. *Trans IChemE*, vol. 71 (B), pp. 89–100.
- Catlin, CA, Fairweather, M and Ibrahim, SS (1995) Prediction of turbulent, premixed flame propagation in explosion tubes. *Combustion and Flame*, vol. 102, pp. 115–128.
- Chaineaux, J, Mavrothalassitis, G and Pineau, J (1991) Modelization and validation of the discharge in air of a vessel pressurized by flammable gas, *Progress in Astronautics and Aeronautics*, vol. 134, pp. 104–137.
- Chakravarthy, VK and Menon, S (2001) Subgrid modelling of turbulent premixed flames in the flamelet regime. *Flow, Turbulence and Combustion*, vol. 65, pp. 133–161.
- Chapman, DL (1899) On the rate of explosion in gases. *Philosophical Magazine*, vol. 47, pp. 90–104.
- Chen, C and Rodi, W (1980) *Vertical turbulent buoyant jets – a review of experimental data*. Pergamon Press, Oxford. ISBN 0-08-024772-5.
- Cheng, TS, Chao, Y-C, Wu, C-Y, Li, Y-H, Nakamura, Y, Lee, K-Y et al. (2005) Experimental and numerical investigation of microscale hydrogen diffusion flames. *Proc Combust Inst*, vol. 30, pp. 2489–2497.
- Cheng, TS, Chen, CP, Chen, CS, Li, YH, Wu, CY and Chao, YC (2006) Characteristics of microjet methane diffusion flames. *Combustion Theory and Modeling*, vol. 10, pp. 861–881.
- Cheng, TS and Chiou, CR (1998) Experimental Investigation on the Characteristics of Turbulent Hydrogen Jet Flames. *Combustion Science and Technology*, vol. 136, pp. 81–94.

Chenoweth, DR (1983) *Gas-transfer analysis. Section H – Real gas results via the van der Waals equation of state and virial-expansion extensions of its limiting Abel-Noble form*. Livermore, CA, Sandia National Laboratories.

Ciccarelli, G and Dorofeev, S (2008) Flame acceleration and transition to detonation in ducts. *Progress in Energy and Combustion Science*, vol. 34, pp. 499–550.

Clavin, P (2004) *Theory of gaseous detonations*. American Institute of Physics.

College of the Desert (2001) *Hydrogen Fuel Cell Engines and Related Technologies, Module 1: Hydrogen Properties*. Energy Technology Training Center, College of the Desert. Available from: <http://www.hydrogensafety.info/resources/courseManual.asp>. [Accessed 29.12.11].

Commission Regulation (EC) No 79/2009 Of The European Parliament & Of The Council of 14 Jan. 2009 on type-approval of hydrogen-powered motor vehicles, & amending Dir.2007/46/EC, Official Journal of the European Union, 4.2.2009.

Commission Regulation (EU) No 406/2010 of 26 April 2010 implementing Regulation (EC) No 79/2009 of the European Parliament and of the Council on type-approval of hydrogen-powered motor vehicles. *Official Journal of the European Union*, vol. 53, 18 May 2010. [Accessed 01.04.12]  
<http://eur-lex.europa.eu/LexUriServ/LexUriServ.do?uri=OJ:L:2010:122:FULL:EN:PDF>.



**I WANT TO CHANGE DIRECTION,  
AND THE WORLD.**

**GOT-THE-ENERGY-TO-LEAD.COM**

We believe that energy suppliers should be renewable, too. We are therefore looking for enthusiastic new colleagues with plenty of ideas who want to join RWE in changing the world. Visit us online to find out what we are offering and how we are working together to ensure the energy of the future.

**RWE**  
The energy to lead

Cooper, MG, Fairweather, M and Tite, JP (1986) On the Mechanisms of Pressure Generation in Vented Explosions. *Combustion and Flame*, vol. 65, pp. 1–14.

Corrsin, S (1943) Investigation of flow in an axially symmetric heated jet of air. National Advisory Committee (NACA); Wartime Report W-94 (Advance Confidential Report 3L23).

Coward, HF and Jones, GW (1952) Limits of flammability of gases and vapors. *Bulletin 503, Bureau of Mines, 1952*. Available from: <http://www.galcit.caltech.edu/EDL/public/flammability/USBM-503.pdf>. [Accessed 25.12.11].

Crank, J (1975) *The Mathematics of Diffusion*, Second ed., Oxford University Press, USA.

Creitz, EC (1961) Inhibition of Diffusion Flames by Methyl Bromide and Trifluoromethyl-Bromide Applied to the Fuel and Oxygen Sides of the Reaction Zone. *Journal of Research for Applied Physics and Chemistry*, vol. 65A, pp. 389–396.

Croce, PA, Grosshandler, WL, Bukowski, RW and Gritzo, LA (2008) The International FORUM of Fire Research Directors: A position paper on performance-based design for fire code applications. *Fire Safety Journal*, vol. 43, pp. 234–236.

Cross, S and Jean, A (1987) *Electrostatics principles, problems and applications*. Bristol: Adam Hilger.

Cubbage, PA and Marshall, MR (1973) Pressures generated by explosions of gas-air mixtures in vented enclosures. *Inst. Gas Engineers Communication*, No. 926.

Cubbage, PA and Simmonds, WA (1955) An investigation of explosion reliefs for industrial drying ovens, I – Top reliefs in box ovens. *The Gas Council Research Communication* GC23, 46 p.

Dahoe, AE and Molkov, VV (2007) On the development of an international curriculum on hydrogen safety engineering and its implementation into educational programmes. *International Journal of Hydrogen Energy*, vol. 32, pp. 1113–1120.

Damkolher, G (1940) *Z. Elektroche.*, vol. 46, p. 601. English translation NACA TM 1112, 1947.

Deakin, G and Cooke, G (1994) Future codes for fire safety design, *Fire Safety Journal*, vol. 23, pp. 193–218.

Delichatsios, M (1993) Transition from momentum to buoyancy-controlled turbulent jet diffusion flames and flame height relationships. *Combustion and Flame*, vol. 92, pp. 349–364.

DNV Technica (2001) Human resistance against thermal effects, explosion effects, toxic effects and obscuration of vision.

Dorofeev, SB (2005) Evaluation of Safety Distances Related to Unconfined Hydrogen Explosions. Proceedings of the 1st International Conference on Hydrogen Safety, Pisa, September 2005.

Dorofeev, SB (2008) Flame acceleration and transition to detonation: a framework for estimating potential explosion hazards in hydrogen mixtures. *Lecture presented at the 3<sup>rd</sup> European Summer School on Hydrogen Safety*, Belfast, UK, 21–30 Jul 2008.

Dorofeev, SB, Bezmelnitsin, AV and Sidorov, VP (1995a) Transition to detonation in vented hydrogen-air explosions. *Combustion and Flame*, vol. 103, pp. 243–246.

Dorofeev, SB, Sidorov, VP and Dvoinishnikov, AE (1995b) Blast parameters from unconfined gaseous detonations *Proc. of 20-th Symp. (Int.) on Shock Waves* (Pasadena, CA, USA, July 1995) pp. 673–678.

Döring, W (1943) Über Detonationsvorgang in Gasen [On detonation processes in gases]. *Ann. Phys.*, vol. 43, pp. 421–436, ISSN 0003-4916.

Dragosavic, M (1973) Structural measures against natural-gas explosions in high-rise blocks of flats. *Heron*, vol. 19(4), pp. 1–51.

Drell, IL and Belles, FE (1958) Survey of hydrogen combustion properties, Report NACA 1383, National Advisory Committee for Aeronautics.

Dryer, FL, Chaos, M, Zhao, Z, Stein, JN, Alpert JY and Homer, CJ (2007) Spontaneous ignition of pressurized releases of hydrogen and natural gas into air. *Combustion Science and Technology*, vol. 179, pp. 663–694.

Dulov, VG and Luk'yanov, GA (1984) *Gasdynamics of the outflow processes*. Nauka, Novosibirsk.

Edwards, DH, Jones, AT and Phillips, DE (1975) The secondary shock wave in supported detonations with flow divergence. *J. Phys. D: Appl. Phys.*, vol. 8, pp. 891–901.

Efimenko, AA, Denkevits, AV, Dorofeev, SB and Breitung, W (1998) Numerical investigations of missiles acceleration by hydrogen explosion. *Archivum combustionis*, vol. 18(1–4), pp. 47–73.

Efimenko, A and Gavrikov, A (2007) Large scale hydrogen-air detonation experiments. The effect of ignition location and hydrogen concentration on loads. *Description of HySafe SBEP V13* ([www.hysafe.org](http://www.hysafe.org)).

Eichert, H (1992) *Gefährdungspotential bei einem verstaerkten Wasserstoffeinsatz*. Deutsche Forschungsanstalt fuer Luft- und Raumfahrt (DLR), Stuttgart, Germany.

Einstein, A (1905) On the motion of small particles suspended in liquids at rest required by molecular kinetic theory of heat. *Annalen der Physik*, vol. 17, pp. 549–560.

Electric Power Research Institute (1991) Modelled and measured infiltration: a detailed study of four electrically heated homes, prepared by ECOTOPE, Inc., Seattle, WA, EPRI Report No. CU-7327, May 1991.

Electric Power Research Institute (1996) Modelled & measured infiltration phase iii, a detailed case study of 3 homes, TR-106228, August 1996, USA.

Emmons, DD (1995) Vent flows. SFPE Handbook, ed. P.J. Di Nenno, 2nd Edition, Ch. 2–5. Society of Fire Protection Engineers, Boston, MA, USA.

EN14994:2007. Gas explosion venting protective systems.

ENDEMAT project (2008) Durability of constituent materials from type-4 compressed gaseous storage tanks, Contract No. ANR-08-PANH-007, ANR, France.

[bookboon.com](http://bookboon.com)

# Corporate eLibrary

See our Business Solutions for employee learning

Click here





- ENVIRONMENTAL GRAFFITI ALPHA (2010) *The Hindenburg Disaster in Pictures*. Available from: <http://www.environmentalgraffiti.com/anthropology-and-history/news-hindenbergdisaster-accident-waiting-happen>. [Accessed 24.12.11].
- Eto, K, Tsuboi, N and Hayashi, AK (2005) Numerical study on three-dimensional C-J detonation waves: detailed propagating mechanism and existence of OH radical. *Proceedings of the Combustion Institute*, vol. 30, pp. 1907–1913.
- European Industrial Gas Association (2007) IGC Doc 75/07/E, Determination of Safety Distances.
- Fairweather, M, Hargrave, GK, Ibrahim, SS and Walker, DG (1999) Studies of premixed flame propagation in explosion tubes. *Combustion and Flame*, vol. 116, pp. 504–518.
- Ferrara, G, Willacy, SK, Phylaktou, HN, Andrews, GE, Di Benedetto, A and Salzano, E (2005) Venting of premixed gas explosions with a relief pipe of the same area as the vent. *Proceedings of the European Combustion Meeting*.
- Fickett, W and Davis, WC (2000) *Detonation: Theory and Experiment*. Dover Publications Inc. Mineola, New York.
- Friedrich, A, Kotchourko, N, Stern, G and Vesper, A (2009) HYPER experiments on catastrophic hydrogen releases inside a fuel cell enclosure. *Proceedings of the Third International Conference on Hydrogen Safety*, Paper ID 118, 16–18 September 2009, Ajaccio, Corsica, France.
- Frolov, SM, Aksenov, VS and Shamshin, IO (2007) Reactive shock and detonation propagation in U-bend tubes. *Journal of Loss Prevention in the Process Industries*, vol. 20, pp. 501–508.
- Fryxell, B, Genin, F and Menon, S (2005) Hybrid large-eddy simulation of detonations in reactive mixtures. *20th ICDERS*, July 31 to August 5, 2005.
- Fujiwara, T and Fukiba, K (2001) Influence of Transport Processes on Two-Dimensional Structure of Detonation. In: *High-Speed Deflagration and Detonation*, Edited by GD Roy et al., Moscow 2001.
- Fureby, C (2005) A fractal flame-wrinkling large eddy simulation model for premixed turbulent combustion. *Proceedings of the Combustion Institute*, vol. 30, pp. 593–601.
- Gamezo, VN and Oran, ES (2005) Computing detonations. *20th ICDERS*, July 31–August 5 2005, Montreal, Canada.

- Gamezo, VN, Ogawa, T and Oran, ES (2007) Numerical simulations of flame propagation and DDT in obstructed channels filled with hydrogen-air mixture. *Proc. Comb. Inst.*, vol. 31, pp. 2463–2471.
- Gamezo, VN, Ogawa, T and Oran, ES (2008) Flame acceleration and DDT in channels with obstacles: Effect of obstacle spacing. *Combustion and Flame*, vol. 155(1-2), pp. 302–315.
- Gavrikov, AI, Efimenko, AA and Dorofeev, SB (2000) A model for detonation cell size prediction from chemical kinetics. *Combustion and Flame*, vol. 120, pp. 19–33.
- Ge, X and Sutton, WH (2006) Analysis and test of compressed hydrogen interface leakage by commercial stainless steel (NPT) fittings. *SAE International*, 35–47.
- Genin, F, Fryxell, B and Menon, S (2005) Simulation of Deonation Propagation in Turbulent Gas-Solid Reactive Mixtures. *41st AIAA/ASME/SAE/ASEE Joint Propulsion Conference and Exhibit*, July 10–13, 2005. Tuscon, AZ.
- Gibson, N and Harper, DJ (1988) Parameters for assessing electrostatic risk from non-conductors – a discussion. *J Electrostatics*, vol. 21, pp. 27–36.
- Golovichev, VI and Yasakov, VA (1972) Analysis of a reacting submerged hydrogen jet. *Combustion, Explosion, and Shock Waves*, vol. 8(1), pp. 41–56.
- Golub, VV (2010b) Private communication.
- Golub, VV, Baklanov, DI, Bazhenova, TV, Bragin, MV, Golovastov, SV, Ivanov, MF and Volodin, VV (2007) Hydrogen auto-ignition during accidental or technical opening of high pressure tank, *Journal of Loss Prevention in the Process Industries*, vol. 20(4–6), pp. 439–446.
- Golub, VV, Baklanov, DI, Golovastov, SV, Ivanov, MF, Laskin, IN, Saveliev, AS, Semin, NV and Volodin, VV (2008) Mechanisms of high-pressure hydrogen gas self-ignition in tubes, *Journal of Loss Prevention in the Process Industries*, vol. 21(2), pp. 185–198.
- Golub, VV, Volodin, VV, Baklanov, DI, Golovastov, SV and Lenkevich, DA (2010a) Experimental investigation of hydrogen ignition at the discharge into channel filled with air, *In: Physics of Extreme States of Matter*, ISBN 978-5-901675-96-0, Chernogolovka, 2010, pp. 110–113.
- Goodwin, D (2005) CANTERA – Object-oriented software for reacting flows. Technical report, California Institute of Technology.

Gorev, VA (1982) Comparison of the air explosion waves from different sources. *Combustion, Explosion and Shock Waves*, vol. 8(1), pp. 77. See also Bystrov, SA and Gorev, VA (1982) Interaction of explosion waves from a spherical deflagration with an obstacle. *Combustion, Explosion and Shock Waves*, vol. 20(1), pp. 113–116.

Gorev, VA, Miroshnikov, SN and Troshin, YaK (1980) Pressure waves from gaseous explosions. In: *Detonation, Proceedings of the VI All-Union Symposium on Combustion and Explosions*, (23–26 September 1980, Almaty), Chernogolovka, Institute of Chemical Physics of Academy of Sciences of USSR, 1980, pp. 110–113.

Gostintsev, YuA, Istratov, AG and Shulenin, YV (1988) Self-similar propagation of a free turbulent flame in mixed gas mixtures. *Combustion, Explosion and Shock Waves*, vol. 24(5), pp. 63–70.

Gostintsev, YuA, Istratov, AG, Kidin, NI and Fortov, VE (1999) *High Temperature Thermophysics (Teplofizika Vysokih Temperatur)*, vol. 37(4), pp. 633–637 (in Russian).

Gouldin, FC (1987) An application of fractals to modelling premixed turbulent flames. *Combustion and Flame*, vol. 68, pp. 249–266.



**Brain power**

By 2020, wind could provide one-tenth of our planet's electricity needs. Already today, SKF's innovative know-how is crucial to running a large proportion of the world's wind turbines.

Up to 25 % of the generating costs relate to maintenance. These can be reduced dramatically thanks to our systems for on-line condition monitoring and automatic lubrication. We help make it more economical to create cleaner, cheaper energy out of thin air.

By sharing our experience, expertise, and creativity, industries can boost performance beyond expectations.

Therefore we need the best employees who can meet this challenge!

**The Power of Knowledge Engineering**

Plug into The Power of Knowledge Engineering.  
Visit us at [www.skf.com/knowledge](http://www.skf.com/knowledge)

**SKF**

- Grigorash, A, Eber, R and Molkov, V (2004) Theoretical Model Of Vented Gaseous Deflagrations In Enclosures With Inertial Vent Covers. *Proceedings of the 4th International Seminar on Fire and Explosion Hazards*, 8-12 September 2003, Londonderry, pp. 445–456.
- Groethe, M, Merilo, E, Colton, J, Chiba, S, Sato, Y and Iwabuchi, H (2005) Large-scale hydrogen deflagrations and detonations, *Proceedings of the 1<sup>st</sup> International Conference on Hydrogen Safety*, 8–10 September 2005, Pisa, Paper 120105.
- Groff, EG (1982) The cellular nature of confined spherical propane-air flames. *Combustion and Flame*, vol. 48, pp. 51–62.
- Gülder, ÖL (1990) Turbulent premixed combustion modelling using fractal geometry. *Proc. Comb. Instit.*, vol. 23, pp. 835–842.
- Gülder, ÖL, Smallwood, GJ, Wong, R., Snelling, DR, Smith, R, Deschamps, BM and Sautet, J-C (2000) Flame front surface characteristics in turbulent premixed propane/air combustion. *Combustion and Flame*, vol. 120, pp. 407–416.
- Gutheil, E, Balakrishnan, G and Williams, FA (1993) Structure and extinction of hydrogen-air diffusion flames, *In: Reduced kinetic mechanisms for applications in combustion systems* (Peters, N. and Rogg, B. Eds.), Springer-Verlag, New York, p. 179.
- Haberman, WL and John, JEA (1988) *Introduction to Fluid Mechanics*, 3<sup>rd</sup> Edition. Englewood Cliffs, NJ, Prentice Hall.
- Hadjisophocleous, GV and Benichou, N (1999) Performance criteria used in fire safety design. *Automation in Construction*, vol. 8, pp. 489–501.
- Harrison, AJ and Eyre, JA (1987) External explosions' as a result of explosion venting. *Combustion Science and Technology*, vol. 52, pp. 91–106.
- Hawkes, ER and Cant, RS (1999) Physical and numerical realizability requirements for flame surface density approaches to large-eddy simulation of premixed turbulent combustion. *Combustion Theory and Modelling*, vol. 5, pp. 699–720.
- Hawkes, ER and Cant, RS (2001) Implication of a flame surface density approach to large eddy simulation of premixed turbulent combustion. *Combustion and Flame*, vol. 126, pp. 1617.

Hawthorne, WR, Weddell, DS and Hottel HC (1949) Mixing and combustion in turbulent gas jets, *Third International Symposium on Combustion, Flame and Explosion Phenomena*, pp. 266–288, Baltimore, USA.

Health and Safety Executive (1975) The Flixborough Disaster: Report of the Court of Inquiry, HMSO, ISBN 0113610750, 1975.

Heidari, A, Ferraris, S, Wen JX and Tam, VHY (2009) Numerical simulation of large scale hydrogen detonation. Proceedings of the 3rd International Conference on Hydrogen Safety, 16-18 September 2009, Corsica, France.

Henrie, JO and Postma, A K (1983) Analysis of the Three Mile Island (TMI-2) hydrogen burn. In: *Thermalhydraulics of nuclear reactors, vol. II*. LaGrange Park, IL: American Nuclear Society (ASME), pp. 1157–1170.

Heskestad, G (1999) Turbulent Jet Diffusion Flames: Consolidation of Flame Height Data. *Combustion and Flame*, vol. 118, pp. 51–60.

Hjertager, BH (2002) Simulation of transient compressible turbulent reactive flows. *Combustion Science and Technology*, vol. 27, pp. 159–170.

Höchst, S and Leuckel, W (1998) On the effect of venting large vessels with mass inert panels. *Journal of Loss Prevention in the Process Industries*, vol. 11, pp. 89–97.

Hottel, H and Hawthorne, WR (1949) Diffusion in laminar flame jets. *Third International Symposium on Combustion, Flame and Explosion Phenomena*. Baltimore: Williams and Wilkins Co; pp. 254–266.

Houf, W and Schefer, R (2008) Analytical and experimental investigation of small-scale unintended releases of hydrogen, *International Journal of Hydrogen Energy*, vol. 33(4), pp. 1435–1444.

HYPER (2008) FP6 STREP project “Installation Permitting Guidance for Hydrogen and Fuel Cells Stationary Applications”. *Deliverable 4.3 Releases, Fires and Explosions*. WP4 Final Report. <http://www.hyperproject.eu/> [Accessed 26.0512].

IEC 61779-1 (1998): Electrical Apparatus for the Detection and Measurement of Flammable Gases - Part 1: General Requirements and Test Methods. Standard IEC 61779-4: Performance requirements for group II apparatus indicating up to a volume fraction of 100% lower explosive limit. International Electrotechnical Commission (IEC).

IEC (2002) Published Technical Report. Electrostatics – code of practice for the avoidance of hazards due to static electricity, TR 50404.

Imamura, T, Hamada, S, Mogi, T, Wada, Y, Horiguchi, S, Miyake, A and Ogawa, T (2008) Experimental investigation on the thermal properties of hydrogen jet flame and hot currents in the downstream region. *International Journal of Hydrogen Energy*, vol. 33, pp. 3426–3435.

International fire code (2006). International Code Council.

InsHyde project “Allowable hydrogen permeation rate for automotive applications”, Deliverable D74 (NoE HySafe), June 2009. Accessible from: <http://www.hysafe.org/download/1855/HySafe%20D74%20Permeation%20Rev7%20Final%20Corr%201.pdf>. [Accessed 14.04.12].

Ishii, R, Fujimoto, H, Hatta, N and Umeda, Y (1999) Experimental and numerical analysis of circular pulse jets. *J. Fluid Mech.*, vol. 392, pp. 129–153.

ISO/IEC Guide 73:2002 Risk management – Vocabulary – Guidelines for use in standard.

ISO/TR 15916:2004. Basic considerations for the safety of hydrogen systems. International Organization for Standardization. ISO Technical Committee 197 Hydrogen Technologies. International Organization for Standardization, Geneva.

ISO 26142:2010. Hydrogen detection apparatus – Stationary applications. ISO Technical Committee 197 Hydrogen Technologies. International Organization for Standardization.

With us you can  
shape the future.  
Every single day.

For more information go to:  
[www.eon-career.com](http://www.eon-career.com)

Your energy shapes the future.

**e-on**



- Jansen, KE (1997) Large-eddy simulation using unstructured grids. In: *Advances in DNS/LES, Proceedings of the first AFOSR International Conference on DNS/LES*, Louisiana Tech University, USA, p. 117.
- Jeary, B (2001) Fast Filling Of Compressed Hydrogen Fuel Storage Containers”, Proc. 11th Canadian Hydrogen Conf., Victoria, Canada, 17–20 June 2001.
- Jouguet, JCE (1905-1906) On the propagation of chemical reactions in gases. *Journal des Mathématiques Pures et Appliquées*, vol. 1, pp. 347–425, 1905; continued vol. 2, pp. 5–85, 1906.
- Kalghatgi, GT (1981) Blow-out stability of gaseous jet diffusion flames. part I: in still air. *Combustion Science and Technology*, vol. 26(5), pp. 233–239.
- Kalghatgi, GT (1984) Lift-off heights and visible lengths of vertical turbulent jet diffusion flames in still air. *Combustion Science and Technology*, vol. 41, pp. 17–29.
- Kao, Chen-Shan and Duh, Yil-Shing (2002) Accident investigation of an ABS plant. *Journal of Loss Prevention in the Process Industries*, vol. 15, pp. 223–232.
- Karlovitz, B, Denniston, DW Jr and Wells, FE (1951) Investigation of turbulent flames. *The Journal of Chemical Physics*, vol. 19(5), pp. 541–547.
- Kaufmann, A, Nicoud, F and Poinso, T (2002) Flow forcing techniques for numerical simulation of combustion instabilities. *Combustion and Flame*, vol. 131(4), pp. 371–385.
- Kee, RJ et al. (2000) CHEMKIN Collection. Reaction Design, Inc., San Diego.
- Korinko, PS, Scogin, JH and Clarck, EA (2001) Development of Aluminide Coatings for Hydrogen Isotope Permeation Resistance. Tritium, Tsukaba, Japan.
- Korotkikh, NI and Baratov, AN (1978) Vent area calculation for enclosures in case of internal gaseous deflagration. Flammability of Substances and Chemical Fire Extinguishing Agents, Transactions of VNIPO, issue 5, pp. 3–15 (in Russian).
- Kumar, RK, Tamm, H and Harrison, WC (1983) Combustion of hydrogen at high concentration including the effect of obstacles. *Combustion Science and Technology*, vol. 35, pp. 175–186.
- Kumar, RK, Dewit, WA and Greig, DR (1989) Vented explosions of hydrogen-air mixtures in a large volume. *Combustion Science and Technology*, vol. 66, pp. 251–266.

- Kumar, RK and Bowles, EM (1990) Flame acceleration in hydrogen/air mixtures in a vertical cylinder filled with obstacles. Proceedings of the 2<sup>nd</sup> Int. Conf. on Containment Design and Operation, Toronto, Canadian Nuclear Society, 14–17 October 1990.
- Kuznetsov, M (2006) FZK. Hydrogen distribution tests in free turbulent jet, SBEP V4. Report No.: SBEP V4.
- Kuznetsov, M (2010) Private communication.
- Kyushu University (2007) Accident of hydrogen stand at Kyushu University investigation committee, “Report on the accident of hydrogen stand at Kyushu University 3rd edition”. Available from: <http://www.kyushu-u.ac.jp/news/hydrogen/hydrogensummary0330.pdf>; <http://www.nsc.go.jp/senmon/shidai/kasai/kasai004/ssiry04-1.pdf>. [Accessed 01.01.12, in Japanese].
- LaChance, JL (2010) Progress in risk assessment methodologies for emerging hydrogen applications. Presented at the Sixth International Short Course and Advanced Research Workshop “Progress in Hydrogen Safety - Regulations, codes, and standards”, 25–29 January 2010, Belfast, Northern Ireland, UK.
- LaChance, J, Tchouvelev, A and Ohi, J (2009) Risk-informed process and tools for permitting hydrogen fueling stations. *International Journal of Hydrogen Energy*, vol. 34, pp. 5855–5861.
- Lamoureux, N, Djebaili-Chaumeix, N and Paillard, C-E (2003) Laminar flame velocity determination for H<sub>2</sub>-air-He-CO<sub>2</sub> mixtures using the spherical bomb. *Experimental Thermal and Fluid Science*, vol. 27, pp. 385–393.
- Landau, LD and Lifshits, EM (1988) *Hydrodynamics*, Nauka, Moscow, p. 733.
- Laskey, KJ, Oran, ES and Boris, JP (1988) The Gradient Method for Interface Tracking. Report, Naval Research Laboratory, 1988.
- Lautkaski, R (1997) Understanding vented gas explosions. Technical Research Centre of Finland, *VTT Research Notes 1812*, 129 p.
- Lavoie, GA and Schlader, AF (1974) A scaling study of NO formation in turbulent diffusion flames of hydrogen burning in air. *Combustion Science and Technology*, vol. 8, pp. 215–224.
- Lecoustre, VR, Sunderland, PB, Chao, BH and Axelbaum, RL (2010) Extremely weak hydrogen flames, *Combustion and Flame*, vo. 157, pp. 2209–2210.

Lee, JHS (1982) Hydrogen air detonations. *2nd International workshop on the impact of hydrogen on water reactor safety*. Albuquerque, New Mexico.

Lee, JHS (1984) Dynamic Parameters of Gaseous Detonations. *Ann. Rev. Fluid. Mech.*, vol. 16, pp. 311–336.

Lee, JHS (2008a) Explosion primer – definitions of basic combustion parameters, Lecture presented at the 3rd European Summer School on Hydrogen Safety, Belfast, 21–30 July 2008.

Lee, JHS (2008b) The detonation phenomenon, Cambridge.

Lee, JHS and Guirao, CM (1982) Pressure development in closed and vented vessels. *Plant/Operations Progress*, vol. 1(2), pp. 75–85.

Lee, ID, Smith, OI and Karagozian, AR (2003) Hydrogen and helium leak rates from micromachined orifices. *AIAA Journal*, vol. 41, pp. 457–463.

Lee, BJ and Jeung, I-S (2009) Numerical study of spontaneous ignition of pressurized hydrogen release by the failure of a rupture disk into a tube. *International Journal of Hydrogen Energy*, vol. 34, pp. 8763–8769.

Lee, JHS, Knystautas, R and Yoshikawa, N (1978) Photochemical Initiation and Gaseous Detonations. *Acta Astronautica*, vol. 5, pp. 971–972.

be > your degree

Bring your talent and passion to a global organization at the forefront of business, technology and innovation. Discover how great you can be.

Visit [accenture.com/bookboon](http://accenture.com/bookboon)

Be greater than.  
consulting | technology | outsourcing

accenture  
High performance. Delivered.

© 2013 Accenture  
All rights reserved.

- Libby, PA and Williams, FA (Eds.) (1993) *Turbulent Reacting Flows*, Academic Press, New York, 646 p., 1993.
- Lind, CD (1975) What Causes Unconfined Vapour Cloud Explosions? *Loss Prevention*, vol. 9, pp. 101–105.
- Liou, MS (1996) A sequel to AUSM: AUSM+. *Journal of Computational Physics*, vol. 129, pp. 364–382.
- Lipatnikov, AN (2007) Turbulent combustion of hydrogen-air mixtures. *Lecture presented at the 2nd European Summer School on Hydrogen Safety*, Belfast, UK, 30 Jul – 8 Aug 2007.
- Lipatnikov, AN and Chomiak, J (2005) Molecular transport effects on turbulent flame propagation and structure. *Progress in Energy and Combustion Science*, vol. 31, pp. 1–73.
- Liu, F, McIntosh, AC and Brindley, J (1993) A numerical investigation of Rayleigh-Taylor effects in pressure wave-premixed flame interactions. *Combust. Sci. Technol.*, vol. 91, pp. 373–386.
- Liu, Y-F, Tsuboi, N, Sato, H, Higashino, F, Hayashi, AK and Gakuin, A (2005) Direct numerical simulation of hydrogen fuel jetting from high pressure tank, *Proceedings of the 20th International Colloquium on the Dynamics of Explosions and Reactive Systems*, 31 July–5 August 2005, Montreal, Canada.
- Magnussen, BF (1981) On the structure of turbulence and a generalized eddy dissipation concept for chemical reactions in turbulent flow. *Proceedings of the 19th American Institute for Aeronautics and Astronautics Aerospace Science Meeting*, 12–15 January 1981, St. Louis.
- Mair G, Novak, P and Anders, S (2007) Methods to describe the impact of special effects on lifetime and reliability, Deliverable D SA6, EC Project StorHy (SPSAR), Revision1, BAM, Germany, May 2007.
- Makarov, D and Molkov, V (2004) Large Eddy Simulation of Gaseous Explosion Dynamics in an Unvented Vessel. *Combustion, Explosion and Shock Waves*, vol. 40(2), pp. 136–144.
- Makarov, D, Molkov, V and Gostintsev, Yu (2007a) Comparison between RNG and fractal combustion models for LES of unconfined explosions. *Combustion Science and Technology*, vol. 179(1–2), pp. 401–416.
- Makarov, D, Molkov, V, Zbikowski, M and Schneider H (2007b) A model for numerical simulations of large-scale deflagrations and detonations. *Proceedings of the 21st International Colloquium on the Dynamics of Explosions and Reactive Systems*, ENSMA, Futuroscope, Poitiers, France, 23–27 July 2007, 4 p.
- Makarov, D and Molkov, V (2013) Hydrogen plane jets. *International Journal of Hydrogen Energy*, (submitted for publication).

- Manton, J and Milliken, BB (1956) Study of pressure dependence of burning velocity by the spherical vessel method. *Proceedings of the Gas Dynamics Symposium on Aerothermochemistry*, Illinois. Northwestern University, pp. 151–157.
- Marshall, M (1983) The effect of ventilation on the accumulation and dispersal of hazardous gases, 4th Int. Symp. on Loss Prevention and Safety Promotion in the Process Industries, Symp. Series No. 82, Vol. 3 Chemical Process Hazards, The Institution of Chemical Engineers, UK.
- Matta, LM, Neumeier, Y, Lemon, B and Zinn, BT (2002) Characteristics of microscale diffusion flames. *Proceedings of the Combustion Institute*, vol. 29, pp. 933–938.
- Medvedev, SP, Polenov, AN, Khomik, SV and Gelfand, BE (1994) 25th Symp. (Int.) on Combustion, The Combustion Institute, vol. 73–78.
- Metghalchi, M and Keck, JC (1982), Burning velocities of mixtures of air with methanol, isooctane and indolene at high pressure and temperature. *Combustion and Flame*, vol. 48, pp. 191–210.
- Metzler, AJ (1952) Minimum ignition energies of six pure hydrocarbon fuels. NACA Report RM E52 F27.
- Michels, A, de Graaf, W and Wolkers GJ (1963) Thermodynamic properties of hydrogen and deuterium between -175°C and 150°C and at pressures up to 2500 atmospheres (Part A). *Appl Sci Res*, vol. 12, pp. 9–32.
- Miles S (2007) Summary of Garage Review for HySafe Internal Project InsHyde, HySafe, Issue 2, April 2007.
- Millet, P, Ranjbari, A, de Guglielmo, F, Grigoriev, SA and Etiévant, C (2011) Cell failure mechanism in PEM water electrolyzers. *Proceedings of the Fourth International Conference on Hydrogen Safety*, paper ID 254, 12–14 September 2011, San Francisco, USA.
- Mitlitsky, F, Weisberg, AH and Blake, M (1999) Vehicular hydrogen storage using lightweight tanks (regenerative fuel cell systems), prepared for U.S. DOE Hydrogen program 1999
- Annual review meeting, CO, USA, 4–6 May 1999.
- Mitlitsky, F, Weisberg, AH and Blake, M (2000) Vehicular hydrogen storage using lightweight tanks, Lawrence Livermore National Laboratory, Proceedings of the 2000 U.S. DOE Hydrogen program review, NREL/CP-570e28890, USA.
- Mogi, T, Nishida, H and Horiguchi, S (2005) Flame Characteristics of high-pressure hydrogen gas jet. *Proceedings of the 1st International Conference on Hydrogen Safety*, Pisa, September 2005.



Mogi, T, Kim, D, Shiina, H and Horiguchi, S (2008) Self-ignition and explosion during discharge of high-pressure hydrogen, *Journal of Loss Prevention in the Process Industries*, vol. 21(2), pp. 199–204.

Mogi, T and Horiguchi, S (2009) Experimental study on the hazards of high-pressure hydrogen jet diffusion flames. *Journal of Loss Prevention in the Process Industries*, vol. 22, pp. 45–51.

Molkov, VV (1995) Theoretical generalization of international experimental data on vented explosion dynamics, *Proceedings of the First International Seminar on Fire and Explosion Hazards*, Moscow, VNIIPO, pp. 166–181.

Molkov, VV (1997) *Venting of gaseous deflagrations*. DSc thesis, VNIIPO, Moscow, (in Russian).

Molkov, VV (1999a) Explosion safety engineering: NFPA 68 and improved vent sizing technology. In: *Interflam '99, 8th International Fire Science Conference*, Edinburgh Conference Centre, Scotland, UK, 29th June–1st July 1999, Interscience Communications, pp. 1129–1134.

Molkov, VV (1999b) Explosions in buildings: modelling and interpretation of real accidents. *Fire Safety Journal*, vol. 33, pp. 45–56.



"I studied English for 16 years but...  
...I finally learned to speak it in just six lessons"

Jane, Chinese architect

ENGLISH OUT THERE

Click to hear me talking before and after my unique course download



- Molkov, VV (2001a) Unified correlations for vent sizing of enclosures at atmospheric and elevated pressures. *Journal of Loss Prevention in the Process Industries*, vol. 14, pp. 567–574.
- Molkov, VV (2001b) Turbulence generated during vented gaseous deflagrations and scaling issue in explosion protection. *Proceedings of the IChemE Symposium “Hazards XVI: Analysing the past, planning the future”*, Manchester, UK, UMIST, 6–8 November, 2001, Symposium Series No. 148, ISBN 0-85295-441-7, pp. 279–292.
- Molkov, VV (2002) Accidental gaseous deflagrations: modelling, scaling and mitigation. *Journal de Physique IV*, vol. 12, pp. 7/19–7/30.
- Molkov, VV (2008) Preface to Special Issue on Hydrogen Safety, *Journal of Loss Prevention in the Process Industries*, vol. 21(2), pp. 129–130.
- Molkov, VV (2009a) Hydrogen non-reacting and reacting jets in stagnant air: overview and state-of-the-art. *Proceedings of the 10th International Conference on Fluid Control, Measurements, and Visualization (FLUCOM 2009)*, 17–21 August 2009, Moscow, Russia.
- Molkov, VV (2009b) Fundamentals of hydrogen safety engineering. *Proceedings of the 4th European Summer School on Hydrogen Safety*. 7–16 September 2009, Corsica, France.
- Molkov, VV (2009c) A multi-phenomena turbulent burning velocity model for large eddy simulation of premixed combustion. In: *Nonequilibrium Phenomena: Plasma, Combustion, Atmosphere*. Eds. Roy GD, Frolov SM and Starik AM, Torus Press, Moscow, pp. 315–323.
- Molkov, VV and Nekrasov, VP (1981) Dynamics of gaseous combustion in a vented constant volume vessel. *Combustion, Explosion and Shock Waves*, vol. 17(4), pp. 363–370.
- Molkov, VV, Nekrasov, VP, Baratov, AN and Lesnyak, SA (1984) Turbulent Gas Combustion in a Vented Vessel. *Combustion, Explosion and Shock Waves*, vol. 20, pp. 149–153.
- Molkov, VV, Baratov, AN and Korolchenko, AY (1993) Dynamics of gas explosions in vented vessels: a critical review and progress. *Progress in Astronautics and Aeronautics*, vol. 154 “Dynamics aspects of Explosion Phenomena”, Proceedings of the 13th International Colloquium on Dynamics of Explosions and Reactive Systems, 28 July–2 August 1991, Nagoya (Japan), 1993, pp. 117–131.
- Molkov, VV, Korolchenko, AY and Alexandrov, SV (1997a) Venting of deflagrations in buildings and equipment: universal correlation. *Proceedings of the Fifth International Symposium on Fire Safety Science*, 3–7 March 1997, Melbourne, Australia, pp. 1249–1260.

- Molkov, VV, Agafonov, VV and Alexandrov, SV (1997b) Deflagration in a vented vessel with internal obstacles. *Combustion, Explosion and Shock Waves*, vol. 33(4), pp. 418–424.
- Molkov, VV, Dobashi, R, Suzuki, M and Hirano, T (1999) Modelling of Vented Hydrogen-Air Deflagrations and Correlations for Vent Sizing. *Journal of Loss Prevention in the Process Industries*, vol. 12, pp. 147–156.
- Molkov, VV, Dobashi, R, Suzuki, M and Hirano, T (2000) Venting of deflagrations: hydrocarbon-air and hydrogen-air systems. *Journal of Loss Prevention in the Process Industries*, vol. 13(3-5), pp. 397–409.
- Molkov, VV, Eber, RM and Grigorash AV (2003) Vented Gaseous Deflagrations: Modelling of Translating Inertial Vent Covers. *Journal of Loss Prevention in the Process Industries*, vol. 16(5), pp. 395–402.
- Molkov, V, Grigorash, A, Eber, R, Tamanini, F and Dobashi, R (2004a) Vented Gaseous Deflagrations with Inertial Vent Covers: State-of-the-Art and Progress. *Process Safety Progress*, vol. 23(1), pp. 29–36.
- Molkov, VV, Grigorash, AV, Eber, RM and Makarov, DV (2004b) Vented Gaseous Deflagrations: Modelling of Hinged Inertial Vent Covers. *Journal of Hazardous Materials*, vol. 116, pp. 1–10.
- Molkov, V, Makarov, D and Grigorash, A (2004c) Cellular Structure of Explosion Flames: Modelling and Large Eddy Simulation. *Combustion Science and Technology*, vol. 176(5–6), pp. 851–885.
- Molkov, VV, Grigorash, AV and Eber, RM (2005) Vented gaseous deflagrations: Modelling of spring-loaded inertial vent covers. *Fire Safety Journal*, vol. 40, pp. 307–319.
- Molkov, V, Makarov, D and Schneider, H (2006a) LES modelling of an unconfined large-scale hydrogen-air deflagration, *Journal of Physics D: Applied Physics*, vol. 39, pp. 4366–4376.
- Molkov, V, Makarov, D and Puttock, J (2006b) The nature and large eddy simulation of coherent deflagrations in a vented enclosure-atmosphere system. *Journal of Loss Prevention in the Process Industries*, vol. 19(2–3), pp. 121–129.
- Molkov, VV and Makarov, DV (2006c) Rethinking the physics of a large-scale vented explosion and its mitigation. *Process Safety and Environmental Protection* (Trans IChemE, Part B), vol. 84(B1), pp. 33–39.
- Molkov, VV, Makarov, DV and Schneider, H (2007a) Hydrogen-air deflagrations in open atmosphere: Large eddy simulation analysis of experimental data. *International Journal of Hydrogen Energy*, vol. 32(13), pp. 2198–2205.

Molkov, VV, Makarov, DV, Verbecke, F and Schneider, H (2007b) Supra LES of accelerating premixed hydrogen-air flames in the open atmosphere. Proceedings of the 3rd International Symposium on Non-Equilibrium Processes, Plasma, Combustion and Atmospheric Phenomena (NEPCAP), Sochi, Russia, June 2007.

Molkov, V, Verbecke, F and Saffers, JB (2008a) Venting of uniform hydrogen-air deflagrations in enclosures and tunnels: vent sizing and prediction of overpressure. Proceedings of the 7th International Symposium on Hazards Prevention and Mitigation of Industrial Explosions, St. Petersburg, Russia, July 7–11, vol. II, pp. 158–167.

Molkov, V, Verbecke, F and Makarov, D (2008b) LES of hydrogen-air deflagrations in a 78.5 m tunnel. *Combustion Science and Technology*, vol. 180(5), pp. 796–808.

Molkov, V and Bragin, M (2009) High-pressure hydrogen leak through a narrow channel. In: *Nonequilibrium Phenomena: Plasma, Combustion, Atmosphere*; Torus Press: Moscow, pp. 332–338.

Molkov, V, Makarov, D and Bragin, M (2009) Physics and modelling of under-expanded jets and hydrogen dispersion in atmosphere, in Fortov VE, et al. (eds) *Physics of extreme state of matter 2009*. Chernogolovka, Russia, pp. 143–145. ISBN 978-5-901675-89-2.



**DUKE**  
THE FUQUA  
SCHOOL  
OF BUSINESS

**BUSINESS HAPPENS**

**HERE.**

[www.fuqua.duke.edu/globalmba](http://www.fuqua.duke.edu/globalmba)

**Learn More >**

Molkov, V, Bragin M, Brennan S, Makarov, D and Saffers, J-B (2010) Hydrogen Safety Engineering: Overview of Recent Progress and Unresolved Issues, *Proceedings of the International Congress on Combustion and Fire Dynamics*, 20–23 October 2010, Santander, Spain.

Molkov, V and Saffers, J-B (2011) The correlation for non-premixed hydrogen jet flame length in still air. *Proceedings of the 10th International Symposium on Fire Safety Science*, June 2011, University of Maryland, USA.

Molkov, V and Saffers J-B (2012) Introduction to hydrogen safety engineering. *International Journal of Hydrogen Energy* (accepted for publication).

Moorehouse, J, Williams, A and Maddison TE (1974) An investigation of the minimum ignition energies of some C1 to C7 hydrocarbons. *Combust Flame*, vol. 23, pp. 203–213.

Moran, MJ and Shapiro, HN (2006) *Fundamentals of Engineering Thermodynamics*. John Wiley & Sons, New York, 5th edition.

Murayama, M and Takeno, T (1988) Fractal-like character of flamelets in turbulent premixed combustion. Twenty-Second Symposium (International) on Combustion, The Combustion Institute, pp. 551–559.

NASA (1997) Safety Standard for Hydrogen and Hydrogen Systems. Guidelines for hydrogen system design, materials selection, operations, storage, and transportation. Technical Report NSS 1740.16, Office of Safety and Mission Assurance, Washington. Available from: <http://www.hq.nasa.gov/office/codeq/doctree/canceled/871916.pdf>. NSS 1740.16 was cancelled on July 25 2005. [Accessed 26.12.11].

Nettleton, MA (1987) *Gaseous Detonations: their nature, effects and control*. Chapman and Hall Ltd. New York.

Neumann, von J (1942) Theory of Detonation Waves. In: John von Neumann, collected works. 1942, vol. 6, ed. A. J. Taub. Macmillan: New York.

NFPA 55 (2010) Standard for the Storage, use, and Handling of Compressed Gases and Cryogenic Fluids in Portable and Stationary Containers, Cylinders, and Tanks. National Fire Protection Association, Quincy, MA, 2010.

NFPA 68 (2007) Guide for venting of deflagrations, NFPA, Quincy, MA, US.

Ng, HD, Yiguang, J and Lee, JHS (2007) Assessment of detonation hazards in high-pressure hydrogen storage from chemical sensitivity analysis. *International Journal of Hydrogen Energy*, vol. 32(1), pp. 93–99.

- North, GL and Santavicca DA (1990) the fractal nature of premixed turbulent flames. *Combustion Science and Technology*, vol. 72, pp. 215–232.
- Novak, P (2009) Private communication, MagnaSteyr.
- Okabayashi, K, Nonaka, T, Sakata, N, Takeno, K, Hirashima, H and Chitose, K (2005) Characteristics of dispersion for leakage of high-pressurized hydrogen gas, *Japan Society for Safety Engineering*, vol. 44 (6), pp. 391–397.
- Okabayashi, K, Hirashima, H, Nonaka, T, Takeno, K, Chitose, K and Hashiguchi, K (2007) Introduction of Technology for Assessment on Hydrogen Safety. *Mitsubishi Heavy Industries Ltd. Technical Review*, vol. 44(1), pp. 1–3.
- Oran, ES (1999) The Structure of Propagating Detonations. In: *Gaseous and Heterogeneous Detonations Science to Applications*, Edited by Roy GD et al., ENAS Publishers, Moscow.
- Oran, ES and Boris, JP (1987) *Numerical simulation of reactive flow*. Elsevier.
- Oran, E, Gamezo, V and Ogawa, T (2008) Flame acceleration and DDT in channels with obstacles. Lecture presented at the 3rd European Summer School on Hydrogen Safety, Belfast 21–30 July 2008.
- Pan, L, Fisher, SA, Jayanti, S and Hewitt, GF (1995) Measurement and prediction of temperature rise following sudden compression in a high-pressure pipeline. *Trans Int Chem Eng*, vol. 73 (Part B), pp. 18–20.
- Pasman, HL, Groothuizen, ThM and de Gooijer, H (1974) Design of pressure relief vents. In: *Loss Prevention and Safety Promotion in the Process Industries*, Ed. by C.H. Buschman, pp. 185–189.
- PENNWELL CORPORATION (2007) *Fuel cell demand to reach \$8.5 billion in 2016*. Available from: <http://www.militaryaerospace.com/>. [Accessed 24.12.11].
- Peters, N (2000) *Turbulent Combustion*, Cambridge. Cambridge University Press.
- Petersen, EL, Davidson, DF and Hanson, RK (1999) Ignition Delay Times of Ram Accelerator CH/O/ Diluent Mixtures, *Journal of Propulsion and Power*, vol. 15(1), pp. 82–91.
- Pförtner, H and Schneider, H (1983) Fraunhofer-institut für treib- und explosivstoffe. ICT-Projektfor- schung 19/83. Forschungsprogramm “Prozeßgasfreisetzung – Explosion in der Gasfabrik und Auswir- kungen von Druckwellen auf das Containment”. Ballonversuche zur Untersuchung der Deflagration von Wasserstoff/Luft-Gemischen (Abschlußbericht). Dezember 1983.

Pförtner, H and Schneider, H (1984) Final Report for Interatom GmbH, Bergish Gladbach, Germany, October, Fraunhofer ICT Internal Report. (in German).

Pförtner, H (1985) The effects of gas explosions in free and partially confined fuel/air mixtures. *Propellants, Explosives, Pyrotechnics*, vol. 10, pp. 151–155.

Pinto, D, Aizawa, K, Liu, YF, Sato, H, Hayashi, AK and Tsuboi, N (2007) Auto-ignition of high pressure hydrogen release. *Proceedings of the 21<sup>st</sup> International Colloquium on the Dynamics of Explosions and Reactive Systems*, 23–27 July 2007, Poitiers, France.

Poinsot, T and Veynante, D (2001) Theoretical and numerical combustion. Edwards.

Pope, SB (1997) Computationally efficient implementation of combustion chemistry using in situ adaptive tabulation. *Combustion Theory and Modelling*, vol. 1, pp. 41–63.

Pope, SB (2004) Ten questions concerning the large-eddy simulation of turbulent flows. *New J. Phys.*, vol. 6, pp. 1–24.

Potter, AE (1960) Flame quenching. *Prog Comb Sci Tech*, vol. 1, pp. 145–181.

## Join American online LIGS University!

Interactive Online programs  
BBA, MBA, MSc, DBA and PhD

### Special Christmas offer:

- ▶ enroll **by December 18th, 2014**
- ▶ **start studying and paying only in 2015**
- ▶ **save up to \$ 1,200** on the tuition!
- ▶ Interactive Online education
- ▶ visit [ligsuniversity.com](http://ligsuniversity.com) to find out more!

Note: LIGS University is not accredited by any nationally recognized accrediting agency listed by the US Secretary of Education. More info [here](http://ligsuniversity.com).





- Pratt, TH (1993) Electrostatic ignitions in enriched oxygen atmospheres: a case history. *Process Saf Prog*, vol. 12, pp. 203–205.
- Proust, C, Jamois, D and Studer, E (2009) High pressure hydrogen fires. *Proceedings of the Third International Conference on Hydrogen Safety*. 16-18 September 2009, Ajaccio, France, paper 214.
- Prudnikov, AG (1967) Combustion of homogeneous fuel-air mixtures in turbulent flows. In: *Physical Principles of the Working Process in Combustion Chambers of Jet Engines*, edited by B.V. Raushenbakh, Chapter 5, pp. 244-336. Clearing House for Federal Scientific & Technical Information, Springfield.
- Puttock, JS, Cresswell, TM, Marks, PR, Samuels, A and Prothero, A (1996) Explosion assessment in confined vented geometries. SOLVEX large-scale explosion tests and scope model development. Project report. Health and Safety Executive, OTO 96 004 (Shell Research Limited, Rep. TRCP 3688R2).
- Radulescu, MI, Sharpe, GJ and Law, CK (2005) The Hydrodynamic Structure of Detonations. *Proceedings of the 20th ICDEERS*, Montreal, Canada 2005.
- Rasmus, DM and Krause, U (2001) Comparison of empirical and semi-empirical calculation methods for venting of gas explosions. *Fire Safety Journal*, vol. 36, pp. 1–23.
- Reider, R, Otway, HJ and Knight HT (1965) An unconfined large volume hydrogen/air explosion. *Pyrodynamics*, 1965, vol. 2, pp. 249–261.
- Report of committee for explosion testing (1958) Kommitten for Explosions Forsok, Bromma 1957, Slutrapport, Stockholm, April 1958.
- Ricci, M, Newsholme, G, Bellaby, P and Flynn, R (2006) Hydrogen: too dangerous to base our future upon?, In: *Proceedings of the IChemE Symposium Hazards XIX, March 2006, Manchester*. Rigby: IChemE, pp. 42–60.
- Ricou, FP and Spalding, DB (1961) Measurements of entrainment by axisymmetrical turbulent jets, *J. Fluid Mech.*, vol. 8, pp. 21–32.
- Ronney, PD (1990) Near-Limit flame structures at Low Lewis Number. *Combustion and Flame*, vol. 82, pp. 1–14.
- Rothe, V (2009) GM Permeation, delivered for presentation to the EC Hydrogen Working Group meeting on 10 March 2009, GM Powertrain Germany.

Royle, M and Willoughby, DB (2009) Consequences of catastrophic releases of ignited and unignited hydrogen jet releases. *Proceedings of the Third International Conference on Hydrogen Safety*, 16-18 September 2009, Ajaccio, France.

Ruffin, E, Mouilleau, Y and Chaineaux, J (1996) Large scale characterization of the concentration field of supercritical jets of hydrogen and methane, *Journal of Loss Prevention in the Process Industries*, vol. 9 (4), pp. 279–284.

Ruggles, AJ and Ekoto, IW (2011) Ignitability and mixing of underexpanded hydrogen jets, *Proceedings of the Fourth International Conference on Hydrogen Safety*, paper ID 125, 12–14 September 2011, San Francisco, USA.

SAE J2578 (2009) Recommended practice for general fuel cell vehicle safety, a Surface Vehicle Recommended Practice, SAE International, Detroit, Michigan, USA, January 2009.

SAE J2579 (2009) Technical information report for fuel systems in fuel cell and other hydrogen vehicles, SAE International, Detroit, Michigan, USA, January 2009.

SAE J2600 (2008) Compressed Hydrogen Surface Vehicle Refueling Connection Devices. SAE work in progress technical standard. Initiated 31 March 2008

Saffers, J-B, Makarov, D and Molkov, V (2011) Modelling and numerical simulation of permeated hydrogen dispersion in a garage with adiabatic walls and still air. *Int J Hydrogen Energy*, vol. 36, pp. 2582–2588.

San Marchi, C, Somerday, BP and Robinson, SL (2007) Permeability, solubility and diffusivity of hydrogen isotopes in stainless steels at high gas pressures. *Int J Hydrogen Energy*, vol. 32, pp. 100–116.

Sato, Y, Merilo, E, Groethe, M, Colton, J, Chiba, S and Iwabuchi, H (2006) Homogeneous hydrogen deflagrations in a sub-scale vehicle tunnel. *Proceedings of the National Hydrogen Association Conference*, Long Beach, CA, USA, 12–16 March 2006.

Schefer, RW, Houf, WG, San Marchi, C, Chernicoff, WP and Englom, L (2006a) Characterisation of leaks from compressed hydrogen dispensing systems and related components. *International Journal of Hydrogen Energy*, vol. 31, pp. 1247–1260.

Schefer, RW, Houf, WG, Bourne, B and Colton, J (2006b) Spatial and radiative properties of an open-flame hydrogen plume, *International Journal of Hydrogen Energy*, vol. 31, pp. 1332–1340.

Schefer, RW, Houf, WG, Williams, TC, Bourne, B and Colton, J (2007) Characterization of high pressure, underexpanded hydrogen-jet flames. *International Journal of Hydrogen Energy*, vol. 32, pp. 2081–2093.

Schröder, V and Holtappels, K (2005) Explosion characteristics of hydrogen-air and hydrogen mixtures at elevated pressures. Proceedings of the First International Conference on Hydrogen Safety. Pisa, Italy, 8–10 September 2005.

Schultheiß, D (2007) Permeation Barrier for Lightweight Liquid Hydrogen Tanks, Der Online-Publikationsserver der Universität Augsburg, 2007.

Shah, RK, Heikal, MR, Thonon, B and Tochnon, P (2001) Progress in the numerical analysis of compact heat exchanger surfaces. In: *Advances in Heat Transfer* (Hartnett, JP, Ed.), vol. 34, San Diego, USA, Academic Press.

Sharpe, GJ and Falle, SAEG (2000) Numerical simulations of pulsating detonations: I. Nonlinear stability of steady detonations. *Combust. Theory Modelling*, vol. 4, pp. 557–574.

Sharpe, GJ (2001) Transverse waves in numerical simulations of cellular detonations. *J. Fluid Mech.*, vol. 447, pp. 31–51.



**ie business school**

**#1 EUROPEAN BUSINESS SCHOOL**  
FINANCIAL TIMES 2013

**#gobeyond**

**MASTER IN MANAGEMENT**

**Because achieving your dreams is your greatest challenge.** IE Business School's Master in Management taught in English, Spanish or bilingually, trains young high performance professionals at the beginning of their career through an innovative and stimulating program that will help them reach their full potential.

- Choose your area of specialization.
- Customize your master through the different options offered.
- Global Immersion Weeks in locations such as Rio de Janeiro, Shanghai or San Francisco.

***Because you change, we change with you.***

www.ie.edu/master-management | mim.admissions@ie.edu | f t in YouTube

- Shebeko, YuN, Tsarichenko, S G, Eremenko, OYa, Keller, VD and Trunev, AV (1990) Combustion of lean hydrogen-air mixtures in an atomized water stream. *Combustion Explosion and Shock Waves*, vol. 26(4), pp. 426–428.
- Shepherd, JE (2006) Structural response of piping to internal gas detonation. *Proceedings of PVP2006-ICPVT-11 2006 ASME Pressure Vessels and Piping Division Conference*, July 23–27, 2006, Vancouver BC, Canada.
- Shepherd, J (2011) Crisis at Fukushima Dai-ichi Nuclear Power Plant. Available from: <http://www.galcit.caltech.edu/~jeshep/fukushima/> [Accessed 04.03.12].
- Shevyakov, GG and Komov, VF (1977) Effect of non-combustible admixtures on length of an axisymmetric on-port turbulent diffusion flame, *Combustion, Explosion and Shock Waves*, vol. 13, pp. 563–566.
- Shevyakov, GG, Tomilin, VP and Kondrashkov, YuA (1980) *Engineering Physical Journal*, deposit with VINITI, N3671-80 (in Russian).
- Shevyakov, GG and Savelieva, NI (2004) Dispersion and combustion of hydrogen jet in the open atmosphere, *International Scientific Journal for Alternative Energy and Ecology*, vol. 1(9), pp. 23–27 (in Russian).
- Shirvill, LC, Roberts, PT, Butler, CJ, Roberts, TA and Royle, M (2005) Characterisation of the hazards from jet releases of hydrogen, *Proceedings of the First International Conference on Hydrogen Safety*, Pisa, Italy, 8–10 September 2005.
- Shirvill, LC, Roberts, PT, Roberts, TA, Butler, CJ and Royle, M (2006) Dispersion of hydrogen from high-pressure sources, *Proceedings of the IChemE Symposium Hazards XIX*, Manchester, UK, 27–30 March 2006.
- Shorin, SN and Ermolaev, ON (1952) *Teploenergetika*, No.2.
- Short, M (2005) Theory and modeling of detonation wave stability; A brief look at the past and toward the future. ICDERS 2005.
- Short, M and Quirk, JJ (1997) On the nonlinear stability and detonability limit of a detonation wave for a model 3-step chain-branching reaction. *J. Fluid. Mech.*, vol. 339, pp. 89–119.
- Smagorinsky, J (1963) General circulation experiments with the primitive equations. I. The basic experiment. *Mon. Wea. Rev.*, vol. 91, pp. 99–164.

- Snee, TJ and Griffiths, JF (1989) Criteria for spontaneous ignition in exothermic, autocatalytic reactions: chain branching and self-heating in the oxidation of cyclohexane in closed vessels. *Combust Flame*, vol. 75, pp. 381–95.
- Solberg, DM, Pappas, JA and Skramstad, E (1980). Experimental investigations on flame acceleration and pressure rise phenomena in large scale vented gas explosions. *Proceedings of the 3<sup>rd</sup> Int. Symposium on Loss Prevention and Safety Promotion in Process Industries*. Basel (p. 16/1295).
- Spence, DA and Woods, BA (1964) A review of theoretical treatments of shock-tube attenuation, *Journal of Fluid Mechanics*, vol. 19, pp. 161–174.
- Stephenson, RR (2005) Fire safety of hydrogen-fuelled vehicles: system-level bonfire test. Proceedings of the 1<sup>st</sup> International Conference on Hydrogen Safety, Pisa, Italy, 2005. Available from: <http://conference.ing.unipi.it/ichs2005>. [Accessed 15.04.12].
- Stodilka, DO, Kherani, NP, Shmayda, WT and Thorpe, SJ (2000) A tritium tracer technique for the measurement of hydrogen permeation in polymeric materials. *Int J Hydrogen Energy*, vol. 25, pp. 1129–1136.
- Strelets, M (2003) Turbulence modelling in convective flow of fires. *Proceedings of the Fourth International Seminar on Fire and Explosion Hazards*, Londonderry, Northern Ireland, UK, 8–12 September 2003, ISBN: 1 85923 186 1, pp. 53–67.
- Studer, E, Jamois, D, Jallais, S, Leroy, G, Hebrard, J and Blanchetière, V (2009) Properties of large-scale methane/hydrogen jet fires. *International Journal of Hydrogen Energy*, vol. 34, pp. 9611–9619.
- Sunavala, PD, Hulse, C and Thring, MW (1957) Mixing and combustion in free and enclosed turbulent jet diffusion flames, *Combustion and Flame*, vol. 1(2), pp. 179–193.
- Sunderland, PB (2010) Hydrogen microflame hazards, Proceedings of the 8th International Short Course and Advanced Research Workshop in the series “Progress in Hydrogen Safety”, Hydrogen and Fuel Cell Early Market Applications, 11–15 October 2010, University of Ulster, Belfast.
- Swain, MR (2001) *Fuel leak simulation*. Available from: <http://evworld.com/library/swainh2vgasVideo.pdf>. [Accessed 24.12.11].
- Swain, MR and Swain, MN (1992) A comparison of H<sub>2</sub>, CH<sub>4</sub> and C<sub>3</sub>H<sub>8</sub> fuel leakage in residential settings. *International Journal of Hydrogen Energy*, vol. 17, pp. 807–815.



Swift, I and Epstein, M (1987) Performance of low-pressure explosion vents. *Plant/Operations Progress*, vol. 6 (2), pp. 98–105.

Takeno, K, Okabayashi, K, Kouchi, A, Nonaka, T, Hashiguchi, K and Chitose, K (2007) Dispersion and explosion field tests for 40MPa pressurized hydrogen. *International Journal of Hydrogen Energy*, vol. 32, pp. 2144–2153.

Tamura, Y, Takabayashi, M, Takeuchi, M and Mitsuishi, H (2011) The spread of fire from adjoining vehicles to a hydrogen fuel cell vehicle. In: *Proceedings of the Fourth International Conference on Hydrogen Safety*, 12–14 September 2011, San Francisco, USA.

Taylor, GI (1950) The dynamics of the combustion products behind plane and spherical detonation fronts in explosives. *Proceedings of the Royal Society of London. Series A, Mathematical and Physical Sciences*, vol. 200, Issue 1061, pp. 235–247.

The Air Tightness Testing & Measurement Association (2010) Technical standard L1. Measuring Air Permeability of building envelopes (dwellings), October 2010 issue. Available from: <http://www.attma.org/>. [Accessed 18.04.12].

Thring, MW and Newby, MP (1953) Combustion length of enclosed turbulent jet flames. *Fourth International Symposium on Combustion*, The Williams & Wilkins Co., pp. 789–796.

**SMS from your computer**  
...Sync'd with your Android phone & number

**FREE**  
30 days trial!

Go to

**BrowserTexting.com**

and start texting from your computer!

BrowserTexting



- TIAX (2004) Safety evaluation of the fuelmaker home refueling concept, presented to: Natural Gas Vehicle Technology Forum, Sacramento, USA, April 15.
- Townsend, AA (1956) The structure of turbulent shear flow, Cambridge University Press.
- Tse, SD, Zhu, DL and Law CK (2000) Morphology and burning rates of expanding spherical flames in H<sub>2</sub>/O<sub>2</sub>/inert mixtures up to 60 atmospheres. *Proceedings of the 28th Symposium (International) on Combustion*, Pittsburgh, PA: The Combustion Institute, pp. 1793–1800.
- Tsuboi, N (2007) Numerical Approach on Hydrogen Detonation: Fundamentals and Applications. 2<sup>nd</sup> European Summer School on Hydrogen Safety, Belfast 31 July–8 August 2007.
- Tsuruda, T and Hirano, T (1987) Growth of flame front turbulence during flame propagation across an obstacle. *Comb. Sci. Techn.*, vol. 51, pp. 323–328.
- Waterland, LR (2005) Safety evaluation of the fuelmaker home refueling concept, Final report, NREL/SR-540-36780, February 2005, NREL, Colorado, USA.
- Weast, RC and Astle, MJ (1979) CRC Handbook of Chemistry and Physics. CRC Press, Inc., West Palm Beach, 59th edition.
- Webster, C (2009) Private communication, Powertech Labs.
- Tieszen, SR, Sherman, MP, Benedick, WB, Shepherd, JE, Knystautas, R and Lee, JHS (1986) Detonation cell size measurements in hydrogen-air-steam mixtures. *Progress in Astronautics Aeronautics*, vol. 106, pp. 205–219.
- Tse, SD, Zhu, DL and Law, CK (2000) Morphology and burning rates of expanding spherical flames in H<sub>2</sub>/O<sub>2</sub>/inert mixtures up to 60 atmospheres. *Proceedings of the 28th Symposium (International) on Combustion*. The Combustion Institute. Pittsburgh, PA, pp. 1793–1800.
- Ungut, A and James, H (2001) Autoignition of gaseous fuel-air mixtures near a hot surface. *Int Chem Eng Symp Ser*, vol. 148, pp. 487–502.
- US DEPARTMENT OF ENERGY (2004) *Basic Research Needs for the Hydrogen Economy*. Washington: US DoE, Office of Science. Available from: [science.energy.gov/~media/bes/pdf/reports/files/nhe\\_rpt.pdf](http://science.energy.gov/~media/bes/pdf/reports/files/nhe_rpt.pdf). [Accessed 24.12.11].
- Vaagsaether, K, Knudsen, V and Bjerketvedt, D (2007) Simulation of flame acceleration and DDT in H<sub>2</sub>-air mixture with a flux limiter centered method. *International Journal of Hydrogen Energy*, vol. 32(13), pp. 2186–2191.

- Verbecke, F (2009) Formation and combustion of non-uniform hydrogen-air mixtures. PhD thesis, University of Ulster.
- Verbecke, F, Makarov, D and Molkov, V (2009) VLES of lean hydrogen-air deflagrations in a closed vessel 5.7 m high. *Proceedings of the 6th Mediterranean Symposium on Combustion*, 7–11 June 2009, Corsica.
- Verfonderen, K. (2008) *Safety considerations of liquid hydrogen*. Forschungszentrum Jülich GmbH, Jülich, 178 p., ISBN 978-3-89336-530-2.
- Vervisch, L and Veynante, D (2000) Interlinks between approaches for modelling turbulent flames. 28th Symp. (Int.) on Combustion, pp. 173–185.
- Veser, A, Kuznetsov, M, Fast, G, Frierish, A, Kotchourko, N, Stern G, et al. (2009) The structure and flame propagation regimes in turbulent hydrogen jets, *Proceedings of the Third International Conference on Hydrogen Safety*, Ajaccio, France, 16–18 September 2009.
- Wancura, H, Mayo, B, Reijalt, M, Mertens, JJ, Maio, P and Claassen, P (2006) Draft implementation report WG5 Cross Cutting Issues (XCI). European Hydrogen and Fuel Cell Technology Platform, Implementation Panel.
- Warren Centre for Advanced Engineering (1989) *Fire Safety and Engineering Project*, Report and Technical Papers, Books 1 and 2, The University of Sydney, Sydney, Australia.
- Watterson, JK, Connel, IJ, Savill, AM and Dawes, WN (1998) A solution adaptive mesh procedure for predicting confined explosions. *International Journal for Numerical Methods in Fluids*, vol. 26, pp. 235–247.
- Weller, H, Tabor, G, Gosman, A and Fureby, C (1998) Application of a flame-wrinkling LES combustion model to a turbulent mixing layer. 27<sup>th</sup> Symp. (Int.) on Combustion, pp. 899–907.
- Wen, JX, Xu, BP and Tam, VHY (2009) Numerical study on spontaneous ignition of pressurized hydrogen release through a length of tube, *Combustion and Flame*, vol. 156(11), pp. 2173–2189.
- Whitehouse, DR, Greig, DR and Koroll, GW (1996) Combustion of stratified hydrogen-air mixtures in the 10.7 m<sup>3</sup> Combustion Test Facility cylinder. *Nucl. Eng. Design.*, vol. 166, pp. 453–462.
- Wikipedia – The Free Encyclopedia. Wikimedia Foundation, Inc. Available from: <http://en.wikipedia.org/>. [Accessed 25.12.11].
- Wilson, MJG (1954) The relief of explosions in closed vessels. PhD thesis, June 1954, Dept. of Chemical Engineering, Imperial College of Science and Technology, London, UK.

van Wingerden, CJM and Zeeuwen, JP (1983) On the role of acoustically driven flame instabilities in vented gas explosions and their elimination. *Combustion and Flame*, vol. 51, pp. 109–111.

Wionsky, SG (1972) Predicting Flammable Material Classifications. *Chemical Engineering*, vol. 79, no. 26, pp. 81-86.

Wolanski, P and Wojcicki, S (1972) Investigation into the mechanism of the diffusion ignition of a combustible gas flowing into an oxidizing atmosphere. *Proceedings of the Combustion Institute*, vol. 14, pp. 1217–1223.

Xiao, H, Makarov, D, Sun J and Molkov, V (2012) Experimental and numerical investigation of premixed flame propagation with distorted tulip shape in a closed duct. *Combustion and Flame*, vol. 159, pp. 1523–1538.

Xu, BP, El Hima, L, Wen, JX, Dembele, S, Tam, VHY and Donchev, T (2008) Numerical study on the spontaneous ignition of pressurized hydrogen releases through a tube into air, *Journal of Loss Prevention in the Process Industries*, vol. 21(2), pp. 205-213.

Xu, BP, Wen, JX, Dembele, S, Tam, VHY and Hawksorth, SJ (2009) The effect of pressure boundary rupture rate on spontaneous ignition of pressurized hydrogen release, *Journal of Loss Prevention in the Process Industries*, vol. 22(3), pp. 279–287.

## The Wake

the only emission we want to leave behind

Low-speed Engines Medium-speed Engines Turbochargers Propellers Propulsion Packages PrimeServ

The design of eco-friendly marine power and propulsion solutions is crucial for MAN Diesel & Turbo. Power competencies are offered with the world's largest engine programme – having outputs spanning from 450 to 87,220 kW per engine. Get up front! Find out more at [www.mandieselturbo.com](http://www.mandieselturbo.com)

Engineering the Future – since 1758.

**MAN Diesel & Turbo**



- Yakhot, V (1988) Propagation velocity of premixed turbulent flames. *Combustion Science and Technology*, vol. 60, pp. 191–214.
- Yakhot, V and Orszag, S (1986) Renormalization group analysis of turbulence. I. Basic theory. *Journal of Scientific Computing*, vol. 1, pp. 3–51.
- Yamada, E, Watanabe, S, Hayashi, AK and Tsuboi, N (2009) Numerical analysis on autoignition of a high-pressure hydrogen jet spouting from a tube, *Proceedings of the Combustion Institute*, vol. 32(2), pp. 2363–2369.
- Yang, JC, Pitts, WM, Fernandez, M and Kuldeep, P (2011) Measurements of effective diffusion coefficients of helium and hydrogen through gypsum. *Proceedings of the Fourth International Conference on Hydrogen Safety*, paper ID 144, 12–14 September 2011, San Francisco, USA.
- Yao, C (1974) Explosion venting of low-strength equipment and structures. *Loss Prevention*, vol. 8, pp. 1–9.
- Zabetakis, MG (1967) *Safety with cryogenic fluids*. Plenum Press, New York.
- Zalosh, RG (1978) Gas explosion Tests in Room-Size Vented Enclosures. *Proceedings of AIChE Loss Prevention Symposium*, vol. 13, pp. 98–108.
- Zbikowski, M (2010) Hydrogen deflagration-to-detonation transition and its mitigation technologies. PhD thesis, University of Ulster, September 2010.
- Zbikowski, M, Makarov, D and Molkov, V (2008) LES model of large scale hydrogen-air planar detonations: Verification by the ZND theory. *International Journal of Hydrogen Energy*, vol. 33, pp. 4884–4892.
- Zbikowski, M, Makarov, D and Molkov, V (2010) Numerical simulations of large-scale detonation tests in the RUT facility by the LES model. *Journal of Hazardous Materials*, vol. 181(1-3), pp. 949–956.
- Zeldovich, YaB (1940) К теории распространения детонации в газообразных системах (On the theory of the propagation of detonations on gaseous system), *Zh. Eksp. Teor. Fiz.*, vol. 10, pp. 542–568. (in Russian).
- Zeldovich, YaB, Librovich, VB, Makhviladze, GM and Sivashinsky, GI (1970) On Development of Detonation in a Non-Uniformly Preheated gas. *Astronautica Acta*, vol. 15, pp. 313–320.
- Zeldovich, YaB, Barenblatt, GI, Librovich, VB and Makhviladze, GM (1980) *Mathematical Theory of Combustion and Explosion*, Moscow: Nauka.
- Zimont, VL and Lipatnikov, AN (1995) A numerical model of premixed turbulent combustion of gases. *Chem. Phys. Reports*, vol. 14, no. 7, pp. 993–1025.